Technische Universität München
TUM School of Natural Sciences

Development of a cellular model system to differentiate HDAC1 from HDAC2 activity

Karl Moritz Ludwig

Vollständiger Abdruck der von der TUM School of Natural Sciences der Technischen Universität München zur Erlangung eines

Doktors der Naturwissenschaften (Dr. rer. Nat.)

genehmigten Dissertation.

Vorsitz: Prof. Dr. Franz Hagn

Prüfer der Dissertation:

1. Prof. Dr. Michael Sattler
2. Prof. Dr. Martin Göttlicher

Die Dissertation wurde am 29.08.2022 bei der Technischen Universität München eingereicht und durch die Fakultät für Chemie am 30.09.2022 angenommen.

Danksagung

Mein aufrichtiger Dank gilt:
Herrn Prof. Dr. Martin Göttlicher für die Möglichkeit, diese am Helmholtz-Zentrum durchzuführen.

Herrn Prof. Dr. Michael Sattler für die Betreuung meiner Doktorarbeit als Lehrstuhlinhaber für Biomolekulare NMR-Spektroskopie.

Meinen Eltern, die mich während meines gesamten Studiums unterstützten, mir den nötigen Rückhalt gaben und diese Arbeit Korrektur lasen.

Den Mitgliedern des Instituts für Molekulare Toxikologie und Pharmakologie, für die vielen beantworteten Fragen und die angenehme Zeit, die ich mit ihnen während meiner Doktorarbeit verbrachte.

Meiner Freundin Catarina Theiß, die mir vor allem, aber nicht nur, in der Endphase der Doktorarbeit zur Seite stand.

Nirav Chhabra für die gute Freundschaft und den hilfreichen Input zu meiner Doktorarbeit.

Allen Mitgliedern der Doktorandeninitiative für die schöne gemeinsame Zeit beim Organisieren von Events für alle Doktoranden.

Contents

List of Figures

List of Tables

List of abbreviations

A

APS - ammoniumperoxodisulfate 42
a.u. - arbitrary units 50

B

BSA - bovine serum albumin 33

C

CHX - cycloheximide 60, 61
CRC - Colorectal cancer 2
CTCL - cutaneous T cell lymphoma 6

D

DMSO - dimethyl sulfoxide 31, 83
DNA - desoxyribonucleic acid 11, 33, 45
DSBs - double strand breaks 45
DTT - dithiothreitol 40

E

E. coli - Escherichia coli 35
EDTA - ethylenediaminetetraacetic acid 36
ELISA - enzyme-linked immunosorbent assay 40, 94

F

FACS - fluorescence activated cell sorting 37, 47, 49
FDA - food and drug administration 6

G

GFP - green fluorescent protein 48, 51, 86

H

HAT - histone acetyl transferase ..... 2, IX
HDAC - histondeacetylase 2–4, 6
HDACi - HDAC inhibitors ..... 9, 11, 13, IX
HEPES - 4-(2-hydroxyethyl)-1-piperazineethanesulfonic acid 41
HMT - histone methyl transferase 2
HPLC - high-performance liquid chromatography 39

I

IF - immunofluorescence 3, 33
IGV - integrative genomics viewer 70, 125

IP - immunoprecipitation 41, 83, 85

K

KDAC - lysine deacetylase 4
KDM - lysine demethylase 2

M

MS - mass spectrometry 82, 87
MWCO - molecular-weight cutoff 41

N

NHEJ - non-homologous end joining 45, 46

P

PAGE - polyacrylamide gel electrophoresis 43
PBS - phosphate buffered saline 31
PCR - polymerase chain reaction 32, 33, 45
PEG - polyethylene glycol 34
PFA - paraformaldehyde 33, 37
POI - protein of interest 44
PRF - Perforin 99
PTC - premature termination codon 45, 46
PTCL - peripheral T cell lymphoma 6, 7
PTMs - post translational modifications 105

R

RNA - ribonucleic acid 38
ROS - reactive oxygen species 11
RT - room temperature 31, 33

S

SAHA - suberanilohydroxamic acid 6–8, 10, 18, 21, 22, 83, 98, 100
SAR - structure activity relationship 7, 8
SDS - sodium dodecyl sulfate 42
SKR - structure kinetic relationship 9

T

TAGLN - Transgelin 99
TEMED - N,N,N,N-tetramethylethane-1,2-diamine 42
TF - transcription factor 99
TFA - trifluoracetic acid 41
TMT - tandem mass tag 84
TSA - trichostatin A 83, 102

V

W

Abstract

The research in this thesis aimed to improve the development of isoform-specific HDAC inhibitors (HDACi). The HDAC family consists of 18 isoforms, eleven of which have a zinc dependent mechanism. Cancer medications were developed targeting some of the zinc dependent isoforms, since the activity loss of the isoform HDAC2 proved to be beneficial for colon cancer treatment. Currently, all available HDAC inhibitors target HDAC2 as well as its structurally most similar relative HDAC1. These inhibitors are constrained in their application by dose-limiting side-effects, which suggests, that a better isoform selectivity of the inhibitors will be required to improve the therapeutic application. The specific goal of the thesis was to differentiate between the potency of small molecules to inhibit HDAC1 and HDAC2 in cells, which advances isoform-selective measurements from *in-vitro* assays to the more relevant cellular assays, improving future HDAC inhibitor development.

For the distinction between HDAC1 and HDAC2, a set of highly homologous clonal cell lines was created, in which the expression of either HDAC1 or HDAC2 can be controlled without triggering compensation of the other HDAC's expression from the endogenous gene. In a first scenario, utilizing the model cell lines with either HDAC1- or HDAC2-expression allowed us to measure the effect of an inhibitor on either HDAC1 or HDAC2 by quantifying a marker of combined HDAC1/2 activity, histone acetylation site Ac-H3K9. At higher inhibitor concentrations we observed HDAC3 inhibition, confirming the need for a more selective marker.

In a second scenario, this set of cell lines enabled to search for markers of specific activity of either HDAC1 or HDAC2. It was reasoned that acetylations on non-histone proteins are modified by fewer histone acetyl transferase (HAT) and HDAC isoforms, therefore we performed LC-MS/MS of acetylation enriched samples of non-histone proteins. In the model cell lines new acetylation sites were identified as well as specific acetylation sites, which may serve as specific marker for either HDAC1 or HDAC2 activity. Acetylated Matrin 3 on K711 and K712 was identified to react on HDAC2 activity loss and the acetylation site on lysine 108 of the heat shock protein HSPA8/HSP7C/Hsp70 was identified to react to the loss of HDAC1 activity. An initial verification of the acetylation site on Matrin 3 showed an increase upon either HDAC1 or HDAC2 loss, making this acetylation site a candidate for the single expression context scenario.

In conclusion, cellular systems were created, in which either HDAC1 or HDAC2 inhibition can be measured. The use of these genetically engineered cell lines combined with markers that are modified by both isoforms creates *in-vivo* conditions, under which the effect of an HDAC inhibitor on a single isoform can be measured. This is a great improvement compared to existing approaches and will enable the development of improved and safer cancer therapies with HDAC-specific targeting inhibitors.

Zusammenfassung

Ziel dieser Arbeit war es, die Entwicklung isoenzym-selektiver Histondeacetylase Inhibitoren zu verbessern. Die Familie der Histondeacetylasen besteht aus 18 Isoformen, von denen elf Isoformen einen Zink-basierten Katalysemechanismus aufweisen. Da sich eine Reduktion der HDAC2 Aktivität als nützlich bei der Behandlung von Darmkrebs heraus gestellt hatte, wurden gegen einige dieser Isoformen Krebsmedikamente entwickelt. Nach aktuellem Entwicklungsstand inhibieren alle bekannten Inhibitoren mehreren Isoformen, insbesondere HDAC1 und HDAC2 werden zusammen inhibiert. Da das therapeutische Fenster dieser Medikamente durch deren starke Nebenwirkungen eingeschränkt wird, verfolgten wir den Ansatz die Entwicklung selektiverer Medikamente zu unterstützen. Das Hauptziel dieser Arbeit war die Unterscheidung HDAC1 und HDAC2 Inhibition in Zellen.

Zur Unterscheidung der Aktivität von HDAC1 und HDAC2 wurde ein Set homologer Zelllinien erstellt, in denen die Expression von HDAC1 und HDAC2 kontrolliert werden konnte, ohne eine Kompensation durch die Expression des edogenenen Gens auszulösen. Zum einen ermöglichten uns diese Zelllinien die Messung der Inhibition von HDAC1 oder HDAC2 mit Markern der gemeinsamen Aktivität von HDAC1/2 in Zellen, die nur eine der beiden Isoformen exprimieren. Zum Anderen ermöglichten uns diese Zelllinien die Suche nach Isoenzymselektiven Biomarkern für HDAC1 oder HDAC2 Aktivität.

Wir konnten zeigen, dass sich die Wirkung eines Inhibitors auf HDAC1 oder HDAC2 quantitativ messen lässt, wenn man die Acetylierungsstelle an Lysin 9 von Histon 3 in Zellen betrachtet, die entweder HDAC1 oder HDAC2 exprimieren. Bei höheren Inhibitor Konzentrationen werden acetylierte Lysine an dieser Stelle zusätzlich durch HDAC3 beeinflusst. Daher werden selektivere Acetylierungsstellen benötigt, die von weniger Isoformen modifiziert werden. Da für viele Lysine in Histonen bekannt ist, dass sie durch mehrere Isoformen modifiziert werden, haben wir unsere Suche nach seletiv modifizierten Stellen auf nicht-Histon Proteine fokussiert. Dabei konnten wir durch LC-MS/MS-Messungen sowohl bisher unbekannte acetylierte Lysine identifizieren, als auch zwei Peptide, die selektiv auf den Verlust von HDAC1 bzw. HDAC2 reagieren. Die acetylierten Lysine K711 und K712 am Protein Matrin 3 nehmen bei HDAC2 Aktivitätsverlust zu und die Acetylierung an K108 an Heat Shock Protein HSPA8 /HSP7C /Hsp70 nimmt bei HDAC1 Aktivitätsverlust ab. Ein initiale Verifizierung durch einen maßgeschneiderten Antikörper hat gezeigt, dass die acetylierten Lysine an Matrin 3 auf HDAC1 und HDAC2 Verlust reagieren. Daher eignet sich dieser Marker für Aktivitätsmessungen in Zelllinien, die entweder HDAC1 oder HDAC2 exprimieren.

Zusammenfassend wurden zelluläre Systeme erstellt, in denen sich die Inhibition von HDAC1 oder HDAC2 individuell messen lässt. Diese Messung der Inhibition einzelner Isoformen *in-vivo* stellt eine große Verbesserung dar und wird die Entwicklung besserer und sicherer Krebstherapeutika mit gezielt HDAC-spezifischen Inhibitoren ermöglichen.

1. Introduction

1.1. Colon Cancer

Cancers are a whole group of diseases, with more than 100 distinct types of cancer, which share the trait of abnormal cellular growth[1]. The malignant, excessive growth of cells is called neoplasm and if this uncoordinated growth forms a mass, it is called tumor. Neoplasms and tumors can occur anywhere in the body, sharing only the abnormal growth. In 2000 Hanahan *et al.* proposed the concept of six hallmarks that regular cells have to acquire in order to become malign[1]. These include evading apoptosis, self-sufficiency in growth signals, insensitivity to anti-growth signals, sustained angiogenesis, limitless replicative potential as well as tissue invasion and metastasis[1]. In 2011 Hanahan *et al.* further refined their hallmark concept, adding two additional hallmarks and two enabling characteristics[2]. The two additional hallmarks are a deregulation of cellular energetics and the avoidance of immune destruction[2]. Cancer enabling characteristics are genome instability and mutation as well as tumor-promoting inflammation[2]. In 2017 the total death toll of cancers worldwide was 10.8 million deaths[3]. The mortality by cancer increases with age, reaching a maximum in the age group around 65-69 year old men and women (based on 2010 data)[4].

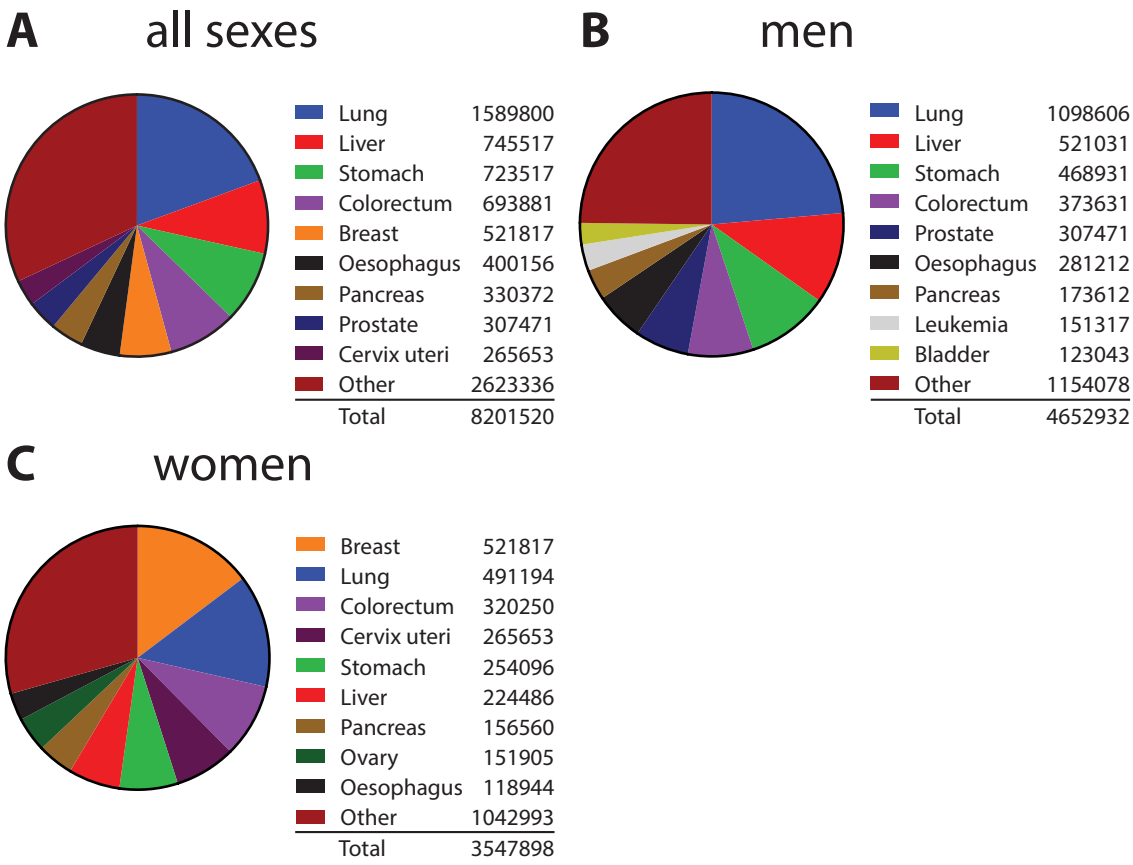

Figure 1.1 Colorectal cancer (colon and rectum) is the fourth most common cause of deaths among cancers worldwide. Estimated deaths for all sexes (**A**), men (**B**) and women (**C**) from the 2014 world cancer report[5].

Colorectal cancer (CRC) is a cancer type with a high death toll (see fig. 1.1) and a lot of time and money has been invested to investigate differences between CRC cells and healthy cells. CRC is the abnormal growth of cells in the colon or rectum and to address differences in CRC and their responses to medication, four consensus molecular subtypes (CMSs) were defined[6]. CMS1 accounts for 14% and is microsatellite instability immune, hypermutated, microsatellite unstable and has strong immune activation. CMS2 is called canonical, accounts for 37% of all cases and is characterized by being epithelial as well as having marked WNT and MYC signaling activation. The metabolic CMS3 accounts for 13% of cases, is epithelial and has metabolic dysregulation. 23% of cases are classified as the mesenchymal CMS4, which shows prominent transforming growth factor-β activation, stromal invasion and angiogenesis[6].

These are four subtypes of fully developed tumors, but sometimes DNA hypo-methylation even precedes initial cancer mutations[7, 8]. Epigenetic marks, like DNA methylation, are heritable from cell to cell and are able to influence the phenotype. In general, epigenetic alterations play an important role in cancer development[9], leading Feinberg *et al.* to a model proposition that cancers in general are caused by epigenetic disruptions in cancer stem/progenitor cells[10]. Epigenetic marks may be influenced by diet, obesity and the lack of exercises, which are life-style related risk factors for the development of CRC[5].

1.2. Epigenetic Regulations and Cancer

In cancers four general types of epigenetic phenotypes were classified by Sarkar *et al.*[11]. A first phenotype and long standing observation is genome-wide DNA hypo-methylation[7, 8]. A second phenotype observed in cancer is the hyper-methylation of promoter regions[12, 13]. Abnormal histone modifications and binding of their readers was classified as a third phenotype. A last class of phenotypes described by Sarkar *et al.* are abnormal chromatin structures. As there are epigenetic alterations in almost every cancer type, it was proposed to add genetic alterations as a hallmark of cancer[11, 14].

In general, three groups of of histone modifying enzymes and proteins exist (see fig. 1.2)[15]. The first group of enzymes catalyzes the addition of chemical residues to histones and are called epigenetic writers (fig. 1.2, panel A). Enzymes like histone methyl transferase (HMT) and HAT belong to this group. A second group is called epigenetic editors and consists of enzymes like lysine demethylase (KDM) and histondeacetylase (HDAC). The third group consists of enzymes and proteins that recognize epigenetic modification, e.g. bromodomain containing proteins. In the 2000s the histone code hypothesis was proposed stating that different histone tail modifications on individual positions act sequentially or in combination to initiate distinct events[16, 17, 18, 19]. Some acetylation sites, like acetylated lysine at position nine of histone three (Ac-H3K9), Ac-H3K18 and Ac-H4K8, are associated with active chromatin regions[20]. In many cancer types histone modifications or patterns of modifications have proven to be prognostic markers of survival[14]. While single modifications have been

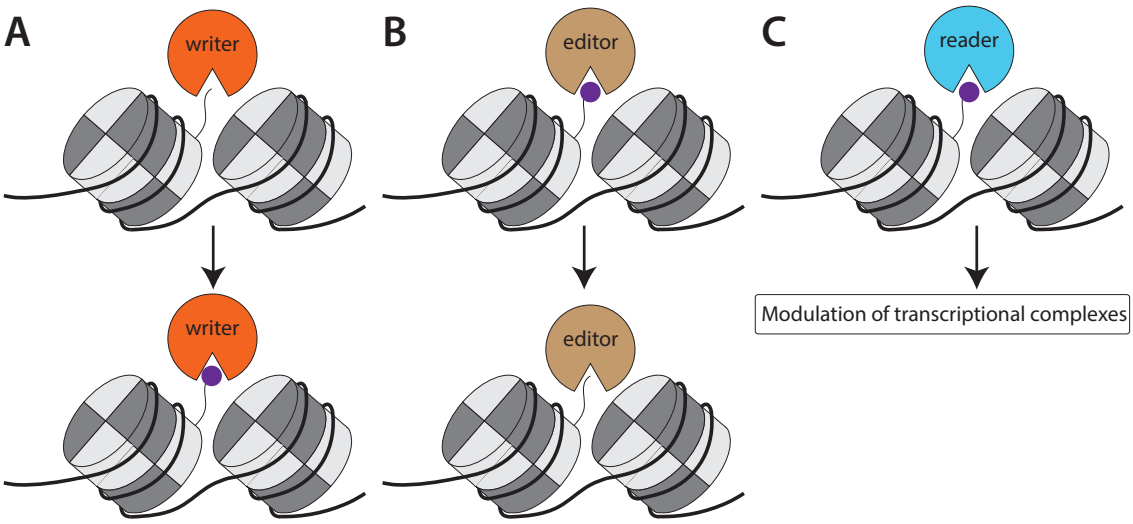

Figure 1.2 Classification of histone modifying enzymes. A) Histone modifications are added by writers like histone methyl transferases (HMTs) or histone acetyl transferases (HATs). **B)** These modifications are removed by editing like demethylases (KDMs) or histone deacetylases (HDACs). **C)** Some enzymes only read certain modifications, e.g. acetyl groups are read by groups of bromodomain proteins. (Figure adapted from [15])

attributed to functions, an overall histone code remains to be fully understood and decoded.

A significant difference between normal colon tissue and colon carcinomas is that isoform two of the HDAC family is overexpressed, which has been shown for patient matched normal tissues compared to colonic tumor samples[21]. In another study, HDAC1 and HDAC2 were found to be overexpressed in colon carcinomas, with HDAC2 being more robustly up-regulated[22]. Without mentioning HDAC2, Ishiama *et al.* found a more intense immunofluorescence (IF) staining of HDAC1 in patient colon cancer samples compared to normal colonic mucosa[23]. One study also found HDAC3 to be up-regulated in colon tumor samples compared to normal tissue, while confirming the previously mentioned HDAC1 and HDAC2 overexpression in the same samples[24].

These results highlight the important role of class I HDACs in cancer development. Depending on the cancer type, different HDAC isoforms seem to be overexpressed. The wide variety of cancer types and their different phenotypes suggest certain differences in HDAC isoform dependency. In other cancer types, e.g. in gastric cancer, HDAC2 was found to be up-regulated[25] and in prostate cancer HDAC1 was up-regulated[26]. When focusing on colon cancer, the isoform HDAC2 is consistently up-regulated, which suggests a key role of this isoform in the formation of colon cancer.

HDACs either modify histone tails causing chromatin condensation[31] and changing the chromatin state from euchromatin to heterochromatin [17] or HDACs remove acetylation sites from non-histone proteins (fig. 1.3). Tubulin was one of the first known non-histone proteins which was found to be acetylated. Now acetylation sites on tubulin are well established and it is known that HDAC6 deacetylates lysine 40[27, 28, 29]. In 2009 Choudhary *et al.* performed the first unbiased comprehensive analysis of acetylations within the mammalian

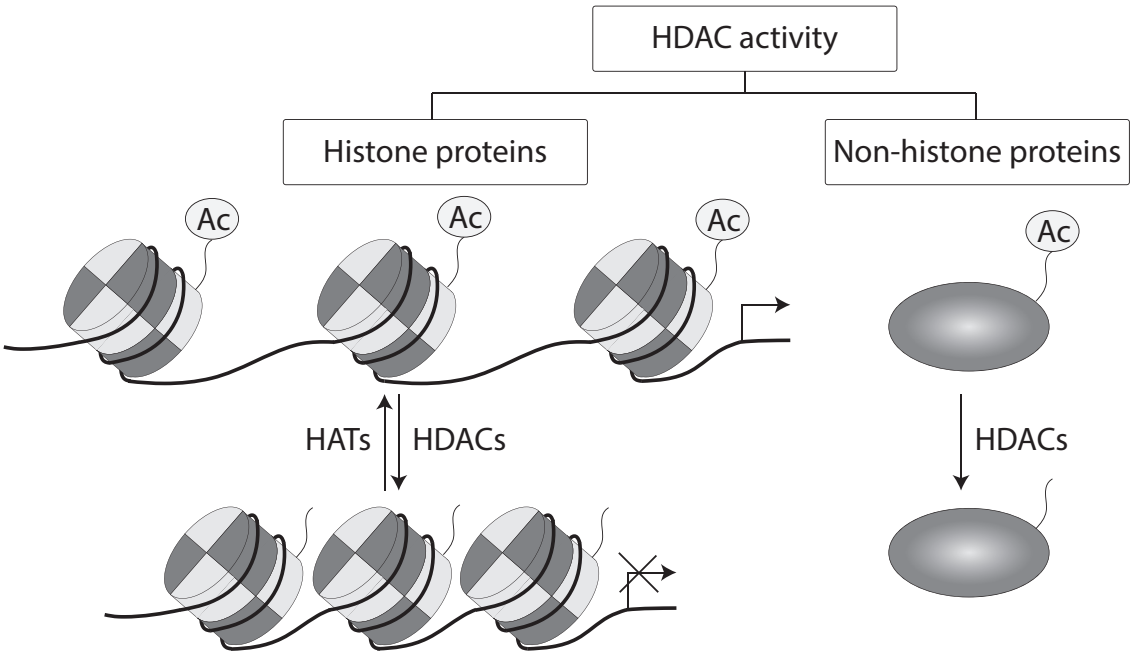

Figure 1.3 HDACs deacetylate histones and non-histone proteins. Histone acetylation influences the chromatin state between euchromatin and heterochromatin [17] as well as non-histone proteins. E.g. the acetylation on lysine 40 of tubulin is well established[27, 28, 29]. (Figure adapted from [30]).

proteome[32]. After having found a total of 3600 acetylation sites on 1750 non-histone proteins, they proposed to rename the HDAC family into lysine deacetylase (KDAC) to convey the function rather than the HDAC target family[32]. To date most publications still use the name HDAC for members of the enzyme family.

1.3. The HDAC Family

The HDAC family consists of 18 individual isoforms, which all function by the removal of ε-N-acetyl from lysines of proteins. By similarities to yeast deacetylases the isoforms are grouped into four classes. Class I,II and IV deacetylate lysines with a Zn^{2+} dependent mechanism. The zinc atom activates the oxygen of the acetyl group, making it prone for a nucleophilic attack of a water molecule, which is activated by a histidin-aspartate charge relay system[33]. After a temporary transition state, the amine group is released from the acetate[33]. Class III enzymes deacetylate lysines with a NAP^{+} dependent mechanism. Class I consists of HDAC1, HDAC2, HDAC3 and HDAC8, which are related to yeast RDP3. Isoforms from this class are mainly nuclear and expressed in all tissue types[34]. HDAC1 and HDAC2 are part of the Sin3, Nurd and CoREST complexes[35, 36, 37, 38, 39, 40]. HDAC3 is part of the N-CoR/SMRT complex[36, 37, 41]. These complexes bind to chromatin through transcription factors and coordinate epigenetic modifications. Class II enzymes are homologous to yeast Sir2[42]. Enzymes from the class IIa (HDAC4, HDAC5, HDAC7 and HDAC9) and from class IIb (HDAC6 and HDAC10) show tissue specific expression with varying functions. Class III isoforms are named Sirtuins after the yeast Sir2 protein and consist of seven isoforms (SIRT1-7). They are structurally unrelated to class I, II and IV. SIRT1, SIRT6 and SIRT7 are

localized in the nucleus and involved in the regulation of metabolic processes, especially the glucose metabolism[43, 44, 45]. SIRT2 is located in the cytoplasm and deacetylates for example lysine 40 of α-tubulin[46]. SIRT3, SIRT4 and SIRT5 are mitochondrial, where no class I, II and IV isoforms are located. HDAC11 differs from the other yeast homologous, forming its own class IV[47]. The only known function of HDAC11 is to regulate interleukin 10, which decides if antigen presenting cells steer towards immune activation or immune tolerance[48].

From the domain structure of the individual HDAC isoforms, it becomes evident that there is a high homology between class I isoforms (see fig. 1.4). Within class I HDACs, HDAC1 and HDAC2 share an overall sequence similarity of 86% and they even share 95% sequence similarity in their catalytic domain[49]. The domain structure of class IIa isoforms is also similar within the subclass. HDAC6 and HDAC10 are very distinct from all other isoforms. A phylogenetic analysis of class I, II and IV HDAC families showed an evolutionary divergence of the isoforms roughly correlating with the structural differences. Within the evolutionary development of class I, HDAC8 diverged first, then HDAC3 did and most recently a gene duplication lead to the two human paralogue HDAC1 and HDAC2[50].

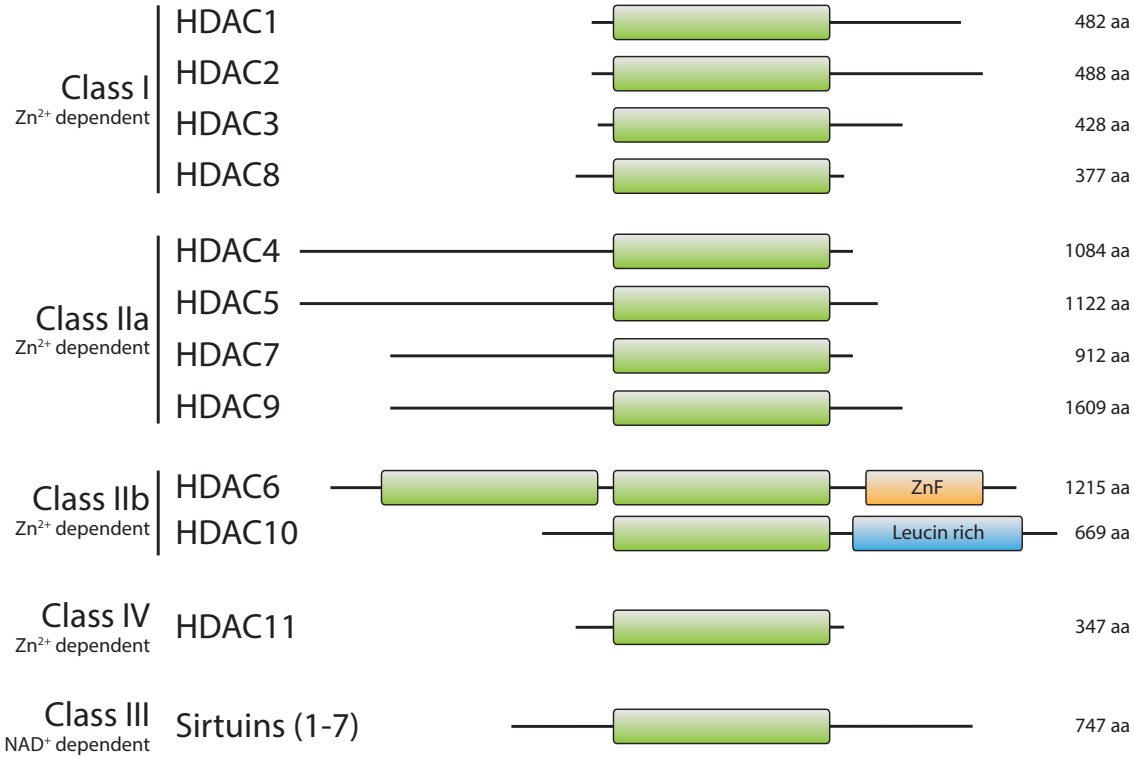

Figure 1.4 HDAC family protein domains. The individual classes of the HDAC family are shown with the individual isoforms belonging to the classes. The green rectangle represents the conserved catalytic domain. (Figure adapted from [30]).

The earlier described aberrant expression of HDAC enzymes in general and HDAC2 in colon carcinoma cells provides a good rationale for the development of inhibitors against HDAC enzymes, especially against HDAC2[51, 52, 53].

When HDAC2 comes into focus for inhibitor development, the close structural similarity between HDAC1 and HDAC2 poses a challenge. The gene duplication suggests little func-

tional divergence from each other. Nevertheless, HDAC1 and HDAC2 cannot fully replace each other. One of the first observations in this direction was that homozygous disruption of HDAC1 in mice leads to early embryonic lethality, while HDAC2 knockout mice survived until the first day after birth[54]. In one study, HDAC2 knockout mice showed lethal heart morphology alterations[55]. In a different viable HDAC2 knockout mouse model, the mice showed reduced body sizes and reduced intestinal tumor rates when paired with a tumor prone mouse model[56]. In contrast to HDAC1, HDAC2 negatively regulates memory formation in mice[57]. Additionally, on the molecular level, there is evidence that histone acetylations are influenced by HDAC1 or HDAC2. Acetylation on histone four lysine five (H4K5) inversely correlates with HDAC1 expression[58] and HDAC2 protein depletion leads to increased H4K16 acetylation levels[59]. These differences pose a rationale to differentiate between HDAC1 and HDAC2 with inhibitors. The next section describes the current state of development of HDAC inhibitors and their selectivity.

1.4. HDAC Inhibitors

Initially, in 1975, butyrate was found to have anti-cancer activity, by inducing differentiation[60]. Shortly afterwards, in 1977, it was discovered that butyrate caused histone hyper-acetylation[61], while it remained unclear that HDACs were the target. The link between HDAC inhibition and tumor growth/survival was established in the 1990s, by showing that the inhibitors TSA and SAHA cause histone hyper-acetylation *in vivo* and that they strongly inhibit purified HDAC isoforms *in vitro*[62, 63]. In 2001, the food and drug administration (FDA) approved anti-epileptic drug valproic acid (VPA) and it was discovered that VPA inhibits HDAC isoforms[64]. This opened the possibility to investigate HDAC inhibition for the treatment of cancer in patients.

Over time several zinc binding groups were discovered and HDAC inhibitors were classed by the dominant chemical group. One class are short chain fatty acids and another class include a hydroxamic acids group[53]. A third class contains the central motive of a benzamide group and a fourth class are cyclic tetrapeptides[53] (see fig. 1.5 for chemical structures). VPA is an example for a short chain fatty acid. The inhibitor suberanilohydroxamic acid (SAHA), which is also called Vorinostat, as well as the inhibitors Belinostat and Panobinostat are examples for hydroxamic acid inhibitors. Entinostat, JQ-12 and Chidamide are HDAC inhibitors based on a benzamide Zn^{2+} binding group. The depsipeptide Romidepsin was found as a natural product produced by *Chromobacterium violaceum* in 1994[65] and belongs to the class of cyclic tetrapeptides.

Five HDAC inhibitors are currently approved for the treatment of different forms of cancer. In 2006 SAHA was approved by the FDA under the name Vorinostat for the treatment of cutaneous T cell lymphoma (CTCL) to be used upon a relapse after two systemic treatments[66] [67]. The next HDAC inhibitor approved by the FDA was Romidepsin, first approved in 2009 for the treatment of CTCL. In 2011 the FDA approval was extended to the treatment of pe-

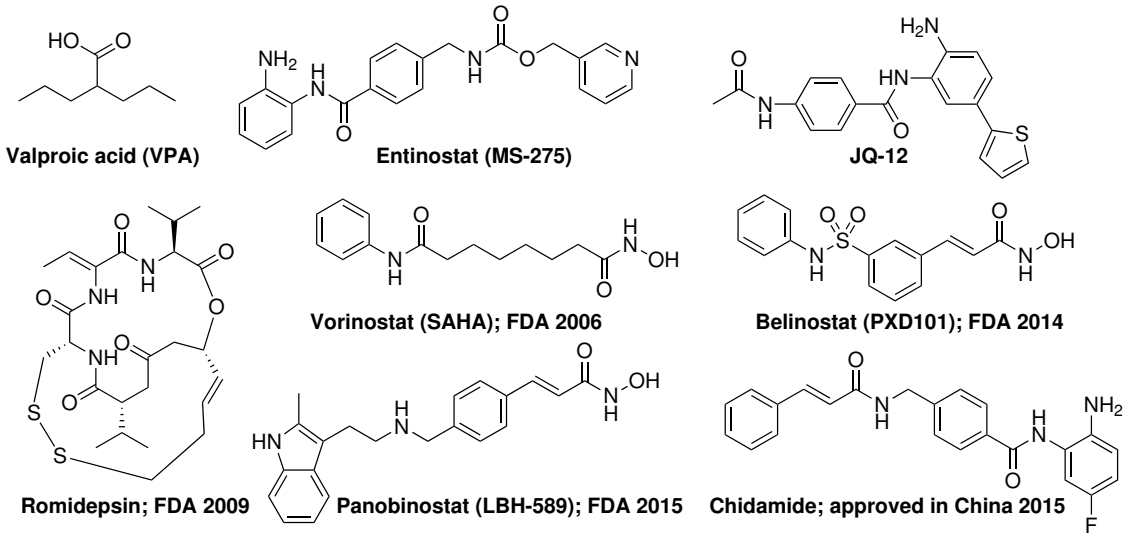

Figure 1.5 Chemical structures of HDAC inhibitors. Small molecule inhibitors are divided into three general classes of HDAC inhibitors. VPA is an example for a short chain fatty acid, MS-275 is an example for the benzimide class of inhibitors and SAHA is an example for a hydroxamic acid. The inhibitor JQ-12 is a research tool used for it's HDAC1/HDAC2 selectivity over other isoforms. VPA is approved for epilepsy and bipolar disorder. Romidepsin, Entinostat, Belinostat, Panobinostat and Chidamide are the five HDAC inhibitors currently approved for specific cancer therapies.

ripheral T cell lymphoma (PTCL)[68, 69]. In 2014 and 2015 two hydroxamic acid-based inhibitors were approved by the FDA. Belinostat was approved for the treatment of PTCL[70] and Panobinostat was approved for the co-treatment of multiple myeloma,[71] which extended the HDAC inhibitor treatable cancer types. The first approved benzamide HDAC inhibitor is Chidamide, which was approved by the Chinese authorities in 2015 for the treatment of relapsed PTCL[72].

Hydroxamic acid- and benzamide-based inhibitors can be described based on a common pharmacophore model. In 1999 crystal structures generated from the HDAC homologue in *Aquifex aeolius* bound to either TSA or SAHA first introduced this model[33]. In general, these inhibitors contain a Zinc chelating group, either the hydroxamic acid or the benzamide group[73]. Other zinc binding groups are possible, but not established. Due to their structure, benzamide-based inhibitors can contain structural elements reaching into a foot pocket of the HDAC enzymes[74]. A second common element of the pharmacophore model is a hydrophobic linker region occupying the narrow tube into the binding pocket[73]. The third part of the model is the surface recognition group, where most of the variability between individual inhibitors is present[73]. In the structure activity relationship (SAR) model of hydroxamic acid and benzamid inhibitors, it is believed that the surface recognition domain is responsible for the class I isoform selectivity profile.

Specifically, VPA shows a two-fold preference over HDAC2 and HDAC3 with IC_{50} values in the millimolar range. The inhibitor JQ-12 preferentially inhibits HDAC1 over HDAC2 in the nanomolar range. A 20-fold difference separates the IC_{50} value for HDAC2 from the one for HDAC3. The other six inhibitors have IC_{50} values in the nanomolar range. Among those the inhibitor LBH-589 is the strongest inhibitor with low nanomolar IC_{50} values for HDAC1, HDAC2

Table 1.1 All approved HDAC inhibitors show selectivity for HDAC1 over HDAC2. HDAC class I *in vitro* IC_{50} values of inhibitors. Chemical structures of inhibitors are shown in figure 1.5. IC_{50} values were collected from the stated studies. (n.a. = not available)

***in vitro* IC_{50} in nM**	**HDAC1**	**HDAC2**	**HDAC3**	**HDAC8**	**source**
Valproic acid (VPA)	1.584.000	3.068.000	3.071.000	7.442.000	[75]
JQ-12	9,2	77,2	1856	>4000	[76]
Entinostat (MS-275)	181	1155	2311	>10.000	[75]
Vorinostat (SAHA)	68	164	48	1524	[75]
Romidepsin (FK228)	36	47	n.a.	n.a.	[77]
Belinostat	41	125	30	216	[75]
Panobinostat (LBH-589)	3	3	4	248	[75]
Chidamide	95	160	67	733	[78]

and HDAC3.

All inhibitors, except LBH-589, show a preference for HDAC1 over HDAC2 with lower IC_{50} values on HDAC1. Most of the presented inhibitors inhibit HDAC3 in addition to HDAC1 and HDAC2. MS-275 shows a two-fold preference for HDAC2 over HDAC3, and JQ-12 is the only inhibitor with a 20-fold preference for HDAC2 over HDAC3. The 20-fold difference in HDAC2 IC_{50} values compared to HDAC3 IC_{50} values makes this inhibitor a valuable research tool to investigate effects on HDAC1 and HDAC2, which do not arise from HDAC3 inhibition. It also becomes clear that no state-of-the-art inhibitor is so far able to achieve a preferential inhibition of HDAC2 when compared with HDAC1. Hence, multiple isoforms are inhibited by all inhibitors. Effects caused by HDAC inhibition can therefore neither be attributed to HDAC1 nor HDAC2 and in most cases the HDAC3 inhibition could also be responsible.

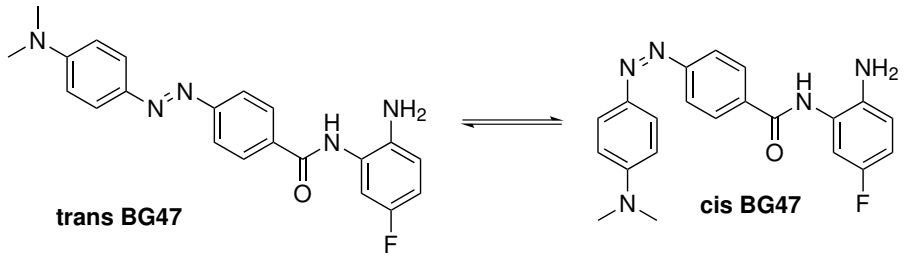

Figure 1.6 Chemical structures of a light switchable HDAC inhibitor. Through blue light exposure, the molecule BG-47 presented by Reis *et al.* switches its azo-group conformation from the relaxed E-state (trans) to a Z-state (cis) effectively deactivating the enzyme[79]. By using the different on and off-rates between HDAC1 and HDAC2, Reis *et al.* plan to expose the HDAC inhibitor to light pulses that activate the inhibitor in a way that can differentiate between HDAC1 and HDAC2.

The rational design of small molecules based on SAR seems to be limited in distinguishing HDAC1 and HDAC2, since both isoforms have 95% similarity within the catalytic binding domains[49]. To circumvent this limit Wagner *et al.* turned to a difference between k_{on} and

k_{off} values in order to achieve a differential target engagement *in vivo*[49, 80]. While the affinity of the molecules designed by structure kinetic relationship (SKR) still remained preferential in their affinity for HDAC1, a faster k_{on} and slower k_{off} for HDAC2 compared to HDAC1 lead to a higher exposure (area under a concentration over time curve) of the inhibitor on HDAC2[80].

To further utilize the kinetic differences, Reis *et al.* developed the molecule, which inhibits HDAC1, HDAC2 and HDAC3 (see fig. 1.6)[79]. Light irradiation switched the central azo group from the active trans conformation to the inactive cis-conformation[79]. Fast thermal relaxation reverts the azo-group to the trans-conformation[79]. Through the modulation of light irradiation frequencies a temporal control of active HDAC inhibitor may be possible, which could use the faster k_{on} values of an inhibitor on HDAC2 over HDAC1 to achieve selectivity.

While independent isoform selectivity has not yet been reached for HDAC inhibitors, the effects of inhibitor treatment nonetheless give an overview of the functions of this enzyme family and certain isoforms of it. The next section describes effects of HDACi treatment.

Effects of HDAC Inhibitors

There are multiple effects that were observed when treating cells or animals with HDAC inhibitors. One of the very first observations was the induction of cancer cell differentiation. Increases in senescence and apoptosis were observed as well as cell cycle arrests in different phases. More recently, an induction of autophagy as well as an increase of tumor immunogenicity were observed upon treatment with various HDAC inhibitors. These effect categories are described in more detail in the following sections.

Senescence

HDAC inhibitor treated cells were observed to enter senescence, with increased expression of $p21^{Cip1/WAF1}$ [82] or independent from $p21^{Cip1/WAF1}$ and p53[83]. Senescence was observed by an increase of a staining of the marker senescence-associated β-Galactosidase (SA-βGal) upon sodium butyrate inhibition[82]. On a molecular level, miRNAs were shown to down-regulate polycomb repressor proteins (senescence inhibitors) BMI1[84] and EZH2 expression[84, 85].

Cell Cycle Arrest

A second field of effects induced by HDAC inhibitors are cell cycle alterations. Upon HDAC inhibitor treatment cells either arrest in G1 or G2/M. Mechanistically it is the current understanding that cell cycle changes are caused by transcription changes of cell cycle regulator genes[52]. The arrest in G2/M phase upon HDACi treatment appears to be independent from DNA damage and is thought to be caused by decreased levels of cycline A and cycline B1[86]. The arrest at the G1/S phase transition checkpoint is thought to arise through increased transcription from the CDKN1A gene[52, 87], which encodes the protein $p21^{Cip1/WAF1}$.

It has been shown in many experiments that $p21^{Cip1/WAF1}$ expression is controlled by HDAC1

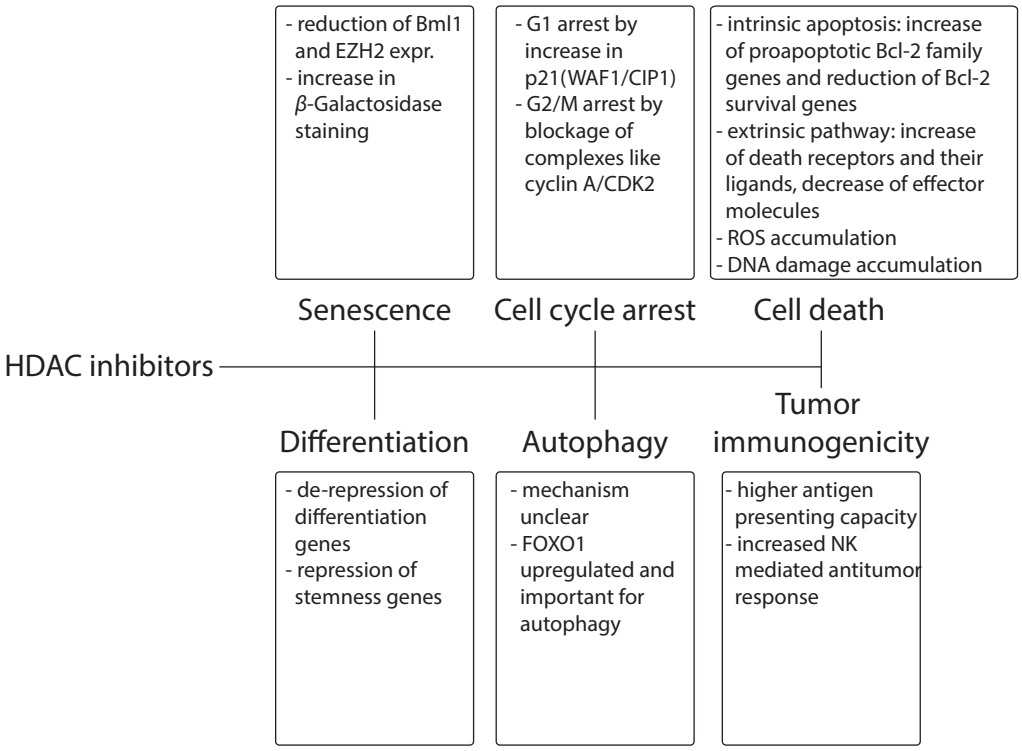

Figure 1.7 Mechanisms of HDAC inhibitor effects in cancer cells. HDAC inhibitors have shown increases in apoptosis, cell cycle arrests and senescence. They induced differentiation and autophagy as well as increasing tumor immunogenicity (figure adapted from [81]).

and HDAC2. A HDAC2 knockdown in HeLa cells caused increased p21 protein levels [22] and HDAC1 deletion in mouse embryonic stem cells leads to an increase in $p21^{Cip1/WAF1}$ mRNA levels, which is reversible by exogenous HDAC1 expression[88]. A strong up-regulation of $p21^{Cip1/WAF1}$ and a weaker up-regulation of p57 were found upon down-regulation of HDAC1 and HDAC2 together[89]. ChIP experiments demonstrated that both HDAC1 and HDAC2 bind to the promoter regions of $p21^{Cip1/WAF1}$ and p53[89]. The binding of HDAC2 to the promoter region of p53 was verified independently[90]. Increased p53 acetylation and lower $p21^{Cip1/WAF1}$ mRNA levels were observed by Li *et al.* in H1299 cells upon HDAC2 stabilization[91]. The p53-HDAC2 interaction was also observed by Brandl *et al.* [92] and HDAC2 up-regulation increases the phosphorylation at Ser-46 of p53[90]. Taken together, this suggests that HDAC1 and HDAC2 directly repress the expression of $p21^{Cip1/WAF1}$ and p53[89].

There is evidence that p21 down-regulation by high HDAC1/2 expression in cancer cells can be reverted by HDAC inhibitor treatment. Increased $p21^{Cip1/WAF1}$ levels upon inhibition by SAHA or Romidepsin in HepG2 and Huh7 cells was observed by Zhou *et al.*[93]. In general $p21^{Cip1/WAF1}$ was one of the first HDAC inhibitor target genes identified[52, 81, 87]. Genetically changing the HDAC1 or HDAC2 expression state by knockdown or knockout further validates that $p21^{Cip1/WAF1}$ is a target gene of these two isoforms. Lagger *et al.* showed a $p21^{Cip1/WAF1}$ and $p27^{Kip1}$ increase in HDAC1 deficient stem cells,[54] which Drazic *et al.* confirmed by depleting HDAC1 in stem cells and observing an increase of $p21^{Cip1/WAF1}$ and $p27^{Kip1}$[94].

Cell Death

Cell death is a well studied phenomenon in pre-clinical tumor models. One mechanism for HDACi induced cell death is through the intrinsic apoptosis pathway, which is accompanied by a coordinated up- and down-regulation of Bcl-2 family genes like Bim, Bid, Bmf, Noxa and Puma[95, 96, 97, 98, 99]. There is experimental evidence that HDACi treatment causes histone hyperacetylation for some of these genes[100, 101, 102], supporting the hypothesis of a direct connection. Additionally or independently Bcl-2 family gene expression may also be altered through HDACi mediated transcription factors like E2F1,[103] FoxO1,[104] p53[105] or Sp1[106]. A second mechanism through which HDAC inhibitors facilitate cell death is the extrinsic apoptosis pathway. An increase in expression of death receptors and a decrease of c-FLIP protein expression make cancer cells more prone to death inducing signals[107, 108]. The accumulation of reactive oxygen species (ROS) in some cases of HDAC inhibitor treatment is a third mechanism, which can lead to cell death[109]. In general ROS accumulation can lead to desoxyribonucleic acid (DNA) damage[110]. A fourth mechanism that leads to cell death in HDACi treated cancer cells is the accumulation of DNA damage. This can happen through ROS accumulation or by down-regulation of DNA repair proteins[111].

Differentiation

Another mode of action of HDAC inhibitors is by inducing differentiation. The very first finding of anti-cancer activity by an HDAC inhibitor was its effect on inducing differentiation[60]. The induction of differentiation by HDACi has been shown for primary sarcoma cell lines[112] as well as liver[113] and breast cancer cell lines[114]. More recently, the induction of myeloid differentiation was discovered together with the de-repression of promyeloid differentiation genes[115]. HDAC inhibitors may also be utilized to induce differentiation and apoptosis in cancer stem cells/leukemia stem cells[116, 117, 118].

Autophagy

An HDAC inhibitor treatment response is the induction of autophagy[119, 120, 121]. This was observed for SAHA treatment in MCF-7 breast cancer cells[121] as well as for butyrate and SAHA in mouse embryonic fibroblasts[120]. The presence of studies showing a reduction of autophagy by HDAC inhibitor treatment questions if this mechanism plays a role in mediating the therapeutic effect[122, 123, 124].

Tumor Immunogenicity

HDAC inhibitors were shown to influence tumor immunogenicity. Treatment with Romidepsin (FK228) promoted immune cell mediated tumor destruction in murine melanoma through an increase in tumor antigens[125]. Cancer recognition and destruction by the immune system could happen through an increase in the expression of MHC I and MHC II associated antigen-processing machinery by HDAC inhibition[126, 127, 128]. In addition, HDAC inhibitor treatment leads to an increase in natural killer cells and an induction of activating ligands[129, 130]. E.g. VPA treatment upregulates NKG2D ligand expression, which enhances the recognition by natural killer cells[131].

Additional Applications of HDAC Inhibitors

With many approved small molecules for the treatment of cancer, HDAC inhibitors are an established field, which has proven benefits in cancer treatment. Currently cancer treatment with HDAC inhibitors is limited to very specific cancer types, e.g. lymphomas. For these types of cancer, HDAC inhibitors are approved for treatment after two previous unsuccessful systemic treatments. The research into the efficiency of these drugs in other types of cancer is ongoing as well as research and clinical trials investigating the combination of HDAC inhibitor treatment with other anti-cancer agents (reviewed in [53]).

Quite differently from cancer treatment, there is research into treating HIV positive patients with HDAC inhibitors. The HDAC inhibitor VPA has been shown to increase HIV production in patients[132]. In 2004, VPA was found to induce acetylation at the HIV proviral promoter[133]. These findings lead to the hypothesis that HDAC inhibitors stimulate HIV production in latent cells. HIV latency is a problem for existing treatments, since infected cells which do not produce virus are very hard to target by treatment. Potentially, the disruption of HIV latency might help in completely eradicating the virus in patients. In 2014 Barton *et al.* used shRNA to narrow down individual isoforms which are responsible for reactivating HIV virus production. Mostly HDAC3 seemed important for the effect, with some influence of HDAC2[134]. This sparked the development of HDAC3 targeted HDAC inhibitors tackling HIV latency[135].

Another well established field of application of HDAC inhibitors are neurodegenerative diseases. In 2009 epigenetic dysregulation in cognitive disorder was already known (reviewed in [136]), when Guan *et al.* showed that HDAC2 is specifically responsible for a negative regulation of memory formation[57]. This HDAC1/2 differential observation gives an additional rationale for the development of HDAC2 selective inhibitors. The potential of existing HDAC inhibitors for the treatment of neurodegenerative diseases is reviewed in [137].

Measuring HDAC Activity

For the development of HDAC inhibitors it is important to measure HDAC activity and how it is influenced by inhibitors. There is an *in vitro* assay, with which the activity of HDACi against certain HDAC isoforms can be measured. This assay is based on a short peptide with lysine, which is coupled to a fluorescent dye. The lysine residue next to the dye is acetylated and while the dye is coupled to the peptide, it does not show fluorescence (fig. 1.8).

The first step is the deacetylation of the synthetic peptide by a HDAC with or without HDACi. The presence of a single HDAC isoform generates the selectivity of the assay. Only after deacetylation by HDAC in the first step, the peptide can be cleaved by trypsin in a second step, which liberates the fluorescent dye. The presence of a high concentration of the HDACi TSA in the second step completely inhibits HDAC activity of every isoform used. Measuring the fluorescence of multiple concentration points HDACi in the first step for a single inhibitor enables the calculation of the IC_{50} value of the inhibition. In the assay only one HDAC isoform is present, which makes it possible to determine selective IC_{50}s for the different isoforms.

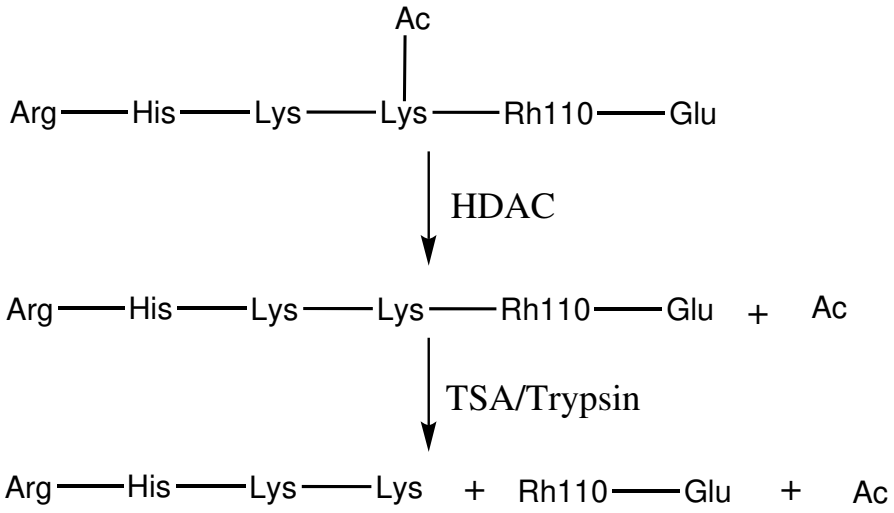

Figure 1.8 Chemical reactions in the HDAC *in vitro* assay. The deacetylation in the first step is followed by cleavage of the synthetic substrate while inhibiting the HDAC with the broad-spectrum inhibitor TSA. Cleavage by Trypsin is only possible after deacetylation.

With the same principle, but slightly varying substrates, this assay is commercially available and widely used. While dyes and peptides may vary most commercial kits are based on this principle.

Limitations of HDAC Inhibitor Development

Inhibition of HDACs has emerged as an important therapeutic strategy in the treatment of malignancies and currently HDAC inhibitors are approved for limited haematological malignancies, but not in solid tumors[138]. HDAC inhibitors are associated with a range of serious class specific adverse effects, in particular myelosuppression and cardiotoxicity as well as gastrointestinal and hepatic effects[138]. Myelosupression is a decrease of the production of immune cells, which was observed in treated patients. In the heart HDAC inhibitors have been observed to prolong QT intervals, which is a measure for the electrical properties of the heart in the electrocardiogram. In the presence of risk factors, the prolongation can be lethal. Gastrointestinal adverse effects of HDACi include nausea, vomiting and diarrhea. Hepatic adverse effects manifest by increased serum levels of transaminases indicating an increase of dead hepatic cells. Each individual inhibitor may additionally show varying agent specific adverse effects. This reassures the need for more selective inhibitors that may reduce class specific side effects. Moreover, for the treatment of cognitive disorders, only HDAC2 and not HDAC1 needs to be inhibited[139], which currently no inhibitor achieves.

While the need for isoforms selective molecules is clear, the selectivity can so far only be measured in *in-vitro* assays. Currently target engagement can be simulated by measuring k_{on} and k_{off} *in-vitro* and extrapolating this data[49, 80]. As the treatment happens in patients where all isoforms are present in parallel and where isoforms HDAC1 and HDAC2 are components of multi-protein complexes, *in-vivo* represents the most relevant environment for patient treatment.

1.5. Objective

With the overarching goal of reducing side effects of HDAC inhibitor based cancer medications as well as making new therapies for other diseases possible, we aimed to enable selective inhibitor development.

In order to improve the selectivity of an inhibitor, the effect on the targeted isoforms needs to be quantified. The objective of this work was to differentiate between the potency of small molecules to inhibit HDAC1 and HDAC2 in cells. Therefore, the following research questions were attempted:

1. Can the individual expression of either HDAC1 or HDAC2 be controlled without triggering compensation of the other isoform's expression from the endogenous gene?
2. Are there individual biomarkers for the activity of HDAC1 and HDAC2?
3. Can we establish an isoform selective *in-vivo* assay to measure HDAC inhibition?

2. Material and Methods

2.1. Material

Table 2.1 Complete list of materials

Material	**Manufacturer**	**Ordering number**
Cell culture		
McCoys Modified Eagle Medium	Sigma	M8403
DMEM	Sigma	D5796
Optimem	Gibco	51985-026
PBS-buffer	Gibco	15326-239
Trypsin-EDTA (0.05%)	Gibco	25300-054
FBS superior	Biochrom	S0615
Penicillin-streptomycin (10000 U/mL)	Gibco	15140-122
Fungizone	ThermoFisher	15290-026
Cell strainer	ThermoFisher	08-771-23
l L-Glutamine 200 mM	Gibco	25030-024
Doxicycline hyclate	Sigma	D9891
FuGENE HD transfection reagent	Promega	E2311
Puromycin dihydrochloride	Sigma	P9620
DMSO	Carl Roth	A994
Cloning		
LB-medium	Carl Roth	X964

Continued on next page

Table 2.1 – *Continued from previous page*

LB-agar	Carl Roth	X965
$MgCl_2$	Th. Geyer	63065
$CaCl_2$	VWR	103464
Glucose	Sigma	G7528
Potassiumacetate	VWR	BDH9254
HEPES	Sigma	H3375
Magnesiumacetate	Fluka	63051
DNA gel loading dye (6x)	ThermoFisher	R0611
Pfu DNA-polymerase	ThermoFisher	EP0501
DeepVent DNA-polymerase	NEB	M0258S
Taq DNA-polymerase	Quiagen	201203
Herculase II	Agilent	600675
MluI	NEB	R0198
ClaI	NEB	R0197
PmeI	NEB	R0560
SpeI	NEB	R0133
Agarose	Roth	2267
TAE buffer (50×)	AppliChem	A1691
SV gel and PCR clean-up system	Promega	A9282
T4 DNA ligase	Thermo	EL0014
Stbl3 *E. coli*	ThermoFisher	C737303
Ampicillin	Merck	171254

Continued on next page

Table 2.1 – *Continued from previous page*

Roti-Phenol/Chloroform	Roth	A156.1
GeneJET plasmid miniprep kit	ThermoFisher	K0503
GeneJET plasmid maxiprep kit	ThermoFisher	K0492
Qiagen plasmid maxi kit	Qiagen	12163
Isopropanole	Merck	109634
Molecular Biology		
Proteinase K	Invitrogen	25530
RNAse A	ThermoFisher	EN0531
Formaldehyde solution	Sigma	47608
Triton X-100	Sigma	T8787
Hoechst 33342	ThermoFisher	H3570
Poly-D-lysine	Sigma	P6407
Biochemistry		
High Pure RNA Isolation Kit	Roche	11828665001
Random hexamer primer	ThermoFisher	10580091
dNTPs	ThermoFisher	R1441
96 well qPCR plate	4titude	4ti-0952
AMV reverse transcriptase	NEB	M0277
Power SYBR green master mix	Applied Biosystems	4367659
Tris	AppliChem	A2264
NaCl	Sigma	S3014
Tween 20	Sigma	P1379

Continued on next page

Table 2.1 – *Continued from previous page*

Glycerol	Sigma	G5516
SDS	Sigma	74255
DTT	Carl Roth	6908
Rotiphorese 10 × SDS-PAGE	Carl Roth	3060
APS	VWR	BDH9214
skim milk power	Sigma	70116
BSA	Roth	T844
BSA conc. standard	ThermoFisher	23208
Comassie Brilliant Blue	VWR	200005
Acetic Acid	Merck	100063
Methanol	Merck	106009
Ethanol	Merck	100983
Ethylenediamine tetraacetic acid	Serva	11280
NP-40	Calbiochem	492016
SAHA	Cayman Chemicals	10009929
Nicotinamide	Merck	481907
Urea	Carl Roth	7638
Trifluoracetic acid (TFA)	Applichem	163317
HPLC grade acetonitrile	Carl Roth	8225
HPLC grade water	VWR	23595
4-Methylmorpholine	Sigma	67870
Hydroxylamide	Sigma	467804

Continued on next page

Table 2.1 – *Continued from previous page*

Acetyl lysine antibody	ImmuneChem	ICP0388
Biotin antibody	ImmuneChem	ICP0615
PTMScan Acetyl-Lysine Motif	Cell Signaling	13416
MOPS	Roth	6979
Acetic acid	Merck	100066
ZipTips	Merck	ZTC18S096
TMTsixplex Isobaric Label Reagent Set	ThermoFisher	90066
Potassiumcarbonate, anhydrous	Sigma	60108
0.22 µm filter	Merck	SLGP033RS
0.45 µm filter	Merck	SLHP033RS
C18 SepPack	Waters	WAT 054955
30 kDa MWCO filter	Pall	OD030C34
10 kDa MWCO filter	Pall	OD010C34
mini-PROTEAN Tetra Cell system	Bio-Rad	1658001
semi-dry electrophoretic transfer cell	Bio-Rad	1703940
TEMED	AppliChem	A1148
Rotiphorese Acrylamid (30%)	Roth	3029
Pierce 660nm Protein Assay Reagent	LifeTechnologies	22660
Ionic Detergent Compatibility Reagent	LifeTechnologies	22663
Precision Plus Protein Standard	Bio-Rad	161-0374
PVDF-membrane, 0.45 µm pore size	Roth	T830.1
Kit ECL prime det. reagent	VWR	RPN2232P

Buffer and Media

Table 2.2 Composition of self-made buffers, media and solutions

Buffer / Medium	**Contents**
Cell culture	
McCoys Modified Eagle Medium	supp.: 10% (v/v) FCS supp.: 1:100 Pen/Strep supp.: 1:100 L-Glutamin
DMEM	supp.: 10% (v/v) FCS supp.: 1:100 Pen/Strep
Cloning	
SOC-medium	LB-medium 0.5% (v/v) $MgCl_2$ (1.0 M) 1.0% (v/v) glucose (2.0 M)
Annealing-buffer (pH 7.4)	100 mM potassiumacetate 30 mM HEPES 2 mM magnesiumacetate
Molecular Biology	
TELysis buffer pH 8.0	10 mM Tris 1 mM EDTA 50 mM KCl 2 mM $MgCl_2$ 200 $\frac{\mu g}{mL}$ RNase A heat inactivated: 15 min, 95°C

Continued on next page

Table 2.2 – *Continued from previous page*

Proteinase K solution pH 8.0	10 mM Tris 1 mM EDTA 100 mg proteinase K per 5 mL
Biochemistry	
TBS-T (1×, pH 7.5)	20 mM Tris-HCl 150 mM NaCl 0.1% (v/v) Tween 20
Lämmli-buffer[140]	63 mM Tris-HCl 10% (w/v) glycerol 2% (w/v) SDS 2.5% (w/v) dithiothreitol
Transfer buffer	1× Rotiphorese SDS-PAGE buffer 20% methanol
Stacking gel buffer (pH 6.8)	0.5 M Tris
Separation gel buffer (pH 8.8)	3.0 M Tris
APS-solution	10% (w/v) APS
Lysis-buffer	20 mM Tris pH 7.5 3 mM EDTA 1% NP40 5 µM SAHA 10 mM Nicotinamide

Continued on next page

Table 2.2 – *Continued from previous page*

4x NaCl containing lysis-buffer	1.2 M NaCl 20 mM Tris pH 7.5 3 mM EDTA 1% NP40 5 µM SAHA 10 mM Nicotinamide
Urea buffer	20 mM HEPES pH 8.0 9 M Urea 4.5 mM DTT 5 µM SAHA 10 mM Nicotinamide
HEPES buffer	20 mM HEPES pH 8.0 5 µM SAHA 10 mM Nicotinamide
Solvent A	0.1% TFA
Wash solvent	0.1% TFA 5% Acetonitrile
Solvent B	0.1% TFA 40% Acetonitrile
Labeling buffer	10 mM 4-Methylmorpholine pH 8.0
Hydroxyamine	5% (v/v) solution in water

Continued on next page

Table 2.2 – *Continued from previous page*

IP buffer	provided with the AB
Solvent C	0.1% TFA 50% Acetonitrile
Solvent D	0.1% TFA
Solvent E	0.1% TFA 40% Acetonitrile

Antibodies

Table 2.3 Antibodies used throughout this study.

Target	**clone**	**ProductNo**	**Manufacturer**
HRP-linked horse anti-mouse		7076	Cell Signaling
HRP-linked goat anti-rabbit		7074	Cell Signaling
HRP-linked polyclonal rabbit anti-goat		sc-2768	SCB
Cy3-linked polyclonal goat anti-rabbit		111-225-144	Jackson Immuno
Cy2-linked polyclonal goat anti-mouse		115-225-003	Jackson Immuno
mouse monoclonal anti-HDAC1	10E2	sc-81598	SCB
mouse monoclonal anti-HDAC2	3F3	sc-81599	SCB
rabbit polyclonal anti-HDAC3	H-99	sc-11417	SCB
rabbit polyclonal anti-HDAC8	H-145	sc-11405	SCB
rabbit monoclonal anti-GAPDH	14C10	2118	Cell Signaling
rabbit monoclonal anti-beta-actin	13E5	4970	Cell Signaling
rabbit polyclonal anti-Ac-K		9441	Cell Signaling

Continued on next page

Table 2.3 – *Continued from previous page*

rabbit monoclonal anti-H3 Ac-K9	C5B11	9649	Cell Signaling
rabbit polyclonal anti-H4 Ac-K05		9672	Cell Signaling
rabbit polyclonal anti-H4 Ac-K08		2594	Cell Signaling
rabbit polyclonal anti-H4 Ac-K12		2591	Cell Signaling
rabbit polyclonal anti-H4 Ac-K16		8804	Cell Signaling
rabbit polyclonal anti-H2A Ac-K5		2576	Cell Signaling
rabbit polyclonal anti-H2B Ac-K5		2574	Cell Signaling
rabbit monoclonal anti-H2B Ac-K20	EPR859	ab177430	Abcam
rabbit polyclonal anti-H3 Ac-K18		07-354	Merck Millipore
rabbit monoclonal anti-histone H3	D1H2	4499P	Cell Signaling
rabbit polyclonal anti-histone H4		2592	Cell Signaling
rabbit polyclonal anti-Ac-H3		06-599	Merck Millipore
rabbit polyclonal anti-Ac-H4		06-598	Merck Millipore
rabbit monoclonal anti-p21 (Cip/waf)	12D1	2947	Cell Signaling
rabbit polyclonal anti-p27 (Kip1)		2552	Cell Signaling
goat polyclonal anti-p57 (kip2)	M-20	sc-1039	SCB
rabbit polyclonal anti-Matrin 3		A300-591A-T	Bethyl Labs
mouse monoclonal anti-HSP70/HSC70	N27F3-4	ADI-SPA-820	Enzo
rabbit polyclonal anti-c-myc		9402	Cell Signaling
mouse monoclonal anti-ubiquitin	P4D1	3936	Cell Signaling

Primer

Table 2.4 Synthesized DNA oligonucleotides and primer pairs used in experiments.

ID	Target	Direction	Sequence
Cloning primer for the pLVTHM vector			
1	HDAC1 PmeI-site	forward	AAAGTTTAAACGCCACCATGGCGCAGACGCAGGGC
1	HDAC1 SpeI-site	reverse	AAAACTAGTTCAGGCCAACTTGACCTCC
2	HDAC2 PmeI-site	forward	AAAGTTTAAACGCCACCATGGCGTACAGTCAAGGAGG
2	HDAC2 SpeI-site	reverse	AAAACTAGTTCAGGGGTTGCTGAGCTGT
sgRNA oligonucleotides for cloning with the pX458 vector			
3	HDAC1 Intron1	forward	CACCGACAGTTAGGCATACACTACC
3	HDAC1 Intron1	reverse	AAACGGTAGTGTATGCCTAACTGTC
4	HDAC1 Intron2	forward	CACCGTCTTGCCATGTTGACCCGGA
4	HDAC1 Intron2	reverse	AAACTCCGGGTCAACATGGCAAGAC
5	HDAC2 Intron1	forward	CACCGTCCATATTAAAGCCCATCA
5	HDAC2 Intron1	reverse	AAACTGATGGGCTTTAATATGGAC
6	HDAC2 Intron2	forward	CACCGAAATTGAGCTCTTCGGAACA
6	HDAC2 Intron2	reverse	AAACTGTTCCGAAGAGCTCAATTTC
Sequencing primer			
7	EF1a	forward	TCAAGCCTCAGACAGTGGTTC
8	GFP	reverse	ACCACCCCGGTGAACAGC
9	HDAC1	forward	GTACCACAGCGATGACTACA
10	HDAC1	forward	TTCAAGCCGGTCATGTCCAA
11	HDAC1	forward	CTCGATCTGCTCCTCTGAC

Continued on next page

Table 2.4 – *Continued from previous page*

12	HDAC1	reverse	CTTCGTCCTCATCGCCACT
13	HDAC1	reverse	GGCCTCATAGGACTCGTCA
14	HDAC1	reverse	TGGACGGATGGAGCGCAAG
15	HDAC2	forward	CTACGGTCAATAAGACCAGAT
16	HDAC2	forward	ATGATGAGTCATATGGGCAGA
17	HDAC2	forward	AGCATCAGACAAGCGGATAG
18	HDAC2	reverse	TATCCGCTTGTCTGATGCTC
19	HDAC2	reverse	GCCCATATGACTCATCATCTA
20	HDAC2	reverse	TGTCATTTCTTCGGCAGTGG
PCR primer			
21	HDAC1 k.o. test	forward	GGAGGTGAATTGTGGCTTCT
21	HDAC1 k.o. test	reverse	CAATCACGGCTCACTGTAAC
22	HDAC2 k.o. test	forward	CAGCAGACACCACCATCTAT
22	HDAC2 k.o. test	reverse	CAAATCCATATGTTCATAAACTC
23	HDAC1 k.o. test	forward	GTGGCAGGTAGTGTGAATTG
23	HDAC1 k.o. test	reverse	CAGGCCAGGATACCAGCTAA
24	HDAC2 k.o. test	forward	GTGATATTGGAAATTATTATTATG
24	HDAC2 k.o. test	reverse	ATATATTTCCATTTTTCTGTATAAG

Table 2.5 qPCR DNA primer pairs.

ID	Target	Direction	Sequence	amplicon size
25	PTGS2	forward	GCTTTATGCTGAAGCCCTATGA	70
25	PTGS2	reverse	TCCAACTCTGCAGACATTTCC	
26	DUSP10	forward	TGAATGTGCGAGTCCATAGC	92
26	DUSP10	reverse	TGGCAATTCAAGAAGAACTCAA	
27	EGR1	forward	AGCCCTACGAGCACCTGAC	92
27	EGR1	reverse	GGTTTGGCTGGGGTAACTG	
28	SNTB1	forward	ATTTTGGAGGCAAAGATGGA	88
28	SNTB1	reverse	GCTGACAGGAAGGAATGAATG	
29	SCNN1A	forward	TGTGACTACAGAAAGCACAGTTCC	76
29	SCNN1A	reverse	CCAGGTGGTCTGAGGAGAAGT	
30	SERPINF1	forward	GTGTGGAGCTGCAGCGTAT	66
30	SERPINF1	reverse	TCCAATGCAGAGGAGTAGCA	
31	GAPDH	forward	ACGGGAAGCTTGTCATCAAT	78
31	GAPDH	reverse	CATCGCCCCACTTGATTTT	
32	ATF3	forward	GGAGCCTGGAGCAAAATG	96
32	ATF3	reverse	AAAGGGCGTCAGGTTAGCA	
33	RPL27	forward	TCGCCAAGAGATCAAAGATAA	121
33	RPL27	reverse	CTGAAGACATCCTTATTGACG	
34	ANKRD1	forward	CAAGAACTGTGCTGGGAAGA	85
34	ANKRD1	reverse	TCTCTCTGAGGCTGTCGAATA	

Continued on next page

Table 2.5 – *Continued from previous page*

35	TAGLN	forward	TGCAGAGGACCCTGATGG	103
35	TAGLN	reverse	TTATGCTCCTGCGCTTTCTT	
36	PRF1	forward	CACTCACAGGCAGCCAACT	111
36	PRF1	reverse	GGGAGTGTGTACCACATGGA	
37	SEMA3A	forward	TGAAATTGGACATCATCCTGAG	65
37	SEMA3A	reverse	GGCCGTTTTCAAAATGTGAG	
38	S100A14	forward	CTTCTGAGCTACGGGACCTG	73
38	S100A14	reverse	TTCTCTTCCAGGCCACAGTT	
39	MAL2	forward	TCAAATTGATGCTAACTGGAACTT	111
39	MAL2	reverse	AAATCATGCAGGGATGTGG	
40	TGM2	forward	CACCCACACCTACAAATACCC	66
40	TGM2	reverse	TGGTTCGCCCTTGTGAAG	
41	CDKN1A	forward	TCACTGTCTTGTACCCTTGTGC	127
41	CDKN1A	reverse	GGCGTTTGGAGTGGTAGAAA	
42	CDKN1B	forward	TTTGACTTGCATGAAGAGAAGC	84
42	CDKN1B	reverse	AGCTGTCTCTGAAAGGGACATT	
43	HDAC1	forward	CGAATCCGCATGACTCATAA	111
43	HDAC1	reverse	ATCGCTGTGGTACTTGGTCA	
44	HDAC1	forward	ACCCGGAGGAAAGTCTGTTAC	121
44	HDAC1	reverse	CATGTTATCTGGACGGATGGA	
45	HDAC1	forward	TACGACGGGGATGTTGGAAA	100
45	HDAC1	reverse	AGAGACCATAGTTGAGCAGCA	

Continued on next page

Table 2.5 – *Continued from previous page*

46	HDAC1	forward	GACAAGGCCACCCAATGAAG	106
46	HDAC1	reverse	TTGGCTTTGTGAGGGCGATA	
47	HDAC2	forward	TTGTTTCAATCTAACAGTCAAAGGTC	110
47	HDAC2	reverse	CAACATTACGGATTGTGTAGCC	
48	HDAC2	forward	TGCTACTACTACGACGGTGAT	91
48	HDAC2	reverse	GCAAGTTATGGGTCATGCGG	
49	HDAC2	forward	TACGACGAGGCCCCATAAAG	116
49	HDAC2	reverse	TCTGCTTACTATACTCAGACATGT	
50	HDAC1	forward	TACTACGACGCGCCCTCA	120
50	HDAC1	reverse	ATCTGCTTGCTGTACTCCGA	
51	GFP	forward	GAAGCGCGATCACATGGT	62
51	GFP	reverse	CCATGCCGAGAGTGATCC	

Computer software

Table 2.6 Specialized computer software used throughout the study.

specialized software	version	origin
Vector NTI	11.5.3	ThermoFisher
Lightcycler 480	1.5.1.62	Roche
FlowJo	10.5.3	FlowJo LLC
Graphpad Prism	6.01	Graphpad Software
Adobe Illustrator CS6	16.0.3	Adobe
Adobe Photoshop CS6	13.01	Adobe
Integrated Genomics Viewer (IGV)	2.4.18	see [141]
Citavi	6.3.0.0	Swiss academic software
ImageJ	1.52a	Wayne Rasband
Python 3	3.7.1	Python software foundation
Fastq groomer	1.0.4	`https://usegalaxy.org/`
TopHat	2.1.0	`https://usegalaxy.org/`
Cufflinks	2.2.1	`https://usegalaxy.org/`
Cuffmerge	2.2.1	`https://usegalaxy.org/`
Cuffdiff	2.2.1.3	`https://usegalaxy.org/`
MultAlign	online	`http://multalin.toulouse.inra.fr`
InteractiVenn	online	`http://www.interactivenn.net`
Columbus	2.8.0	PerkinElmer

2.2. Methods

Buffers, media and solutions are summarized in table 2.2. If not stated differently, the components were dissolved in pure, deionized water. This water was produced with a Veolia water Purelab Flex 2. The pH had been measured with a Satorius PB-11 electrode and if necessary, the pH-value was adjusted with 2 M sodium hydroxide or 2 M hydrochloric acid. All materials are summarized in table 2.1.

2.2.1. Cell culture

Basic cell lines used in cell culture experiments are summarized in table 2.7. Complete media were prepared as described in table 2.2. In the appendix in table 6.1 on p. 126 the amounts of cells seeded per culture flasks are given for different times, when the cells are supposed to be 80–90% confluent.

Table 2.7 Basic cell lines used in cell culture experiments.

Name	Origin	Tissue	Culture	Medium
HCT 116	ATCC CCL-247	colon	adherent	McCoy's Modified Eagle Medium
Co-115	establishment [142]	colon	adherent	McCoy's Modified Eagle Medium
HEK293T	ATCC CRL-3216	kidney	adherent	DMEM

Cell Passaging and Sub-Cultivation

Before the trypsination of the cells, they were washed with sterile phosphate buffered saline (PBS). Then they were incubated with trypsin for about 3–5 min at 37°C. HT29 cells needed about 5-7 min incubation time to be completely separated from each other. Single cells in trypsin were diluted in a three-fold excess of medium. The number of cells given in table 6.1 in the appendix on page 126 was seeded in a new, sterile culture flask.

Harvesting Cells for WB Analysis

Cells were lysed in Lämmli-buffer without bromophenol blue. The amount of buffer was adjusted to just cover the cells in the well, to ensure a high protein concentration. For full denaturation of the lysate, the samples were heated to 95°C for 2 min. From there on the lysates were always kept on ice and stored at -20°C. Samples were sonicated for seven pulses with 90% intensity with a UP200S sonicator (Hielscher) until the lysate was completely liquid.

Freezing and Defrosting Cells

Cells were passaged as described before. But after stopping the trypsin reaction with medium, the cell suspension was centrifuged (700 g, 7 min, room temperature (RT)), the supernatant was discarded and the cells were resuspended to a density of about one million cells per mL. In cryo-vials 0.9 mL of the cell suspension was mixed with cold freezing-medium (medium with regular supplements and 20% (v/v) DMSO) to a final concentration of 10% (v/v) dimethyl sulfoxide (DMSO). The cells were frozen in Nalgene Cryo 1°C freezing containers

and stored in liquid nitrogen.

For defrosting, the content of the cryo-vial was thawed quickly and mixed with about 20 mL of medium at 37°C to dilute the DMSO. After centrifugation (700 g, 7 min, RT) and removal of the DMSO containing medium, the cells were seeded in fresh medium. The day after the defrosting, cells were washed with PBS and fed with new medium.

Stable HDAC1/HDAC2 Knockout

For each knockout 1-2 million HCT116 cells were seeded on a 10 cm plate one day prior to the transfection. 4 µg of the two vectors containing Cas9 and one sgRNA each were cotransfected with 0.625 µg of the pPGK-puro vector (addgene ID of empty backbone: 35094) encoding a puromycin marker. This corresponded to a molar ratio of 3:3:1. The plasmids had first been mixed with 100 µL of OpiMEM and then 10 µL of Fugene HD transfection reagent was added. After carefully pipetting the mixture up and down and an incubation at RT for 30 min, the mixture was added dropwise to the cells. One day after the transfection 3 $\frac{\mu g}{mL}$ = 6.363 µM puromycin were added to the cells overnight. On the next day, cells were washed with fresh PBS and the remaining cells were allowed to grow until colonies formed. These colonies were picked and transferred to a 96-well plate. When the first wells of the plate reached confluency, the cells were split on three 96-well plates. These plates were grown for 1-3 days. Then two plates were frozen with 10% DMSO containing complete medium to -80°C in a polystyrene box and the third plate was frozen at -80°C without medium and served as polymerase chain reaction (PCR) input material to test the knockout. The verification of the knockouts is described in the methods section part 2.2.3.

Lentivirus Production

To produce lentiviruses for the infection of target cells, 1.0 to 1.5 million HEK293T cells were seeded in a 10 cm dish. The following day, these cells were transfected with 1 µg pMD2G (addgene ID: 12259), 1.5 µg psPAX (addgene ID: 12260) and 2 µg of the plasmid of interest (usually modified pLVTHM, base version addgene ID: 12247). The plasmids had first been mixed with 100 µL of Opimem and then 10 µL of Fugene HD transfection reagent was added. After carefully pipetting the mixture up and down and letting it rest for 30 min, the mixture was added dropwise to the HEK293T cells. Three days after the transfection, the supernatant containing the virus was harvested. To exclude HEK293T cells, the supernatant was filtered with a sterile 45 µm filter.

Lentiviral Transduction

For HCT116 cells, the filtered supernatant was mixed in a 3:1 ratio with the cell culture medium on the target cells. After one day the cells were washed with PBS and new medium is added.

Co-115 cells were transduced by a spin-infection with additional polybrene added to overcome their lower infection rate. After harvesting the supernatant, the target cells are washed with PBS and the supernatant is added as well as polybrene $\left(1:1000, c_{stock} = 8\ \frac{mg}{mL}\right)$. After

centrifugation (60 min, 37°C, 1500 g), the cells were washed with PBS and fresh medium was added.

Induction with Doxicycline

The repressor of the Trono vector systems leaves the Tet operator sequence, when doxicycline is present. A sterile filtered, 1000× stock solution $\left(0.1\ \frac{\text{mg}}{\text{mL}}\right)$ = 195 µM was added to the medium of the cultured cells.

Immunofluorescence

For IF analysis, cells were washed two times with PBS and they were fixed with paraformaldehyde (PFA) (4% in PBS) for 20 min at RT. Afterwards cells were washed two times with PBS and blocked with bovine serum albumin (BSA) (2% in PBS with 0.1% Triton-X) for 1 h at RT. The cells were incubated with the primary antibody / antibodies overnight at 4°C, followed by three PBS washing steps. After a one-hour RT incubation with the secondary antibody / antibodies and washing the cells three times with PBS, the cell's nuclei were counter stained with Hoechst 33342. After this procedure, fluorescence images were collected with an EVOS F1 (life technologies) or an operetta high content imaging system (PerkinElmer).

2.2.2. Cloning

PCR

To prepare the DNA inserts for cloning experiments, a polymerase with proof reading function was used in the PCR. This was either Pfu DNA-polymerase or DeepVent DNA-polymerase. For analytic and long template PCRs Taq polymerase or Herculase II is used.

The template is either cDNA, produced in a reverse transcription, or a previous vector with the gene of interest present. Primers were designed by hand and are summarized in table 2.4. The melting temperature of the primers was calculated according to the formula T_m = 4 × G/C + 2 × A/T and the primers were designed in a way that T_m is between 58–62°C. A standard PCR protocol is shown in table 2.8.

Table 2.8 Standard-PCR reaction

	amount [µL]	**conc. of the parent solution**
Forward primer	1	10 $\frac{\text{pmol}}{\mu\text{L}}$
Reverse primer	1	10 $\frac{\text{pmol}}{\mu\text{L}}$
Template	variable	50–100 ng of vector with template
dNTP-Mix	1	each 10 mM
PCR-buffer	5	10×
H_2O	to 50 µL	
Polymerase	1	

The temperature program consisted of an initial 2 min denaturation step at 95°C followed by a series of three repeated steps. This cycle consisted of a 45 s denaturation step, a 45 s annealing step at 55°C and an extension step at 68°C for the DeepVent-Polymerase or 70°C for the Pfu-Polymerase or 72°C for the Taq-Polymerase and also for the Herculase II. The time of the elongation step depended on the polymerase syntheses speed and the length of the PCR product. For Taq polymerase and Herculase this was about 1000 bp/min and for DeepVent- and Pfu-polmerase the speed is about 500 bp/min. The duration of the elongation step in the cycle was adjusted to match the length of the PCR product. A final single elongation step, which took the same time as in the cycle before, finished the PCR.

Restriction Digest

Digestion of DNA was performed with New England Biolabs enzymes. Analytic digestions were carried out in a 20 µL volume with at least 500 ng of DNA and preparatory digestions were done in 50 µL with a maximum of 2 µg of DNA. The volume of the enzyme solutions stayed below 10% of the total reaction volume. The supplied buffer systems were used and double digest were done, according to the manufacturer's instructions. A preparatory digestion was incubated with 1-2 µL enzyme for 2 h at 37°C and for an analytic digestion between 0.2 and 0.5 µL enzyme was used for 20 min at 37°C. The digestion was controlled through agarose-gelelectrophoresis. The agarose content of the gels was between 0.5% and 2.0% depending on the DNA fragment size. Small fragments needed gels with higher agarose contents. After checking for full digestion, the samples were heated to 70°C to inactivate the restriction enzymes.

Purification and Concentration of DNA

For the purification of PCR samples and the purification of samples from preparatory agarose gels, Wizard SV Gel and PCR Clean-Up System were used according to the manufacturer's instructions. Under high salt concentrations, the DNA bound to a silica-membrane, when other contaminants passed the membrane. After washing, the DNA comes off the membrane under low salt concentrations. The purified DNA was eluted in 20–50 µL water.

DNA Concentration Determination

The concentration of DNA samples was determined with a NanoDrop 2000 (Thermo scientific) using 1.5 µL of the sample.

Ligation of DNA Fragments

Ligation of DNA fragments was done with T4 DNA ligase according to the manufacture's instructions with 50 ng of vector DNA and three to five times as much insert in a molar ratio. The total volume of the reaction was 20 µL and for blunt end ligations polyethylene glycol (PEG) 4000 was added to a final concentration of 5%. The reactions were incubated for 1 h at RT. After the incubation, 10 µL of the reaction were immediately transformed into *E. coli* cells. The rest was stored at -20°C. Differences in RT especially in summer influenced the experiment negatively and, in this case, the samples were cooled to 25°C in a thermo shaker.

Chemical Transformation of Bacteria

Cells of an overnight culture of the *E. coli* strains Stbl3 were seeded 1:100 in a 100 mL culture and cultivated to an optical density of about 0,3. The cells were incubated in pre-cooled 50 mL tubes on ice for 10 min. After sedimentation of the cells (10 min, 4°C, 4000 g) the pellet was resuspended in 10 mL 0.1 M $CaCl_2$ at 4°C. After a second centrifugation under the same conditions, the cells were resuspended in 2 mL of cold medium and stored on ice until the transformation (min. 3 h, max. 24 h). Cells not used in this time period were mixed with glycerol to a final concentration of 25%, separated into 200 µL aliquots and stored at -80°C.

Each defrosted aliquot of cells was carefully mixed with the DNA that is supposed to be transformed and the cells were incubated for at least 30 min on ice. This incubation was followed by a heat shock of 42°C for 90 s and an immediate cooling to 4°C for 2 min. After addition of 0.5 mL SOC medium, the cells were incubated at 37°C for 45 min under gentle shaking and plated on selective agar plates (containing 125 $\frac{\mu g}{mL}$ ampicillin). To grow clonal cultures, the plates were incubated over night at 37°C.

Microplasmid-Preparation

Overnight cultures of *Escherichia coli* (*E. coli*) cells had been analyzed before the plasmids were extracted from the culture. Due to the small experimental effort, a lot of clones were analyzed in a short time. This method was able to find differences between an empty vector and a vector with insert, but the change in size had to be substantial.

100 µL of an overnight culture were transferred to a 1.5 mL eppendorf tube and mixed with 50 µL phenol/chloroform and 10 µL DNA loading buffer. This mixture was vortexed for 10 s and after centrifugation (3 min, RT, 18000 g), 25 µL of the supernatant were loaded onto a 1% agarose gel. After running the gel with 125 V for 20–25 min, with a negative and a positive control, positive clones were identified with good accuracy.

Plasmid Preparation

For analytic purposes plasmids were extracted from overnight cultures with the GeneJET plasmid miniprep kit. 3 mL of the overnight culture were treated as stated in the manufacturer's instructions. The elution was carried out in 50 µL water.

For preparative studies, *E. coli* cells from a 4 mL overnight culture were seeded 1:1000 in a 125 mL overnight culture from which the plasmids are extracted with the GeneJET plasmid maxiprep kit or the Qiagen plasmid maxi kit. Here as well, the elution was carried out in water, with the minimum amount indicated in the instructions.

Isopropane/Ethanol Precipitation

Before the precipitation a 100 mM NaCl concentration had been adjusted in the sample, then the DNA was precipitated with two-fold volume excess of pure isopropanol. After centrifugation (10 min, RT, 18000 g) the supernatant was removed and the sample was redissolved in

0.5 mL of 70% ethanol. After another centrifugation (10 min, RT, 18000 g), the supernatant was removed again and 20 µL of pure ethanol were put on the DNA pellet. After the evaporation and drying of the pellet, it was redissolved in water and an EDTA concentration of 0.1 mM was adjusted (stock solution: 0.1 M, pH 8.0). The ethylenediaminetetraacetic acid (EDTA) complexes bivalent cations, which inhibits restriction enzymes. DNA samples were kept at -20°C for short term storage and at -80°C for long term storage.

DNA Sequencing

DNA sequencing was carried out by Eurofins. Samples were submitted with a template concentration between 50 and 100 $\frac{ng}{\mu L}$. Primers were premixed with the sample before submission.

sgRNA Design for CRISPR-Cas9 Targeting

The single guide RNAs were designed using an online tool at crispr.mit.edu, which, at the time of writing, was offline. For a provided DNA sequence, the tool found PAM sequences and estimate potential off-target sites through a BLAST like search. Guides were chosen according to the potential off-target score and according to their location in the genome. For both HDAC1 and HDAC2 the second exon was cut out and the sgRNAs were designed within the intron to be at least 300 bp away from the exon to either side. Oligos and the restriction site were designed according to established methods[143]. The ordered oligos are summarized in table 2.4. The vector pSpCas9(BB)-2A-GFP (pX458) was a gift from Feng Zhang (Addgene plasmid # 48138 ; `https://www.addgene.org/48138/` ; RRID:Addgene_48138).

2.2.3. Molecular Biology

Cell Cycle Analysis

The cell cycle was analyzed by flow cytometry using Hoechst dye to stain the DNA content of cells. After treating cells according to the individual experimental setup, they were trypsinized. The trypsinization reaction was stopped with complete cell culture medium in the ratio 1:2. A brief centrifugation (500 g, 5 min, RT) resulted in a cell pellet and the supernatant was removed. Redissolving the cells in 0.5 mL PBS was important to mitigate cell chunks when adding 0.5 mL 2x formaldehyde solution (c_{final} = 4%) and mixing softly but thoroughly. After a 10 min incubation at RT, 110 µL of 1% Triton X-100 solution and 11 µL of a 100x Hoechst33342 solution (c_{final} = 0.1 $\frac{\mu g}{mL}$) were added to permeabilize and stain the fixed cells. The cells were recorded with a BD LSR II after an incubation of 45-60 min at RT. Instrument settings were optimized for each experiment individually.

Flow Cytometry Analysis of the Cell Fluorescence

Similar to the method above, after treating cells according to the individual experimental setup, they were trypsinized. The trypsinization reaction was stopped with complete cell culture medium in the ratio 1:2. A brief centrifugation (500 g, 5 min, RT) resulted in a cell pellet and the supernatant was removed. The cells were redissolved in PBS (e.g. 1 mL PBS for cell from a well of a 6-well plate) and recorded with a BD LSR II instrument. Settings were optimized for each experiment individually.

FACS

Similar to the method above, after treating cells according to the individual experimental setup, they were trypsinized. The trypsinization reaction was stopped with complete cell culture medium in the ratio 1:2. A brief centrifugation (500 g, 5 min, RT) resulted in a cell pellet and the supernatant is removed. The cells were redissolved in PBS containing 0.5 mM EDTA and cell aggregates were removed by pipetting them through a cell strainer cap. The fluorescence activated cell sorting (FACS) was performed with a Beckman Coulter MoFlo instrument. Analytic flow cytometry runs were used as controls to calibrate the gates in the sorting runs. After sorting, the cells were plated in complete cell culture medium with Fungizone. Sorted cells were collected as a pool and cultured as modified cell line.

Knockout Verification

The frozen plates without medium were defrosted on ice and 30 µL TELysis buffer with RNAse A and 2 µL of proteinase K solution were added to each well. After a short gentle shaking and spinning down the liquid, the 96-well plate was sealed with aluminum foil and was kept overnight at 60°C in a plastic box covered with wet paper towels. The next morning, after another gentle shaking, the enzymes were inactivated by heating the plate to 95°C for 2 min. 1-2 µL of this lysate were used for a PCR reaction with the primer pairs 21-24 in table 2.4. The product size of these PCR reactions showed if a knockout was present.

Proliferation Assay

Cell proliferation was measured by counting the Hoechst stained nuclei of fixed cells with an operetta high content imaging system. Cells were seeded on a 96-well plate. The right seeding number was important to not overgrow the culture which makes counting impossible. For HCT116 cells a seeding number of 1000 cells/well, as counted by a Beckmann Coulter ViCell XR, worked well for a six day growth experiment. In experiments with Co-115 cells, the plates need to be pre-coated with 50 $\frac{\mu g}{mL}$ poly-D-lysine in pure water. In experiments with HCT116 cells no pre-coating was applied. For each day of the experiment one replicate plate was seeded. On each day of the growth experiment one plate was fixed with 50 µL 4% PFA solution in PBS for 10 min at RT. After washing the fixed cells three times with 50 µL PBS, they were stored at 4°C in PBS, sealed with PCR seal. Before counting, the fixed cells were stained with 0.1 $\frac{\mu g}{mL}$ Hoechst33342 solution for 10 min at RT in the dark. Images were processed with the Columbus software with a nuclei identification program which was kindly provided by Dr. Schorpp. Parameters were adjusted to work best with the HCT116 cell line. The individual steps to identify nuclei were as follows:

1. Input image
2. Find nuclei (method C)
3. Calculate morphology properties (standard method)
4. Calculate intensity properties (standard method)

5. Select population (nucleus area < 1000, nucleus roundness > 0.75, nucleus area > 90, intensity nucleus > 300)

6. Define Results

RNA-Seq analysis

Total RNA was isolated according to standard methods. The mRNA enrichment, library generation and RNASeq read generation was performed by the company ABM (website: `https://www.abmgood.com/`, last visited on the 14.02.2021). After receiving the raw data, we analyzed the data by using the tuxedo suite of programs (fig. 2.1). At first the read file format was changed to sanger format .fastq files with the Fastq groomer program, then the reads were aligned to the human reference genome (Human, Feb. 2009, GRCh37/hg19) with the alignment program TopHat2[144]. Using the aligned reads, a transcript file was created for each sample containing information on the presence of transcripts by the program Cufflinks[145]. These transcripts were merged to one file containing all transcripts from all samples by the program Cuffmerge[145]. In a final digital data analysis step, we used the Program Cuffdiff[145].

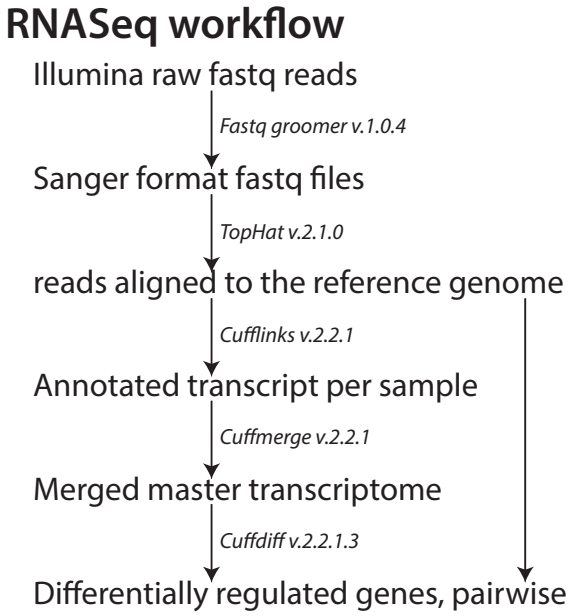

Figure 2.1 RNA-Seq data analysis. The data was analyzed with the Tuxedo suite of tools on the online galaxy cluster (`https://usegalaxy.org/`). Programs and their respective versions are depicted.

2-Step qPCR

Cells were harvested according to the instructions of the High Pure RNA Isolation Kit. The concentration of ribonucleic acid (RNA) samples was determined with a NanoDrop 2000 (Thermo scientific) using 1.5 µL of the sample.

Samples were kept on ice if not otherwise stated. For the reverse transcription 400 ng of RNA were diluted with HPLC grade water to 12 µL and 3 µL of a mastermix of random hexamers (2 µL per sample) and dNTP (1 µL per sample) were added to a final volume of

15 µL which was heated to 65°C for 10 min. After immediately cooling on ice 10 µL of a mastermix containing 2.5 µL 10x RWV buffer, 0.5 µL RMV reverse transcriptase and 7 µL HPLC grade water were added to the RNA mixture. Heating the samples to 25°C for 5 min, to 42°C for 60 min and to 95°C for 5 min completed the reverse transcription.

The qPCR reaction was performed in a LightCycler 480 from Roche. Samples, dilution and mixes were kept on ice. For each biological sample 5 ng of cDNA were diluted to 4 µL in a master dilution. The reaction master mix consisted of 5 µL SYBR green reaction mix, 0.05 µL of each of the two primers and 0.9 µL high-performance liquid chromatography (HPLC) grade water per sample. The combination of 4 µL master dilution and 6 µL mastermix was pipetted shortly before the start of the qPCR. The qPCR program is summarized in table 2.9.

Table 2.9 Temperature program of a qPCR reaction

	repetitions	**temperature**	**duration**
Denaturation	1	95°C	10 min
Amplification	40	95°C	15 s
		60°C	60 s
Melting curve	1	95°C	10 s
		65°C	15 s
		$+2.2\frac{°C}{s}$	
		95°C	10 s
Cooling	1	40°C	forever

qPCR Primer Design

In general primer pairs were designed with an online tool by Roche (`https://lifescience.roche.com/en_de/brands/universal-probe-library.html`, last checked 17.06.2019). In general, the name of the target gene was entered and the tool suggested primer pairs. If a specific exon-exon junction was targeted the sequences of both exons were supplied to the online tool. In a second step the primer pair location was manually compared to the aligned read from the RNASeq experiment to check if there were reads over the exon-exon junction.

Custom Antibody Generation

Together with the Helmholtz center Munich core facility for monoclonal antibodies peptides containing the acetylation sites with predicted high immunogenic potential were designed. These peptides were ordered from Peps4LS in Heidelberg and are summarized in table 2.10. Two peptides with N-terminal cysteine were coupled to ovalbumine by Peps4LS.

In accordance to German animal rights regulations, one mouse and two rats were immunized with the ovalbumine coupled target peptides. Three days after a boost injection of adjuvant,

Table 2.10 Peptides ordered for custom antibody generation.

target	sequence
HSPA8/HSP7C	C-VQVEYK(Ac)GETKS
HSPA8/HSP7C	eBio-VQVEYK(Ac)GETKS-HHHHHH
HSPA8/HSP7C	eBio-VQVEYKGETKS-HHHHHH
MATR3	C-SASAAAK(Ac)K(Ac)KLKKVD
MATR3	eBio-SASAAAK(Ac)K(Ac)KLKKVD-HHHHHH
MATR3	eBio-SASAAAK(Ac)KKLKKVD-HHHHHH
MATR3	eBio-SASAAAKK(Ac)KLKKVD-HHHHHH
MATR3	eBio-SASAAAKKKLKKVD-HHHHHH

which was performed six to eight weeks after the primary immunization, the animals were sacrificed, splenocytes were collected and fused with the myeloma cell line P3X63-Ag8.653.

11-14 days after fusion, the supernatants were enzyme-linked immunosorbent assay (ELISA) screened for the presence of targeted antibodies. Animal handling and ELISA experiments were performed by the core facility. After a further expanding of positive cells, supernatants were tested on western blot (WB) level for an identification of the right sized product. ELISA and WB positive hybridoma lines were single cell cloned to create stable cell lines.

2.2.4. Biochemistry

Sample Preparation for Mass Spectrometry – Part 1: Lysis and Digestion

All buffers were prepared with HPLC grade water and were filtered through a 0.22 µm filter. Per condition, ten 15 cm dishes with subconfluent cells were lysed in 3 mL lysis buffer. The remaining nuclei were scraped from the plate. To increase the protein concentration the lysed cells and remaining nuclei were transferred from plate to plate, consecutively lysing all ten plates. After transferring the cell nuclei in the lysis buffer to a 50 mL falcon and cooling them on ice, 4x NaCl solution was added to a final concentration of 300 mM NaCl. The nuclei were incubated with the 300 mM salt concentration to release chromatin bound proteins. Then the solution was centrifuged (3250 g, 4 °C, 5 min) and the supernatant was transferred to a fresh 50 mL falcon. The proteins in the supernatant were precipitated with 4 parts ice cold acetone and stored at -20 °C overnight. The next morning the precipitated proteins were collected by centrifugation (2000 g, 4 °C, 10 min) and washed twice, once with 70% acetone and another time with 50% acetone. Afterwards, the almost fully dried pellet was redissolved in 8 mL urea buffer and incubated at 55 °C for 30 min. After letting the redissolved proteins cool to RT on ice, 1 mL of freshly prepared iodoacetamide solution (103 mM) was added and the solution was incubated for 15 min in the dark. The remaining iodoacetamide was quenched by adding 36 µL of 1.25 M dithiothreitol (DTT). Then 5 µg LysC were added to each sample

and incubated for 2 h at 37 °C. The solution was diluted two-fold with 4-(2-hydroxyethyl)-1-piperazineethanesulfonic acid (HEPES) buffer to 4 M Urea and incubated for another 2 h at 37 °C. After another two-fold dilution to 2 M Urea, 10 µg of trypsin were added and the solution was incubated at 37 °C overnight. In the morning the digested peptide solution was acidified with 20% trifluoracetic acid (TFA) to a final concentration of 1% TFA. After a 15 min incubation on ice, the solution was centrifuged (2000 g, 4 °C, 10 min). This supernatant was used for the Sep-Pak purification.

Part 2: C18 Sep-Pak Purification

The C18 Sep-Pak column had been pre-wetted with 5 mL of HPLC grade acetonitrile and was then sequentially washed with 1 mL, 5 mL and 6 mL of solvent A. The peptide containing solution was loaded and sucked through the column, which was washed again sequentially with 1 mL, 5 mL and 6 mL of solvent A. After another washing step with 2 mL of wash solvent, the peptides were eluted with 3x 2 mL solvent B. Solvents are removed by freeze-drying the samples.

Part 3: TMT6plex-Labeling

To prepare the labeling, the samples were dissolved in labeling buffer, centrifuged (10,000 g, 4 °C, 5 min) and the supernatant was filtered through a 10 kDa molecular-weight cutoff (MWCO) filter. The protein / peptide concentration in the filtrate was measured with the Nano-Drop. 500 µg of peptides were prepared in 400 µL labeling buffer. The TMT labeling reagent was dissolved in 164 µL of K_2CO_3 dried acetonitrile in 5 min under occasional vortexing. After adding the dissolved TMT reagent to the peptide solution and incubating for 1 h at RT, 32 µL of 5% hydroxylamine were added to quench the reaction for 15 min. At this stage a small part of the sample was used as immunoprecipitation (IP) input analysis. After freezing the samples, the solvents and buffers were removed by lyophilization.

Part 4: Sequential Immunoprecipitation

All the labeled dry peptides were dissolved in a total of 1 mL of IP buffer and the differently labeled peptides were mixed together. The pH of the mixture was controlled and if it was below pH 6, adjusted with 1 M Tris buffer (pH 9-10, when dissolved). After initially centrifuging the beads (2000 g, 4 °C, 30 s) and removing the storage solution, they were washed with with PBS four times. Beads were resuspended in 40 µL IP buffer, the peptide solution was transferred to the beads and incubated overnight on a rotational wheel at 4 °C. The beads were centrifuged (2000 g, 4 °C, 30 s) and the supernatant (flow-through fraction) was used for the consecutive second IP. The beads were washed twice with 1 mL IP buffer and three times with 1 mL of HPLC grade water. At the last washing step, the complete supernatant was removed and the peptides were eluted with 55 µL of 0.15% TFA by letting it stand for 10 min at RT with occasional mixing every 2 min. A second elution with 50 µL of 0.15% TFA finished the first IP. These combined fractions are used in the ZipTip purification.

To prepare the second IP, 50 µL of antibody-agarose conjugate were dissolved in 2% acetic acid solution in water, centrifuged (2000 g, 4 °C, 30 s) and washed twice with PBS and once

with IP buffer. After the last washing step, the beads were resuspended in 40 µL IP buffer and the flow-trough fraction from the previous IP was added. The mixture was incubated at 4 °C overnight on a rotational wheel. Then the beads were centrifuged (2000 g, 4 °C, 30 s) and washed twice with 1 mL IP buffer and once with 1 mL HPLC grade water. After the last washing step as much supernatant as possible was removed and the elution was performed as described above. The eluate from this IP was also used in the ZipTip purification.

Part 5: ZipTip Purification

The C18 ZipTip was equilibrated by passing 50 µL of HPLC grade acetonitrile, 50 µL of solvent C and two times 50 µL of solvent D through. After the eluates from the previous steps had been passed through individual ZipTips, the tips were washed two times with 55 µL of solvent D. The peptides were eluted from the C18 tip by passing 10 µL of solvent E through two times. Pooling the two fractions and freeze-drying the samples completes the MS preparation procedure.

LC-MS/MS Measurements

Approximately 0.5 µg of digested pooled input sample or enriched acetylated peptides was analyzed on a Q-Exactive-HF mass spectrometer online coupled to an Ulimate 3000 RSLC (Thermo Scientific) by the core facility. Injected peptides were automatically loaded on a trap column (300 µm inner diameter (ID) $\times$ 5 mm, Acclaim PepMap100 C18, 5 µm, 100 Å, LC Packings) prior to C18 reversed phase chromatography on the analytical column (nanoEase MZ HSS T3 Column, 100 Å, 1.8 µm, 75 µm x 250 mm, Waters) at 250 nl/min flow rate in a 95 min non-linear acetonitrile gradient from 3 to 40% in 0.1% formic acid. Profile precursor spectra from 300 to 1500 m/z were recorded at 120000 resolution with an automatic gain control (AGC) target of 3e6 and a maximum injection time of 50 ms. TOP10 fragment spectra from 200 to 2000 m/z with a fixed first mass of 100 m/z were recorded at 60000 resolution with an AGC target of 1e5, a maximum injection time of 100 ms and an isolation window of 1.2 m/z. Normalized collision energy was set to 30, unassigned and +1 charges were excluded and dynamic exclusion was set to 30 s.

SDS-PAGE and Western Blot

Gels were cast according to standard procedures with acrylamide contents between 6% and 15% depending on the protein masses that were analyzed. The reagents acrylamide (30%), 1.5 M Tris (pH 8.8), 10% sodium dodecyl sulfate (SDS) solution, ammoniumperoxodisulfate (APS) and N,N,N,N-tetramethylethane-1,2-diamine (TEMED) were used for the polymerization of the gels. Gels were cast and run with the mini-PROTEAN Tetra Cell system.

After mixing the protein samples with bromophenol blue solution to a final concentration of 10 µM (1 µL of 1 mM stock solution per 100 µL lysate), they were heated to 95°C for 2 min. A total amount of protein between 4 and 40 µg was loaded per lane and 3 µL of protein marker were used. The gel was run in two steps. In a first step, the samples passed the stacking gel in 12 min at 100 V and about 3 A. In the second step, the gel was run for about 1 h at 160 V and roughly 3 A until the colored bromphenol blue band just left the gel

chamber. After the SDS-polyacrylamide gel electrophoresis (PAGE), the gel was equilibrated in transfer buffer for at least 5 min. The PVDF membrane was activated in pure methanol (min. 2 min) and equilibrated in transfer buffer for at least 5 min. Blotting of the proteins on the membrane was performed with a trans-blot semi-dry electrophoretic transfer cell for 1 h 40 min at a current of 1 mA/cm^2. After washing of the membrane with TBS-T buffer once, the membrane was blocked with a 5% (w/v) milk powder solution in TBS-T for 1 h at RT. After washing, the membrane was incubated overnight with the primary antibody at 4°C. A list of the antibodies used is given in table 2.3. The next day, the membrane was washed again three times with TBS-T solution and incubated with fresh secondary antibody at RT for 1 h. After another washing step, the membrane was incubated with the ECL kit and chemiluminescence is recorded with a INTAS ECL Chemocam Imager system.

Determination of the Protein Concentration

The protein concentration for western blots was determined with the Pierce 660 nm Protein Assay Kit. To mask the SDS in the samples, 1 g ionic detergent compatibility reagent was added to 20 mL of protein assay reagent. For the assay 5 µL of the sample and 5 µL PBS were mixed with 100 µL protein assay reagent containing the compatibility reagent in a 96 well plate. For each individual measurement a calibration curve was created with BSA standards with the concentrations 0, 125, 250, 500, 750, 1000, 1500 and 2000 $\frac{\mu g}{\mu l}$. After 5 min incubation of the sample with the reagent, the shift of the absorption maximum of the dye was measured. A comparison with the standard curve resulted in the total proteins concentrations.

2.2.5. Statistics and Bioinformatics

Statistical analysis was performed using Prism 6.0. Values shown are reported as mean $\pm$SEM, if not stated otherwise. Each experiment was repeated multiple times on different days and a representative image is shown. Depending on the type of dataset, significance was either determined using a Student's unpaired t-test against a control, a 1-way ANOVA with a Tukey's multiple comparisons test or 2-way ANOVA with a Sidak's multiple comparisons test. Significance levels are states as: * $p < 0.05$; ** $p < 0.01$; *** $p< 0.001$; **** $p < 0.0001$.

Quantification of Western Blot Signals with the Tool ImageJ

A rectangular selection was placed around the furthest left band of the blot and marked as reference. Selections with the exact same size were placed from left to right over all western blot bands. In the density plots of the bands, the bases of the peaks were closed with a line in order to adjust for the background. The peak area was used as quantification of the western blot band.

TMT Quantifications in Proteome Discoverer 2.2

Mass spectrometric raw files were analyzed by the core facility in Proteome Discoverer 2.2 (Thermo Scientific), using the provided Processing and Consensus work-flows for reporter based quantifications, with the following settings: Mascot (Matrix Science) was used a search engine with trypsin as enzyme and 2 missed cleavages allowed. Spectra were searched in the Swissprot human database with a precursor mass tolerance of 10 ppm and a fragment

mass tolerance of 20 mmu. Carbamidomethylation of cysteine was set as fixed modification additionally allowing for the following variable modifications: acetyl (K), oxidation (M), TMT-6plex (K, N-term). Peptide identifications were scored in the percolator node with a strict target FDR of 1%. Quantifications were based on unique and razor peptides with normalization on total peptide amount and calculation based on summed abundances. Resulting lists of proteins and peptide groups with corresponding scaled abundances of TMT channels were exported and used for further analyses like calculations of TMT abundance ratios between channels.

Counting Cells with Cytosolic Protein

The image analysis was performed with the Columbus software on data acquired with the operetta system. The identification steps in the software were as follows:

1. Input image
2. Find nuclei (Hoechst, method M)
3. Find surrounding region (fluorescence channel of protein of interest (POI), method B)
4. Calculate morphology properties (standard method)
5. Select population (nucleus area > 25, nucleus area < 150, nucleus roundness > 0.67, POI surrounding area > 160)
6. Select population (common filter: remove border objects)
7. Define Results (formula a/b: selected population / total nuclei)

3. Results

3.1. Cell Culture Models for the Distinction between HDAC1 and HDAC2

An important objective to assay selective HDAC1/HDAC2 activity markers was to create genetically modified colon cancer cell lines. These cell lines allowed us to manipulate the HDAC1/HDAC2 expression individually. For our genetic modifications we choose the CRISPR-Cas9 method as well as a conditional overexpression system.

Design of the HDAC Knockout *via* CRISPR-Cas9

For the creation of our model cell lines, we aimed to reliably create knockouts, which were easily verifiable by PCR. CRISPR-Cas9 knockouts were often created by targeting Cas9 to a single site within an exon with one single guide RNA (sgRNA)[146]. The desired outcome of this approach was a random mutation in the non-homologous end joining (NHEJ) repairing process[143]. In some cases random mutations lead to a shift of the gene's reading frame, which can cause a premature termination codon (PTC) to appear in the new reading frame. This PTC impairs the correct translation of the target protein and causes the knockout. This Cas9 targeting strategy is a stochastic approach.

This was the reason why we decided for a knockout system in which the complete exon two was excised, since this reliably lead to a PTC (see figure 3.1). The targeting of Cas9 for this excision was performed by sgRNAs, which were expressed from a transfected vector. Four individual sgRNAs were designed to direct Cas9 to intron 1-2 and intron 2-3 of HDAC1 and HDAC2 respectively, which created four versions of the vector pSpCas9(BB)-2A-GFP (pX458) (addgene ID: 48138). Guide RNA targeting of Cas9 to a DNA sequence lead to double strand breaks (DSBs), which were presumably repaired by the NHEJ repair pathway. The two resulting DNA ends in intron 1-2 and intron 2-3 were joined together leaving out exon two of HDAC1 or HDAC2, respectively. With this strategy, the exact DNA sequence of the repair site is irrelevant, since the cut site is located in an intron, which is removed during splicing.

To control for successful knockout, genomic DNA was isolated from cells and used as template in a PCR. The excision of exon two was confirmed for both isoforms by a size reduction of the PCR product generated with primer pairs spanning from exon one to exon three. The expected PCR amplicon size of the wild type locus was 1499 bp for HDAC1 and 1839 bp for HDAC2, and the faster migrating bands of PCR products from the knockout modification were found in the range of 750-850 for HDAC1 and 500-600 for HDAC2. This means, the DNA damage in the form of two DSBs was repaired through the NHEJ pathway and not by recombination. Therefore, we were able to confirm a successful knockout. The position of the

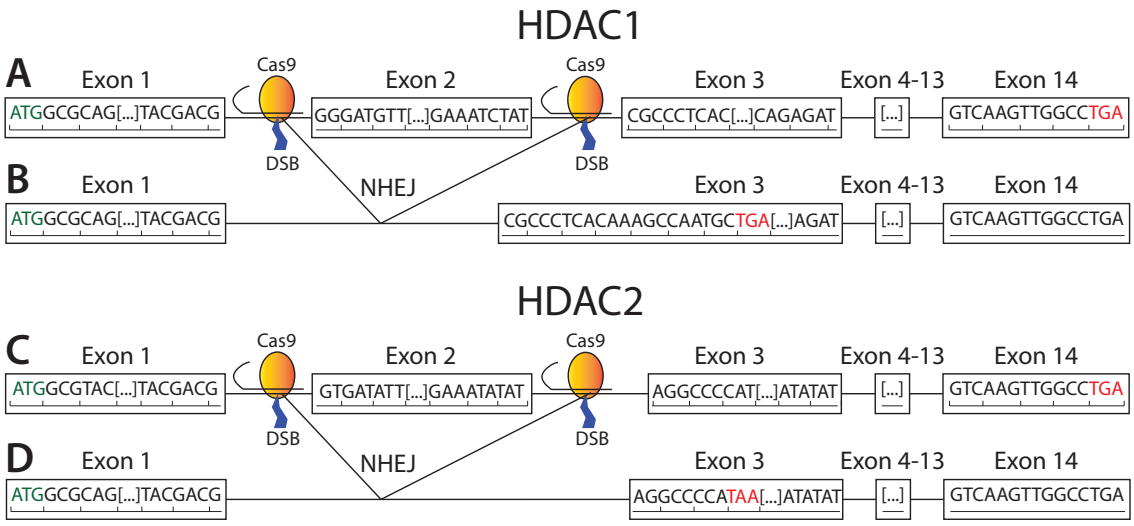

Figure 3.1 CRISPR-Cas9 strategy to knockout HDAC1 or HDAC2. A) The DNA of native HDAC1 was cleaved in intron 1-2 and intron 2-3. **B)** Through NHEJ exon 2 of HDAC1 was excised. This resulted in a premature stop codon in exon 3. **C+D**) The HDAC2 gene was modified in a similar manner. Transcriptional start sites are marked in green and stop codons are marked in red. (DSB: double strand break)

PTCs in the former exon three strongly suggested that the resulting fragments did not lead to functional protein, which represented the knockout.

The HDAC Overexpression System

The second set of genetic modifications was the stable integration of a conditional expression system. This conditional overexpression system of HDAC1 or HDAC2 was based on two vectors created by Trono *et al.*[147]. In their system, one vector encoded the KRAB repressor protein fused to the tTR binding domain of the tet-on system. The KRAB protein suppressed polymerase II and polymerase III transcription, irrespective of orientation, because KRAB was thought to change the chromatin structure to a heterochromatin like state, effectively blocking transcription[147]. KRAB interacted with the corepressor protein KAP-1 (KRAB associated protein) and heterochromatin protein 1 (HP1), which in turn recruited chromatin remodeling complexes leading to heterochromatin in the surrounding region[148]. The pLVTHM vector of the Trono system was modified by M. Vincendeau at our institute, who included an expression cassette for a gene of interest upstream of the GFP site (method described in [149, 150]). By cloning HDAC1 or HDAC2 into this expression cassette, we created a vector containing an EF1α-HDAC-T2A-GFP sequence. Close to the expression cassette, a tet-operator sequence was located, to which the repressor fusion protein can bind in the absence of doxicycline, causing repression of the expression cassette in close proximity. The combination of both vectors enabled the conditional overexpression of either HDAC1 or HDAC2.

The basic functionality of the tTR - tetO interaction was doxicycline dependent (see fig. 3.2). Without doxicycline, the tTR-KRAB fusion protein bound to the operator sequence (tetO), blocking the transcription of DNA in close proximity (panel A). With doxicycline the fusion protein was released and the transcription of the target protein, either HDAC1 or HDAC2, was activated (panel B). Hence, addition or removal of the substance doxicycline controls the

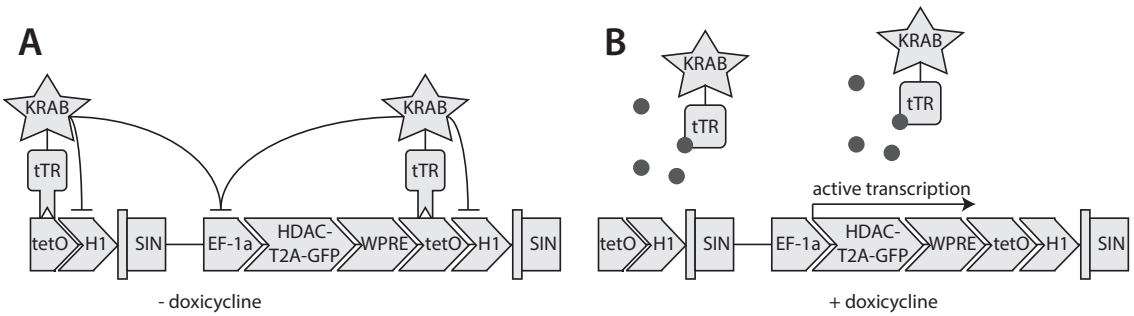

Figure 3.2 Tetracycline regulated expression of HDAC1 or HDAC2. A) Without doxicycline, the trans repressor domain (tTR) of the tTR-KRAB fusion protein binds to the tet Operator sequence (tetO) in the DNA. The KRAB domain blocks the transcription of nearby DNA. **B)** Upon addition of doxicycline, the tTR domain is released from operator sequence and the HDAC-T2A-GFP sequence is transcribed driven by the EF1α promoter. Figure adapted from Trono *et al.*[147].

expression of a single HDAC isoform. We used this conditional expression system to control the expression of HDAC1 and HDAC2 in our model cells.

Genetic Modifications in HCT116 Based Model Cell Lines

With the previously described genetic modification strategies, we aimed to create a genetic system to analyze the unique consequences of either HDAC1 or HDAC2 activity level changes in HCT116 cells. Previous research found that HDAC1 / HDAC2 double knockouts in mouse embryonic fibroblasts severely impair cellular growth[151]. To avoid growth impairment, we modified HCT116 cells in a four-step process (fig. 3.3). The process ensured that either HDAC1 or HDAC2 were expressed throughout all modification steps. At the last stage dying of cells within days could be acceptable. The order of the four modification steps excluded synthetic lethality by a double knockout during the creation process.

In a first step the vector pLV-tTRKRAB was incorporated in the host genome of HCT116 cells by lentiviral infection. The vector encodes the dsRED fluorescence marker and the tTR-KRAB fusion protein, responsible for transcriptional repression (depicted in red in fig. 3.3). This genetically modified cell line was created during previous work for a master's thesis at the same institute[152]. Cells were sorted *via* FACS for positive dsRED fluorescence and the pool of dsRED positive cells was used in the next step.

In this second step either HDAC1 or HDAC2 were knocked out by using the CRISPR-Cas9 system[143]. For the knockout three vectors were cotransfected. The first two vectors refer to two versions of the vector pSpCas9(BB)-2A-GFP, which encoded Cas9 and differently targeted sgRNAs. The third vector was pPGK-puro (addgene ID of empty backbone: 35094), which encodes a puromycin resistance marker. Because of the assumption that either all vectors enter a cell or none, the third vector pPGK-puro was added for selection. As Puromycin kills cells without a resistance, the surviving cells express the resistance marker and were likely to also contain both pSpCas9(BB)-2A-GFP vectors, which induce the knockout. After this Puromycin selection, single cell clones were picked and analyzed by PCR for a successful knockout. For both the HDAC1 k.o. and the HDAC2 k.o. one positive single cell clone was expanded and used in the next step (step 3). Since the knockouts were performed in the pre-

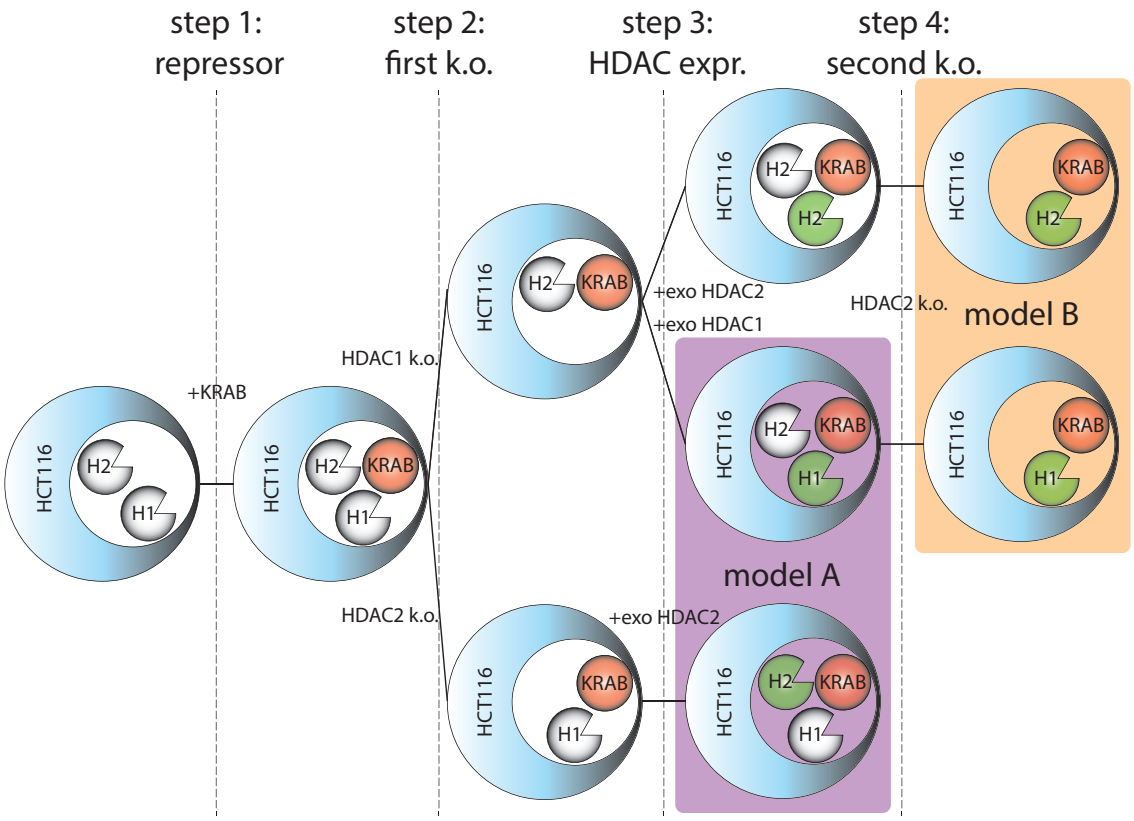

Figure 3.3 Genetic modifications in HCT116 cells for the distinction between HDAC1 and HDAC2 dependent processes. **Step 1:** The repressor KRAB and a dsRED fluorescence marker were introduced into the HCT116 cell genome *via* lentiviral infection. **Step 2:** HDAC1 or HDAC2 were knocked out individually. **Step 3:** Transduction of HDAC1 or HDAC2 in combination with a green fluorescence marker by lentiviral infection. The two lines in the purple box form model A cell lines. **Step 4:** In this step a knockout of endogenous HDAC2 was performed in the two lines from the previous step. These knockouts created two individual sets of modifications, where both endogenous isoforms were knocked out and either HDAC1 or HDAC2 was expressed from the transgene. For each set of final genetic modifications, three individual HDAC2 knockout clones were created. The cell lines with these two sets of genetic modifications form model B. White symbols represent endogenous HDAC isoforms, red symbols represent cells that were infected with a viral vector encoding the repressor KRAB with a dsRED fluorescence marker, and green symbols represent cells that were infected with a viral vector encoding HDAC expression and green fluorescent protein (GFP) as fluorescence marker. (H1 = HDAC1, H2 = HDAC2, exo = exogenous, endo = endogenous)

viously infected cells, both lines also contain the repressor tTR-KRAB (fig. 3.3 after step two modification).

In a third step a HDAC isoform cloned on a pLVTHM based vector was introduced *via* lentiviral infection into the cellular genome with a GFP marker (depicted in green in figure 3.3). Together with the KRAB repressor inserted in the first step, these two stably integrated vectors completed the conditional expression system (described in figure 3.2). Three individual combinations of genetic modifications were created in this third step. In the first case (top row), the HDAC2 expressing transgene was introduced in the previous knockout of endogenous HDAC1. The resulting cell line has endogenous HDAC2 expression and also a conditional expression of HDAC2 (depicted in green) as well as the repressor and a knockout of the endogenous HDAC1 isoform. In a second case (middle row), the exogenous HDAC1 expressing vector was introduced in the same HDAC1 k.o. cells from step two. This cell line has an endogenous HDAC1 knockout and a conditional expression of HDAC1 from the transgene. In the third case (lower row), the HDAC2 encoding pLVTHM vector was introduced in

HDAC2 k.o. cells. This cell line has an endogenous HDAC2 knockout and a conditional expression of HDAC2 from the integrated transgene. The cell lines marked by the purple box in figure 3.3 form model A cell lines. This pair of cell lines enables control over the expression of a single HDAC isoform by doxicycline presence in the background of the endogenous presence of the corresponding isoform. For the conditional HDAC1 expression, endogenous HDAC2 is present and for the conditional HDAC2 expression, HDAC1 is present. The three combinations of genetic modifications created in step three contain both the repressor and the conditional expression transgene, which can be controlled by the presence of doxicycline. These three lines were sorted by FACS for dual dsRED/GFP positive cells and the pool of collected cells was used in further experiments and the fourth modification step.

The fourth and final step was a knockout of the remaining endogenous HDAC2 isoform using the CRISPR-Cas9 system in two cell lines. Similar to the process in step two, the cells were co-transfected with the three vectors and puromycin selected. In this fourth step, both endogenous loci were checked for the knockout by PCR. The two final cell lines created in this step carry a double knockout of both endogenous isoforms, HDAC1 and HDAC2. In one line HDAC2 is conditionally expressed from the integrated transgene (top row) and in the other line HDAC1 is conditionally expressed (middle row). It was necessary to leave the expression of the conditional HDAC isoform active in order to sustain the growth of these cell lines. For each cell line, three positively tested knockout clones were cultured as biological replicates. These clonal cell lines form model B (orange box in figure 3.3). This set of modifications created a series of highly homologous clonal cell lines, in which the expression of either HDAC1 or HDAC2 can be controlled by addition or removal of doxicycline independent from the endogenous expression of HDAC1 and HDAC2.

FACS of HCT116 Cells Containing both Vectors for the Conditional HDAC Expression

During the infection step of the model cell lines creation, we expected the rate of infection to be below 100%. To ensure that we created stable cell lines and that unmodified cells could not outgrow the modified cells, we sorted the cells carrying the intended modifications by FACS.

The two vectors of the conditional expression system encoded dsRED or GFP as fluorescence markers. HCT116 wild-type cells served as control for the auto-fluorescence of this cell line (fig. 3.4, panel A). Cells expressing dsRED or GFP served as controls for the respective fluorescence (panel B and panel C).

A representative dot blot of dsRED and GFP fluorescence of a sorting run of cells after the third modification step shows 22.1% cells fall into quadrant two, showing both GFP and dsRED fluorescence (panel D). This means both vectors were included in the genome of the cells. After the last transduction step, we assumed a stable integration of both vectors, since lentivirus based vectors stably transduce a variety of targets. We confirmed the expression

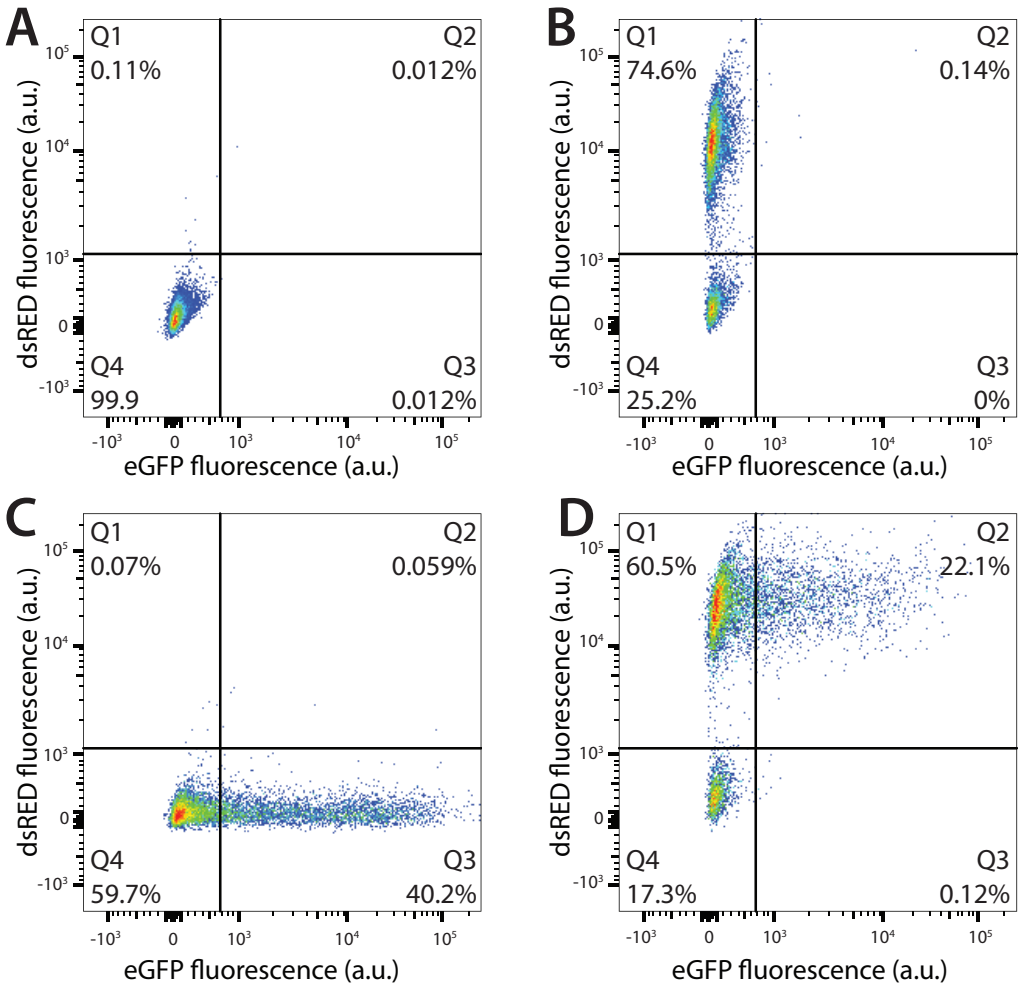

Figure 3.4 Flow cytometry and FACS of HCT116 cells which incorporated the expression system. A) dsRED and GFP fluorescence of HCT116 wild type cells. **B)** dsRED and GFP fluorescence of HCT116 cells infected with the pLV-tTRKRAB vector encoding dsRED and the KRAB repressor. **C)** dsRED and GFP fluorescence of HCT116 cells infected with the pLVTHM vector encoding GFP and HDAC. Panels A-C represent analytic flow cytometry runs, with which the gates for the sorting runs were set. **D)** Representative dsRED and GFP fluorescence in a sorting run after step three in the cell line creating process (refer to fig. 3.3). Cells positive in dsRED and GFP fluorescence were collected and this pool of cells was cultured as new cell line. arbitrary units (a.u.)

and absence of expression of HDAC1/2 by monthly western blots.

Genetic Modifications for Conditional HDAC2 Expression in a Co-115 Based Cell Line

In order to verify results in a second parental cell line, we evaluated a transduction of conditional HDAC2 expression in the Co-115 cell line. The Co-115 cell line was established by Carrel *et al.* [142] and was found to lack expression of HDAC2[153]. HCT116 and Co-115 cell lines are both adherent colon cancer cell lines, thus the Co-115 cells have a similar origin compared to HCT116 cells. Therefore, the modified Co-115 line provided complementary data to minimize the risk to rely on phenomena occurring in the context of one specific parental cell line.

To achieve a conditional HDAC2 expression in Co115 cells, we applied a two-step strategy

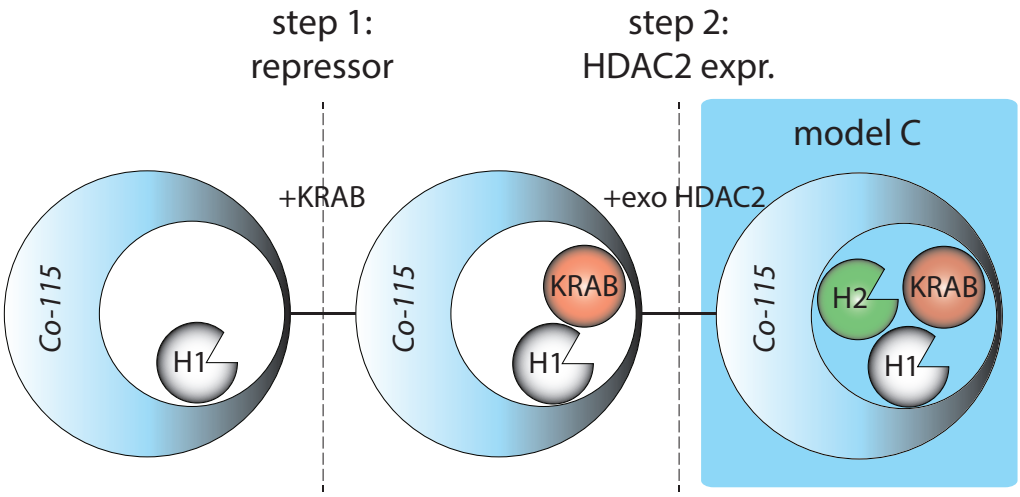

Figure 3.5 Design of the conditional expression of HDAC2 in natively HDAC2 deficient Co-115 cells. A conditional expression of HDAC2 was introduced in a two step process. **Step 1:** The KRAB repressor was transduced *via* lentiviral infection. **Step 2:** The HDAC2 expression was transduced *via* lentiviral infection, creating the model C cell line, where HDAC2 expression was controllable by doxicycline presence. White symbols represent the endogenous HDAC1 isoform, red symbols represent cells that were infected with a vector encoding a dsRED fluorescence marker and green symbols represent cells that were infected with a vector encoding GFP as fluorescence marker. (H1 = HDAC1, H2 = HDAC2, exo = exogenous)

(fig. 3.5). Similar to the conditional expression for models A and B, in a first step, the KRAB repressor protein was virally transduced and in a second step the HDAC2 containing pLVTHM vector was transduced. After sorting the cells in the same way as HCT116 cells (described in figure 3.4), the pool of dsRED and GFP positive cells form the model C cell line (blue box). Addition or removal of doxicycline control the HDAC2 expression in the model C cells. The genetic modifications in this model C line are analogous to model A cells with a knockout of endogenous HDAC2 and HDAC2 conditional expression of HDAC2.

In summary, we created HCT116 based model A cell lines, in which the expression of either HDAC1 or HDAC2 is controlled by doxicycline in the background of the knockout of the endogenous isoform. In the HCT116 based model B cell lines, either HDAC1 or HDAC2 are conditionally expressed in the background of the knockout of both HDAC1 and HDAC2 together. The model C cell line is based on Co-115 and transgenic HDAC2 expression can be controlled by doxicycline presence. Model A-C cell lines enabled us to investigate effects of HDAC1/2 expression gain and loss. We used these effects to search for specific markers for either HDAC1- or HDAC2-activity.

3.2. HDAC1 and HDAC2 Reconstitution and Regulation in the Model Systems

In this chapter we validated the HDAC expression patterns generated through the genetic modifications and further investigated the interaction of HDAC1 and HDAC2 expression levels.

Validation of HDAC1/2 Reconstitution in HCT116 Based Model A Cell Lines

After introducing the genetic modifications described in the previous chapter and verifying them on DNA level, we investigated the result of the knockout and the conditional overexpression on protein level. We expected the knockout as well as the inactive conditional expression system to reduce protein levels to undetectable amounts. For the active conditional expression system, we expected either HDAC1 or HDAC2 expression.

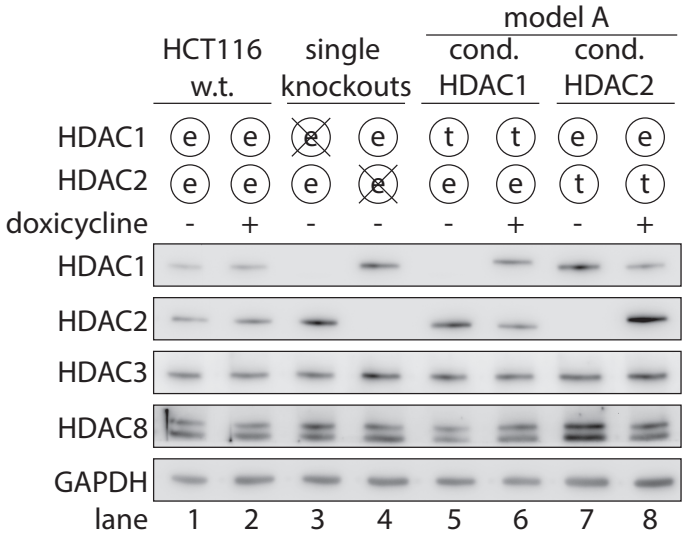

Figure 3.6 Class I HDAC protein expression and inducibility in model A cell lines.
Representative images of class I HDAC steady state protein expression. HCT116 wild type cells cultured with or without doxicycline were compared to single HDAC1 or single HDAC2 knockout cells, as well as model A cells with conditional HDAC1 or HDAC2 expression in the background of a knockout of the respective endogenous isoform. Whole cell lysates were extracted from cultured cells and a representative of more than ten experiments is shown. (e = endogenous, t = transgenes of the conditional system introduced into the host cell genome with a background knockout of the endogenous isoform)

We examined class I HDAC protein levels as well as GAPDH as protein amount loading control in five cell lines: HCT116 wild type cells, HCT116 cells with a suspected single knockout of either HDAC1 or HDAC2 and the two model A cell lines with either a suspected conditional HDAC1 or HDAC2 expression (fig. 3.6). In order to examine the conditional expression, both model A were cultured with or without the expression activator doxicycline. HCT116 wild type cells with and without doxicycline served as a control for the treatment. The absence of detectable HDAC1 and HDAC2 protein confirmed the effective knockout of HDAC1 or HDAC2 in the single knockout cell lines. A similar absence of detectable HDAC1 and HDAC2 protein in model A cell lines additionally confirmed the ability of the conditional expression system to effectively suppress the expression of the respective isoform. For both model A cell

lines, we detected the conditionally expressed isoform in the presence of doxicycline. These HDAC protein levels were slightly elevated compared to wild type HDAC1 or HDAC2 levels. Exogenous expression of the HDAC isoforms resulted in the expression of a protein with increased molecular weight. Combining this observation with the fact that the design of the HDAC-T2A-GFP cassette of the transgenic expression system resulted in residual amino acid tail originating from the self-cleaving T2A peptide, strongly suggested that the expression of HDAC1 originated from the transgene. These data showed that the conditional reconstitution was effective. We additionally observed an increase of native HDAC1 or HDAC2 expression, when the corresponding isoform's expression was reduced to undetectable levels. Furthermore, we observed a reduction of the corresponding native isoform's expression levels upon active conditional expression. This result hinted towards a regulation between HDAC1 and HDAC2.

To further analyze the conditional expression system in model A cell lines and to reproduce the regulation between HDAC1 and HDAC2, we decided to perform a time course experiment of the onset of the conditionally expressed isoform (fig. 3.7).

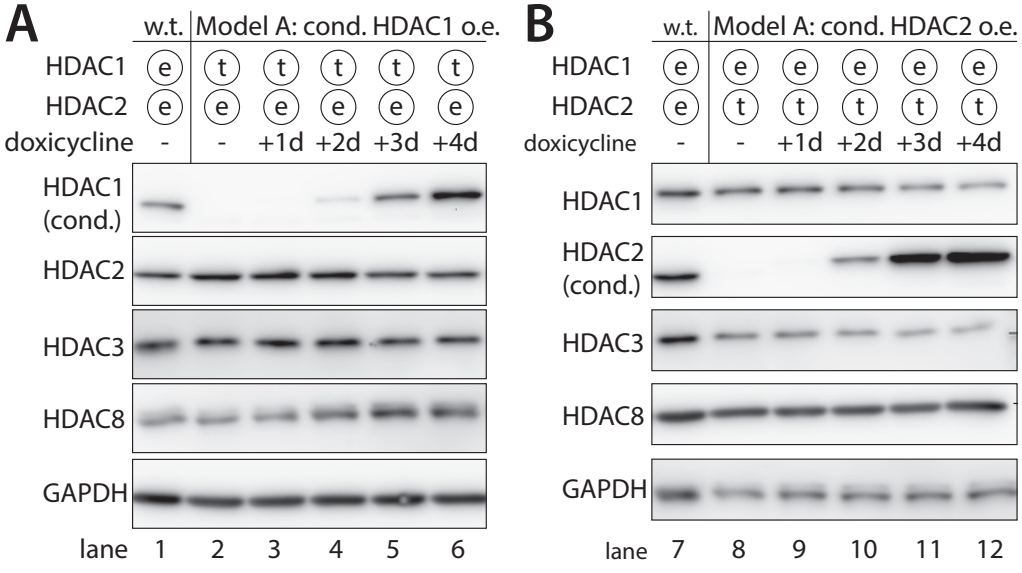

Figure 3.7 Time course of HDAC1/2 expression gain in model A cell lines.
Representative images of class I protein expression in model A cell lines. **A)** Time course of the gain of the conditional expression of HDAC1. Doxicycline was added for up to four days. **B)** Analog to panel A, a time course of the gain of the conditional expression of HDAC2 is shown. For both panels A and B, a representative of three individual experiments are shown. Western blots were measured from whole cell lysates. (e = endogenous, t = transgenes of the conditional system introduced into the host cell genome with a background knockout of the endogenous isoform)

The conditional HDAC1 expression was induced by doxicycline addition to cells previously cultured without doxicycline and compared to the expression of class I HDACs in HCT116 wild type cells (fig. 3.7, panel A). In lanes two to six model A cells with previously inactive conditional HDAC1 expression were treated with doxicycline for the indicated times. HDAC1 protein appeared after two days of doxicycline treatment and the abundance increased until day four. We showed that the conditional system took three days to reach HDAC1 protein levels comparable to the levels in wild type cells. On day three and four after doxicycline

addition, a light decrease of HDAC2 protein abundance and an increase of HDAC8 protein abundance was observed. The slight decrease in endogenous HDAC2 upon HDAC1 induction (5^{th} and 6^{th} lane) may correspond to the decrease of HDAC2 upon permanent induction of HDAC1 (fig. 3.6). The increase of HDAC8 protein levels was only observed once (fig. 3.7, panel A). As HDAC1 and HDAC2 were the primary focus, we did not follow up on the HDAC8 protein abundance observation.

In analogy to the time course of conditional HDAC1 induction we observed the gain of conditionally expressed HDAC2 over time (panel B). A HDAC2 protein band appeared already after two days of doxicycline induction and the abundance increased until day four. The HDAC2 maximum was slightly elevated above wild type levels. With the increase in HDAC2 protein abundance, HDAC1 protein expression from the endogenous gene decreased. HDAC3 appeared to be expressed less in model A cells with conditional HDAC2 expression compared to wild type HCT116 cells. This observation did not reproduce over several experiments and was therefore considered to be an artifact. One repetition of the experiment was performed with longer doxicycline induction times and showed a plateau of HDAC1 or HDAC2 protein levels after four days of activation of the conditional HDAC1 or HDAC2 expression system. We deduced that after four days of activation of the conditional system, effects of the expression of the isoform should have taken place. Therefore, most repetitions of this experiment and further studies were performed over a time course of four days.

In conclusion, we demonstrated an efficient knockout of HDAC1 or HDAC2, the suppression of HDAC1/2 expression below detectable limits in the inactive conditional expression system and the expression of HDAC1 or HDAC2 after three days of induction under doxicycline treatment.

Validation of HDAC1/2 Reconstitution in HCT116 Based Model B Cell Lines

We validated the genetic modifications in model B cell lines described in chapter 3.1 on protein level (fig. 3.8). There were two sets of genetic modifications. Both include two knockouts of the endogenous HDAC1 and HDAC2 isoforms. One additionally included a conditional expression of HDAC1 and the other one a conditional expression of HDAC2 respectively. For each of the two sets of genetic modifications, three clonal cell lines were created and tested.

We compared clonal model B cell lines with a conditional expression of HDAC1 or HDAC2 to the expression of class I HDACs in HCT116 wild type cells. HDAC1, 2, 3 and 8 as well as GAPDH as a protein amount loading control are shown. Clonal lines were cultured for at least two weeks with doxicycline prior to the experiment, then doxicycline was removed for up to four days as indicated. For cell lines with a conditional expression of HDAC1 (panel A), HDAC2 protein was not detected, confirming the efficiency of the knockout in model B cells. HDAC1 expression started to decrease after two days of doxicycline withdrawal and disappeared completely after four days. Upon expression loss of HDAC1, an increase of HDAC3 protein was detected. Around day three to day four after doxicycline removal, HDAC8 protein

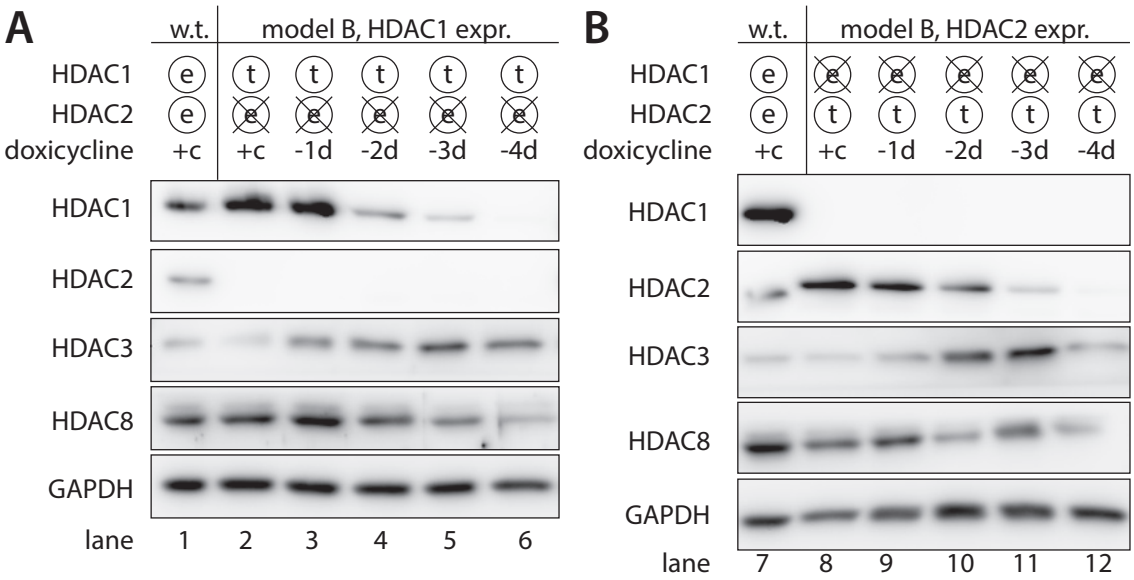

Figure 3.8 Validation of the class I HDAC protein expression pattern in model B cell lines.
Representative images of class I HDAC protein expression in model B cell lines. **A)** Model B cells with conditional HDAC1 expression in the background of a double knockout of endogenous HDAC1 and HDAC2 were cultured with doxicycline present. Doxicycline was withdrawn over a period of four days. In lane one, HCT116 wild type cell extracts were loaded for comparison. **B)** In analogy to panel A, doxicycline was removed in model B cells with conditional expression of HDAC2 in the background of a knockout of both endogenous HDAC1 and HDAC2. Western blots were performed from whole cell lysates and show a representative image of a clonal cell line of three cell lines per genetic condition. (d = day, +c = cultured with, e = endogenous, t = transgenes of the conditional system introduced into the host cell genome with a background knockout of the endogenous isoform)

levels decreased. For cell lines with a conditional expression of HDAC2 (panel B), HDAC1 protein was only detected in the wild type sample, confirming the efficiency of the HDAC1 knockout in these clones. HDAC2 expression from the transgene started to decrease after two days of doxicycline removal and was completely lost after four days. Upon HDAC2 expression loss, HDAC3 protein levels started to increase. HDAC3 and HDAC8 protein abundance decreased at day four of doxicycline removal. Similar for both model B cell lines, HDAC3 protein levels increased, when the conditional expression was lost. The increase was consistent with previous work, which found an HDAC3 up-regulation in mouse embryonic stem cells upon knocking out HDAC1 and HDAC2[154]. The observed reduction of HDAC8 protein levels upon loss of HDAC1 and HDAC2 (in fig. 3.8) suggested that the synthetic lethality of the double knockout caused this reduction. This analysis is supported by the observation that individual expression level changes of either HDAC1 or HDAC2 did not alter HDAC8 protein levels (see fig. 3.6).

In summary, we confirmed the efficiency of the double knockout of both endogenous HDAC1 and HDAC2 in model B cells. We also showed that the conditional expression can be turned off by doxicycline withdrawal in model B cells, without triggering compensation from the corresponding endogenous isoform. These data suggest that model B cell lines are a useful tool to investigate effects depending on a single isoform.

Validation of Conditional HDAC2 Expression in the Co-115 Model C Cell Line

The third model cell lines created was based on the Co-115 parental cell line (cell line creation described in chapter 3.1). Here, we examined the conditional expression of HDAC2 in the background of an endogenous knockout of HDAC2 in model C cells. Next to the validation of the HDAC expression pattern, we tested if we would be able to observe a cross regulation of the native isoform similar to the regulation previously observed in HCT116 based cell lines models.

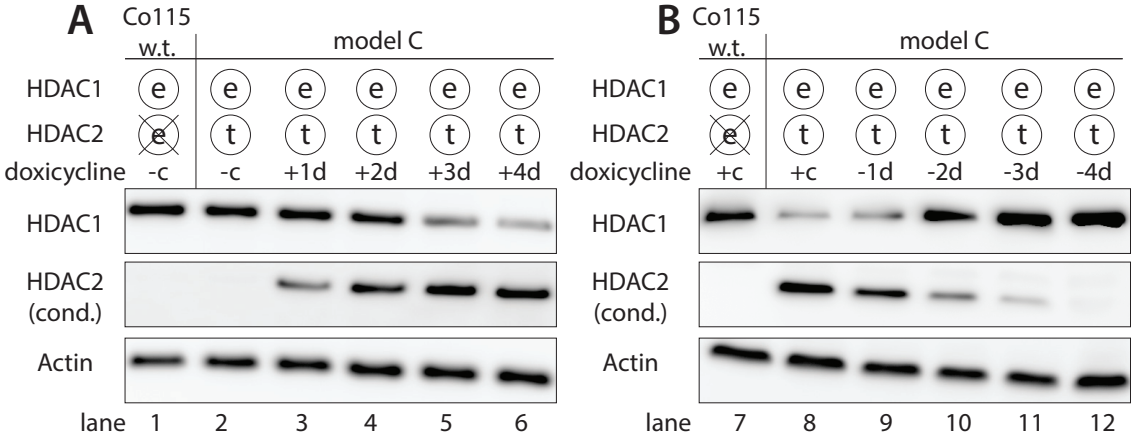

Figure 3.9 Verification of HDAC2 conditional expression in model C cells.
A) Time course of doxicycline addition in Co-115 wild type cells and model C cells with transgenic conditional expression of HDAC2. Before the experiment wild type cells and model C cells were cultured for at least two weeks without doxicycline. **B)** Time course of doxicycline removal in model C cells. Before the experiment wild type cells and model C cells were cultured for at least two weeks with doxicycline. Western blots were measured from whole cell lysates and show representative western blots of two experiments. (e = endogenous, crossed out e = natively deficient, t = transgenes of the conditional system introduced into the host cell genome)

We investigated HDAC1 and HDAC2 protein levels after doxicycline addition (panel A) or removal (panel B) over several days in model C cells. Upon activation (panel A), HDAC2 expression became detectable after one day and reached a maximum after three days. Similarly, HDAC2 expression decreased after one day of doxicycline withdrawal and the protein levels were undetectable after four days (panel B). These observations confirmed the successful transduction of the conditional expression of HDAC2 in the model C cell line. Additionally, we observed a reduction of native HDAC1 protein levels upon HDAC2 expression, as well as a return to native HDAC1 protein levels, when the conditional expression of HDAC2 was lost after inactivation of the system. Thus, our data suggested that a certain compensatory regulation of the overall HDAC1/2 protein amount exists in human cells, which we chose to further investigate.

Compensation between HDAC1 and HDAC2 on Protein Level

We verified the genetic modifications, which were introduced into HCT116 cells and Co-115 cells. In the process of this verification, we observed a cell type independent compensation between HDAC1 and HDAC2 protein levels. Changing the expression of either HDAC1 or HDAC2 influences the protein levels of the corresponding native isoform in a compensatory way (fig. 3.6 and 3.7). This effect was also observed in the Co-115 based model C cell line (fig. 3.9).

Compensation between HDAC1 and HDAC2 describes a process, in which cells try to maintain a constant amount of both isoforms together. The artificial disruption of one isoform's expression lead to an increase of the other isoform. Overexpression of one isoform lead to a reduction of the other isoform. We observed this compensation between HDAC1 and HDAC2 for each isoform in HCT116 cells and independently in Co-115 cells, which raised the question where the regulation of endogenous isoforms takes place.

Regulation of Compensation on the Post-Transcriptional Level

After observing the compensation of HDAC1/2 on protein level, we wanted to further pinpoint the underlying mechanism to the mRNA or protein level. We isolated total protein extracts as well as mRNA from identical samples and compared the reduction in protein levels with the reduction in mRNA levels over time (fig. 3.10).

We analyzed protein levels, where doxicycline was removed for increasing time periods in model A cells with the conditional expression system of HDAC1 in the background of the knockout of endogenous HDAC1 (panel A). In the leftmost lane, the cells were cultured with doxicycline and in the rightmost lane they were cultured without doxicycline. In between, doxicycline was removed for the indicated times. To compare protein levels with mRNA, we isolated RNA from identical samples. For the purpose of normalization, mRNA levels in an additional HCT116 wild type sample were measured and the mRNA sample of model A cells without doxicycline was omitted (-c). In analogy to the previous HDAC1 expression loss, model A cells with the conditional expression system of HDAC2 in the background of a knockout of endogenous HDAC2 were analyzed (panel C and D).

The protein expression of HDAC1 started to decrease at the first day and was lost completely after three days (panel A). Together with this loss, an increase of HDAC2 protein was observed, which correlated in a timely manner to the loss of HDAC1. Relative HDAC1 mRNA levels showed a ten-fold higher mRNA level in model A cells cultured with doxicycline compared to wild type levels. These high mRNA levels decreased within two days. The relative HDAC2 mRNA levels stayed constant around wild type levels over the course of the four day doxicycline removal. The rapid loss of HDAC1 mRNA is an expected property of the conditional expression system and correlated with the loss of HDAC1 protein in panel A. The result of constant HDAC2 mRNA levels excluded a regulation on transcript level and thereby indicated that the regulation of endogenous HDAC2 protein abundance happened on a post-transcriptional level. In the second half, HDAC2 protein expression started to decrease after two days and was lost after three to four days of doxicycline removal (panel C). Simultaneously to the loss of HDAC2 protein, the abundance of HDAC1 protein increased. On mRNA level, we revealed a 60-fold difference between wild type cells and model B cells cultured with doxicycline (panel D). Upon removal of doxicycline the mRNA level dropped within four days to almost zero. The high HDAC2 mRNA levels resulted from the active transgene, and the loss of mRNA correlated well with the loss of protein over time. Endogenous HDAC mRNA levels stayed constant during the loss of the conditionally expressed HDAC protein and mRNA.

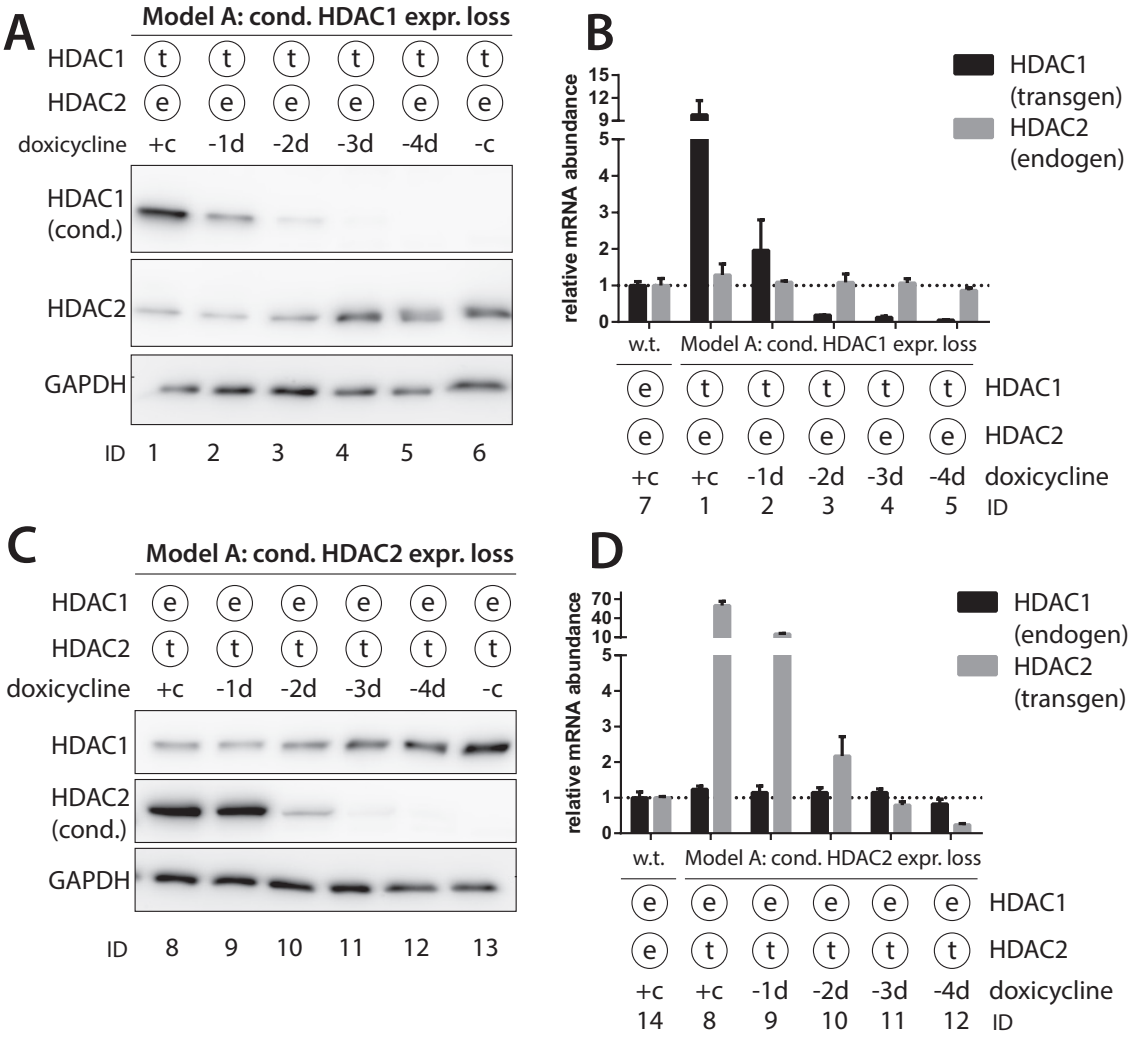

Figure 3.10 HDAC1/HDAC2 compensation on protein level is not reflected on mRNA levels.
A) Time course of doxicycline withdrawal in model A cells with a conditional overexpression of HDAC1 in the background of a knockout of endogenous HDAC1. Doxicycline was removed for the indicated times and these samples were compared to the same line cultured with or without doxicycline (indicated by +c or -c). Cells not marked by -c were cultured for at least two weeks with doxicycline prior to the experiment. **B)** Relative mRNA levels are shown for HDAC1 and HDAC2 for the time course shown in panel A. HDAC1 and HDAC2 mRNA levels were normalized to HCT116 wild type levels. **C)** In model A cells with a conditional expression of HDAC2 in the background of a knockout of endogenous HDAC2 doxicycline was withdrawn over time in a similar manner to panel A. **D)** Relative mRNA levels are shown for HDAC1 and HDAC2 for the time course shown in panel C. Identical samples were split for protein and mRNA analysis. Western blots were measured from whole cell lysates and show representative western blots of two experiments. Relative mRNA levels are shown by mean values with SEM error bars of three technical mRNA replicates of reverse transcriptase reactions of a single experiment.

Taken together, the compensation of HDAC1/2 protein levels was not observed at the mRNA level. These data indicate a mechanism on protein level, which could be either a difference in the translation speed of the mRNA or a difference in protein turnover (either by degradation of low stability). For the isoforms transcribed from the transgene, we observed high mRNA levels compared to wild type mRNA levels, which did only result into protein levels comparable to wild type protein levels of HDAC1 and HDAC2. We chose to further investigate this discrepancy.

Higher Overall Translation of HDAC1 or HDAC2 Expressed from the Transgene Compared to Endogenous Expression

We hypothesized that observing high mRNA levels and moderate protein levels could be explained by a high level of protein synthesis and a fast proteasomal degradation. Under the assumption of equal translation speeds for the exogenous and endogenous HDAC1 and HDAC2 mRNA, we tested if exogenously introduced HDAC1 or HDAC2 protein accumulated faster than protein transcribed and translated from the endogenous gene, when the proteasomal degradation pathway was inhibited. A validation of the hypothesis would be an accumulation of HDAC2 or HDAC2 protein originating from the transgene, when compared with the endogenous HDAC1 or HDAC2 levels respectively.

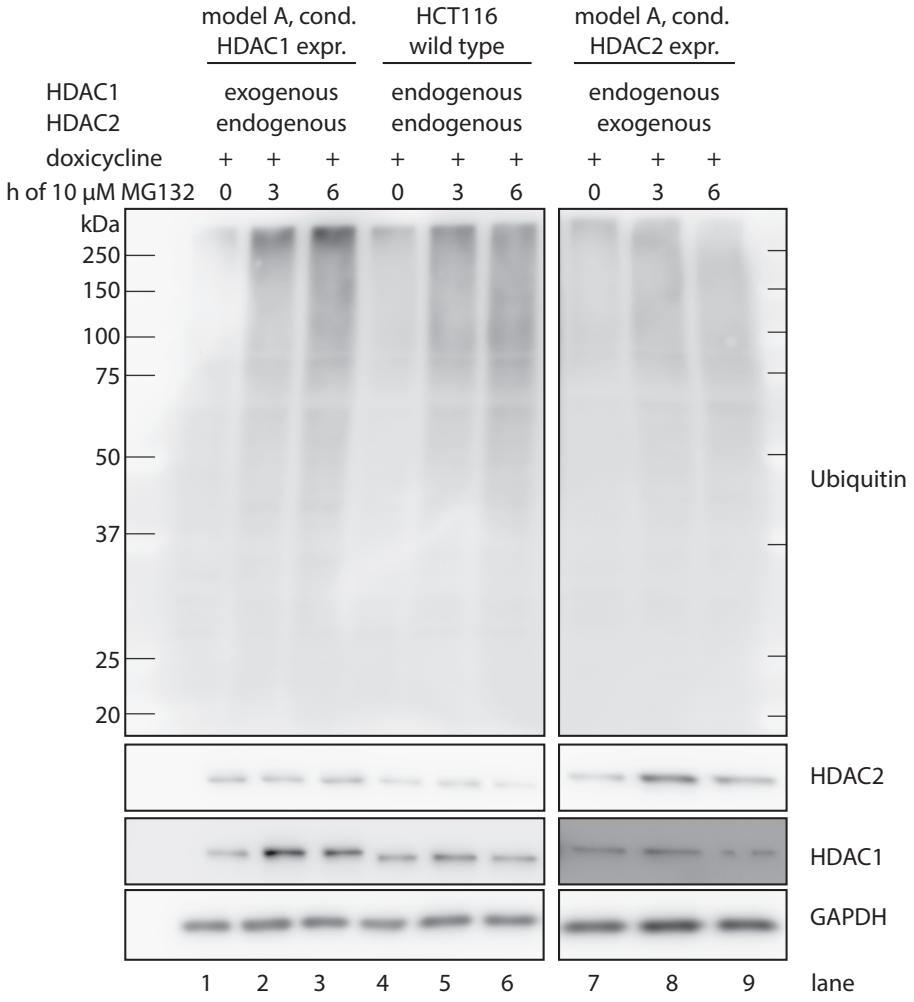

Figure 3.11 HDAC1 and HDAC2 expressed from the transgene accumulate faster than the endogenous isoforms. HCT116 wild type cells and both model A cell lines with active conditional expression of HDAC1 or HDAC2 were treated with 10 µM of the protasome inhibitor MG132 for zero, three or six hours. Cells were cultured with doxicycline for at least two weeks prior to the experiment. Model A cells with a conditional expression of HDAC2 in the background of a knockout of the endogenous isoform were measured on a separate blot. Whole protein extracts were loaded to measure protein and ubiquitination levels.

HCT116 wild type cells and model A cells were cultured with doxicycline and treated with the proteasomal inhibitor MG132 for the indicated times (fig. 3.11). Over three and six hours of treatment, the general amount of ubiquitinated proteins increased in all tested cell lines, proving that the proteasomal inhibition was working with this concentration and in this time

frame. For model A cells with active conditional HDAC1 expression (left three lanes), endogenous HDAC2 and GAPDH did not accumulate nor show a band at higher molecular weights, which would indicate ubiquitination. In these three samples, HDAC1 expressed from the transgene showed a three-fold accumulation upon proteasomal inhibition, but no slower migrating band at higher molecular weights. In the three wild type samples neither the expression of endogenous HDAC1, HDAC2 or GAPDH showed an accumulation upon proteasomal inhibition (mid three lanes). For model A cells with an active conditional expression of HDAC2 neither endogenous HDAC1 nor GAPDH accumulated upon MG132 inhibition (right three lanes). HDAC2 expressed from the transgene accumulated three-fold. From the three-fold accumulation, we inferred a three times faster proteasomal degradation of the exogenously introduced isoforms. While the result of increased degradation of exogenous isoforms may explain some of the discrepancy between HDAC1/2 mRNA and protein levels originating from the transgene, we assumed that another mechanism was at play too.

The proteasome is one of the major degradation pathways in human cells, but cellular protein abundance could also be influenced by degradation by non-proteasomal proteases or by the inherent stability of a protein itself. To test, if non-proteasomal proteases or protein stability differs between HDAC1 and HDAC2 between exogenous or endogenous origin, we inhibited translation by cycloheximide (CHX) treatment. If the exogenous HDAC isoforms were to disappear faster than the endogenous isoforms, then this would be an explanation for high exogenous mRNA levels and moderate resulting protein levels. We compared HDAC1 and HDAC2 protein levels in HCT116 wild type and model A cells by treatment with the translation elongation inhibitors CHX and puromycin (fig. 3.12).

First, we treated HCT116 wild type cells and model A cells containing a conditional expression of HDAC1 with 180 µM CHX for the indicated times or 2 µM puromycin for eight hours. CHX treatment concentrations were based on a previous study that reduced HDAC1/2 levels performed by Zhang *et al.*[155] C-myc protein levels served as a control. CHX treatment successfully reduced c-myc protein levels to an undetectable amount after four hours, proving that the CHX treatment was working with this concentration and in this time frame. On the other hand, the puromycin treatment did not reduce c-myc protein abundance and was therefore considered to be ineffective. For HCT116 wild type cells, HDAC2 and GAPDH protein levels did not decrease within the treatment time frame (panel A, left half). HDAC1 abundance seemed to decrease after eight hours of CHX treatment. For model A cells with a conditional expression of HDAC1 neither HDAC1 nor HDAC2 nor GAPDH abundance decreased upon CHX treatment (panel A, right half). The unchanged protein abundances of HDAC2, GAPDH and transgenic HDAC1 meant that these proteins did not decay and were not degraded in this time frame, since new production of protein was inhibited by the translation elongation inhibitor CHX.

For validation, we performed a repetition of identical wild type samples (panel B, left half). We analyzed model A cells with active conditional expression of HDAC2, under identical

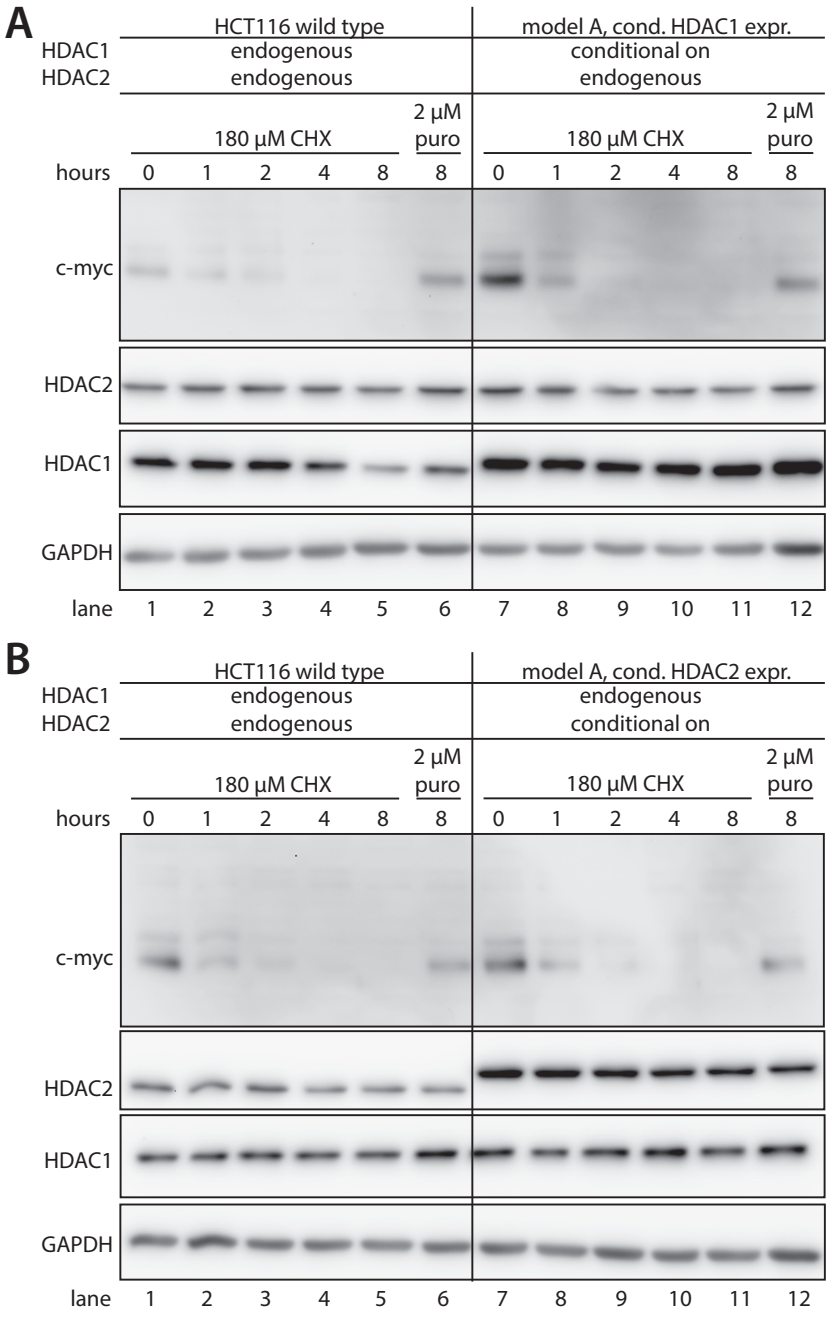

Figure 3.12 Comparable protein stability between endogenous and exogenous HDAC1 or HDAC2 expression.
A) HCT116 wild type cells and model A cell with doxicycline induced HDAC1 expression were treated with CHX or puromycin for increasing times. **B)** In a similar manner, HCT116 wild type cells and model A cell with active conditional HDAC2 expression were treated with CHX and puromycin. Protein levels were measured by western blot from whole cell lysates. (CHX = Cycloheximide, puro = puromycin)

conditions (panel B, right half). For wild type cells neither GAPDH nor HDAC1 nor HDAC2 showed a decrease in the eight hour time frame. As the wild type HDAC1 protein levels did not decrease, we considered the observation of the reduction in panel A as an artifact. While CHX treatment proved to be effective in the reduction of the control protein c-myc, non of the other proteins in these western blots showed a reduction upon treatment. This meant that there was no difference in the degradation and stability of endogenous HDAC1/2 compared to the isoforms expressed from the transgene.

The proteasomal inhibition data indicated either an increased stability or an increased overall translation of HDAC1 or HDAC2 expressed from the transgene. The protein level comparison indicated a similar protein stability and degradation of HDAC1/2 expressed from the transgene compared to the endogenous isoforms. Nonetheless, the increase in translation can only explain some of the mRNA-protein discrepancy observed (see fig. 3.10). Therefore, we suspected a difference in the translation rate between the mRNAs from the endogenous gene and the transgene. This lead us to question our assumption of equal translation speeds from endogenous mRNA compared to mRNA transcribed from the transgene.

Lower Protein Expression from the T2A Containing Transcript Compared to non-T2A Control Transcript

We postulated the hypothesis that the mRNA translation rate was reduced in the transgene, which might explain a part of the mRNA - protein discrepancy (observed in figure 3.10). In the active conditional expression system, one transcription read produced a single transcript encoding a HDAC-T2A-GFP mRNA sequence. The T2A sequence causes a ribosomal skip producing two individual proteins from one transcript with every translation start[156, 157]. Alternatively, during translation 2A sequences can cause the ribosome to fall off or read through the 2A sequence[157]. Since the T2A sequence shows a high efficiency for ribosomal skipping[156, 157], a near one to one ratio between the protein connected by a T2A sequence was assumed[158]. Because of this 1:1 ratio between HDAC and GFP, which results from the sequence, GFP fluorescence was an indicator for the corresponding HDAC protein levels.

During the cell line creation process, we noticed a low GFP fluorescence of cells with the conditional HDAC1 or HDAC2 expression system compared to control cell lines with conditional GFP expression. Fluorescence microscopy was barely able to detect GFP fluorescence in model B cells (see figure 6.3 in the appendix). We quantified the observation of low GFP fluorescence translated from the EF1α-HDAC-T2A-GFP mRNA sequence and compared it to the fluorescence of the translated EF1α-GFP mRNA sequence in a flow cytometry analysis.

In a flow cytometry analysis, GFP fluorescence was plotted against dsRED fluorescence (figure 3.13 panel A-D). The analysis of HCT116 wild type cells served as a control for the autofluorescence of individual cells (panel A). HCT116 cells infected with the base version of the pLVTHM vector and the repressor containing vector show two distinct populations, separated by their GFP fluorescence intensity (panel B). GFP positive cells carried the empty conditional system with the EF1α-GFP transgene. GFP negative cells only carried the repressor part of the conditional expression system.

One representative clone of either HDAC1 or HDAC2 expressing cells with a double knockout of the endogenous isoforms (model B) where GFP was expressed from the EF1α-HDAC-T2A-GFP transgene was measured. The green fluorescence of model B cells was lower (panel C and D) compared to the green fluorescence of GFP positive cells (panel B). We visualized

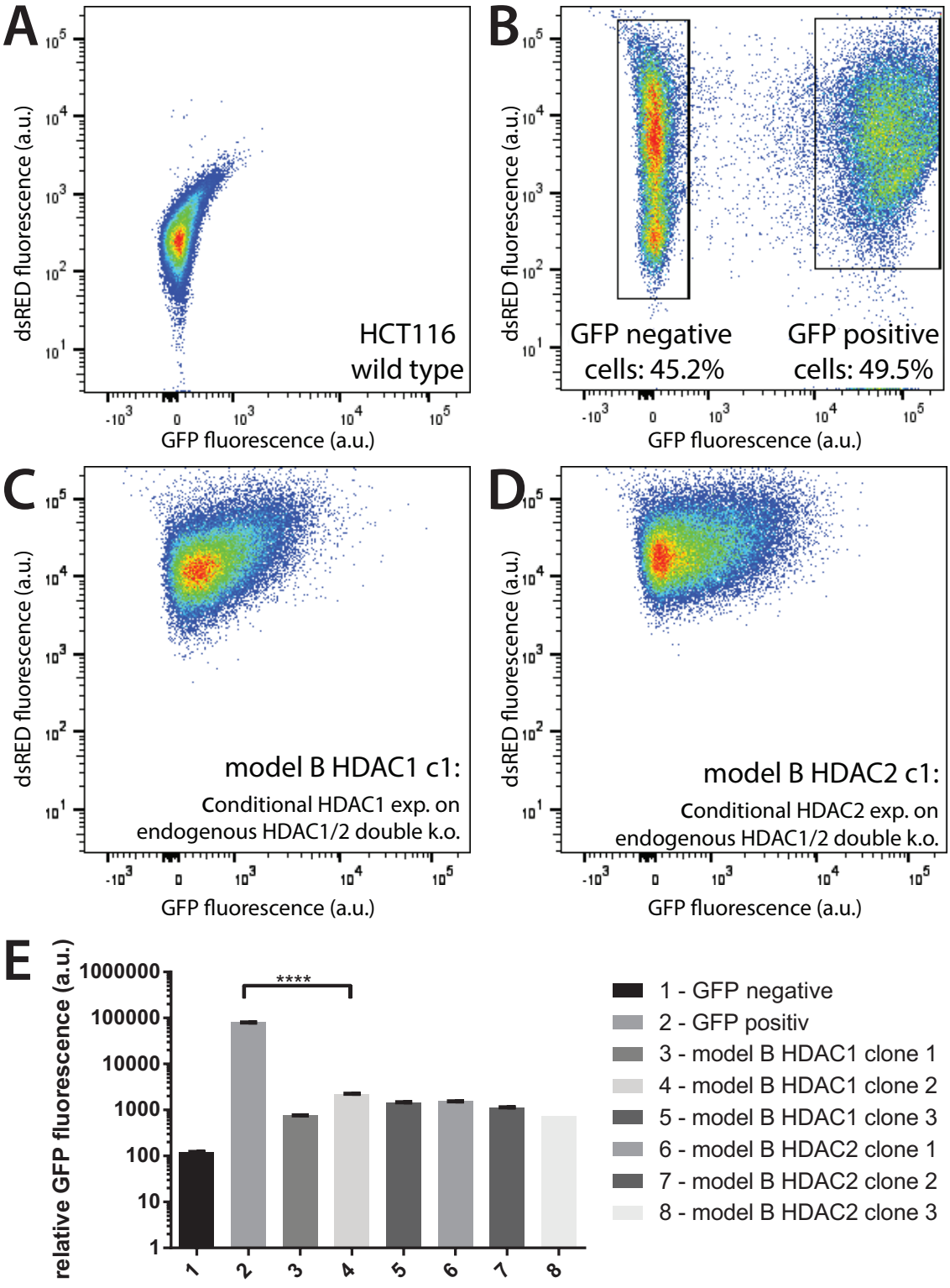

Figure 3.13 Quantification of the lower fluorescence of the EF1α-HDAC-T2A-GFP transgene by flow cytometry.
A) Flow cytometry analysis of dsRED and GFP fluorescence of HCT116 wild type cells. **B)** Unsorted population of HCT116 cells with dsRED fluorescence of the pLV-tTRKRAB vector and GFP fluorescence from the base pLVTHM vector. Two populations, which are separated by their GFP fluorescence, are marked. **C)** dsRED and GFP fluorescence from model B cells expressing HDAC1 in the background of a knockout of both endogenous HDAC1 and HDAC2 isoforms. **D)** dsRED and GFP fluorescence from model B cells expressing HDAC2 in the background of the double knockout. One representative flow cytometry analysis out of three individual clones is shown for each part of model B in panels C and D. **E)** Quantification of the GFP fluorescence in panels B-D. For clarity only one significance bar is shown. Mean values with SEM error bars of FACS events are depicted and significance was determined with a 1-way ANOVA test. (c1 = clone number one)

this difference in a bar diagram, which showed a 100-fold difference in GFP fluorescence between all six clonal modal B cell lines compared to the cells expressing GFP without the T2A sequence (panel E). These data showed that the EF1α-HDAC-T2A-GFP construct resulted into less protein than the EF1α-GFP construct.

Because HDAC and GFP are present on the same transcript, the high HDAC mRNA levels from the EF1α-HDAC-T2A-GFP transgene also imply that there is an equally high amount of GFP mRNA. This in turn, suggested high GFP protein levels. Because of the 1:1 ratio between GFP and HDAC during translation[156], the difference of the GFP protein expression between the EF1α-GFP and the EF1α-HDAC-T2A-GFP transgene showed a negative impact of this particular HDAC expression transgene on protein yields. While HDAC1 and HDAC2 appear to be regulated to maintain a constant overall activity, GFP is of non-mammalian origin and it's expression should therefore not be specifically regulated. This suggested that the T2A sequence may have slowed translation of the complete transcript and thereby reduced the translation of the upstream and downstream gene sequences. This in turn could explain the mRNA/protein discrepancy of the conditional expression system.

Concluding from this chapter, we were able to confirm the genetic modifications concerning HDAC1 and HDAC2 in models A through C. In this process, we observed a counter regulation between the isoforms on protein level, but not on mRNA level. The expression from the transgene produced high mRNA levels relative to the wild type cells. This discrepancy was in part attributed an altered translation originating from the ribosomal skip introduced by the T2A-sequence in the transgene. We decided to further analyze the phenotype of the model cell lines.

3.3. Comparable Effects of HDAC1 and HDAC2 on Proliferation and the Cell Cycle Profile

In this chapter we followed up on the observation that model B cell lines did not grow when HDAC1 and HDAC2 expression were lost. We investigated if HDAC1 or HDAC2 protein expression loss had a differential effect on proliferation and the cell cycle profile.

HCT116 Proliferation Tolerates HDAC1 or HDAC2 Single Knockouts and is Impeded by the Knockout of both Isoforms Together.

Since it was known that HDAC1 and HDAC2 knockouts impair the proliferation of various cell lines [151, 154], we investigated the effect of single and double knockouts of HDAC1 and/or HDAC2 on the proliferation of HCT116 cells. We compared the proliferation of model B cells cultured with and without doxicycline to HCT116 wild type cells and single HDAC1 or HDAC2 knockout cell lines and examined if there were differences between cells expressing HDAC1 or HDAC2 with regards to proliferation (fig. 3.14).

To assess proliferation, we grew cells over a time frame of six days and counted Hoechst stained nuclei. When model B cells with a conditional HDAC1 expression in the background of a knockout of endogenous HDAC1 and HDAC2 were treated with doxicycline, the number of counted nuclei increased until day five of the experiment and stayed constant from day five to day six (panel A). Upon doxicycline withdrawal at day zero the proliferation was unchanged until day three, but from day three until day six the number of counted nuclei did not increase further. Similarly, when model B cells with a conditional HDAC2 expression in the background of the knockout of both endogenous isoforms were continuously treated with doxicycline, the amount of counted nuclei increased until day five of the experiment and stayed constant from day five to day six (panel B). After doxicycline withdrawal in these model B cells, the amount of nuclei increased until day two of the experiment and then stayed in the same magnitude until day six. The time courses of the proliferation arrest correlated with the time courses of protein level loss (see fig. 3.8 on page 55). In this regard both isoforms HDAC1 and HDAC2 were equal. This means that the loss of protein expression of both HDAC1 and HDAC2 together lead to a growth stop of this HCT116 model B cell lines.

For HCT116 wild type cells as well as cell lines with single HDAC1 or HDAC2 knockouts, the number of counted nuclei increased until day five and stayed constant from day five to day six. The proliferation of HCT116 wild cells was similar to the proliferation of model B cell lines when cultured with doxicycline and neither doxicycline, nor single HDAC1 or HDAC2 knockouts influenced the increase in cell numbers (3.14, panel C). This meant that genetic modifications resulting in a single knockout protein state in model B cells did not impede cellular proliferation. The stagnating increase at day six visible under all conditions without impediment was due to the cells growing confluent on the 96 well plate in the experimental setup.

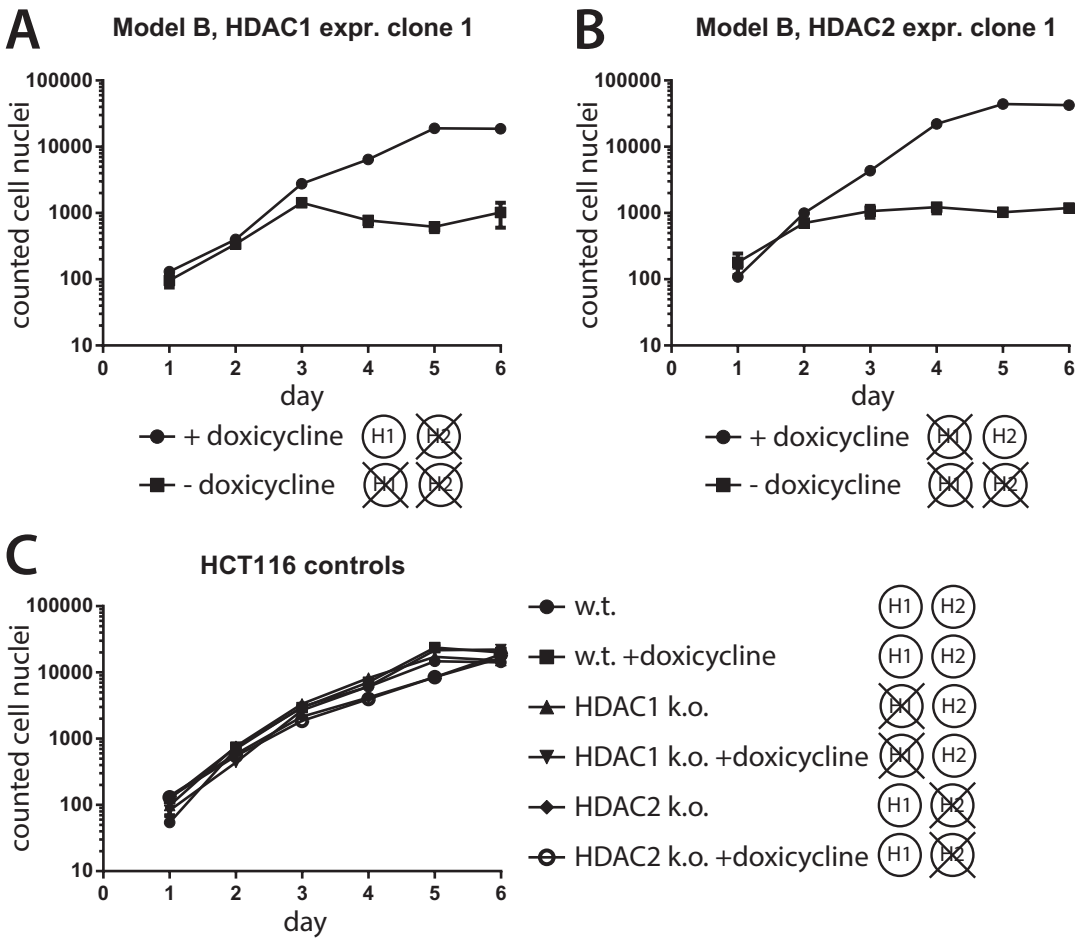

Figure 3.14 Loss of HDAC1 and HDAC2 together lead to a stop in cell proliferation.
A) Clone one of model B cell lines with a conditional expression of HDAC1 in the background of the knockout of endogenous HDAC1 and HDAC2 was cultured with doxicycline prior to the experiment. The continued treatment with doxicycline and the withdrawal at day zero of the experiment are shown. **B)** Similar to panel A, clone one of model B cells with a conditional expression of HDAC2 in the background of the double knockout are shown. **C)** HCT116 wild type cells, HCT116 cell with a single knockout of HDAC1 and HCT116 cells with a single knockout of HDAC2 were either cultured with or without doxicycline. Cells were seeded in 96 well plates and Hoechst stained nuclei were counted in an Operetta System. Mean values ±SEM of three technical replicates per cell lines and condition are shown. Clones two and three of each model B cell line are depicted in the appendix in fig. 6.1 on page 124.

We were able to show that both isoforms were individually sufficient to sustain the proliferation of HCT116 cells. We have observed that the cell numbers stayed roughly constant after the growth arrest, which opened the question in which cell cycle state these HDAC1/2 deficient cells arrested.

HDAC1 together with HDAC2 Expression Loss Lead to a G2/M Phase Block

In direct follow-up, an analysis of the cell cycle was performed to determine in which cell cycle phase the proliferation stop happened. Once more, we examined if there was a difference between cells that just lost residual HDAC1 or HDAC2 protein expression.

To precisely analyze this question, six conditions were compared by flow cytometry analysis of DNA content of Hoechst-33342 stained nuclei (fig. 3.15). Doxicycline treatment in wild-type cells showed no significant difference in any cell cycle phase, when doxicycline was

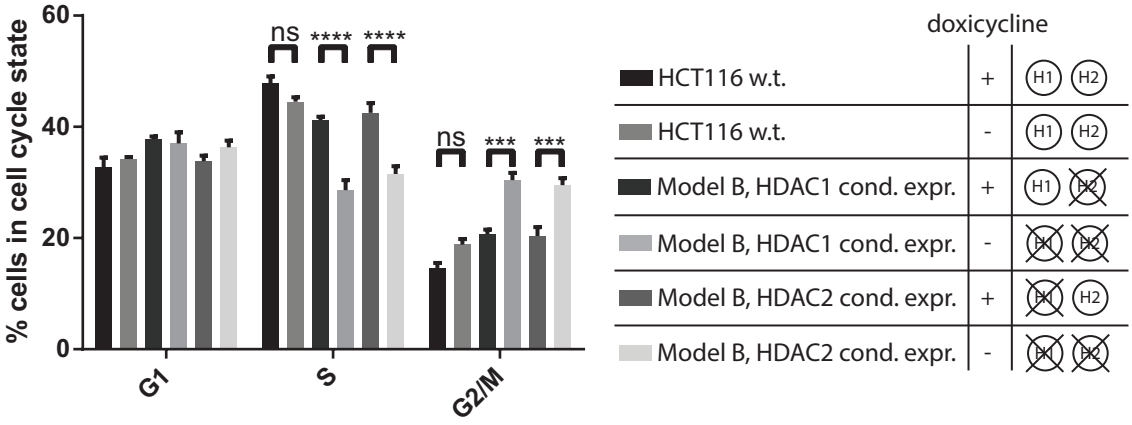

Figure 3.15 Loss of HDAC1 and HDAC2 together lead to a reduction in S phase cells and an increase in G2/M phase cells. Cell cycle analysis by flow cytometry of Hoechst-33342 stained DNA content of fixed cells. Three cell lines were either treated with doxicycline or doxicycline was removed at day zero of the experiment: HCT116 wild type cells, model B cell lines with a conditional HDAC1 expression and model B cell lines with a conditional HDAC2 expression. Means ±SEM from three clonal replicated for each model B condition and two technical replicates for HCT116 wild type cells are shown. Statistical significance was determined using a 2-way ANOVA test. (ns = not significant)

withdrawn in HCT116 wild type cells. This means doxicycline by itself did not alter the cell cycle. Doxicycline removal in both model B cell lines showed a relative reduction of S-phase cells and a relative increase in G2/M phase cells, when doxicycline was withdrawn. This meant that the loss of HDAC1 and HDAC2 together lead to a cell cycle block either in the G2- or M-phase, suggesting a block at the G2/M-phase transition checkpoint. Taken together, these results showed that both HDAC1 and HDAC2 protein expression were sufficient to maintain a wild type like cell cycle profile.

Since cellular proliferation and the cell cycle profile were influenced by HDAC1 and HDAC2 in a similar manner, we concluded that these two phenotypic readouts were not isoform selective. While searching for isoform selective effects between HDAC1 and HDAC2, this leaves molecular readouts like transcripts and acetylations sites to be investigated.

3.4. Transcriptome Analysis of HDAC1- and HDAC2-Knockout Cells

In the previous chapter, we observed growth limitations and a G2/M phase cell cycle block in HCT116 cells upon loss of the expression of both HDAC1 and HDAC2. Single knockouts of either isoform did not show a phenotype in these readouts. In order to further investigate less pronounced effects of individual isoforms, we performed a comprehensive transcriptome analysis.

Design of the Transcriptome Analysis

The presence of HDAC1 and HDAC2 in multiprotein complexes let us build the hypothesis that through HDAC1 or HDAC2 dependent binding of these complexes to promoter regions of genes, the transcription of some of these genes was influenced differently by either HDAC1 or HDAC2. The untargeted nature of a transcriptome analysis was specifically intended to help in this search for isoenzyme selectivity.

We compared relative mRNA levels of the HCT116 wild type line with model B lines with either active conditional expression of HDAC1 or HDAC2 in the background of the knockout of HDAC1 and HDAC2 (fig. 3.16, panel A). By design, the software analysis program was limited to compare two conditions, but it was able to take replicates into account.

The three genetic conditions we compared led to three comparisons (figure 3.16, panel B). In comparison number one, HCT116 wild type mRNA levels were compared to model B cells with active conditional expression of HDAC1 in the background of a double knockout of endogenous HDAC1 and HDAC2. These model B cells correspond to a single knockout of HDAC2 in their class I HDAC protein expression. In comparison number two, wild type cells were compared to model B cells with active conditional expression of HDAC2 in the background of a double knockout of endogenous HDAC1 and HDAC2. These cells correspond to single knockouts of HDAC1 in their class I HDAC expression. The third comparison was between the lines expressing either HDAC1 or HDAC2. In all comparisons, we found a total of 771 up-regulated and 605 down-regulated genes (fig. 3.16, panel C). With respect to the total number of 23219 identified transcripts in all datasets, this represents 5.9 %. Notably, there were more genes up-regulated than down-regulated in the single HDAC knockouts compared to HCT116 wild type cells. This means the loss of the expression of either HDAC1 or HDAC2 lead to more active transcription. In a model, where HDAC loss leads to increased acetylation levels, which in turn lead to more euchromatin regions and elevated levels of transcription, more up-regulated genes were an expected result. This transcriptome analysis setup enabled us to investigate effects of single knockouts on individual transcripts. Before the investigation, we wanted to confirm the genetic modifications in the measured samples.

A RNASeq dataset

HCT116 cell line	HDAC1 status	HDAC2 status	replicates
wild type	endogenous	endogenous	2x technical
model B cond. HDAC1	exogenous	knockout	3x clonal
model B cond. HDAC2	knockout	exogenous	3x clonal

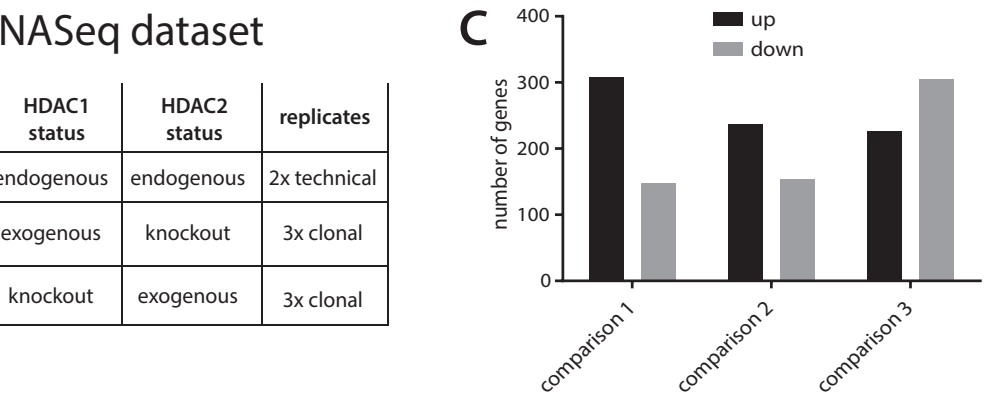

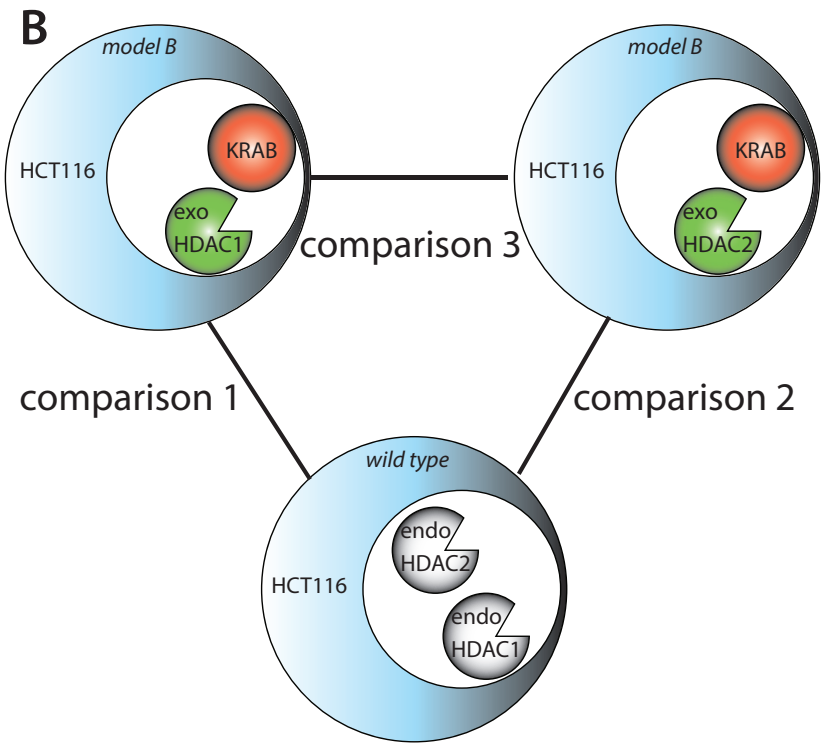

Figure 3.16 Comparison of the transcriptomes of HDAC1 k.o., HDAC2 k.o. and HCT116 wild type cells.
A) The HDAC status of the three compared conditions is depicted and the replicates are stated. All cell lines were cultured with doxicycline to ensure active conditional expression in model B cells. **B)** In the transcription analysis three conditions with two or three replicates each were compared pairwise leading to three comparisons. **C)** Transcripts significantly up- or down-regulated in comparison to wild type cells are shown from the dataset of a total 23219 unique transcripts. For comparison three, up- or down-regulation refers to the status in HDAC2 k.o. cell lines compared to HDAC1 k.o. cell lines. Transcript levels were considered significantly different if a p-value below 0.05 was reached. (exo = exogenous, endo = endogenous)

Verification of HDAC1 and HDAC2 Status in the Transcriptome Analysis Data

In order to confirm the genetic modifications in RNASeq data from the samples, we used the sequence alignment information. As the knockouts were achieved by two cuts around exon two of HDAC1 and/or HDAC2 the sequence alignment of all individual reads enabled us to analyze the splicing of matured HDAC1 and HDAC2 mRNA. By analyzing intron spanning reads of HDAC1 and HDAC2, these reads would identify the splicing, which resulted from knockout or non-knockout reads. A Sashimi plot visualizes the intron spanning mRNA reads. Each exon was condensed to a small line and the amount of raw reads between two exons was counted (fig. 3.17). In general the numbers of raw reads were not comparable, since the overall read count may have differed from sample to sample. Within this experiment all eight

samples showed similar total read counts (table 6.2 on page 127 in the appendix), which meant that the relative read counts of intron spanning reads gave a rough representation of the relative transcript levels. Most importantly, the presence of certain intron spanning reads proved either the presence of splicing or the lack of introns.

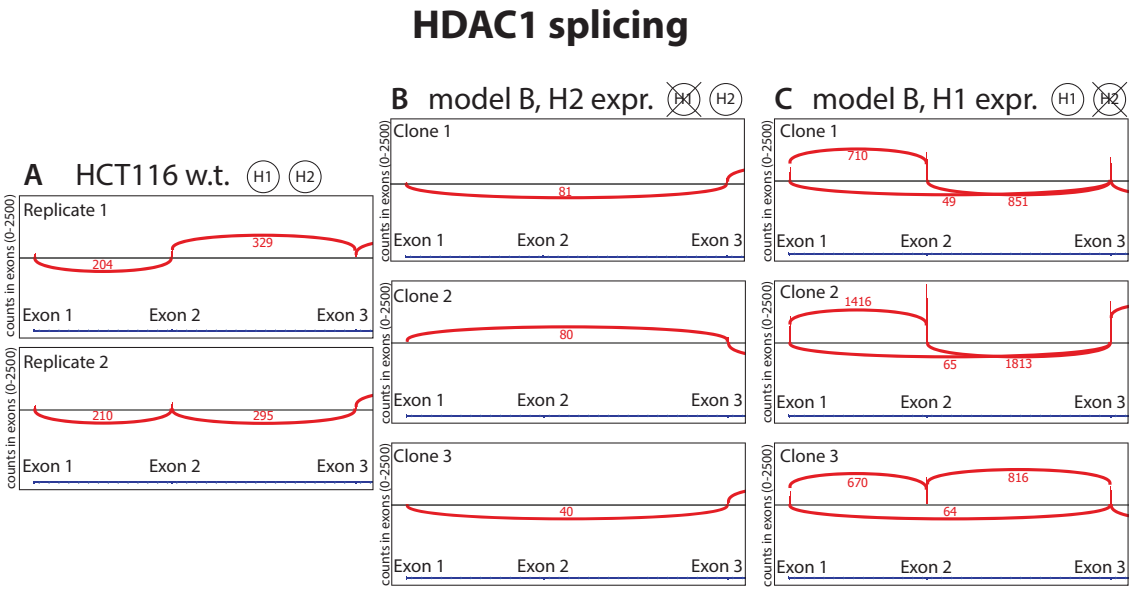

Figure 3.17 Verification of HDAC1 splicing between exons 1-2-3. RNASeq reads between intron one, intron two and intron three of HDAC1 are shown for two replicates of HCT116 wild type cells (panel **A**), three clones of the model B cells with a conditional HDAC2 expression and a double knockout of the endogenous isoforms (panel **B**) as well as three clones with a conditional HDAC1 expression and the double knockouts (panel **C**). Sashimi plots were generated with the tool integrative genomics viewer (IGV)[141].

For both wild type replicates (panel A) the presence of reads between exon one and exon two as well as between exon two and exon three represent the regular splicing. In the model B cell lines with a knockout of both endogenous HDAC1/2 isoforms and a HDAC2 conditional expression (clones 1-3, panel B), the HDAC1 splicing showed reads from exon one to exon three. As the endogenous exon two was removed to create the knockouts, reads from exon one to exon three are proof of the presence of this genetic modification. For the model B cell lines with a HDAC1/2 double knockout and a conditional HDAC1 expression (clone 1-3, panel C) there are reads from exon one to exon two, from exon two to exon three and reads from exon one to exon three. The regular exon one to exon two to exon three splice pattern resulted from the active conditional overexpression system, where the transgene did not contain introns.

These plots confirmed the intended splicing of HDAC1 as introduced during the model cell line creation process. The same analysis was also performed for the first three exons of HDAC2 (fig. 6.2 on page 125 in the appendix). There, the knockout splicing from exon one to exon three was identified in all model B clones and the regular splicing was only identified in the wild type line as well as in the clonal lines with active conditional expression of HDAC2. Taken together, these results confirmed the modified splicing of HDAC1 and HDAC2 in all model B cell line clones and wild type cells on mRNA level.

Identification of Individual Transcripts Influenced by a HDAC1 or HDAC2 Knockout

After gaining confidence in the dataset, we tested our hypothesis that individual transcripts were influenced by the lack of HDAC1 or HDAC2 expression. An individual transcript expression change, which was caused by one set of genetic modifications, should have appeared in two comparisons, since each condition was compared twice. For example, we expected a mRNA level change induced by the loss of HDAC1 protein expression to be identified in the comparison between wild type cells and HDAC1 k.o. cells as well as in the comparison between the HDAC1 k.o. and the HDAC2 k.o. Changes induced by the genetic system should have been identified in both comparisons against wild type cells. To identify relevant transcript level changes, we visualized the overlap of the three comparisons in a Venn diagrams (fig. 3.18). To identify overlapping transcripts that show different expression levels between the HDAC1 k.o. and the HDAC2 k.o. in model B cells, all significantly ($p < 0.05$) altered genes were compared (panel A). The large number of transcripts was narrowed down by only showing transcripts with a fold change above four (panel B).

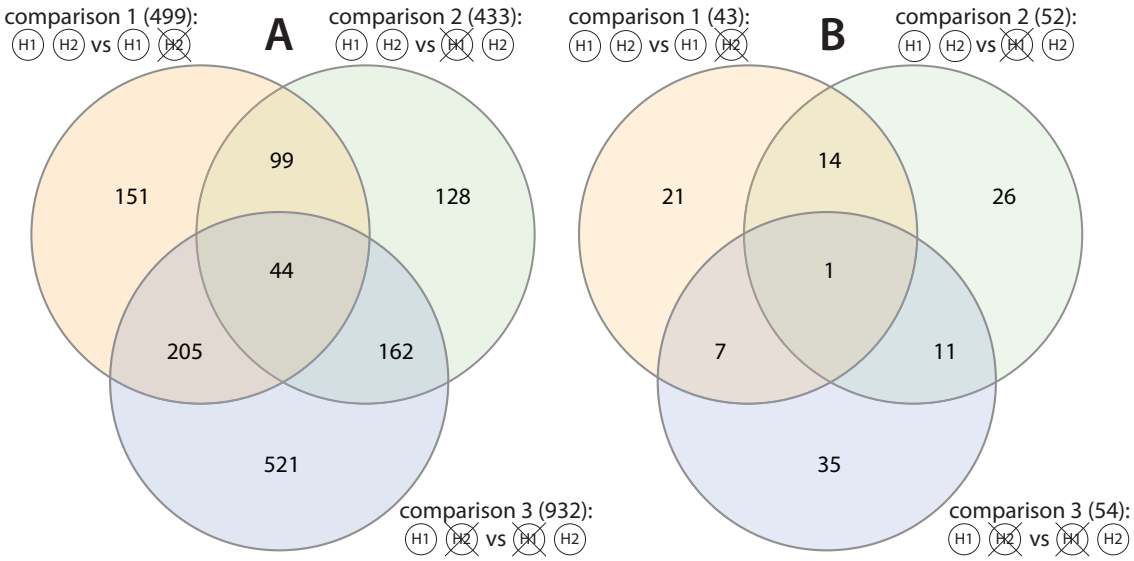

Figure 3.18 Identification of HDAC1- or HDAC2-dependent transcripts. A) Transcripts, which were significantly effected in the three comparisons were compared in a Venn diagram. Transcripts were considered significant with a p-value below 0.05. **B)** To reduce the amount of transcripts, those with an expression difference above four-fold were chosen for further investigation. Venn diagrams were created with the online tool InteractiVenn [159].

Seven transcripts were identified in the overlap between comparison one and comparison three and eleven transcripts in the overlap between comparison two and comparison three. A single transcript was identified in all three comparisons. Transcripts that showed up in the comparisons including the HDAC2 knockout cells seemed to be selectively influenced by the HDAC2 knockout. Similarly, transcripts that showed up in the comparisons including the HDAC1 knockout cells seemed to be selectively influenced by the HDAC1 knockout. The transcript identified in all three comparisons and therefore in the middle of the Venn diagram seemed to differential between HDAC1 and HDAC2 knockouts in the RNASeq data. From this total of 18 transcripts (see table 6.3 in the appendix on page 128) qPCR validations under the same conditions were attempted.

Since these previously identified transcript level changes did not reproduce in qPCR experiments, we were neither able to confirm nor reject our hypothesis. Therefore, we modified our strategy to reproduce transcripts with high fold changes and low p-values.

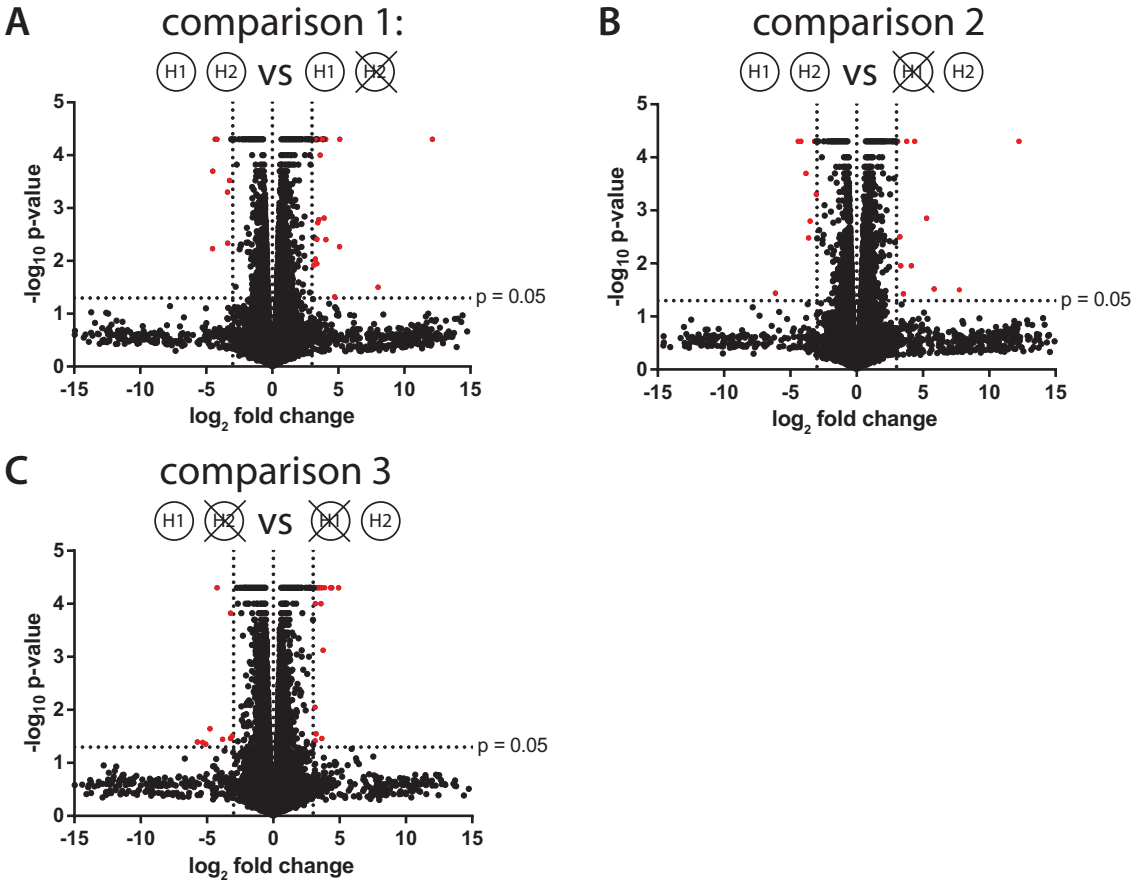

Figure 3.19 Identification of transcript level changes between HDAC1 k.o., HDAC2 k.o. and HCT116 wild type cells. Volcano plot analysis of RNASeq data. The three different conditions with their replicates lead to three pairwise comparisons: **A)** comparison 1, **B)** comparison 2 and **C)** comparison 3 (fig. 3.16 panel A). Individual significant transcript level changes with a fold change above eight are marked in red and summarized in table 3.1.

The altered approach to continue to test our hypothesis consisted of identifying transcripts which combine high fold changes and low p-values. This altered approach would identify transcripts, which could be analyzed for the dependence on HDAC1 and HDAC2 expression in a second step. Plotting negative $\log_{10}$ p-values against the $\log_2$ based fold change of all transcripts in a volcano plot revealed such transcripts. Every point represented a transcript in each of our three comparisons. From the three volcano plots, we selected transcripts with fold changes higher than eight-fold ($\log_2 > 3$) and a p-values below 0.05 ($-\log_{10} > 1.3$). These cutoffs are marked by dotted lines. All three comparisons resulted in transcripts above the threshold criteria. The Cuffdiff calculation also resulted in relative expression values representing the abundance of the transcript ranging from 0-4839. The list of transcripts with significant high fold changes was sorted into higher and lower expression around the arbitrary Cuffdiff expression cutoff of 40 (see table 3.1). The Cuffdiff tool assigned reads from the KRAB repressor to the transcript of ZNF10. Since the repressor was artificially transduced into the cell's genome, this transcript was not influenced by the knockouts and was therefore

excluded from further validation. Multiple other transcripts were identified as candidates for HDAC1 and HDAC2 knockout effects and chosen for qPCR validation.

Table 3.1 RNASeq transcripts with significant and high fold changes.

	wild type	**HDAC2 k.o.**	**HDAC1 k.o.**
higher expression			
ZNF10	0,077762	377,588	346,597
PRF1	6,99979	95,4571	105,404
MAL2	67,6689	18,5817	8,28625
S100A14	66,6125	20,6771	7,69171
NR4A1	2,39846	41,8691	9,00708
SEMA3A	3,67341	23,0045	45,6424
TAGLN	12,1555	5,88316	74,9962
TGM2	18,6073	6,12647	54,0595
lower expression			
PRKAA2	0,915962	0,0432123	0,298849
NRP1	1,28103	26,4427	18,3587
TNFSF4	0,681224	13,6364	23,5982
TM4SF18	1,26675	0,0896069	2,70922
NRG1	1,23535	0,108256	0,256587
CYP4F11	5,4479	0,604146	1,19381
ACTL8	0,304939	2,61376	1,19416
PTGS2	0,094392	0,802839	0,180836
LOC388553	2,01021	0,244778	0,191439

Continued on next page

Table 3.1 – *Continued from previous page*

TACSTD2	9,51878	1,16161	0,520285
PLEKHA7	1,6374	13,1111	16,4697
GPAM	10,3492	8,63039	0,454772
SPARC	0,951532	2,25558	15,7274
EFNA5	0,142549	0,51846	1,7639
SMARCA4	1,26221	14,5184	15,5321
GCNT4	0,047323	0,0685445	0,544131
APOBEC3G	0,232207	0,295326	2,43978
TNFRSF19	0,12085	0,674916	1,18036
LIPG	0,710454	0,479269	0,0748845
GPR110	17,5025	6,12588	2,12498
ANKRD1	2,53474	0,553065	11,082
ITGBL1	1,11495	0,180099	2,65822
CEACAM1	0,073791	0,0904651	1,2307
LOC100507127	0,473849	0,158482	1,77128
PRSS33	0,912185	0,235488	2,59174
SLCO2A1	0,143914	0,0809516	0,804988
ZNF702P	0,312612	0,0786411	0,706953

qPCR Validation of Individual Transcripts from the Transcriptome Analysis

The transcripts identified with the RNASeq analysis from in the previous section needed to be verified by a targeted method in order to confirm our hypothesis about transcripts that are influenced by the knockout of either HDAC1 or HDAC2. In order to verify these previously identified candidates, highly expressed genes (table 3.1) were tested by qPCR for relative mRNA expression levels. A qPCR reproduction of the transcripts PRF1, TAGLN and S100A14 under

the conditions tested in the RNASeq analysis was compared to the RNASeq data (fig. 3.20, panel A). In the qPCR experiment mRNA levels of HCT116 wild type cells were compared to mRNA levels from model B cells with an active conditional expression of either HDAC1 or HDAC2 in the background of the knockout of both endogenous isoforms. The mRNA levels in wild type cells were normalized to one, since both the qPCR and the RNASeq measure relative expression levels. The transcript PRF1 (perforin 1) increased substantially in both sets of genetic modifications in model B cells (fig. 3.20, panel A). qPCR and RNASeq results were in accordance. For the transcript of TAGLN (transgelin), mRNA levels measured by qPCR increased in model B cells. In the RNASeq experiment, the transcript levels decreased in the HDAC2 knockout and increased in the HDAC1 knockout. For the HDAC2 knockout qPCR and RNASeq data of TAGLN pointed in opposite directions, but both methods confirmed the increase of the TAGLN transcript in HDAC1 knockout cells. The relative transcript level of S100A14 decreased in the RNASeq experiment in the knockouts compared to HCT116 wild type cells. For the targeted reproduction of the transcript S100A14 by qPCR, the mRNA level stayed constant in the HDAC2 knockout cells and decreased in the HDAC1 knockout cells. The comparison of these three transcripts showed that the effect of single knockouts was partially reproducible by qPCR. This reproduction of HDAC1 or HDAC2 knockout influence on these transcripts lead to the question if the transcripts are also influenced by the loss of the expression of one isoform or by inhibition of both isoforms together, which would qualify them as activity readouts.

These three genes were further tested by qPCR with model A cells, to detect if the transcript levels react to HDAC1 or HDAC2 protein level changes or if they result from the genetic modifications in model B cell lines (fig. 3.20, panel B). As previously shown, withdrawal of doxicycline in these model A cells lead to the loss of either HDAC1 or HDAC2 protein expression (see fig. 3.6 on page 52). Model A cell lines showed higher PRF1 mRNA levels (left side) and lower S100A14 mRNA levels (right side) compared to wild type mRNA levels. Doxicycline and the induced HDAC1 and HDAC2 expression showed no effect on mRNA levels. Hence, we can say that these two transcripts seemed to be influenced by the genetic modifications introduced into these cells. The transcript level of the gene TAGLN decreased when the conditional system was turned off for both HDAC1 and HDAC2. This meant that this transcript reacted to HDAC1 and HDAC2 expression changes in a similar manner. Model A cells with inactive conditional expression (-doxicycline) have a similar HDAC1/2 expression pattern as the corresponding model B cells with active conditional expression. The reduction of TAGLN transcript upon the loss of a single isoform in model A cells compared to wild type cells was inconsistent with the increase observed in panel A, where the knockout cell lines were compared to HCT116 wild type cells. This data suggested that a short term loss of HDAC1 or HDAC2 expression and long term expression deficiency of one of the isoforms have opposing effects.

To clarify if the effect on TAGLN was caused by HDAC activity or by activation of the overexpression system, HDAC1 and HDAC2 were inhibited with 1 µM JQ-12 in HCT116 wild type

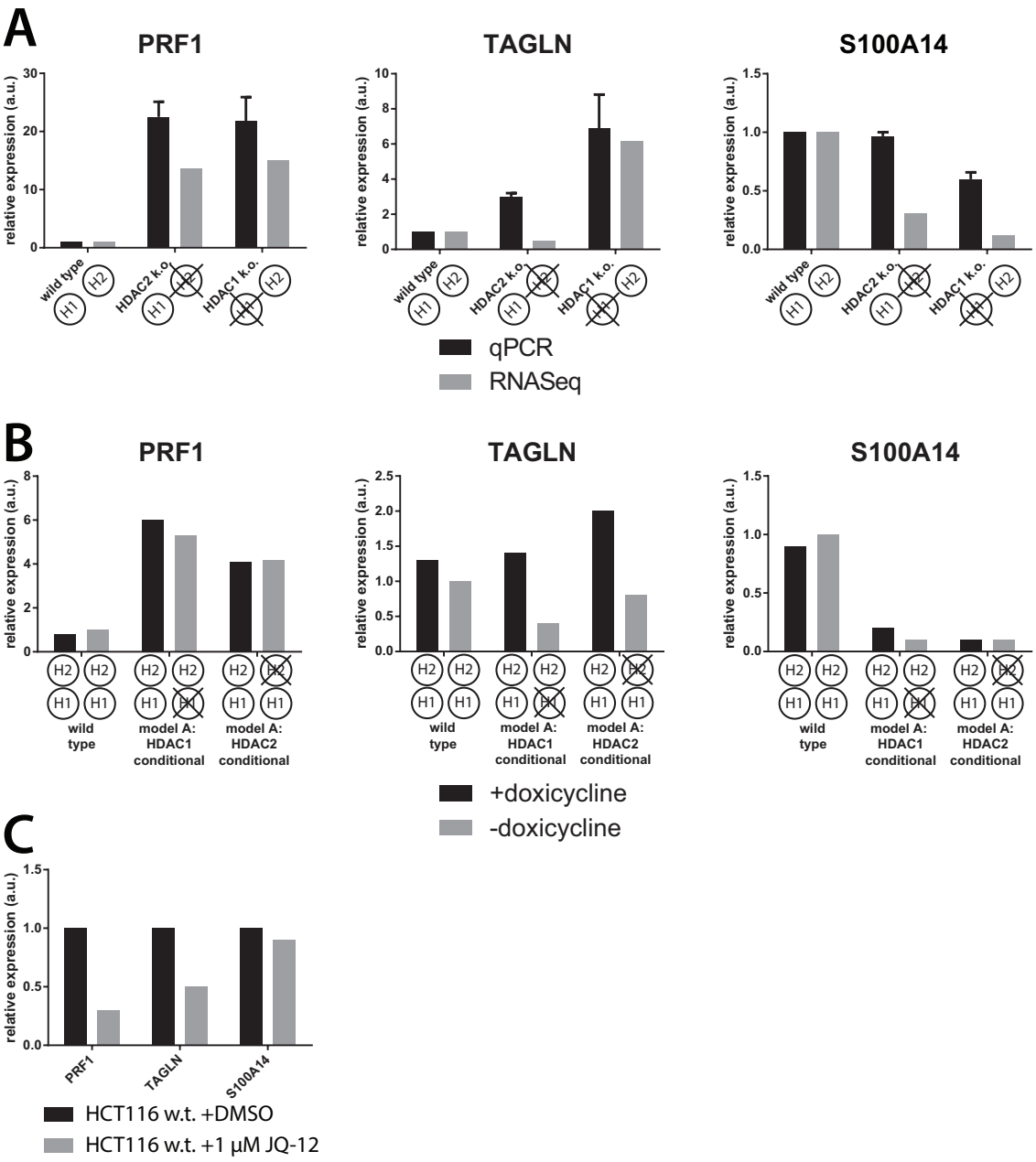

Figure 3.20 Validation of individual transcripts of the transcriptome analysis by qPCR. A) mRNA levels of the genes PRF1, TAGLN and S100A14 were measured by qPCR and compared to the RNASeq data. **B)** Different expression states of HDAC1 and HDAC2 were measured in the model A cell lines. **C)** HCT116 wild type cells were either treated with 1 µM JQ-12 for 16 h or an equal concentration of DMSO. Panel A qPCR bars show the mean of three individual clonal cell lines per set of genetic modification, error bar represent +SEM. In panel B and C, technical triplicates were performed for all samples.

cells (figure 3.20 panel C). The inhibition concentration was chosen to act on HDAC1 and HDAC2 and not on any other HDAC isoforms. Inhibition of HDAC1 and HDAC2 reduced the level of TAGLN. This decrease was consistent with the reduction of TAGLN transcript levels in model A cells with inactive HDAC1 or HDAC2 expression compared to wild type cells. This meant, the transcript level was influenced by HDAC1/2 activity without differentiating between isoform one and isoform two.

The transcript level of S100A14 did not depend immediately upon inhibition indicating that

S100A14 was largely influenced by the genetic system and not by HDAC activity. The PRF1 transcript level decreased upon HDAC1/2 inhibition. In the model A cells the overall HDAC1/2 levels were regulated through compensation of HDAC1 or HDAC2 protein loss by increased expression of the still present isoform (see figure 3.7 on page 53). If the compensation is enough to keep PRF1 levels up, then HDAC1/2 inhibition cannot maintain the high level, explaining the reaction to the HDAC inhibitor, but not to the single knockouts. PRF1 transcript was therefore increased by the genetic modifications in the model A (panel B) and model B cells (panel A) and additionally an overall HDAC1/2 activity reduction through inhibition lead to decreased transcript levels (panel C).

In the presented transcriptome analysis many significant, but small effects of HDAC1 or HDAC2 knockout were identified, of which some were reproduced by qPCR. The dependency of the transgelin (TAGLN) gene on HDAC1 and HDAC2 was verified, but we could not verify other transcripts with a differential reaction to either HDAC1 or HDAC2. This finding points in the direction that multiprotein complexes containing either HDAC1 and/or HDAC2 bind to similar chromatin regions. In general, we considered our hypothesis as confirmed, because we were able to identify and verify the influence of single knockouts on individual transcripts, like transgelin.

The transcripts we identified and investigated did not show consistent selectivity between the activity loss of HDAC1 or HDAC2 respectively. Nonetheless, some transcripts could serve as selective biomarkers for combined HDAC1/2 activity in the context of single HDAC1 or HDAC2 expression. This option remains to be investigated. Since we were investigating selectivity between HDAC1 and HDAC2, we decided to continue the search for such markers in the realm of histone acetylation sites, since they were known to be direct targets of histone deacetylases and individual sites may be modified by individual isoforms.

3.5. Measuring HDAC1/HDAC2 Selectivity in Model Cell Lines

In this chapter, we looked for specific acetylation sites that were either modified by HDAC1 or by HDAC2 as well as investigated the concentration dependency of the acetylation in relation to the inhibitor JQ-12 for one specific acetylation site.

In the first case we assumed, that there were acetylation sites that would only be modified by one of the enzyme isoforms. To show this, we used Co-115 wild type cells and the model C cell line to compare the extent of acetylation for several sites upon inhibition of HDAC1 and HDAC2.

In the second approach we expected that the preference of the inhibitor towards a certain enzyme isoform would result in different EC_{50} values, when a single isoform is expressed. We choose one specific histone acetylation site in wild type HCT116 cells as well as single-knockout cell lines and measured the dose-response curves.

Non-Selective Response of HDAC1/2 Inhibition in Co-115 Based Model C Cell Line

To test our first hypothesis we used the colon adenocarcinoma cell line Co-115 as well as our model C cell line to compare eight different acetylation sites when treated with the inhibitor JQ-12 (fig. 3.21). Using cell lines with different HDAC expression patterns allowed us to investigate the effect of inhibition for HDAC1 and HDAC2.

Wild-type Co-115 cells only expressed HDAC1 and our model C cell line expressed both isoforms, depending on doxicycline treatment. This enabled us to control the expression of HDAC2 between not being expressed (without doxicycline) and being expressed (with doxicycline). We previously showed that the activation of HDAC2 expression led to a reduction in native HDAC1 protein levels (chapter 3.2, fig. 3.9). Meaning, for the case where HDAC2 was not expressed, only HDAC1 can be inhibited (lane 4). Then again, in the case where HDAC2 was expressed from the transgene, the native HDAC1 expression is reduced and the inhibition will mostly act on HDAC2 (lane 6). The set of acetylation sites was chosen according to published data considering the commercial availability of antibodies. The JQ-12 inhibition in Co-115 wild type cells served as a control (lane 1& 2). JQ-12 inhibits HDAC1 and HDAC2 at nano-molar concentrations and the inhibition of other isoforms only starts in a micro-molar range (see table 1.1 in the introduction). Thus, we assumed that the observed effects, with a concentration of 1 µM, should only result from the inhibition of HDAC1 and HDAC2.

We investigated the impact of conditional HDAC2 expression without addition of the inhibitor in the model C cell line (comparing lanes 1 & 3 against lane 5). For the acetylation sites Ac-H3K18 and Ac-H2AK5 we were able to observe an increase in the extent of acetylation for active expression of HDAC2 and reduced HDAC1 expression (lane 5), compared to the expression of HDAC1 (lanes 1 & 3), indicating a potential HDAC1 selective site. This promis-

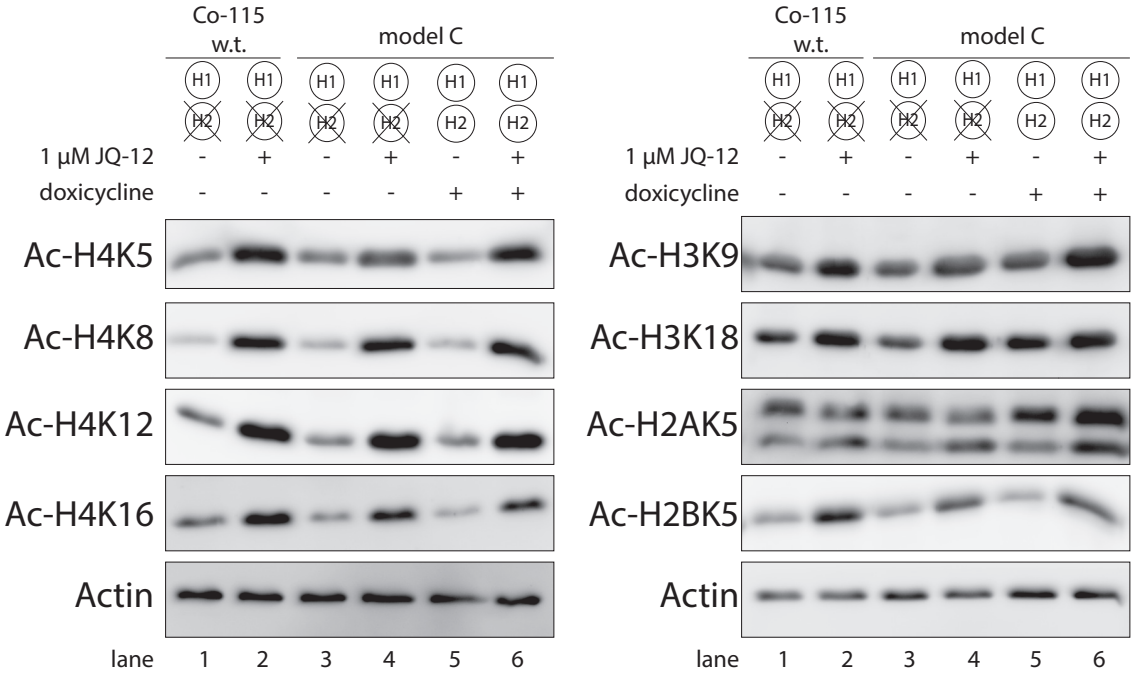

Figure 3.21 Acetylation levels of histone lysine sites to the HDAC1/HDAC2 selective inhibitor JQ-12 in model C cells. Co-115 wild type cells were treated with out without 1 µM JQ-12 (16 h) and compared to model C cells under four treatments. Model C cells were or were not treated with doxicycline at least 5 d prior to the experiment and model C cells were also treated with or without 1 µM JQ-12 (16 h). The indicated acetylated sites were detected *via* western-blot analysis from whole cell lysates (n = 1). β-actin served as a protein amount loading control. (H1 = HDAC1, H2 = HDAC2, Ac = acetylated)

ing result remains to be further investigated. The other acetylation sites showed no notable impact of HDAC2 expression.

We additionally evaluated if the selectivity of the inhibitor towards one of the isoforms would show a difference in the extent of acetylation (lanes 4 & 6). When inhibiting HDAC1 in the absence of HDAC2 (lane 3 vs. lane 4), we noted an increase in the extent of acetylation for all of the sites, showing that these sites were modified by HDAC1. But for the sites Ac-H4K5, Ac-H2AK5 and Ac-H3K9 we were able to observe a higher extent of acetylation for the HDAC2 expressed condition (lane 6) compared to the condition, where only HDAC1 is expressed (lane 4). Combining, that these sites were modified by HDAC1 and that we observed a higher extent of acetylation when HDAC2 was expressed, we can not exclude the possibility that the sites are also modified by HDAC2.

In summary, we found three acetylation sites, for which our results hinted towards isoform selectivity, but need to be further investigated to distinguish between HDAC1 and HDAC2. We moved to HCT116 cell lines with knockouts of either HDAC1 or HDAC2. Because of the relatively high difference between acetylation levels in JQ-12 treated model C cells with complementary HDAC1/2 expression pattern, we chose to investigate the Ac-H3K9 site further in the context of the expression of either HDAC1 or HDAC2 respectively.

HDAC1/2 Selectivity Determination of Inhibitors in HCT116 Based Cell Lines

In the second step we targeted our approach more precisely and chose to quantify the inhibition at different concentrations, aiming to find selectivity in the concentration dependency of the acetylation site. We assumed that the inhibitor would only effect one isoform if the corresponding one was genetically knocked out. We chose to measure dose-response-curves in single knockout cell lines, which allowed us to calculate EC_{50} values.

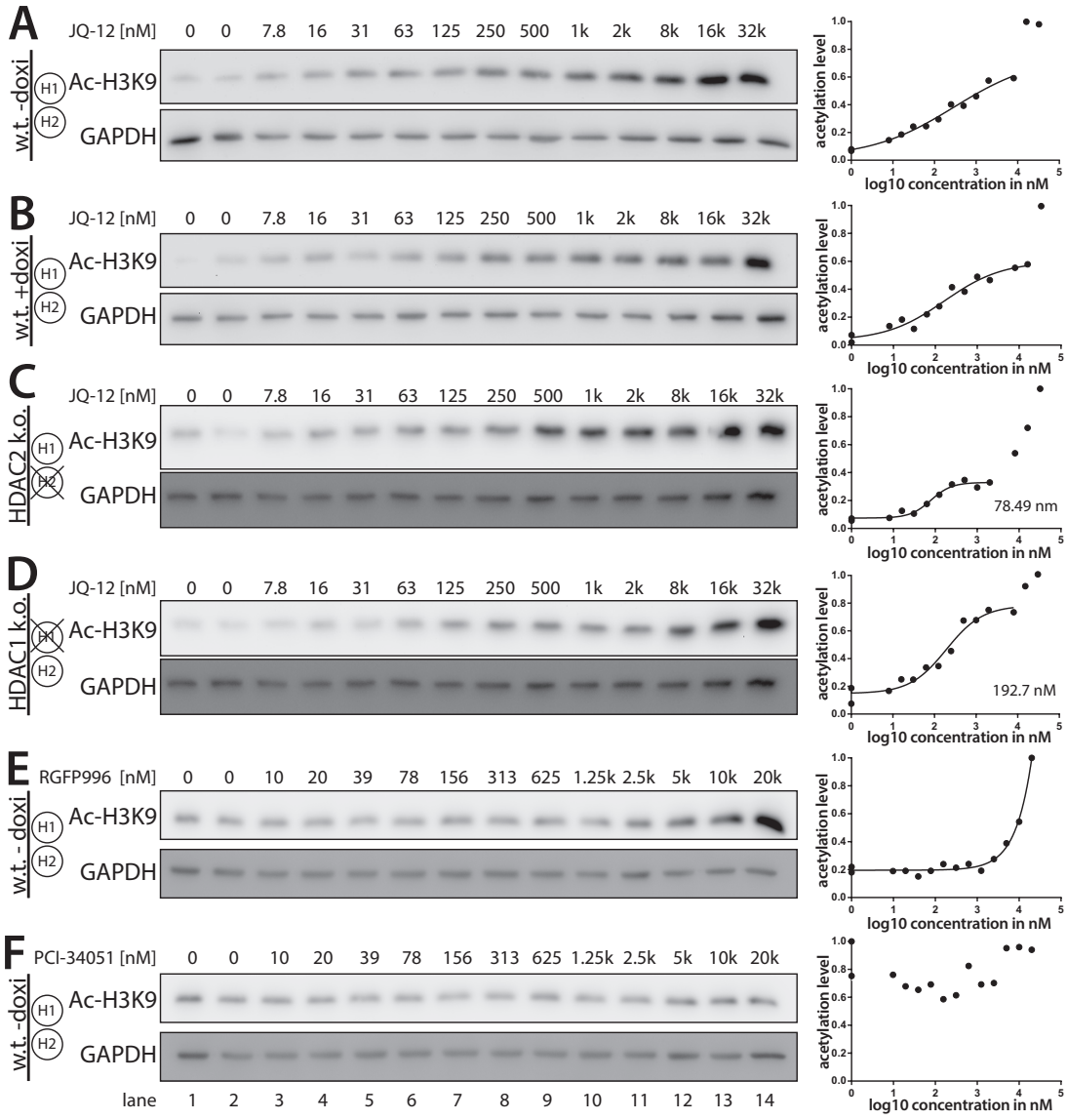

Figure 3.22 The histone acetylation site on histone 3 lysine 9 (Ac-H3K9) enables the measurement of either HDAC1 or HDAC2 EC_{50} values of inhibitors. Representative images of histone 3 acetylated on lysine 18 after 16 h treatment with increasing concentrations of HDAC inhibitors (n=2). HCT116 wild type cells were treated without **(A)** and with **(B)** doxicycline in addition to the indicated concentrations of JQ-12. HCT116 cells with a genetic knockout of either HDAC2 **(C)** or HDAC1 **(D)** were treated with the same concentrations of JQ-12 as the wild-type cells. HCT116 wild type cells were treated with the indicated concentrations of the HDAC3 selective inhibitor RGFP996 **(E)** or the HDAC8 selective inhibitor PCI-34051 **(F)**. Logarithmic concentration plots of the Western-Blot quantifications are shown for each concentration curve. The respective maximum value was normalized to one. The turning point (EC_{50}) of the dose-response curve was determined with a sigmoidal fit in Prism 6.

HCT116 wild type cells were treated with or without doxicycline, respectively, to serve as control (panel A & B). For the measurement of the inhibition of a single isoform, we used HCT116 cells with a single knockout, either of HDAC1 or of HDAC2 (panel C & D). As the

inhibition profile of JQ-12 (HDAC1: 9.2 nM, HDAC2: 77.2 nM, HDAC3: 1856 nM and HDAC8: > 4000 nM [76]) also includes the inhibition of HDAC3 at higher concentrations, we controlled for inhibition of the isoforms HDAC3 and HDAC8 with the selective inhibitors RGFP996 and PCI-34051 (panel E & F). The range of inhibitor concentrations was chosen to cover a range above and below published *in-vitro* IC_{50} values [76].

The dose-response-curves for the inhibitor JQ-12 showed a biphasic increase of the extent of acetylation. For lower concentrations we observed a light increase and a strong increase at the top end of our concentration range (panel A-D). For both single knockout cell lines we calculated the EC_{50} values at lower concentrations, which showed a stronger inhibition in those cells expressing HDAC1, compared to the ones expressing HDAC2 (panel C & D). These results agree with *in-vitro* IC_{50} values established for the inhibitor JQ-12 in literature [76]. The absolute EC_{50} values are higher compared to the *in-vitro* values, which is often the case when comparing these to *in-vivo* values. For the strong increase at higher concentrations we have to take in account the dose-response-curve for the inhibitor RGFP996, which is selective for HDAC3 (panel E). This curve, too, showed an increase of the acetylation, suggesting that the biphasic increase at higher concentrations for the Ac-H3K9 site upon treatment with JQ-12 resulted from the inhibition of HDAC3. For the inhibitor PCI-34051, selective for HDAC8, we did not observe inhibition (panel F).

Since we measured a preference of JQ-12 for HDAC1 over HDAC2 and also over HDAC3, we were able to reproduce the selectivity profile of the inhibitor JQ-12 in live cells, where these HDAC are mostly present in multi-protein complexes. However, our approach is limited to the class I HDAC inhibition profile. Our method can only differentiate between HDAC1 and HDAC2, if the inhibitor in question is already specific for these two isoforms and does not inhibit HDAC3.

All together our data demonstrate that the acetylation site Ac-H3K9 can be used to measure the extent of inhibition of one of the isoforms in homologous cell lines with either an HDAC1 or an HDAC2 knockout. Limited by the extent of inhibition of HDAC3 by the tested inhibitor molecule, the determined EC_{50}-values enabled us to understand and quantify the preference for either HDAC1 or HDAC2 of the molecule. Assuming that the presented method is transferable to other inhibitor molecules, this is an advancement with regards to the determination of HDAC1/HDAC2 selectivity measurements in the context of fully functioning protein complexes in intact cells.

3.6. Few Acetylated Lysines on Non-Histone Proteins Selectively Regulated by either HDAC1 or HDAC2

In order to identify acetylation sites which were selectively modified by either HDAC1 or HDAC2, we established an acetylomics work-flow in our lab to measure enriched acetylated peptides by LC-MS/MS.

We followed the hypothesis that individual non-histone acetylations were selectively modified by either HDAC1 or HDAC2. For this investigation we needed a method that was able to identify and quantify acetylation sites on non-histone proteins. In 2009, Choudhary *et al.* showed by mass spectrometry (MS) that over 1500 non-histone proteins were acetylated[32]. With this acetylomics work-flow we were able to leverage model B cells to observe specific effects of HDAC1 or HDAC2 activity loss by either expression loss or inhibition of the remaining isoform.

Establishment of an Acetylomics Workflow

In the process of the establishment of the acetylomics work flow, we performed three pre-tests. A first pre-test resulted from a previous try to measure acetylation sites with a standard MS method, where we observed very few acetylation sites. This lead to the hypothesis that lysine acetylations were not stable during the sample preparation procedure. A second pre-test assessed, if it was possible to clear non-specific binders to the antibody-agarose conjugate in a sample preparation step prior to the acetylation immunoprecipitation. The third pre-test determined to molar ratio at which the isotope label reagent needed to be used.

Pre-test no. 1: Mitigation of Acetylation Loss during Sample Preparation

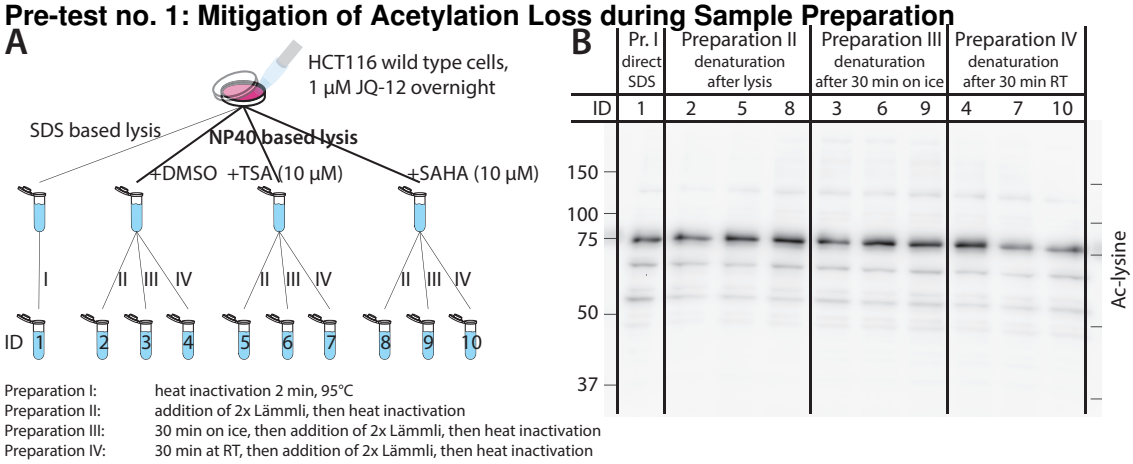

Figure 3.23 Evaluation of the stability of acetylation sites during the lysis.
A) HCT116 wild type cells were treated with JQ-12 overnight and lysed in SDS or NP40 based lysis buffers with or without the HDAC inhibitors TSA (10 µM) or SAHA (10 µM) as indicated. Cells lysed in SDS buffer were heat inactivated for 2 min at 95°C after the lysis (preparation I). Another part of the cells was mixed with 2x SDS buffer after the lysis and heat inactivated (preparation II). A third part was kept on ice for 30 min and then, mixed with 2x SDS and heat inactivated (preparation III) and a fourth part was kept at RT for 30 min, then mixed with 2x SDS buffer and heat inactivated (preparation IV). **B)** Relative amounts of acetylated proteins after the different preparation procedures. Equal amounts of total protein were loaded on each lane.

In order to assess the stability of lysine acetylations during the procedure, we tested different

buffer and sample preparation conditions. We compared unspecific acetylation levels after complete lysis by SDS and partial lysis by NP40 (fig. 3.23). The partial NP40 based lysis buffer represents the method used in MS experiments. A single sample of HCT116 wild type cells was treated with 1 µM JQ-12 overnight. Cells of this sample were either lysed in Lämmli buffer or in three NP40 based MS lysis buffers, either containing trichostatin A (TSA), SAHA or DMSO (panel A). To check the stability of acetylation sites in sample preparation steps after the lysis, a part of the MS lysis buffer samples was quenched directly by addition of 2x Lämmli buffer and treated with a consecutive heat denaturation. Two other parts of the same lysis sample were either kept for 30 min on ice or for 30 min at RT and were consecutively quenched. In panel B, non-histone acetylation WB signals above 37 kDa are shown.

Samples with the IDs 1, 2, 5, 8, 3, 6 and 9 showed equal acetylations levels. Two out of three samples that were kept at RT for 30 min (IDs 4, 7 and 10), showed a reduction of the prominent acetylation band around 75 kDa. This data suggests that other acetylated proteins with lower abundance also lost their acetylation under these conditions. This pre-test indicated that no deacetylation occurred in a time frame of 30 min when working on ice and using HDACi.

Generally, acetylation sites are chemically stable, since commercial acetylated peptides do not lose their acetylation by them self over time. This lead us to the conclusion that the acetylation loss we observed was due to residual catalytic activity in the unquenched lysates. Further studies were designed to incorporate the procedure under which acetylations were stable.

Pre-test no. 2: Pre-Clearing Acetylomics Samples does not Increase Sample Quality

In a second pre-test, we determined if it was possible to clear non-specific binders to the antibody-agarose conjugate in a sample preparation step prior to an acetylation immunoprecipitation. We suspected that certain non-acetylated peptides bind to the agarose-beads or the antibody itself and that we would be able to clear these peptides from samples. We hypothesized that implementing a pre-clearing step in the acetylations work flow would improve sample quality, quantified by an increased identification rate in cleared samples.

We prepared peptides from HCT116 wild type cells, treated with 1 µM JQ-12 over night, and performed an IP with an anti-biotin antibody bound to agarose beads. The anti-biotin antibody did not target peptides and therefore the antibody-agarose conjugate was supposed to represent only unspecific binding. From this IP, we compared the input with the fraction that did not bind the antibody (cleared sample) by LC-MS/MS (fig. 3.24, panel A). Each input sample, as well as the cleared fraction identified about 11000 unique peptides, of which 8042 overlapped (70-72%). The similar number of overall identified peptides means that this was the amount of unique peptides that were identifiable in a single run. The observed 70% overlap between the two MS runs meant that the peptide composition in both runs was nearly identical. Two MS runs of an identical sample would also not fully overlap, since peptides with abundances

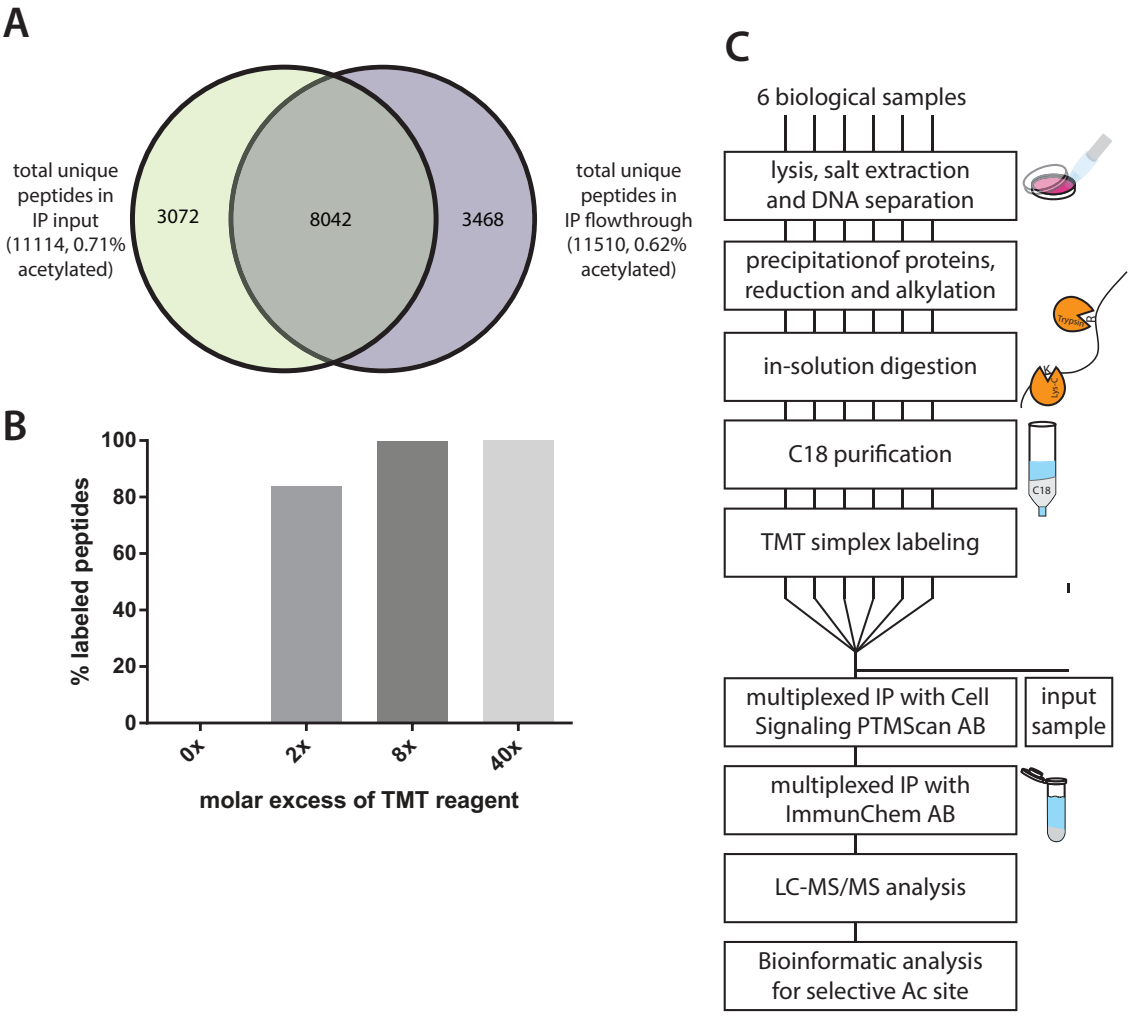

Figure 3.24 Establishment of the sample preparation procedure to measure acetylation sites by LC-MS/MS.
A) Comparison of unique identified peptides between IP-input and flowtrough of an anti-biotin AB conjugate (ICP0615). HCT116 wild type cells were treated with 1 µM JQ-12 over night. The Venn diagram was created with the online tool InteractiVenn [159]. **B)** Equal amounts of peptides from the same biological sample were reacted with different molar excesses of the TMT reagent. The percentage of TMT labeled peptides identified by MS is depicted. **C)** Schematic MS preparation and data analysis procedure.

at the edge of detectability would only be detected irregularly. The cleared fraction represents a sample, where peptides that unspecifically bound the antibody-agarose conjugate should have been removed. The equal percentage of peptides with acetylation sites identified in both samples means that the pre-clearing of the sample did not improve the identification rate of acetylated peptides, falsifying our hypothesis. The pre-clearing step was therefore not included in the sample preparation procedure.

Pre-test no. 3: Adjustment of the Molar Ratio between Labeling Reagent and Peptides

For a relative comparison between acetylation levels, we used a peptide labeling strategy with tandem mass tag (TMT) labels. TMT labels offer the advantage of the same overall molecular weight for each tag. During the mass spectrometer run the tags release a unique fragment, which can be identified and quantified.

For the labeling reagent, we aimed to optimize the molar peptide to reagent ratio. The goal was to mark as many peptides as possible in order to increase the detection rate of acetylated peptides in the LC-MS/MS runs. In the pre-test, we quantified how many peptides were labeled with an all natural isotope reagent with different molar ratios (fig. 3.24, panel B). HCT116 wild type cells were treated with 1 µM JQ-12 overnight and peptides were prepared. Equal amounts of peptides from the same biological sample were reacted with molar excesses of TMT labeling reagent as indicated and measured by LC-MS/MS. We compared the percentages of TMT labeled peptides to the total number of identified peptides. Without the labeling reagent (0x), no peptides were labeled. A two-fold molar excess of TMT reagent labeled about 80% of all identified peptides and an eight-fold molar excess was sufficient to label 99,6% of all peptides identified by mass spectrometry. Using the 40-fold molar excess labeled about 99.9% of all peptides. Showing that an eight-fold molar excess was sufficient to label 99.6% of all identified peptides led us to the decision to use this molar excess for further studies.

After the pre-tests, we finalized the sample preparation and data analysis work-flow (visualized in fig. 3.24, panel C). The cells were lysed, the chromatin was separated and the proteins were acetone precipitated less than 30 min after the lysis. It was crucial to precipitate the proteins quickly to inactivate any enzyme activity and avoid deacetylation. After the digestion and purification, the peptides from six individual samples were labeled individually with different TMT labels and mixed together. The input and bound fractions from two consecutive IPs were analyzed by LC-MS/MS. We designed this work-flow to identify non-histone acetylation sites and to quantify relative differences of abundance of individual acetylation sites.

Experimental Design to Identify Isoform Selective Acetylation Sites

After establishing the acetylomics procedure, the LC-MS/MS experiment was designed to distinguish acetylation sites influenced by HDAC1 from those influenced by HDAC2.

The challenge was to compare nine different conditions, while the TMT labeling reagent only allowed us to directly compare six samples in a single LC-MS/MS run. The nine different conditions resulted from treating three cell lines in three ways. We solved this challenge with an intelligent overlap of five MS sets including six samples of a total of 30 samples (set called V, W, X, Y, Z in fig. 3.25). In a first treatment, doxicycline was either withdrawn from cells for three days (treatment 1, first row). In samples labeled '-doxicycline', a doxicycline withdrawal of three days was chosen, because after this period the cells had lost about 80-90% of HDAC1 or HDAC2 expression (see figure 3.8) and they did still show regular growth (figure 3.14 part A & B). In a second treatment, cells were cultured with doxicycline (treatment 2, second row). In a third treatment, cells were grown with doxicycline and treated with 1 µM JQ-12 for 16 h (treatment 3, third row). The HDAC inhibitor JQ-12 was used at a concentration far below the IC_{50}s of HDAC3 and HDAC8, which ensured that these two isoforms were not inhibited and effects originated from HDAC1 or HDAC2 inhibition. Both the first and second treatment were mock treated with DMSO to match the DMSO concentration of the third treatment. Cell lines

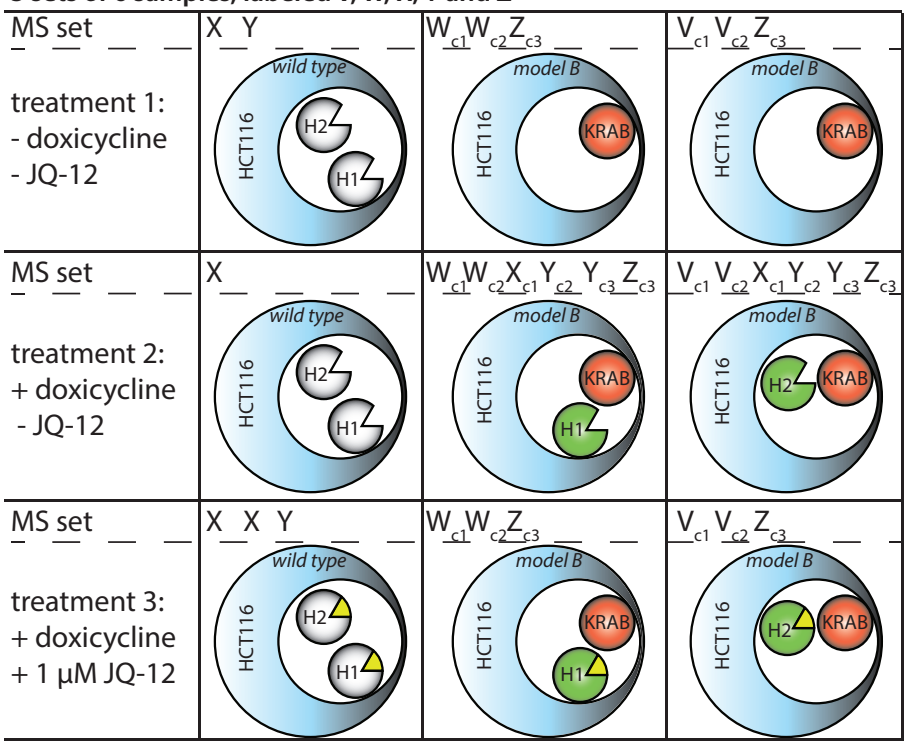

Figure 3.25 Experimental conditions to identify HDAC1 / HDAC2 specific acetylation sites.
Schematic representations of three HDAC1/2 genetic states and three treatments resulting in nine conditions. In total, 30 partly overlapping samples were measured in five multiplex sets of six samples (MS sets). The letters V-Z indicate which sample was measured in which MS set, e.g. all samples marked with V were labeled, pooled and measured in one MS run. The subscript of the set letter indicates which clone of the model B cell lines was used. White symbols represent endogenous HDAC isoforms, red symbols represent cells that were infected with a vector encoding the repressor KRAB with a dsRED fluorescence marker and green symbols represent cells that were infected with a vector encoding HDAC expression and GFP as fluorescence marker. A yellow slice depicts JQ-12 inhibition of HDAC1 and/or HDAC2. (H1 = HDAC1, H2 = HDAC2)

with three sets of HDAC1/2 expression patterns were analyzed. These expression patterns include wild type cells and model B cell lines with either a HDAC1 conditional expression or a HDAC2 conditional expression in the background of the knockout of both endogenous HDAC1 and HDAC2. For each model B genetic state three highly similar clonal cell lines served as replicates.

In MS set V the three treatments of clone one and clone two of model B cells with a conditional HDAC2 expression were compared. Similarly, set W compared the three treatments of clones one and two of model B cells with a conditional HDAC1 expression. Set X compared wild type cells cultured with doxicycline to those where doxicycline was withdrawn as well as two replicates of wild type cells treated with the inhibitor JQ-12. Set X also contained clone one of both genetic variants of model B cells cultured with doxicycline. In set Y HCT116 wild type cells with and without inhibitor treatment were compared to clones two and three of both variants of model B cells cultured with doxicycline. MS set Z compared samples of the three treatments of one clone of each model B cell line. The overlap of all sets in certain conditions allowed the comparison of all samples after a normalization step. Including all six model B

cell lines minimized the risk for artifacts arising from individual knockout clones.

Verification of the DNA Clearing Procedure and HDAC Expression Patterns in MS Samples

After designing the experiment and directly after creating the samples, the step prior to the LC-MS/MS measurement was a verification of HDAC1/2 expression patterns as well as the confirmation of the DNA clearing step. As described in the methods section (2.2.4, starting on p. 40), the MS sample preparation included a salt extraction step, before the DNA and all tighly DNA-bound proteins were removed from the analyzed fraction. Through the salt extraction most nuclear proteins should remain in the sample fraction, which we tested by checking HDAC1/2 presence before and after the clearing step. We expected to clear DNA as well as histones, which we verified for each of the five MS sets (representative example in fig. 3.26).

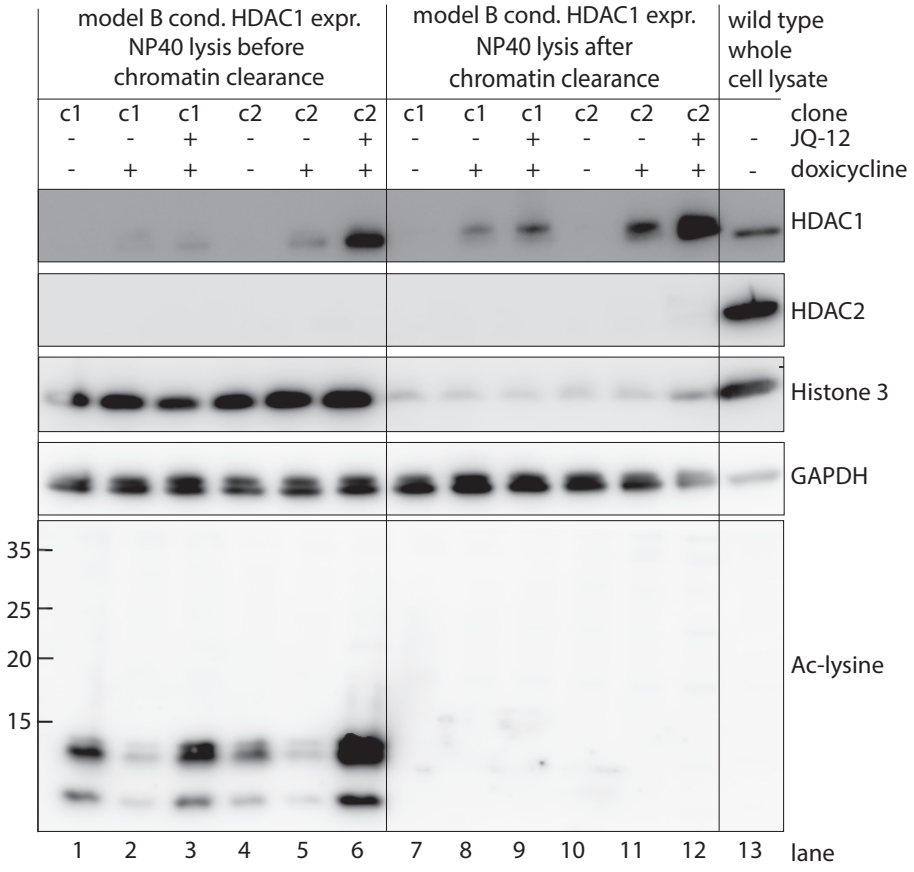

Figure 3.26 Confirmation of HDAC1/2 protein expression before LC-MS/MS analysis.
Representative confirmation of the HDAC1/2 expression pattern and effective clearing of chromatin associated proteins in MS set "W". During the preparation of the samples in MS set W, small portions were taken aside and analyzed by WB. The left six lanes show samples before chromatin clearing. Lanes 7-12 show the same samples after clearing. HCT116 wild type cells are shown for reference in lane #13.

Samples from set W were taken before and after the DNA clearing step of the MS sample preparation procedure and compared to a untreated wild type complete lysate control. For the confirmation of the effectiveness of the DNA clearing step, we observed histone three protein and acetylated histones. The disappearance of these signals in the samples taken after the clearing step confirmed an effective removal of histones as representative for tightly DNA-

bound proteins. Detecting HDAC1 after the clearing step served as an example if nuclear proteins were released by the salt extraction and remained in the analyzed sample fraction. For the verification of HDAC1/2 expression pattern, we observed HDAC1 and HDAC2 protein amounts. HDAC2 protein was not detectable in these model B cell lines, confirming the successful knockout. HDAC1 expression followed the presence of the conditional expression activator doxicycline, confirming the designed expression pattern. We additionally observed an increase in acetylated histones for both the loss of HDAC1 expression and inhibition of HDAC1 (lanes 1-6, from left to right). This observation confirms that the treatments indeed influenced acetylation levels in cells.

Successfully performing this verification step with the exact same samples, which were analyzed by LC-MS/MS, increased the confidence in the results gained from the analysis of the data.

Acetylation Enrichment by IP in MS Samples

Since the WB controls successfully confirmed the expected experimental conditions, we were certain enough to have our samples measured by the Helmholtz core facility for proteomics. In a first analysis of the data, we asked how many acetylated peptides were detected. We compared the percentage of acetylated peptides before the immunoprecipitation (input) with the percentage of acetylated peptides identified after the two immunoprecipitations (summarized in table 3.2).

Table 3.2 Total number of unique acetylated and non-acetylated peptides identified in all 30 samples.

	peptides		
dataset	acetylated	total	% acetylated
input datasets	73	2593	2.82%
IPs with Cell Signaling antibody, # I	1225	2438	50.2%
IPs with ImmuneChem antibody, # II	788	5554	14.2%

In the input dataset 2.8% of all identified peptides were acetylated, compared to 50% with the Cell Signaling antibody (# I) enrichment and 14% with the ImmuneChem antibody (# II) enrichment. This was an 18-fold enrichment for the antibody # I and a five-fold enrichment for antibody # II. The Cell Signaling product was a mixture of monoclonal antibodies and the ImmuneChem product was a polyclonal antibody. Both antibodies were used consecutively to maximize the identification rate of different individual peptides and to increase confidence in data for acetylated peptides identified in both enrichments.

In conclusion, the IPs showed an enrichment of acetylated peptides compared to the IP input samples. With the dataset at hand, the question arose if the two IP antibodies showed bias in enriching certain amino acid sequence motives.

Acetylation Enrichment by IP is Amino Acid Motive Free

To test if the identification of acetylation sites in the dataset depended of the amino acid sequence, we performed an amino acid sequence motive analysis with the online tool IceLogo[160] (fig. 3.27).

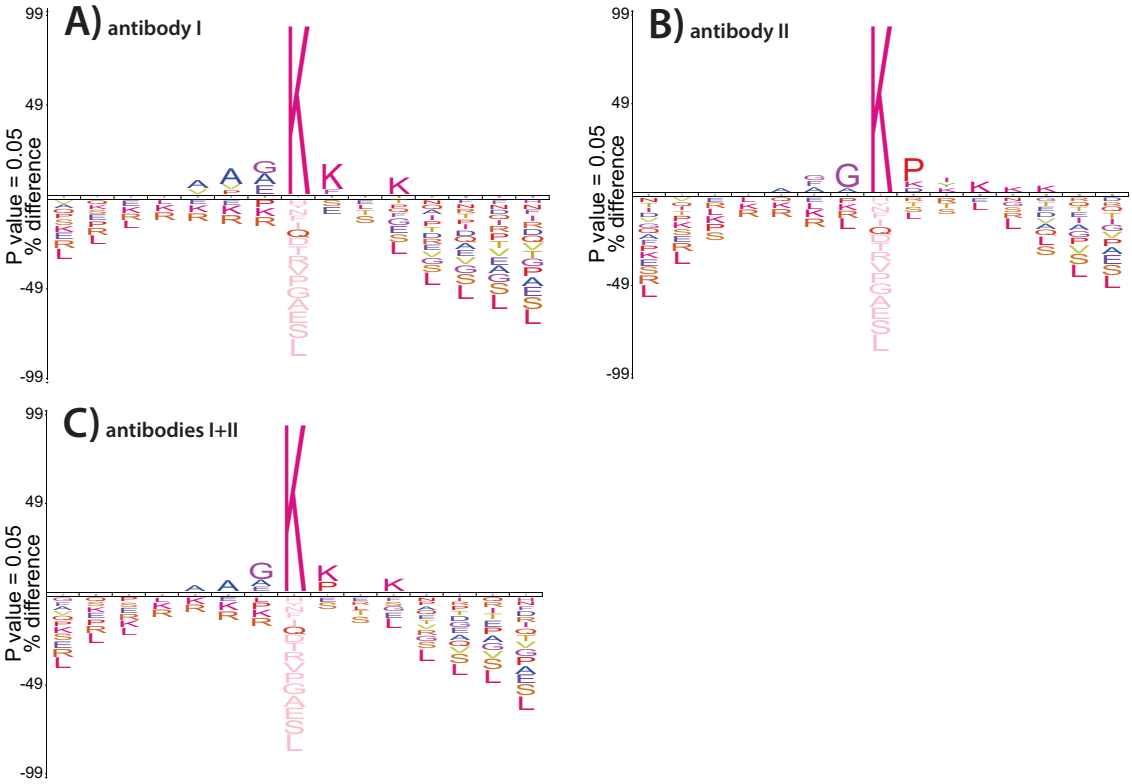

Figure 3.27 IP enrichment showed sequence independent identification of acetylation sites.
A) Sequence motive analysis of unique acetylation sites identified by MS, previously enriched with the PTMScan acetyl lysine motive kit by cell signaling (AB I). **B)** Analogous sequence motive analysis of acetylation sites identified with the polyclonal antibody ICP0388 from Immunchem (AB II). **C)** Sequence motive analysis of all unique acetylation sites (combination of unique peptides from panel A and B). Amino acid sequence motive analysis were performed with the online tool IceLogo [160]. Amino acids of a sequence around the acetylation site are shown that either appear more often (top section of graph) or less often (bottom section of graph) when compared to the general distribution of amino acids in *homo sapiens*.

According to the documentation, the IceLogo analysis is based on probability theory. The tool compares the frequency percentage of an amino acid at a certain location in the multiple sequence alignment of the acetylation sites with a general *homo sapiens* reference set and shows the differences. Peptide sequences with ± 7 amino acids around the acetylation site were extracted from the MS data and formatted by a custom written Python script to have a central acetylation site. For the analysis the script cropped longer peptide sequences and filled up shorter sequences with the letter X, which stood for an undefined amino acid in the IcoLogo tool. Deviations from a general reference *homo sapiens* amino acid composition appeared above or below the x-axis. A letter above the axis symbolizes an enrichment of the amino acid and a letter below symbolizes a lower occurrence compared to the human reference dataset. The size of the letter corresponds to how strong the deviation was. In all three panels, only small letters are depicted around the central lysine. This meant that the amino acid distribution was similar to the general distribution in *homo sapiens* peptides. Therefore, neither the acetylation sites identified by the monoclonal antibody mixture from

Cell Signaling (panel A), nor the acetylation sites identified by the polyclonal antibody from ImmuneChem (panel B) showed a clear binding motive by themselves. From this observation it was evident that there was also no preferentially identified sequence motive in the complete dataset of acetylated peptides (panel C). In conclusion, this analysis indicates an identification of acetylation sites unbiased by the surrounding amino acid sequence. For a next step, this lead to the question, if we were able to identify previously unknown acetylation sites.

Identification of Known and Unknown Acetylation Sites

To evaluate, if we identified previously unknown acetylation sites, we compared our complete dataset to two previous datasets from Choudhary *et al.* [32] and Schölz *et al.* [76] in a Venn diagram (fig. 3.28, panel A). Since we used a similar technique, we expected a certain overlap of our identified acetylation sites compared to the acetylation sites identified by the two other datasets.

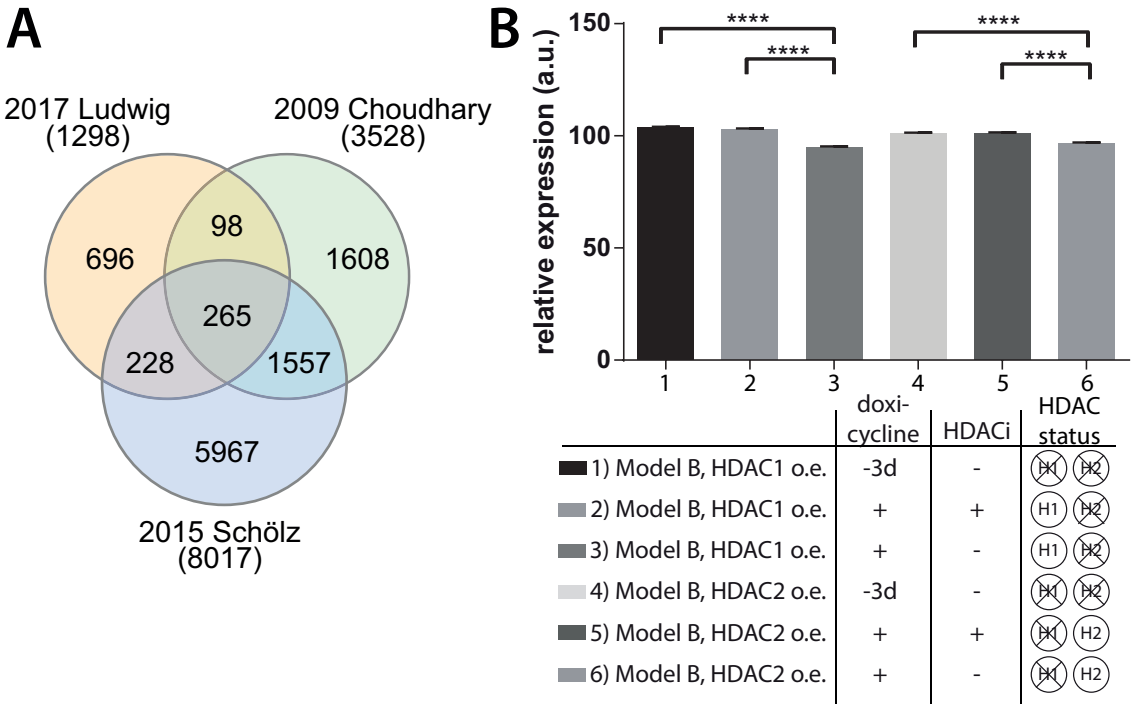

Figure 3.28 Increase of the average proteome-wide acetylation levels upon HDAC1 / HDAC2 activity loss.
A) Venn diagram comparison between acetylated peptides in the dataset and previous datasets from Choudhary *et al.*[32] and Schölz *et al.*[76]. The Venn diagram was created with the online tool InteractiVenn [159]. **B)** Overall relative acetylated peptide abundances are compared for treatments in model B cells in the bar graph. Mean ±SEM of all acetylated peptides are shown. Significance was determined by 1-way ANOVA (****: $p < 0.0001$). (H1: HDAC1, H2: HDAC2)

This comparison showed an overlap of 44% with the previous two datasets, which was comparable to the overlap between these two previous datasets created by the same research groups. The identification differences arose, because in current state of the art MS measurements each individual dataset measures a subset of all existing acetylations and therefore acetylation sites with abundances around the detection limit of the method are sometimes identified and sometimes not. In this comparison 696 acetylation sites were uniquely identified by us and not present in the two reference datasets. Since the two reference datasets do not cover all known acetylation sites, an automated request for all 696 acetylation sites to the

uniprot database (website: `https://uniprot.org` last checked at the 23.08.2019) revealed 529 unregistered acetylation sites. These acetylation sites were assumed to be unknown (table 6.5 in the appendix, starting on page 149).

While we identified new acetylation sites, we were also interested if our experimental conditions influenced acetylation levels, when taking all identified sites into account. After correcting relative abundances for protein level differences, we compared all conditions involving model B cell lines (fig. 3.28, panel B). The conditions with residual HDAC1 (lane 3) and HDAC2 (lane 6) expression showed lower overall acetylation levels compared to the conditions with HDAC1/2 expression loss or inhibition. Due to the high number of acetylation sites identified, the small overall difference was highly significant. The increase of the abundance of acetylated peptides upon inhibition of expression loss of HDAC1 or HDAC2 provided good evidence to continue with the data analysis on the level of individual acetylation sites.

Identification of Acetylation Sites with HDAC1-HDAC2 Differential Effects

An important goal of the analysis of the presented dataset was to find differences in the abundance of individual acetylated peptides between the activity loss of HDAC1 compared to HDAC2. Such sites would represent markers of either HDAC1 or HDAC2 activity in cells. Conceptually, if the activity of HDAC1 or HDAC2 is lost either by inhibition of by loss of protein expression, the abundance of an acetylated peptide with an acetylation site modified by the respective isoform should increase.

In order to analyze individual acetylation sites, the data of each individual acetylation site was extracted and corrected for the input protein levels, if the whole protein was identified and quantified. Individual acetylation sites were identified in one or up to all five of the performed multiplex measurements, which reduced the amount of available data points for some peptides. Since all multiplexed sets were designed to have an overlap, the same conditions measured in two different multiplex sets were used to normalize MS sets to each other, which prepared the data for statistical analysis.

The statistical analysis by the Helmholtz Center Core Facility for Statistics revealed 26 acetylation sites with significant differences between their HDAC1 and HDAC2 response in a dataset of 1298 unique acetylation sites. These 26 sites represented potentially HDAC1 or HDAC2 selective acetylation sites. Since the inhibition of the remaining isoform and the expression loss were both expected to reduce the activity of the remaining isoform, we expected both conditions to have a similar effect on individual acetylation sites. This internal control helped us to chose two peptides with acetylation sites showing a selective pattern for HDAC1 or HDAC2: VQVEYK(ac)GETK from HSPA8 and DGSASAAAK(ac)K(ac)K from MATR3. The first site is lysine K108 on the heat shock protein A8 (HSPA8/HSP7C) and the second is a double acetylation site on lysines K711/K712 on the protein Matrin 3, where the peptide with two post translational modifications showed a selective pattern in the MS data.

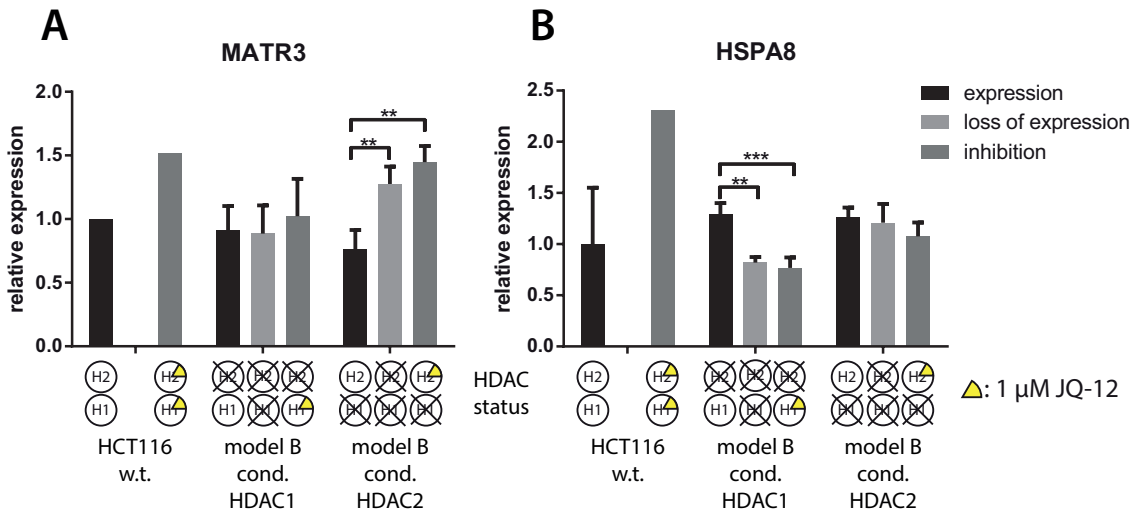

Figure 3.29 Ratios of acetylated MATR3 and HSPA8 peptides upon HDAC1 or HDAC2 activity loss indicate selectivity between HDAC1 and HDAC2.
A) Relative levels of the double acetylated peptide from Matrin 3 (MATR3). Bars were normalized to uninhibited wild type cells. **B)** Relative levels of the acetylated heat shock protein A8 (HSPA8/HSP7C) peptide. The HDAC expression of the cells in the presented conditions is depicted below each bar. Lack of HDAC1 expression is indicated by a crossed our H1/H2 circle. Inhibition by 1 µM JQ-12 is indicated by a yellow pie slice in the circles, which represent HDAC1 or HDAC2. Mean ±SEM of replicates described in figure 3.25 are shown. Significance was determined by a two-way ANOVA test on all data points from model B cell samples (**: $p < 0.01$).

The relative amounts of these two acetylated peptides were visualized (fig. 3.29). Inhibition with JQ-12 in wild type cells increased the abundance of the acetylated peptide. The relative amount of this acetylated peptide from Matrin 3 was significantly increased, when HDAC2 expression was either lost or HDAC2 was inhibited (panel A). For the acetylated peptides from heat shock protein A8 the relative acetylation amount decreased, when HDAC1 expression was lost or when residual HDAC1 was inhibited (panel B). Relative fold changed for both peptides amounted to a difference of about 40%. The abundance increase of the acetylated Matrin 3 peptide suggests that the acetylation site was directly modified by HDAC2, since the direction of the change is conceptually concurring. The abundance decrease of the acetylated peptide of HSPA8 is conceptually inconsistent with a direct modification of the acetylation site by HDAC1. This suggests an indirect mechanism of modification of the acetylation site on HSPA8.

The increase of the abundance of the acetylated Matrin 3 peptide upon HDAC2 inhibition and expression loss and the reduction of abundance of the acetylated heat shock protein A8 peptide upon HDAC1 inhibition or expression loss presented these two acetylation sites as candidates for HDAC2 or HDAC1 activity marker. Further validation of this result was needed.

Intra-Cellular Distribution of Matrin 3 Independent from HDAC1/2 Activity

The acetylation level changes of Matrin 3 and heat shock protein A8 from the previous section could have either resulted from the HDAC1/2 activity changes, or from a difference in the cellular distribution of the proteins, since our sample preparation procedure cleared DNA and

proteins bound tightly to DNA. With Matrin 3 being a nuclear protein, there was the possibility that our sample preparation influenced the result of the MS experiment. Due to the cytosolic location of the protein HSPA8, the lysis method and and HDAC activity changes should not have influenced how tightly the protein was bound to DNA and should therefore not have introduced a bias. If HDAC activity changes would result into changes in the cellular distribution and/or how tightly a protein is bound to the DNA, this would influence how much of this particular protein would make it into the analyzed fraction, faking and effect of HDAC activity on the identified acetylated peptide. We assumed that the observed acetylation level changes resulted from HDAC activity differences between samples, but this had to be tested.

To exclude this potential bias, we visualized DNA, Matrin 3 and HDAC2 by immunofluorescence staining upon HDAC1/2 inhibition and compared how often Matrin 3 and HDAC2 were found in the nucleus compared to cells with a cytosolic localization of the proteins. Not finding an influence of HDAC1/2 activity on the cellular localization of Matrin 3 would confirm our assumption.

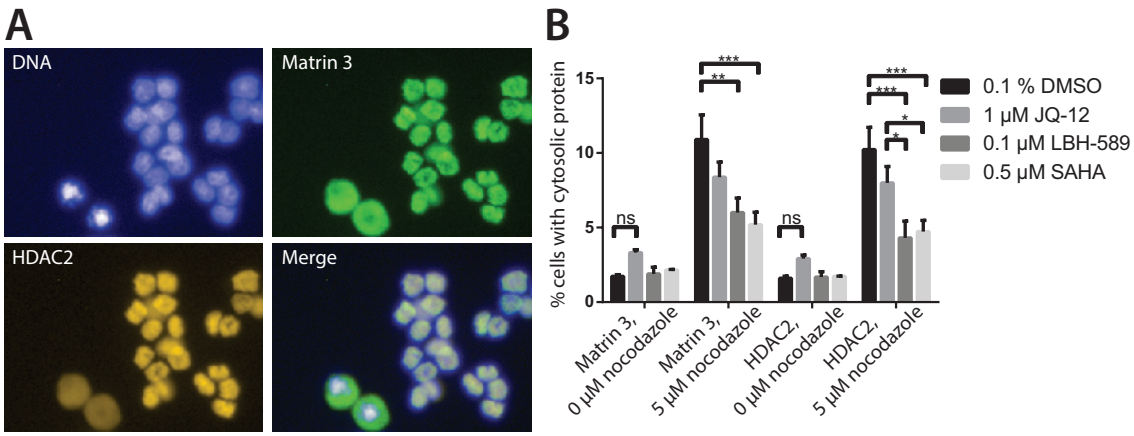

Figure 3.30 Intracellular distribution of Matrin 3 was independent from HDAC1/2 activity.
A) Immunofluorescence of Matrin 3 protein was visualized with Cy2, HDAC2 with Cy3 and nuclei were counter stained with Hoechst in HCT116 wild type cells. Images were collected with an Operetta high content imaging system. **B)** The percentage of cells with cytosolic Matrin 3 and HDAC2 were counted in HCT116 wild type cells, when treated with the indicated HDAC inhibitors and/or nocodazole. Means ±SEM of three identical wells in one experiment replicates are shown. Significance was determined with a two-way ANOVA test (*: $p < 0.05$, **: $p < 0.01$, ***: $p < 0.001$).

Expectantly, we found Matrin 3 and HDAC2 to be mostly nuclear (panel A for representative images). In a small percentage of the cells, Matrin 3 and HDAC2 were located in the cytosole. This percentage was not altered by HDAC inhibitor treatment, which suggested that our mass spectrometry results were not influenced by the cellular distribution of target protein.

From the cell shape in the images and the patterns of Hoechst stained DNA, we hypothesized that the nuclear proteins HDAC2 and Matrin 3 were only released during mitosis, where nuclei are not present. In order to confirm this hypothesis, we additionally treated cells with the cell cycle blocker nocodazole. Nocodazole inhibits the formation of microtubules and as a consequence cells which enter mitosis cannot form metaphase spindles, which arrests them in prometaphase[161]. Blocking the cell cycle during mitosis should increase the cells with cy-

tosolic Matrin 3 according to our hypothesis. Comparing the percentage of cells with cytosolic Matrin 3 and HDAC2 in nocodazole treated cells to untreated cells shows an increased percentage with the treatment (panel B). This increase confirmed the hypothesis that Matrin 3 was only detected in the cytosole during mitosis. An additional observation was, that the percentage of cells with either cytosolic Matrin 3 or HDAC2 was influenced by HDAC inhibitors, when the cells were co-treated with nocodazole. Since HDAC inhibitors were reported to stop cells either in G1 or G2/M phase[94, 162], a reduced proliferation through HDAC inhibition explained the reduction of mitotic cells in the HDAC inhibitor - nocodazole co-treated cells.

Not finding a significant difference upon HDAC1/2 inhibition for the matrin 3 cellular distribution is consistent with the assumption that the results obtained for Matrin 3 in the acetylomics analysis result from the preferences of HDAC1 and HDAC2 for the acetylation sites and are not biased by the protein isolation method.

Verification of Custom Antibodies Targeting the Identified Acetylation Sites

The discovery of a HDAC1 specific effect on an acetylation site on heat shock protein A8 (HSPA8/HSP7C) and of a HDAC2 specific effect on an acetylation site on Matrin 3 (MATR3) by mass spectrometry opened the question if we could observe the same selectivity of HDAC1 and HDAC2 with an independent method. For both acetylation sites, we assessed the creation of specific custom antibodies in cooperation with the Helmholtz core facility for monoclonal antibodies for measuring acetylation levels of specific sites by western blot.

Among the 111 tested hybridoma lines isolated by the core facility to identify HSPA8 / HSP7C acetylation, no antibody correctly identified HSPA8 / HSP7C as measured by protein size in western blots. For the double acetylated site on Matrin 3, one clone produced an antibody which identified a JQ-12 inducible band at the right size in western blot tests. ELISA assays performed by the core facility showed that this antibody recognized individual acetylation on either of the neighboring lysine residues as well as the double acetylation. The clone, from which this antibody was generated, produced one small batch of supernatant with antibody, but failed to create a stable hybridoma cell line.

We used the limited supernatant containing the custom antibody created by the Helmholtz core facility to identify the acetylation level of the site on Matrin 3 (fig. 3.31). We reproduced the conditions of the mass spectrometry setup for three model B clonal cell lines with a conditional expression of HDAC1 in the background of the knockouts of both endogenous isoforms (fig. 3.29, panel A) and the respective three clonal cell lines with a conditional HDAC2 expression in the same background (panel B). Wild type cells were either treated with 1 µM JQ-12 overnight or they received a control DMSO treatment (0.1%). Inhibition of HDAC1 and HDAC2 increased the acetylation level in wild type cells, which was consistent with the MS experiment. Model B clones with conditional HDAC1 expression were subjected to three treatments. In a first condition they were cultured with doxicycline (indicated by "+"). In a second condition, doxicycline was removed for three days (indicated by "-") and in a third condition,

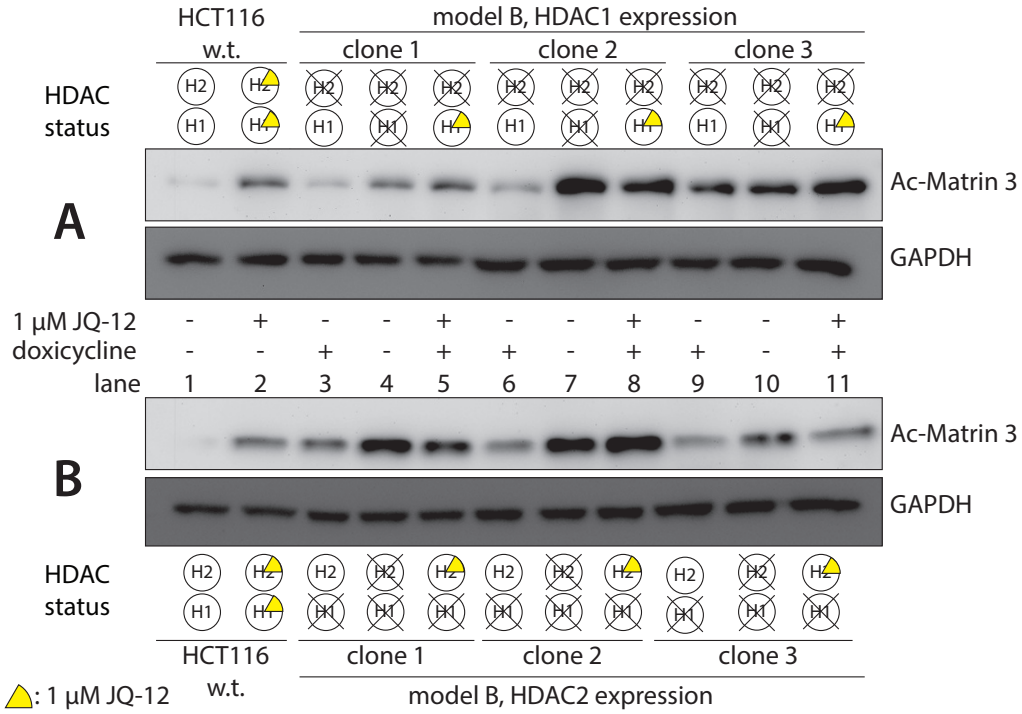

Figure 3.31 Initial verification of a custom antibody targeting Ac-K711/K712 on Matrin 3.
A) Relative amounts of acetylated Matrin 3 in HCT116 wild type cells and model B cells with conditional HDAC1 expression. Conditions of the MS experiment were reproduced (figure 3.29 panel A, wild type and HDAC1 clones). **B)** Relative amounts of acetylated Matrin 3, analogous to panel B with model B cells with a conditional expression of HDAC2. A custom made antibody was used to identify Matrin 3 acetylation. HDAC expression is depicted by circles (expression) or crossed our circles (no expression). Inhibition by 1 µM JQ-12 is indicated by a yellow pie slice in the circles, which represent HDAC1 or HDAC2. Images were recorded by western blot from whole cell lysates. Due to the limited availability of the antibody against acetylated Matrin 3, these western blots were performed once (n=1).

model B cells cultured with doxicycline were treated with 1 µM JQ-12 overnight (indicated by "+"). Expression loss and inhibition of HDAC1 in model B cells increased the acetylation level for clone one, two and less for clone three. For HDAC2 inhibition and HDAC2 expression loss, the acetylation level increased for clone one and two. Clone three only shows an increase for expression loss (panel B).

The data from the MS experiment suggested that a HDAC2 activity reduction increases the acetylation level, but not the loss of HDAC1 activity. This singular western blot did not reproduce the MS pattern. The data indicate that the double acetylation site identified in this study may have a distinct function compared to the single acetylations on this protein. To further investigate this question a more selective antibody for this acetylation site is needed. A second series of antibodies was prepared in cooperation with the Helmholtz core facility for monoclonal antibodies. For this second series, antibody selectivity and HDAC activity dependence remain to be investigated.

In our experiments, a multitude of new acetylation sites were identified and acetylation sites of the protein Matrin 3 (MATR3) and heat shock protein A8 (HSPA8) showed responses in the MS that differentiate between HDAC1 and HDAC2 activity, which establishes these acetylation sites as promising candidates for isoenzyme-selective activity markers.

4. Discussion

The main goal of the thesis was to differentiate between the potency of small molecules to inhibit HDAC1 and HDAC2 in cells. In *in-vitro* assays, the selectivity is achieved by the presence of a single isoform. When measuring the HDAC activity in cells, all HDAC isoforms are present in parallel and the selectivity needs to be achieved through a marker.

4.1. HCT116 Cellular Model to Distinguish HDAC1 from HDAC2 Activity

To find a selective marker we needed a cellular model system, which allowed for the measurement of either HDAC1 or HDAC2 activity loss. So far single HDAC1 or HDAC2 knockout systems in different cell lines were widely applied[151] [163]. Such single knockouts or activity loss systems of either HDAC1 or HDAC2 were accompanied by an increase in the corresponding isoform's expression[55, 151, 164, 165]. For our goal, this meant that we would always measure the activity loss of one isoform and the activity increase of the corresponding isoform. This interdependence of the expression of multiple class I isoforms was the motivation to create cell lines, which have both endogenous HDAC1 and HDAC2 knocked out and which continued their growth by conditionally expressing either HDAC1 or HDAC2. This means, our systems uniquely allows the study of activity loss effects of either HDAC1 or HDAC2. Upon knocking out HDAC1 and HDAC2 in mouse embryonic stem cells, HDAC3 was found to be up-regulated at the protein level[154]. For our model system this means that HDAC3 expression could be up-regulated as well, which remains to be investigated. Because the double knockout of HDAC1 and HDAC2 already lead to a proliferation stop, an additional HDAC3 knockout, to exclude a HDAC3 compensatory effect, was thought to further impede the cell line. Hence, an additional HDAC3 knockout would have made the model cell line more artificial and was deferred. This did not pose a limitation to our study goal, since HDAC inhibitors are already selective enough for HDAC1/2 over HDAC3 and we wanted to differentiate between HDAC1 and HDAC2.

A study of Schölz *et al.* showed that HDAC inhibition lead to increases and decreases of acetylation site abundances[76]. Therefore, it seems that acetylation sites were either modified directly by HDAC and the inhibition increased the abundance of acetylation, or the acetylation site was modified through an indirect mechanism, which decreased the abundance of acetylation. This meant that the direction of the abundance change of an acetylation site cannot be used as an indication of the origin of the change. Since no purely HDAC1 or HDAC2 specific inhibitors exist, the study was only able to evaluate a combined HDAC1 and HDAC2 activity loss. In comparison, by introducing our HCT116 cellular model system, it enabled us to compare two modes of selective HDAC1 or HDAC2 activity loss per isoform. The uniqueness of our model cell lines is the ability to loose the expression of the conditionally expressed

isoform without triggering regulation of the endogenous HDAC1 or HDAC2 isoforms.

We observed the onset of the conditional ectopic expression of HDAC1 or HDAC2 after two to three days (figures 3.7, 3.8, 3.9, 3.10). This is consistent with results shown by Trono *et al.* and Du *et al.*. Trono *et al.* observed expression of GFP protein from the pLVTHM vector starting 48 h in MCF-7 cells [147]. Implementing a shRNA knockdown of HDAC1, Du *et al.* observed the reduction of HDAC1 levels after 48 h in RKO cells [166]. Especially, for *in-vivo* assays, this means that the observation time point needs to be planned accordingly. Should therapies be developed, which influence HDAC expression, the therapeutic effect would be expected to be delayed by roughly two days.

During the process of the cell line creation, we found that transcripts containing an HDACx-T2A-GFP sequence were inefficiently translated. The original system was designed for shRNA knockdowns of target genes and did include GFP instead [147]. The inefficient translation limits the use of this system for explicit overexpression studies, but represented a fortunate coincidence in our case, since it allowed for the expression of near native protein levels. We have also identified a regulation of constant HDAC1/2 activity. Combining the inefficient translation efficiency and the knowledge about a potential regulation between isoforms, this opens the question if the amount of ectopic HDAC1 or HDAC2 expression is regulated.

4.2. Differentiating HDAC1 from HDAC2 Activity

Bringing our cellular model systems to use, we knew that HDACs catalyze the deacetylation of acetylated-lysine residues on histone and non-histone proteins. The deacetylation of histones influences the chromatin state, leading to gene silencing. With this in mind, there were three domains we chose in the search for activity readouts / biomarkers: Firstly, we analyzed the role of HDAC isoforms on histone modifications, then we investigated how these alter transcription of target genes, and lastly we explored how acetylation frequency is affected on non-histone proteins.

4.2.1. Histone Acetylation Sites Serve as Activity Marker in Single HDAC1 or HDAC2 Expression Contexts

For a set of histone acetylation sites (H4K5, H4K8, H4K12, H4K16, H3K9, H3K18, H2AK5 and H2BK5), we observed a dependency on both HDAC1 and HDAC2 activity (fig. 3.21 on p. 79). For the acetylation sites H3K18, our data suggest a preferential deacetylation by HDAC1. Acetylation amounts on sites Ac-H4K5, Ac-H2AK5 and Ac-H3K9 showed a higher dependency on the inhibition of HDAC2 compared to HDAC1 inhibition. There was already evidence that histone acetylations sites are influenced by HDAC1 or HDAC2. For example the acetylation on histone four lysine five (H4K5) inversely correlated with HDAC1 expression[58] and HDAC2 protein depletion lead to increased H4K16 acetylation levels[59]. While some acetylation sites have diagnostic value, for example within differentiated tumor samples more H4K12 and H3K18 acetylation was observed, compared to poorly differentiated tumor samples[167],

this does not make them candidates for biomarkers for the activity of a single isoform. Through our results we were able to show, that the above mentioned sites are modified by both HDAC1 and HDAC2. This further adds to the hypothesis that no acetylation site exists that is modified by a single isoform alone.

In this context it was not surprising that we found Ac-H3K9 to depend on HDAC3 activity (fig. 3.22 on p. 80). We additionally excluded a dependency of this site on HDAC8. Knowing that this site reacted to HDAC inhibition, we established an assay to differentiate the effect of a model inhibitor on either HDAC1 or HDAC2. Concentrations measured as result of the assay were in accordance with *in-vitro* assay results, which measured a lower IC_{50} value of JQ-12 with the HDAC1 compared to HDAC2[76]. To create the assay, we leveraged our unique model system. Previous studies did show that this acetylation site was influenced by inhibitors, e.g. romidepsin and vorinostat (SAHA)[20]. From this finding and our results we can deduct that our assay will be able to measure multiple chemical categories of inhibitors. The assay is performed in genetically modified cells and cannot be translated into human tumor samples, which represents a limitation of this particular assay. We tackled this limitation by searching for more specific biomarkers for either HDAC1 or HDAC2 activity.

Transcription factors specifically bind to certain gene sequences and recruit HDAC containing complexes to modify the chromatin specifically around this genetic sequence[168, 169]. HDAC1 and HDAC2 are for example part of the CoREST, the Sin3 and the NuRD complexes [35, 36, 37, 38, 39, 40]. In the end, genes are individually regulated by PTMs, depending on the physiological need. In the context of a fine tune histone code[16, 17, 18, 19], we expected that most histone acetylation sites would be modified by multiple HDAC enzymes. We hypothesized that selectivity could be found in transcripts, where selectivity would originate from a specific interaction of the transcription factor with the genetic sequence.

4.2.2. Transcriptomics Reveals Many Small Significant Changes

HDACs are chromatin modifiers and we investigated if single transcripts were influenced by either HDAC1 knockout or HDAC2 knockout by RNASeq analysis. Our study identified 771 significantly up-regulated and 605 down-regulated transcripts upon HDAC1 or HDAC2 knockout in a dataset of 23219 identified transcripts. Other transcriptomics studies focused on the effect of inhibitors: Singh *et al.* showed that treatment of glioblastoma cells with SAHA resulted in 4065 up-regulated and 3518 down-regulated genes in an analysis of 7583 transcripts[170]. Laporte *et al.* revealed that HDAC inhibition by quisinostat in six sarcoma cell lines resulted in 609 down-regulated genes and 1967 up-regulated genes in a dataset of a total of 22794 identified transcripts[171]. These studies and other -omics approaches of HDACi treatments are reviewed by Li *et al.*[172]. We took a closer look on the distinction between HDAC1 and HDAC2 leveraging our model system, which generated a uniquely new dataset. From our transcriptomics data, we identified the transcripts of Perforin 1, Transgelin and S100A14 as being influenced by HDAC1 or HDAC2.

We know that individual T-cell clones can lyse cells *via* Perforin (PRF) mediated cytotoxicity[173] and that Perforin is produced by cytotoxic lymphocytes to clear tumor or virus infected cells by forming transmembrane pores[174]. Both use cases of Perforin 1 are related to the immune system. Since the cell lines were infected twice with virus carrying the conditional expression system and we could not confirm a HDAC dependency of the transcript by qPCR (see fig. 3.20 on p. 76), the most likely explanation for the alteration in knockout cell lines is a result from the genetic system introduction. Our results suggest that Perforin 1 function is not limited to immune cells.

Reviewing the state of Transgelin (TAGLN) knowledge reveals that it promotes motility by binding actin[175]. In a study published in pre-print, Arnaud *et al.* found that HDAC inhibition by SAHA in astrocytes increased TAGLN3 expression[176]. We found and confirmed a more specific link between HDAC1, HDAC2 protein expression and Transgelin mRNA levels. We also observed a dependency of Transgelin mRNA levels on a HDAC1/2 selective inhibitor, which is in line with the results from Arnaud *et al.* For HCT116 cells, Zhou *et al.* showed that attenuation of transgelin expression by stable transfection of microRNA containing vector decreased the number of metastases in a mouse model[175]. We observed an increase of mRNA upon HDAC knockout. In combination, this opens the question if HDAC inhibition may lead to increased levels of Transgelin, which in turn may lead to more metastases.

For the transcript S100A14, we confirmed an alteration of mRNA levels in our knockout cell lines, but we did not observe a HDAC activity dependency of the transcript. Since such a connection was also not observed in the literature, this could mean that S100A14 transcript levels do not depend on HDAC1/2 activity.

We found many small significant changes, but overall the transcriptomes of HDAC1 knockout cells were very similar to HDAC2 knockout cells. Assuming that each HDAC containing complex is recruited by a transcription factor (TF) [168, 169], the selectivity of transcription depends on the interaction between the TFs and the genetic sequence. When complexes like the Sin3, the NuRD or the CoREST are recruited to modify the chromatin, these complexes contain either HDAC1 or HDAC2[35, 36, 37, 38, 39, 40]. Transcripts to which these complexes are directed therefore depend on both HDAC1 and HDAC2 activity. In a single HDAC1 or HDAC2 knockout these complexes can only contain the remaining isoform. As HDACs do not seem to be selective for specific histone acetylation sites, the simple recruitment would make them modify sites in close proximity. In this scenario, the isoforms are replaceable as long as they can form the same complexes, which is the case for most HDAC1 and HDAC2 containing complexes. We continued to search for isoform selectivity on non-histone protein acetylation.

4.2.3. Non-Histone Protein Acetylation as Activity Marker

We identified a total of 1298 individual acetylation sites on non-histone proteins, with 26 with significant differences between expression of a single isoform and the respective inhibition or

expression loss. Among the identified acetylation sites in our dataset were 529 sites that were not listed in the Uniprot database at the time of the analysis. Previous research investigated the influence of a multitude of HDAC inhibitors on proteome wide acetylations, the acetylome. In 2015, Schölz *et al.* treated HeLa cells with a set of 18 HDAC inhibitors and quantified the responses of acetylation sites, identifying up- and down-regulated acetylation sites for each inhibitor[76]. In a different study, the inhibitors VPA and SAHA caused a differential induction of the acetylome of HL60 cells, a human promyelocytic leukemia cell line[177]. The HDAC inhibitor romidepsin (FK228) was investigated in an acetylome comparison of treated versus untreated EC109 cells (derived from human esophageal squamous cell carcinoma), identifying effects of FK228 treatment on proteins in multiple biological functions and metabolic pathways[178]. In contrast to previous studies, we focused on the distinction of HDAC1 and HDAC2 deacetylation targets by leveraging our HCT116 based model cell lines. This dataset with the 26 non-histone acetylation site open many doors for further validation of these potentially selective acetylation sites for HDAC1 and HDAC2. Identifying many candidates was important, since not every site may be targeted well by monoclonal antibodies and when looking at markers in human cells, it may happen that a certain acetylation site is not present in a certain cell type. Having an arsenal of markers would circumvent this problem.

In line with previous studies, for example Schölz *et al.*[76], we found that decreased HDAC activity lead to abundance increases and decreases of specific acetylation sites. This suggested the presence of an indirect mechanism, which lead to decreased amounts of acetylated peptides. This mechanism remains to be further investigated.

We observed a HDAC1 selective MS response on K108 on the heat shock protein A8 (HSPA8 / HSP7C / Hsp70) and a HDAC2 selective MS response by two acetylated lysines (K711 / K712) on Matrin 3 (see fig. 3.29 on p. 92). Matrin 3 is a nuclear matrix protein with a zinc finger domain which binds Ca^{2+} [179]. Matrin 3 was also observed to specifically binds several miRNA[180]. Upon the loss of HDAC2 activity either by expression loss or by inhibition, the double acetylation site on Matrin 3 increased in abundance in the MS data. This suggested a direct interaction of HDAC2 with Matrin 3, since less deacetylase activity lead to more acetylation.

For the acetylation site on heat shock protein A8 (HSPA8/HSP7C), the loss of HDAC1 activity lead to less acetylation on HSPA8. In general, HDAC activity loss leads to increased acetylation levels (see fig. 3.26 on p. 87). Observing a reduction through HDAC1 activity loss suggested an indirect mechanism, where HDAC1 does not directly deacetylate HSPA8/HSP7C. Nonetheless, a proteomics study revealed a protein-protein interaction between HDAC1 and HSP7C in HepG2 cells[181]. HSP7C belongs to a group of Hsp70 proteins and epigenetic alterations of this group were reviewed by Ban *et al.*[182]. In summary, HSPA8/HSP7C is a molecular chaperone implicated in a variety of cellular processes[183], opening a wide range of possibilities where HDAC1 activity loss may interfere and consecutively cause the decrease in HSPA8/HSP7C acetylation. This particular acetylation site could serve as starting point to

solve how HDAC activity loss leads to increases of individual acetylation sites.

Both Matrin 3 and the heat shock protein A8 have been found together in a complex which is based on the interaction of both proteins with the NRC interacting factor 1 (NIF-1)[184]. While there was not much further evidence for this specific complex in the literature, the acetylation sites on both proteins may influence this complex composition.

For non-histone acetylation sites the interaction between the HDAC isoform and the target most likely results from a protein-protein interaction and not from complex-DNA interaction, which results in a pool of modified histones located at different genes. As a result, the acetylations of the non-histone protein are much less likely deacetylated by multiple HDAC isoforms. The high structural similarity of the HDAC1 and HDAC2 catalytic sites lead to many overlapping non-histone targets, as seen in our dataset. In conclusion, our data suggested that individual targets of either HDAC1 or HDAC2 exist.

4.3. HDAC1/2 Activity Phenotype in HCT116 cells

While our approach was focused on the distinction between HDAC1 and HDAC2 activity, we also improved the understanding of mechanisms behind observed phenotypes, especially with regards to the cell cycle block in G2/M phase and the mechanism behind the regulation of total HDAC1 and HDAC2 activity.

4.3.1. HDAC1/2 Loss Arrests Growth and Increases G2/M Phase Cells

In the HCT116 cell line we found the combined loss of HDAC1 and HDAC2 expression to lead to an increase in G2/M phase cells and a proliferation stop. In general, HDAC inhibitors influence the cell cycle of cancer cells in various ways. For example phenylbutyrate treatment in WB-F344 rat liver cells and butyrate treatment in mouse embryonic fibroplasts lead to an increase in G1 phase cells[185, 82]. In the neuroblastoma cell line UKF-NB-4 valproic acid leads to increased G1 phase cells[186]. This leads to the impression that short chain fatty acid based inhibitors tend to arrest cells in G1 phase. For other HDAC inhibitors, like MS-275 (Entiostat), the cell's reaction seemed to depend on the cell line, a 24 h treatment in HCT116 cells leads to increased G1 phase cells [187], but treatment in HepG2 and Huh7 lines increases the percentage of G2/M phase cells[93]. Similarly, in HepG2 and Huh7 lines, treatment with HDAC inhibitor FK228 (Rhomidepsin) lead to more G2/M phase cells[93]. These results give a mixed impression, of which inhibitor will cause the cell to be blocked in which cell cycle phase. Looking at genetically altered cell lines, for more HDAC isoform specific effects, Yamaguchi *et al.* showed that a double knockout of HDAC1 and HDAC2 in primary mouse fibroblasts led the cells arrest in G1[89]. Targeting HDAC1 expression by siRNA in U2OS cell arrested some cells in G1 phase, but also increased the part of G2/M phase, where the HDAC1 knockdown cells died during mitosis[162]. Cells carrying a HDAC1 and HDAC2 double knockout stopped proliferating [151, 154], which could neither be rescued by catalytic inactive HDAC1 nor catalytic inactive HDAC2[151]. While our result adds to the complexity of the field of cell cycle

blocks, a clear pattern remains to be identified.

Since we and others found that single knockouts are being tolerated, this suggests that some cancer types will tolerate inhibition of a single HDAC isoform. While HDAC inhibitor treatment is an approved cancer therapy and is therefore known to help, our results mean that a truly HDAC2 selective inhibitor will not act through a proliferation stop or a cell cycle block, but rather through other various epigenetic effects.

In HeLa cells a HDAC2 knockdown leads to an increase of $p21^{Cip1/WAF1}$ protein expression and to no significant change in the cell cycle profile, except for an increase of apoptotic cells[22]. HDAC1 deficient cells derived from embryonic knockout mice have increased levels of $p21^{Cip1/WAF1}$ and $p27^{Kip1}$ [54]. In mice embryonic stem cells $p21^{Cip1/WAF1}$ mRNA levels increased upon treatment with TSA or upon HDAC1 knockout, which was reversible by reintroduction of HDAC1[88]. $p21^{Cip1/WAF1}$ is a common target of HDAC inhibitors and plays a major role in their effect on the cell cycle[188, 87]. $p21^{Cip1/WAF1}$ induction is supposed to lead to a block at the G1/S barrier[52].

Drawing from previous studies on $p21^{Cip1/WAF1}$, the increased amount of G2/M phase cells we observed upon HDAC1/2 protein loss (see fig. 3.15 on p. 67), implied that the cell cycle block was not mediated by $p21^{Cip1/WAF1}$, since induction of $p21^{Cip1/WAF1}$ was supposed to lead to a block at the G1/S phase transition. As the G2/M phase transition check point controls for DNA integrity, damage to DNA may explain our observation.

4.3.2. Cellular Mechanism for a Constant HDAC1/2 Total Activity

We observed an increase in the endogenous isoforms protein expression upon knocking out one isoform of the HDAC1/2 pair, which was reversible by the reintroduction of the knocked out isoform. This compensatory effect was not observable on transcript level. Our results suggest a model, where cells try to maintain constant HDAC1/2 overall activity. We found that the mechanism of the regulation must either act during translation or by altering protein turnover. Jurkin *et al.* observed crosstalk between HDAC1 and HDAC2 on protein level, but not on mRNA level in mouse embryonic stem-cells, fibroblasts and F9 cell lines upon knockout of either HDAC1 or HDAC2, respectively[163]. One of the earliest observations of this crosstalk was a siRNA mediated knockdown of either HDAC1 or HDAC2 in U2OS cells, which lead to slight increases in the corresponding native isoform[162]. shRNA knockdowns of either HDAC1 or HDAC2 in MEF cells lead to increases of the corresponding native isoform[89]. MEF cells isolated from HDAC2 conditional knockout mice showed elevated HDAC1 protein levels after activating the HDAC2 knockout[151]. Our results as well as other studies imply the existence of an ability of the cells to sense the HDAC1/2 activity levels and react. Dissecting and influencing this cellular mechanism would enable investigators to influence HDAC expression and therefore activity levels without directly inhibiting HDACs. Should it prove impossible to generate fully HDAC2 selective inhibitors, this pathway could be a solution.

In 2016, Serebryannyy *et al.* found that HDAC1 and HDAC2 interacted with nuclear actin, where the data suggested a preferential binding with monomeric actin. While excluding that actin acted as a competitive substrate, actin inhibited HDAC1 and HDAC2 activity in *in-vitro* assays. Additionally, HDAC inhibition reduced the interaction between actin and the respective isoform[189]. The ability of actin to interact with HDAC1 and HDAC2 suggested a stabilization mechanism, since complexes are in a lower thermodynamic state and therefore more stable. We observed no difference in stability between the endogenous HDAC isoforms and the exogenous isoforms (see fig. 3.12 on p. 61). If nuclear actin increased the stability of HDAC1 and HDAC2, this suggested that the additional peptide tail of the exogenous isoform did not influence the actin-HDAC interaction. On a speculative note, since nuclear monomeric actin interacts with HDAC1 and HDAC2, this could influence the actin monomer-polymer composition, which in turn could represent a HDAC1/2 activity sensor of the cells.

In 2014 Yang *et al.* presented that the transcription factors Sp1 and Sp3 are involved in the regulation of HDAC1 and HDAC2 mRNA levels[190]. Sp1 and Sp3 bind to the promoter region of HDAC1 and HDAC2 and recruit SET1, a methyltransferase, and p300, an acetyltransferase[190]. Further dissecting the cross-talk of epigenetic modifications at the HDAC1 and HDAC2 promoters may shed light on the mechanisms of HDAC1/HDAC2 overexpression in cancers[21, 22, 23]. Since we did not observe any compensation between HDAC1 and HDAC2 at the transcript level, the mechanism described by Yang *et al.* is not responsible for the compensation between HDAC1 and HDAC2 in the presented model cell lines.

A phylogenetic analysis of the HDAC family enzymes revealed the order of class I isoform divergence. HDAC8 diverged first, then HDAC3 evolution diverged and most recently HDAC1 and HDAC2 split apart[50]. In evolutionary terms, these two isoforms only split up very recently[50]. The recent divergence of HDAC1 and HDAC2 explains the many shared functions of HDAC1 and HDAC2, which in turn gave a rationale, why a compensation between the two isoforms may be able to maintain similar cellular processes.

4.4. Limitations of the Study

Every new insight generated comes with certain limitations and it is advisable to be aware of such limitations. For the presented study, the following limitations should be considered:

- The presented work was performed *in-vitro* and in many cases *in-vitro* work is not translatable to patients. This risk accompanies all *in-vitro* studies. Through carefully chosen controls, we have ourselves identified and excluded results that originated from our own genetic modifications, increasing our confidence in our findings.
- While the HCT116 cell lines is a well established and an often used colon cancer cell line, many results from this study were obtained from this single cell line. This poses the risk that results were specific to this cell lines and would not translate to other cell lines or to

patients.

- The assay we created based on the commonly known histone acetylation site Ac-H3K9 relies on the presence of either HDAC1 or HDAC2 protein in cells for selectivity. Therefore, this assay is not translatable to measure HDAC inhibition efficacy in patient samples. This limitation drove us to further evaluate non-histone acetylation sites for selectivity, which enable a translation to patient samples.
- With regards to the unknown acetylation sites that we identified, there is the risk that these sites are stochasticly acetylated as a sort of "background acetylation", carrying no specific function. As we showed dependency on HDAC1/2 activity, we consider this risk as minimal.

4.5. Conclusion and Outlook

To improve cancer therapeutics, this study aimed to differentiate between the potency of small molecules to inhibit HDAC1 and HDAC2 in cells. The distinction can facilitate the development of isoenzyme-selective cancer therapy drugs and if drugs get more selective, the rationale is that they lose some of their dose-limiting side-effects.

We approached activity readouts in two ways: A readout is either selective between HDAC1 and HDAC2, or the readout depends on the activity of both isoforms. The first case would be a measurable indicator of activity of a single isoform, which could be used as a biomarker. The second case would be an indicator of combined HDAC1/2 activity. For the distinction between HDAC1 and HDAC2, a set of highly homologous clonal cell lines was created, in which the expression of either HDAC1 or HDAC2 can be controlled without triggering compensation of the other HDAC's expression from the endogenous gene. In a first scenario, the model cell lines allowed us to measure the effect of an inhibitor on either HDAC1 or HDAC2 by quantifying a marker of combined HDAC1/2 activity in the context of the expression of a single isoform. In a second scenario, this set of cell lines enabled us to search for markers of the individual activity of either HDAC1 or HDAC2.

For the first scenario, we showed that the measurement of the inhibition of either HDAC1 or HDAC2 with the histone acetylation site Ac-H3K9 as marker is possible in the context of single expression. The same histone acetylation sites may be modified differently in proximity of different genes, which is not separated by measuring the pool. Acetylations on non-histone proteins change the charge of the surface and interact with other post translational modifications (PTMs), e.g. the proteome and the ubiquitylome [191, 192]. We reasoned that these acetylations would be less DNA-context dependent compared to histone acetylations. In the model cell lines new acetylation sites were identified as well as specific acetylation sites, which may serve as marker for either HDAC1 or HDAC2 activity. Acetylated Matrin 3 on K711 and K712 was identified to react on HDAC2 activity loss and the acetylation site on lysine 108 of the heat shock protein HSPA8/HSP7C/Hsp70 was identified to react to the loss of HDAC1 activity. An initial verification of the acetylation site on Matrin 3 showed an increase upon either HDAC1 or HDAC2 loss, which makes this acetylation site a good candidate for the scenario in which sites are used in a single expression context.

To further elucidate the identified acetylation sites more selective antibodies targeting these sites are needed and a new set of monoclonal antibodies was created, which remain to be validated. Such antibodies can further validate the acetylomics data for the HSPA8 peptide and dissect the predictability of two acetylations on the MATR3 peptide. Each antibody could enable a sandwich ELISA assay. A commercial capture antibody would bind the target protein and the detecting antibody would target the acetylation site. The high sensitivity and specificity of an ELISA assay may enable the characterization of the activity of individual HDAC isoforms in tumor samples, which could be used in personalized medicine.

5. Bibliography

[1] Douglas Hanahan and Robert A. Weinberg. The Hallmarks of Cancer. *Cell*, 100: 57–70, **2000**.

[2] Douglas Hanahan and Robert A. Weinberg. Hallmarks of cancer: the next generation. *Cell*, 144: 646–674, **2011**.

[3] Spencer L. James, Degu Abate, Kalkidan Hassen Abate, et al. Global, regional, and national incidence, prevalence, and years lived with disability for 354 diseases and injuries for 195 countries and territories, 1990–2017: a systematic analysis for the Global Burden of Disease Study 2017. *The Lancet*, 392(10159): 1789–1858, **2018**.

[4] Rafael Lozano, Mohsen Naghavi, Kyle Foreman, et al. Global and regional mortality from 235 causes of death for 20 age groups in 1990 and 2010: a systematic analysis for the Global Burden of Disease Study 2010. *The Lancet*, 380: 2095–2128, **2012**.

[5] Bernard W. Stewart and Christopher P. Wild. World Cancer Report 2014. *Lyon: IARC Press*, **2014**.

[6] Justin Guinney, Rodrigo Dienstmann, Xin Wang, et al. The consensus molecular subtypes of colorectal cancer. *Nature Medicine*, 21: 1350–1356, **2015**.

[7] Andrew P. Feinberg and Bert Vogelstein. Hypomethylation distinguishes genes of some human cancers from their normal counterparts. *Nature*, 301: 89–92, **1983**.

[8] Susan E. Goelz, Bert Vogelstein, Stanley R. Hamilton, and Andrew P. Feinberg. Hypomethylation of DNA from benign and malignant human colon neoplasms. *Science*, 228: 187, **1985**.

[9] Peter A. Jones and Stephen B. Baylin. The fundamental role of epigenetic events in cancer. *Nature Reviews Genetics*, 3: 415–428, **2002**.

[10] Andrew P. Feinberg, Rolf Ohlsson, and Steven Henikoff. The epigenetic progenitor origin of human cancer. *Nature Reviews Genetics*, 7: 21–33, **2006**.

[11] Sibaji Sarkar, Garrick Horn, Kimberly Moulton, et al. Cancer development, progression, and therapy: An epigenetic overview. *International Journal of Molecular Sciences*, 14: 21087, **2013**.

[12] Peter A. Jones and Peter W. Laird. Cancer-epigenetics comes of age. *Nature Genetics*, 21: 163–167, **1999**.

[13] Stephen B. Baylin and James G. Herman. DNA hypermethylation in tumorigenesis: epigenetics joins genetics. *Trends in Genetics*, 16: 168–174, **2000**.

[14] Yana Chervona and Max Costa. Histone modifications and cancer: biomarkers of prognosis? *American Journal of Cancer Research*, 2: 589–597, **2012**.

[15] Christoph Plass, Stefan M. Pfister, Anders M. Lindroth, et al. Mutations in regulators of the epigenome and their connections to global chromatin patterns in cancer. *Nature Reviews Genetics*, 14: 765–780, **2013**.

[16] Wolfgang Fischle, Yanming Wang, and C. David Allis. Histone and chromatin cross-talk. *Current Opinion in Cell Biology*, 15: 172–183, **2003**.

[17] Thomas Jenuwein and C. David Allis. Translating the histone code. *Science*, 293: 1074, **2001**.

[18] Brian D. Strahl and C. David Allis. The language of covalent histone modifications. *Nature*, 403: 41–45, **2000**.

[19] Bryan M. Turner. Histone acetylation and an epigenetic code. *BioEssays*, 22: 836–845, **2000**.

[20] Victoria L. Luchenko, Thomas Litman, Arup R. Chakraborty, et al. Histone deacetylase inhibitor-mediated cell death is distinct from its global effect on chromatin. *Molecular Oncology*, 8: 1379–1392, **2014**.

[21] Ping Zhu, Elke Martin, Jörg Mengwasser, et al. Induction of HDAC2 expression upon loss of APC in colorectal tumorigenesis. *Cancer Cell*, 5: 455–463, **2004**.

[22] Bao H. Huang, Mirtha Laban, Chung H-W Leung, et al. Inhibition of histone deacetylase 2 increases apoptosis and $p21^{Cip1/WAF1}$ expression, independent of histone deacetylase 1. *Cell Death and Differentiation*, 12: 395–404, **2005**.

[23] Katsuyoshi Ishihama, Mitsunori Yamakawa, Shuho Semba, et al. Expression of HDAC1 and CBP/p300 in human colorectal carcinomas. *Journal of Clinical Pathology*, 60: 1205, **2007**.

[24] Andrew J. Wilson, Do-Sun Byun, Natalia Popova, et al. Histone Deacetylase 3 (HDAC3) and Other Class I HDACs Regulate Colon Cell Maturation and p21 Expression and Are

Deregulated in Human Colon Cancer. *Journal of Biological Chemistry*, 281: 13548–13558, **2006**.

[25] Jaehwi Song, J. Heoni Noh, Jong Heun Lee, et al. Increased expression of histone deacetylase 2 is found in human gastric cancer. *APMIS*, 113: 264–268, **2005**.

[26] Kalipso Halkidou, Luke Gaughan, Susan Cook, et al. Upregulation and nuclear recruitment of HDAC1 in hormone refractory prostate cancer. *The Prostate*, 59: 177–189, **2004**.

[27] Lisa Eshun-Wilson, Rui Zhang, Didier Portran, et al. Effects of α-tubulin acetylation on microtubule structure and stability. *Proceedings of the National Academy of Sciences*, 116: 10366, **2019**.

[28] Carsten Janke. The tubulin code: Molecular components, readout mechanisms, and functions. *Journal of Cell Biology*, 206: 461, **2014**.

[29] Carsten Janke and Guillaume Montagnac. Causes and consequences of microtubule acetylation. *Current Biology*, 27: 1287–1292, **2017**.

[30] Lucia Di Marcotullio, Gianluca Canettieri, Paola Infante, Azzura Greco, and Alberto Gulino. Protected from the inside: Endogenous histone deacetylase inhibitors and the road to cancer. *Biochimica Et Biophysica Acta*, 1815: 241–252, **2011**.

[31] Guohong Li, Raphael Margueron, Guobin Hu, et al. Highly compacted chromatin formed in vitro reflects the dynamics of transcription activation in vivo. *Molecular Cell*, 38: 41–53, **2010**.

[32] Chunaram Choudhary, Chanchal Kumar, Florian Gnad, et al. Lysine acetylation targets protein complexes and co-regulates major cellular functions. *Science*, 325: 834–840, **2009**.

[33] Michael S. Finnin, Jill R. Donigian, Alona Cohen, et al. Structures of a histone deacetylase homologue bound to the TSA and SAHA inhibitors. *Nature*, 401: 188–193, **1999**.

[34] Wen-Ming Yang, Ya-Li Yao, Jian-Min Sun, James R. Davie, and Edward Seto. Isolation and characterization of cDNAs corresponding to an additional member of the human histone deacetylase gene family. *Journal of Biological Chemistry*, 272: 28001–28007, **1997**.

[35] Julie Ahringer. NuRD and SIN3: histone deacetylase complexes in development. *Trends in Genetics*, 16: 351–356, **2000**.

[36] Thorsten Heinzel, Robert M. Lavinsky, Tina-Marie Mullen, et al. A complex containing N-CoR, mSin3 and histone deacetylase mediates transcriptional repression. *Nature*, 387: 43–48, **1997**.

[37] Eric Y. Huang, Jinsong Zhang, Eric A. Miska, et al. Nuclear receptor corepressors partner with class II histone deacetylases in a Sin3-independent repression pathway. *Genes and Development*, 14: 45–54, **2000**.

[38] Carol D. Laherty, Wen-Ming Yang, Jian-Min Sun, et al. Histone deacetylases associated with the mSin3 corepressor mediate mad transcriptional repression. *Cell*, 89: 349–356, **1997**.

[39] Laszlo Nagy, Hung-Ying Kao, Debabrata Chakravarti, et al. Nuclear Receptor Repression Mediated by a Complex Containing SMRT, mSin3A, and Histone Deacetylase. *Cell*, 89: 373–380, **1997**.

[40] Angie You, Jeffrey K. Tong, Christina M. Grozinger, and Stuart L. Schreiber. CoREST is an integral component of the CoREST- human histone deacetylase complex. *Proceedings of the National Academy of Sciences*, 98: 1454, **2001**.

[41] Lelia Alland, Rebecca Muhle, Harry Hou, et al. Role for N-CoR and histone deacetylase in Sin3-mediated transcriptional repression. *Nature*, 387: 49–55, **1997**.

[42] Eric Verdin, Franck Dequiedt, and Herbert G. Kasler. Class II histone deacetylases: versatile regulators. *Trends in Genetics*, 19: 286–293, **2003**.

[43] Işin Çakir, Mario Perello, Omar Lansari, et al. Hypothalamic Sirt1 regulates food intake in a rodent model system. *PLoS One*, 4: e8322, **2009**.

[44] Lei Zhong, Agustina D'Urso, Debra Toiber, et al. The histone deacetylase sirt6 regulates glucose homeostasis via hif1α. *Cell*, 140: 280–293, **2010**.

[45] Tatsuya Yoshizawa, Md. Fazlul Karim, Yoshifumi Sato, et al. SIRT7 controls hepatic lipid metabolism by regulating the ubiquitin-proteasome pathway. *Cell Metabolism*, 19: 712–721, **2014**.

[46] Brian J. North, Brett L. Marshall, Margie T. Borra, John M. Denu, and Eric Verdin. The human Sir2 ortholog, SIRT2, is an NAD^+-dependent tubulin deacetylase. *Molecular Cell*, 11: 437–444, **2003**.

[47] Annemieke J.M. de Ruijter, Albert H. van Gennip, Huib N. Caron, Stephan Kemp, and

André B.P. van Kuilenburg. Histone deacetylases (HDACs): characterization of the classical HDAC family. *Biochemical Journal*, 370: 737, **2003**.

[48] Alejandro Villagra, Fengdong Cheng, Hong-Wei Wang, et al. The histone deacetylase HDAC11 regulates the expression of interleukin 10 and immune tolerance. *Nature Immunology*, 10: 92, **2008**.

[49] F. F. Wagner, Y. L. Zhang, D. M. Fass, et al. Kinetically selective inhibitors of histone deacetylase 2 (HDAC2) as cognition enhancers. *Chemical Science*, 6: 804–815, **2015**.

[50] Ivan V. Gregoretti, Yun-Mi Lee, and Holly V. Goodson. Molecular evolution of the histone deacetylase family: functional implications of phylogenetic analysis: functional implications of phylogenetic analysis. *Journal of Molecular Biology*, 338: 17–31, **2004**.

[51] Milin R. Acharya, Alex Sparreboom, Jürgen Venitz, and William D. Figg. Rational development of histone deacetylase inhibitors as anticancer agents: A review. *Molecular Pharmacology*, 68: 917, **2005**.

[52] Jessica E. Bolden, Melissa J. Peart, and Ricky W. Johnstone. Anticancer activities of histone deacetylase inhibitors. *Nature Reviews Drug Discovery*, 5: 769–784, **2006**.

[53] Tomas Eckschlager, Johana Plch, Marie Stiborova, and Jan Hrabeta. Histone deacetylase inhibitors as anticancer drugs. *International Journal of Molecular Sciences*, 18, **2017**.

[54] Gerda Lagger, Dónal O'Carroll, Martina Rembold, et al. Essential function of histone deacetylase 1 in proliferation control and CDK inhibitor repression. *EMBO Journal*, 21: 2672–2681, **2002**.

[55] Rusty L. Montgomery, Christopher A. Davis, Matthew J. Potthoff, et al. Histone deacetylases 1 and 2 redundantly regulate cardiac morphogenesis, growth, and contractility. *Genes and Development*, 21: 1790–1802, **2007**.

[56] Stephan Zimmermann, Franz Kiefer, Michela Prudenziati, et al. Reduced body size and decreased intestinal tumor rates in HDAC2-mutant mice. *Cancer Research*, 67: 9047–9054, **2007**.

[57] J. S. Guan, S. J. Haggarty, E. Giacometti, et al. HDAC2 negatively regulates memory formation and synaptic plasticity. *Nature*, 459: 55–60, **2009**.

[58] Pengpeng Ma and Richard M. Schultz. Histone deacetylase 1 (HDAC1) regulates hi-

stone acetylation, development, and gene expression in preimplantation mouse embryos. *Developmental Biology*, 319: 110–120, **2008**.

[59] Pengpeng Ma and Richard M. Schultz. Histone deacetylase 2 (HDAC2) regulates chromosome segregation and kinetochore function via H4K16 deacetylation during oocyte maturation in mouse. *PLoS Genetics*, 9: e1003377, **2013**.

[60] A. Leder, S. Orkin, and P. Leder. Differentiation of erythroleukemic cells in the presence of inhibitors of DNA synthesis. *Science*, 190: 893, **1975**.

[61] M. G. Riggs, R. G. Whittaker, J. R. Neumann, and V. M. Ingram. n-Butyrate causes histone modification in HeLa and Friend erythroleukaemia cells. *Nature*, 268: 462–464, **1977**.

[62] M. Yoshida, M. Kijima, M. Akita, and T. Beppu. Potent and specific inhibition of mammalian histone deacetylase both in vivo and in vitro by trichostatin A. *Journal of Biological Chemistry*, 265: 17174–17179, **1990**.

[63] Victoria M. Richon, Stephane Emiliani, Eric Verdin, et al. A class of hybrid polar inducers of transformed cell differentiation inhibits histone deacetylases. *Proceedings of the National Academy of Sciences*, 95: 3003, **1998**.

[64] Martin Göttlicher, S. Minucci, P. Zhu, et al. Valproic acid defines a novel class of HDAC inhibitors inducing differentiation of transformed cells. *EMBO Journal*, 20: 6969–6978, **2001**.

[65] Hirotsugu Ueda, Nakajima, Hidenori, Hori, Yasuhiro, Takashi Fujita, et al. FR901228, a novel antitumor bicyclic depsipeptide. *Journal of Antibiotics*, 47: 301–310, **1994**.

[66] Elise A. Olsen, Youn H. Kim, Timothy M. Kuzel, et al. Phase IIB multicenter trial of vorinostat in patients with persistent, progressive, or treatment refractory cutaneous T-cell lymphoma. *Journal of Clinical Oncology*, 25: 3109–3115, **2007**.

[67] Madeleine Duvic, Rakshandra Talpur, Xiao Ni, et al. Phase 2 trial of oral vorinostat (suberoylanilide hydroxamic acid, SAHA) for refractory cutaneous T-cell lymphoma (CTCL). *Blood*, 109: 31, **2007**.

[68] John C. Byrd, Guido Marcucci, Mark R. Parthun, et al. A phase 1 and pharmacodynamic study of depsipeptide (FK228) in chronic lymphocytic leukemia and acute myeloid leukemia. *Blood*, 105: 959, **2005**.

[69] Richard L. Piekarz, Robin Frye, Maria Turner, et al. Phase II multi-institutional trial of the

histone deacetylase inhibitor romidepsin as monotherapy for patients with cutaneous T-cell lymphoma. *Journal of Clinical Oncology*, 27: 5410–5417, **2009**.

[70] Hyon-Zu Lee, Virginia E. Kwitkowski, Pedro L. Del Valle, et al. FDA approval: belinostat for the treatment of patients with relapsed or refractory peripheral T-cell lymphoma. *Clinical Cancer Research*, 21: 2666, **2015**.

[71] Karly P. Garnock-Jones. Panobinostat: first global approval. *Drugs*, 75: 695–704, **2015**.

[72] Xianping Lu, Zhiqiang Ning, Zhibin Li, Haixiang Cao, and Xinhao Wang. Development of chidamide for peripheral T-cell lymphoma, the first orphan drug approved in China. *Intractable and Rare Diseases Research*, pages 1–7, **2016**.

[73] Jin Cai, Hongtao Wei, Kwon Ho Hong, et al. Discovery, bioactivity and docking simulation of Vorinostat analogues containing 1,2,4-oxadiazole moiety as potent histone deacetylase inhibitors and antitumor agents. *Bioorganic & Medicinal Chemistry*, 23: 3457–3471, **2015**.

[74] Jerome C. Bressi, Andy J. Jennings, Robert Skene, et al. Exploration of the HDAC2 foot pocket: Synthesis and SAR of substituted N-(2-aminophenyl)benzamides. *Bioorg Med Chem Lett*, 20: 3142–3145, **2010**.

[75] Nagma Khan, Michael Jeffers, Sampath Kumar, et al. Determination of the class and isoform selectivity of small-molecule histone deacetylase inhibitors. *Biochemical Journal*, 409: 581, **2008**.

[76] Christian Schölz, Brian T. Weinert, Sebastian A. Wagner, et al. Acetylation site specificities of lysine deacetylase inhibitors in human cells. *Nature Biotechnology*, 33: 415–423, **2015**.

[77] Ryohei Furumai, Akihisa Matsuyama, Nobuyuki Kobashi, et al. FK228 (Depsipeptide) as a natural prodrug that inhibits class I histone deacetylases. *Cancer Research*, 62: 4916, **2002**.

[78] Zhi-Qiang Ning, Zhi-Bin Li, Michael J. Newman, et al. Chidamide (CS055/HBI-8000): a new histone deacetylase inhibitor of the benzamide class with antitumor activity and the ability to enhance immune cell-mediated tumor cell cytotoxicity. *Cancer Chemotherapy and Pharmacology*, 69: 901–909, **2012**.

[79] Surya A. Reis, Balaram Ghosh, J. Adam Hendricks, et al. Light-controlled modulation of gene expression by chemical optoepigenetic probes. *Nature Chemical Biology*, 12: 317–323, **2016**.

[80] Florence F. Wagner, Michel Weïwer, Stefan Steinbacher, et al. Kinetic and structural insights into the binding of histone deacetylase 1 and 2 (HDAC1, 2) inhibitors. *Bioorganic & Medicinal Chemistry*, **2016**.

[81] Andrea Newbold, Katrina J. Falkenberg, H. Miles Prince, and Ricky W. Johnstone. How do tumor cells respond to HDAC inhibition? *FEBS Journal*, 283: 4032–4046, **2016**.

[82] Romanov, Vasily S., Abramova, Maria V., Svetlikova, Svetlana B., et al. p21(Waf1) is required for cellular senescence but not for cell cycle arrest induced by the HDAC inhibitor sodium butyrate. *Cell Cycle*, 9: 3945–3955, **2010**.

[83] Wei-Sheng Xu, Gisela Perez, Lang Ngo, Chang-Yun Gui, and Paul A. Marks. Induction of polyploidy by histone deacetylase inhibitor: A pathway for antitumor effects. *Cancer Research*, 65: 7832, **2005**.

[84] Joon-Ho Cho, Manjari Dimri, and Goberdhan P. Dimri. MicroRNA-31 Is a Transcriptional Target of Histone Deacetylase Inhibitors and a Regulator of Cellular Senescence. *Journal of Biological Chemistry*, 290: 10555–10567, **2015**.

[85] Warren Fiskus, Michael Pranpat, Maria Balasis, et al. Histone deacetylase inhibitors deplete enhancer of zeste 2 and associated polycomb repressive complex 2 proteins in human acute leukemia cells. *Molecular Cancer Therapeutics*, 5: 3096, **2006**.

[86] Ling Qiu, Andrew Burgess, David P. Fairlie, et al. Histone deacetylase inhibitors trigger a G2 checkpoint in normal cells that is defective in tumor cells. *Molecular Biology of the Cell*, 11: 2069–2083, **2000**.

[87] Ralph K. Lindemann, Brian Gabrielli, and Ricky W. Johnstone. Histone-Deacetylase Inhibitors for the Treatment of Cancer. *Cell Cycle*, 3: 777–786, **2004**.

[88] Gordin Zupkovitz, Julia Tischler, Markus Posch, et al. Negative and positive regulation of gene expression by mouse histone deacetylase 1. *Molecular and Cellular Biology*, 26: 7913, **2006**.

[89] Teppei Yamaguchi, Fabien Cubizolles, Yu Zhang, et al. Histone deacetylases 1 and 2 act in concert to promote the G1-to-S progression. *Genes and Development*, 24: 455–469, **2010**.

[90] Jeyran Shahbazi, Christopher J. Scarlett, Murray D. Norris, et al. Histone deacetylase 2 and N-Myc reduce p53 protein phosphorylation at serine 46 by repressing gene transcription of tumor protein 53-induced nuclear protein 1. *Oncotarget*, 5: 4257–4268, **2014**.

[91] Z. Li, Q. Hao, J. Luo, et al. USP4 inhibits p53 and NF-κB through deubiquitinating and stabilizing HDAC2. *Oncogene*, **2015**.

[92] André Brandl, Tobias Wagner, Katharina M. Uhlig, et al. Dynamically regulated sumoylation of HDAC2 controls p53 deacetylation and restricts apoptosis following genotoxic stress. *Journal of Molecular Cell Biology*, 4: 284–293, **2012**.

[93] Hengyu Zhou, Ying Cai, Dina Liu, et al. Pharmacological or transcriptional inhibition of both HDAC1 and 2 leads to cell cycle blockage and apoptosis via $p21^{Waf1/Cip1}$ and p19INK4d upregulation in hepatocellular carcinoma. *Cell Proliferation*, 51: e12447, **2018**.

[94] Adrian Drazic, Line M. Myklebust, Rasmus Ree, and Thomas Arnesen. The world of protein acetylation. *Biochimica Et Biophysica Acta*, 1864: 1372–1401, **2016**.

[95] Jessica E. Bolden, W. Shi, K. Jankowski, et al. HDAC inhibitors induce tumor-cell-selective pro-apoptotic transcriptional responses. *Cell Death and Disease*, 4: e519, **2013**.

[96] Alba Pérez-Perarnau, Llorenç Coll-Mulet, Camila Rubio-Patiño, et al. Analysis of apoptosis regulatory genes altered by histone deacetylase inhibitors in chronic lymphocytic leukemia cells. *Epigenetics*, 6: 1228–1235, **2011**.

[97] S. Inoue, J. Riley, T. W. Gant, M. J. S. Dyer, and G. M. Cohen. Apoptosis induced by histone deacetylase inhibitors in leukemic cells is mediated by Bim and Noxa. *Leukemia*, 21: 1773, **2007**.

[98] Feng Chen, Xueyi Li, Emily Aquadro, et al. Inhibition of histone deacetylase reduces transcription of NADPH oxidases and ROS production and ameliorates pulmonary arterial hypertension. *Free Radical Biology and Medicine*, 99: 167–178, **2016**.

[99] Nichola Cruickshanks, Hossein A. Hamed, Laurence Booth, et al. Histone deacetylase inhibitors restore toxic BH3 domain protein expression in anoikis-resistant mammary and brain cancer stem cells, thereby enhancing the response to anti-ERBB1/ERBB2 therapy. *Cancer Biology and Therapy*, 14: 982–996, **2013**.

[100] Y. Zhang, M. Adachi, R. Kawamura, and K. Imai. Bmf is a possible mediator in histone deacetylase inhibitors FK228 and CBHA-induced apoptosis. *Cell Death and Differentiation*, 13: 129–140, **2006**.

[101] Sílvia Xargay-Torrent, Mónica López-Guerra, Ifigènia Saborit-Villarroya, et al.

Vorinostat-induced apoptosis in mantle cell lymphoma is mediated by acetylation of proapoptotic BH3-only gene promoters. *Clinical Cancer Research*, 17: 3956, **2011**.

[102] Matthew R. Ramsey, Lei He, Nicole Forster, Benjamin Ory, and Leif W. Ellisen. Physical association of HDAC1 and HDAC2 with p63 mediates transcriptional repression and tumor maintenance in squamous cell carcinoma. *Cancer Research*, 71: 4373, **2011**.

[103] Yan Zhao, Jing Tan, Li Zhuang, et al. Inhibitors of histone deacetylases target the Rb-E2F1 pathway for apoptosis induction through activation of proapoptotic protein Bim. *Proceedings of the National Academy of Sciences*, 102: 16090, **2005**.

[104] Yang Yang, Ying Zhao, Wenjuan Liao, et al. Acetylation of FoxO1 activates Bim expression to induce apoptosis in response to histone deacetylase inhibitor depsipeptide treatment. *Neoplasia*, 11: 313–324, **2009**.

[105] Camille Brochier, Gretel Dennis, Mark A. Rivieccio, et al. Specific Acetylation of p53 by HDAC Inhibition Prevents DNA Damage-Induced Apoptosis in Neurons. *The Journal of Neuroscience*, 33: 8621, **2013**.

[106] Jennifer S. Waby, Haridasan Chirakkal, ChenWei Yu, et al. Sp1 acetylation is associated with loss of DNA binding at promoters associated with cell cycle arrest and cell death in a colon cell line. *Molecular Cancer*, 9: 275, **2010**.

[107] Tabitha E. Wood, Shadi Dalili, Craig D. Simpson, et al. Selective inhibition of histone deacetylases sensitizes malignant cells to death receptor ligands. *Molecular Cancer Therapeutics*, 9: 246, **2010**.

[108] Clare McCourt, Pamela Maxwell, Roberta Mazzucchelli, et al. Elevation of c-FLIP in castrate-resistant prostate cancer antagonizes therapeutic response to androgen receptor–targeted therapy. *Clinical Cancer Research*, 18: 3822, **2012**.

[109] Yun Dai, Mohamed Rahmani, Paul Dent, and Steven Grant. Blockade of histone deacetylase inhibitor-induced RelA/p65 acetylation and NF-κB activation potentiates apoptosis in leukemia cells through a process mediated by oxidative damage, XIAP downregulation, and c-Jun N-terminal kinase 1 activation. *Molecular and Cellular Biology*, 25: 5429, **2005**.

[110] Luca A. Petruccelli, Daphné Dupéré-Richer, Filippa Pettersson, et al. Vorinostat induces reactive oxygen species and DNA damage in acute myeloid leukemia cells. *PLoS One*, 6: e20987, **2011**.

[111] Sushant K. Kachhap, Nadine Rosmus, Spencer J. Collis, et al. Downregulation of

homologous recombination DNA repair genes by HDAC inhibition in prostate cancer is mediated through the E2F1 transcription factor. *PLoS One*, 5: e11208, **2010**.

[112] Andelko Hrzenjak, Farid Moinfar, Marie-Luise Kremser, et al. Valproate inhibition of histone deacetylase 2 affects differentiation and decreases proliferation of endometrial stromal sarcoma cells. *Molecular Cancer Therapeutics*, 5: 2203, **2006**.

[113] Yo-ichi Yamashita, Mitsuo Shimada, Norifumi Harimoto, et al. Histone deacetylase inhibitor trichostatin A induces cell-cycle arrest/apoptosis and hepatocyte differentiation in human hepatoma cells. *International Journal of Cancer*, 103: 572–576, **2003**.

[114] Pamela N. Munster, Tiffany Troso-Sandoval, Neal Rosen, et al. The histone deacetylase inhibitor suberoylanilide hydroxamic acid induces differentiation of human breast cancer cells. *Cancer Research*, 61: 8492, **2001**.

[115] Michael Bots, Inge Verbrugge, Benjamin P. Martin, et al. Differentiation therapy for the treatment of t(8;21) acute myeloid leukemia using histone deacetylase inhibitors. *Blood*, 123: 1341, **2014**.

[116] Monica L. Guzman, Neng Yang, Krishan K. Sharma, et al. Selective activity of the histone deacetylase inhibitor AR-42 against leukemia stem cells: A novel potential strategy in acute myelogenous leukemia. *Molecular Cancer Therapeutics*, 13: 1979, **2014**.

[117] Michael Dickinson, Ricky W. Johnstone, and H. Miles Prince. Histone deacetylase inhibitors: potential targets responsible for their anti-cancer effect. *Investigational New Drugs*, 28: 3–20, **2010**.

[118] Bin Zhang, Adam C. Strauss, Su Chu, et al. Effective targeting of quiescent chronic myelogenous leukemia stem cells by histone deacetylase inhibitors in combination with imatinib mesylate. *Cancer Cell*, 17: 427–442, **2010**.

[119] Thomas Robert, Fabio Vanoli, Irene Chiolo, et al. HDACs link the DNA damage response, processing of double-strand breaks and autophagy. *Nature*, 471: 74, **2011**.

[120] Yufang Shao, Zhonghua Gao, Paul A. Marks, and Xuejun Jiang. Apoptotic and autophagic cell death induced by histone deacetylase inhibitors. *Proceedings of the National Academy of Sciences*, 101: 18030, **2004**.

[121] Young Ju Lee, A. Jin Won, Jaewon Lee, et al. Molecular mechanism of SAHA on regulation of autophagic cell death in tamoxifen-resistant MCF-7 breast cancer cells. *International Journal of Medical Sciences*, 9: 881–893, **2012**.

[122] V. El-Khoury, S. Pierson, E. Szwarcbart, et al. Disruption of autophagy by the histone deacetylase inhibitor MGCD0103 and its therapeutic implication in B-cell chronic lymphocytic leukemia. *Leukemia*, 28: 1636, **2014**.

[123] Ina Oehme, Jan-Peter Linke, Barbara C. Böck, et al. Histone deacetylase 10 promotes autophagy-mediated cell survival. *Proceedings of the National Academy of Sciences*, 110: E2592, **2013**.

[124] M. V. Stankov, M. El Khatib, B. Kumar Thakur, et al. Histone deacetylase inhibitors induce apoptosis in myeloid leukemia by suppressing autophagy. *Leukemia*, 28: 577, **2013**.

[125] Takashi Murakami, Atsuko Sato, Nicole A.L. Chun, et al. Transcriptional modulation using HDACi depsipeptide promotes immune cell-mediated tumor destruction of murine B16 melanoma. *Journal of Investigative Dermatology*, 128: 1506–1516, **2008**.

[126] William J. Magner and Thomas B. Tomasi. Chromatin-immune connections: regulation of MHC and other genes. *Journal of Reproductive Immunology*, 48: 1–15, **2000**.

[127] Jasper Manning, Marie Indrova, Barbora Lubyova, et al. Induction of MHC class I molecule cell surface expression and epigenetic activation of antigen-processing machinery components in a murine model for human papilloma virus 16-associated tumours. *Immunology*, 123: 218–227, **2008**.

[128] A. Francesca Setiadi, Kyla Omilusik, Muriel D. David, et al. Epigenetic enhancement of antigen processing and presentation promotes immune recognition of tumors. *Cancer Research*, 68: 9601, **2008**.

[129] Sorin Armeanu, Michael Bitzer, Ulrich M. Lauer, et al. Natural killer cell–mediated lysis of hepatoma cells via specific induction of NKG2D ligands by the histone deacetylase inhibitor sodium valproate. *Cancer Research*, 65: 6321, **2005**.

[130] Søren Skov, Marianne Terndrup Pedersen, Lars Andresen, et al. Cancer cells become susceptible to natural killer cell killing after exposure to histone deacetylase inhibitors due to glycogen synthase kinase-3–dependent expression of MHC class I–related chain A and B. *Cancer Research*, 65: 11136, **2005**.

[131] Xiaosong Wu, Yi Tao, Jun Hou, Xiuqin Meng, and Jumei Shi. Valproic acid upregulates NKG2D ligand expression through an ERK-dependent mechanism and potentially enhances NK cell-mediated lysis of myeloma. *Neoplasia*, 14: 1178–1189, **2012**.

[132] Myriam Witvrouw, Jean-Claude Schmit, Barbara van Remoortel, et al. Cell type-

dependent effect of sodium valproate on human immunodeficiency virus type 1 replication in vitro. *AIDS Research and Human Retroviruses*, 13: 187–192, **1997**.

[133] Loyda Ylisastigui, Nancie M. Archin, Ginger Lehrman, Ronald J. Bosch, and David M. Margolis. Coaxing HIV-1 from resting CD4 T cells: histone deacetylase inhibition allows latent viral expression. *AIDS*, 18, **2004**.

[134] Kirston M. Barton, Nancie M. Archin, Kara S. Keedy, et al. Selective HDAC inhibition for the disruption of latent HIV-1 infection. *PLoS One*, 9: e102684, **2014**.

[135] Roger Badia, Judith Grau, Eva Riveira-Muñoz, et al. The thioacetate-ω(γ-lactam carboxamide) HDAC inhibitor ST7612AA1 as HIV-1 latency reactivation agent. *Antiviral Research*, 123: 62–69, **2015**.

[136] Johannes Gräff and Isabelle M. Mansuy. Epigenetic dysregulation in cognitive disorders. *European Journal of Neuroscience*, 30: 1–8, **2009**.

[137] Johannes Gräff and Li-Huei Tsai. The potential of HDAC inhibitors as cognitive enhancers. *Annual Review of Pharmacology Toxicology*, 53: 311–330, **2013**.

[138] Rashmi R. Shah. Safety and tolerability of histone deacetylase (HDAC) inhibitors in oncology. *Drug Safety*, 42: 235–245, **2019**.

[139] Jay Penney and Li-Huei Tsai. Histone deacetylases in memory and cognition. *Science Signaling*, 7: re12, **2014**.

[140] Ulrich K. Lämmli. Cleavage of Structural Proteins during the Assembly of the Head of Bacteriophage T4. *Nature*, 227: 680, **1970**.

[141] James T. Robinson, Helga Thorvaldsdóttir, Wendy Winckler, et al. Integrative genomics viewer. *Nature Biotechnology*, 29: 24, **2011**.

[142] S. Carrel, B. Sordat, and C. Merenda. Establishment of a cell line (Co-115) from a human colon carcinoma transplanted into nude mice. *Cancer Research*, 36: 3978, **1976**.

[143] F. Ann Ran, Patrick D. Hsu, Jason Wright, et al. Genome engineering using the CRISPR-Cas9 system. *Nature Protocols*, 8: 2281–2308, **2013**.

[144] Daehwan Kim, Geo Pertea, Cole Trapnell, et al. TopHat2: accurate alignment of transcriptomes in the presence of insertions, deletions and gene fusions. *Genome biology*, 14: R36, **2013**.

[145] Cole Trapnell, Brian A. Williams, Geo Pertea, et al. Transcript assembly and quantification by RNA-Seq reveals unannotated transcripts and isoform switching during cell differentiation. *Nature Biotechnology*, 28: 511–515, **2010**.

[146] Priyanka Somanath, Rachel Herndon Klein, and Paul S. Knoepfler. CRISPR-mediated HDAC2 disruption identifies two distinct classes of target genes in human cells. *PLoS One*, 12: e0185627, **2017**.

[147] Maciej Wiznerowicz and Didier Trono. Conditional suppression of cellular genes: lentivirus vector-mediated drug-inducible RNA interference. *Journal of Virology*, 77: 8957–8961, **2003**.

[148] Angelo Lupo, Elena Cesaro, Giorgia Montano, et al. KRAB-zinc finger proteins: A repressor family displaying multiple biological functions. *Current Genomics*, 14: 268–278, **2013**.

[149] Kamyar Hadian, Richard A. Griesbach, Scarlett Dornauer, et al. NF-κB essential modulator (NEMO) interaction with linear and lys-63 ubiquitin chains contributes to NF-κB activation. *The Journal of biological chemistry*, 286(29): 26107–26117, **2011**.

[150] Daniel Nagel, Stefani Spranger, Michelle Vincendeau, et al. Pharmacologic inhibition of MALT1 protease by phenothiazines as a therapeutic approach for the treatment of aggressive ABC-DLBCL. *Cancer Cell*, 22: 825–837, **2012**.

[151] Roel H. Wilting, Eva Yanover, Marinus R. Heideman, et al. Overlapping functions of HDAC1 and HDAC2 in cell cycle regulation and haematopoiesis. *EMBO Journal*, 29: 2586–2597, **2010**.

[152] Moritz Ludwig. Design of HDAC expression patterns in colon carcinoma cells: a tool for inhibitor screening. *TUM master's thesis*, **2013**.

[153] Santiago Ropero, Mario F. Fraga, Esteban Ballestar, et al. A truncating mutation of HDAC2 in human cancers confers resistance to histone deacetylase inhibition. *Nature Genetics*, 38: 566–569, **2006**.

[154] Shereen Jamaladdin, Richard D. W. Kelly, Laura O'Regan, et al. Histone deacetylase (HDAC) 1 and 2 are essential for accurate cell division and the pluripotency of embryonic stem cells. *Proceedings of the National Academy of Sciences*, 111: 9840–9845, **2014**.

[155] Jing Zhang, Shu Kan, Brian Huang, et al. Mule determines the apoptotic response

to HDAC inhibitors by targeted ubiquitination and destruction of HDAC2. *Genes and Development*, 25: 2610–2618, **2011**.

[156] Jin Hee Kim, Sang-Rok Lee, Li-Hua Li, et al. High cleavage efficiency of a 2A peptide derived from porcine teschovirus-1 in human cell lines, zebrafish and mice. *PLoS One*, 6: e18556, **2011**.

[157] Ziqing Liu, Olivia Chen, J. Blake Joseph Wall, et al. Systematic comparison of 2A peptides for cloning multi-genes in a polycistronic vector. *Scientific Reports*, 7(1): 2193, **2017**.

[158] Andrea L. Szymczak-Workman, Kate M. Vignali, and Dario A.A. Vignali. Design and Construction of 2A Peptide-Linked Multicistronic Vectors. *Cold Spring Harbor Protocols*, 2012(2): pdb.ip067876, **2012**.

[159] Henry Heberle, Gabriela Vaz Meirelles, Felipe R. da Silva, Guilherme P. Telles, and Rosane Minghim. InteractiVenn: A web-based tool for the analysis of sets through Venn diagrams. *BMC Bioinformatics*, 16: 169, **2015**.

[160] Niklaas Colaert, Kenny Helsens, Lennart Martens, Joël Vandekerckhove, and Kris Gevaert. Improved visualization of protein consensus sequences by iceLogo. *Nature Methods*, 6: 786–787, **2009**.

[161] Yumi Uetake and Greenfield Sluder. Prolonged prometaphase blocks daughter cell proliferation despite normal completion of mitosis. *Current Biology*, 20: 1666–1671, **2010**.

[162] Silvia Senese, Katrin Zaragoza, Simone Minardi, et al. Role for histone deacetylase 1 in human tumor cell proliferation. *Molecular and Cellular Biology*, 27: 4784–4795, **2007**.

[163] Jennifer Jurkin, Gordin Zupkovitz, Sabine Lagger, et al. Distinct and redundant functions of histone deacetylases HDAC1 and HDAC2 in proliferation and tumorigenesis. *Cell Cycle*, 10: 406–412, **2011**.

[164] Alexis Gonneaud, Julie M. Gagne, Naomie Turgeon, and Claude Asselin. The histone deacetylase HDAC1 regulates inflammatory signalling in intestinal epithelial cells. *Journal of Inflammation*, 11: 43, **2014**.

[165] Michael Haberland, Rusty L. Montgomery, and Eric N. Olson. The many roles of histone deacetylases in development and physiology: implications for disease and therapy. *Nature Reviews Genetics*, 10: 32, **2009**.

[166] Zhanwen Du, Jing Song, Yong Wang, et al. DNMT1 Stability Is Regulated by Proteins Coordinating Deubiquitination and Acetylation-Driven Ubiquitination. *Science Signaling*, 3(146): ra80, **2010**.

[167] Hassan Ashktorab, Kevin Belgrave, Fatemeh Hosseinkhah, et al. Global Histone H4 Acetylation and HDAC2 Expression in Colon Adenoma and Carcinoma. *Digestive Diseases and Sciences*, 54(10): 2109, **2008**.

[168] Shen-Hsi Yang, Elaine Vickers, Alexander Brehm, Tony Kouzarides, and Andrew D. Sharrocks. Temporal recruitment of the mSin3A-histone deacetylase corepressor complex to the ETS domain transcription factor Elk-1. *Molecular and Cellular Biology*, 21: 2802, **2001**.

[169] Hector Peinado, Esteban Ballestar, Manel Esteller, and Amparo Cano. Snail mediates E-cadherin repression by the recruitment of the Sin3A/histone deacetylase 1 (HDAC1)/HDAC2 complex. *Molecular and Cellular Biology*, 24: 306, **2004**.

[170] Melissa M. Singh, Blake Johnson, Avinashnarayan Venkatarayan, et al. Preclinical activity of combined HDAC and KDM1A inhibition in glioblastoma. *Neuro-Oncology*, 17(11): 1463–1473, **2015**.

[171] Aimée N. Laporte, Neal M. Poulin, Jared J. Barrott, et al. Death by HDAC Inhibition in Synovial Sarcoma Cells. *Molecular Cancer Therapeutics*, 16(12): 2656, **2017**.

[172] Ching-Ling Lin, Ming-Lin Tsai, Chun-Yu Lin, et al. HDAC1 and HDAC2 Double Knockout Triggers Cell Apoptosis in Advanced Thyroid Cancer. *International Journal of Molecular Sciences*, 20: 454, **2019**.

[173] M. Vergelli, B. Hemmer, P. A. Muraro, et al. Human autoreactive CD4+ T cell clones use perforin- or Fas/Fas ligand-mediated pathways for target cell lysis. *The Journal of Immunology*, 158(6): 2756, **1997**.

[174] Tilen Praper, Andreas Sonnen, Gabriella Viero, et al. Human perforin employs different avenues to damage membranes. *Journal of Biological Chemistry*, 286(4): 2946–2955, **2011**.

[175] Hui-Min Zhou, Yuan-Yuan Fang, Paul M. Weinberger, et al. Transgelin increases metastatic potential of colorectal cancer cells in vivo and alters expression of genes involved in cell motility. *BMC Cancer*, 16: 55, **2016**.

[176] Laurie Arnaud, Philippe Benech, Louise Greetham, et al. The Alzheimer's disease

risk factor APOE4 drives pro-inflammation in human astrocytes *via* HDAC-dependent repression of TAGLN3. *bioRxiv*, page 2021.04.16.440108, **2021**.

[177] Xiaoyu Zhu, Xin Liu, Zhongyi Cheng, et al. Quantitative analysis of global proteome and lysine acetylome reveal the differential impacts of VPA and SAHA on HL60 cells. *Scientific Reports*, 6: 19926, **2016**.

[178] Zhiwen Pan, Mingli Wang, Zhen Ye, Shengjie Zhang, and Xiaohong Xu. Global analysis of histone lysine acetylation and proteomic changes in EC109 cells treated with the histone deacetylase inhibitor FK228. *Oncology letters*, 15: 7973–7980, **2018**.

[179] C. Alexander Valencia, Wujian Ju, and Rihe Liu. Matrin 3 is a Ca2+/calmodulin binding protein cleaved by caspases. *Biochemical and Biophysical Research Communications*, 361: 281–286, **2007**.

[180] Thomas Treiber, Nora Treiber, Uwe Plessmann, et al. A Compendium of RNA-Binding Proteins that Regulate MicroRNA Biogenesis. *Molecular Cell*, 66(2): 270–284.e13, **2017**.

[181] Muhammad Farooq, Wael N. Hozzein, Elsayed A. Elsayed, Nael A. Taha, and Mohammad am Wadaan. Identification of histone deacetylase 1 protein complexes in liver cancer cells. *Asian Pacific journal of cancer prevention : APJCP*, 14(2): 915–921, **2013**.

[182] Hyun S. Ban, Tae-Su Han, Keun Hur, and Hyun-Soo Cho. *Epigenetic Alterations of Heat Shock Proteins (HSPs) in Cancer*, volume 20 of *International Journal of Molecular Sciences*. 2019.

[183] François Stricher, Christophe Macri, Marc Ruff, and Sylviane Muller. HSPA8/HSC70 chaperone protein. *Autophagy*, 9: 1937–1954, **2013**.

[184] Shivani Garapaty, Chong-Feng Xu, Patrick Trojer, et al. Identification and characterization of a novel nuclear protein complex involved in nuclear hormone receptor-mediated gene regulation. *Journal of Biological Chemistry*, 284: 7542–7552, **2009**.

[185] Amna Ali, Timothy J. Burns, Jacob D. Lucrezi, et al. Amidation inhibitors 4-phenyl-3-butenoic acid and 5-(acetylamino)-4-oxo-6-phenyl-2-hexenoic acid methyl ester are novel HDAC inhibitors with anti-tumorigenic properties. *Investigational New Drugs*, 33: 827–834, **2015**.

[186] Tereza Cerna, Jan Hrabeta, Tomas Eckschlager, et al. The histone deacetylase inhibitor valproic acid exerts a synergistic cytotoxicity with the DNA-damaging drug ellipticine in neuroblastoma cells. *International Journal of Molecular Sciences*, 19, **2018**.

[187] Anja Göder, Claudia Emmerich, Teodora Nikolova, et al. HDAC1 and HDAC2 integrate checkpoint kinase phosphorylation and cell fate through the phosphatase-2A subunit PR130. *Nature Communications*, 9: 764, **2018**.

[188] Ricky W. Johnstone. Histone-deacetylase inhibitors: Novel drugs for the treatment of cancer. *Nature Reviews Drug Discovery*, 1: 287–299, **2002**.

[189] Leonid A. Serebryannyy, Christina M. Cruz, and Primal de Lanerolle. A Role for Nuclear Actin in HDAC 1 and 2 Regulation. *Scientific Reports*, 6(1): 28460, **2016**.

[190] Hui Yang, Tal Salz, Maria Zajac-Kaye, et al. Overexpression of histone deacetylases in cancer cells is controlled by interplay of transcription factors and epigenetic modulators. *FASEB journal*, 28: 4265–4279, **2014**.

[191] Quan Wu, Weiqing Xu, Lejie Cao, et al. Saha treatment reveals the link between histone lysine acetylation and proteome in nonsmall cell lung cancer a549 cells. *Journal of Proteome Research*, 12(9): 4064–4073, **2013**. PMID: 23909948.

[192] Quan Wu, Zhongyi Cheng, Jun Zhu, et al. Suberoylanilide hydroxamic acid treatment reveals crosstalks among proteome, ubiquitylome and acetylome in non-small cell lung cancer a549 cell line. *Scientific Reports*, 5(1): 2045–2322, **2015**.

6. Appendix

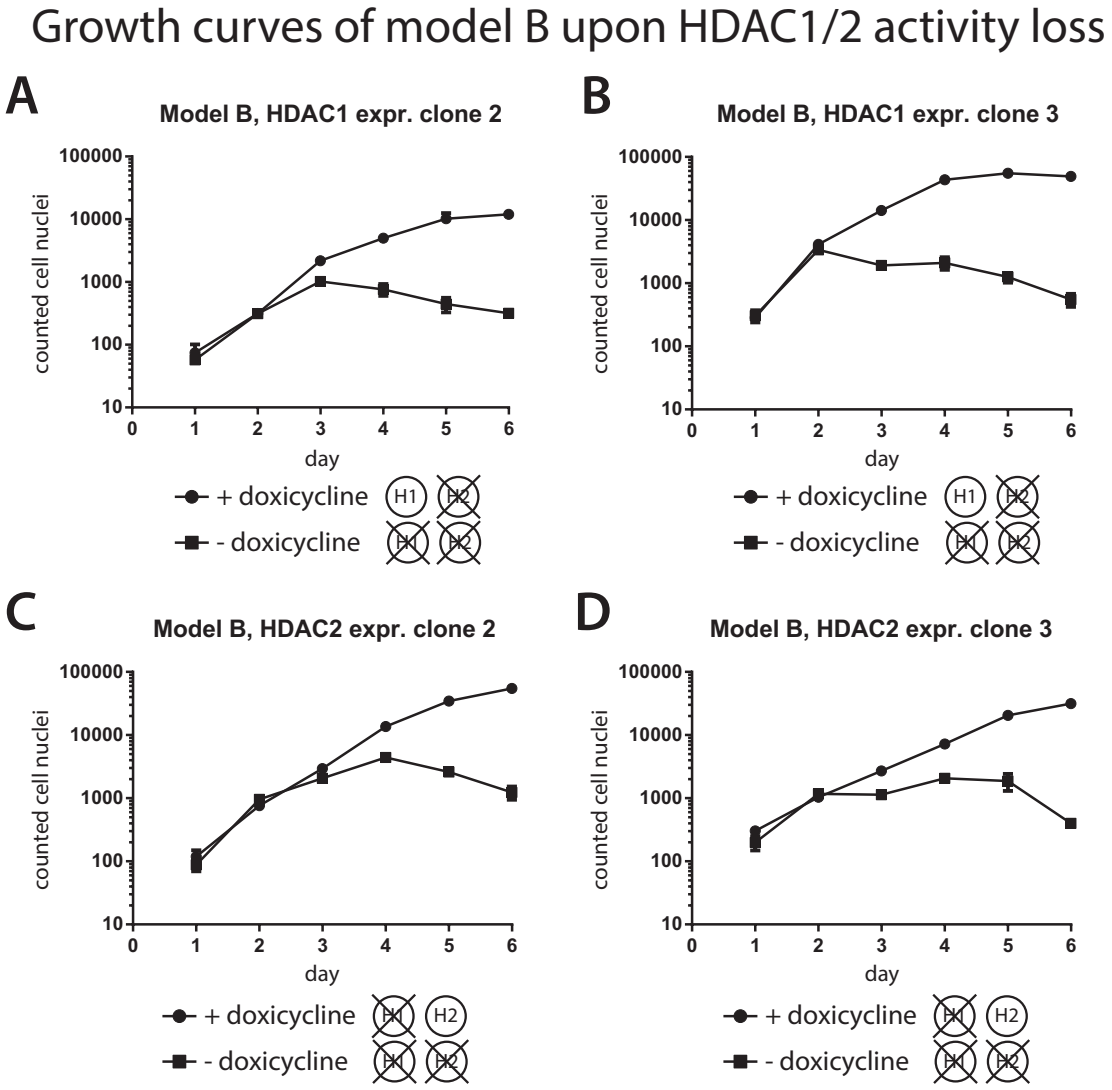

Figure 6.1 Loss of HDAC1 and HDAC2 together leads to a stop in cell growth – additional clones. HCT116 cells suffering from the loss of both HDAC1 and HDAC2 stop proliferating. Cells were cultured in 96 well plates and Hoechst stained nuclei were counted in an Operetta System. HCT116 cells with a HDAC1/2 double knockout and conditional overexpression of HDAC1 **(A & B)** or HDAC2 **(C & D)** are compared to HCT116 wt growth.

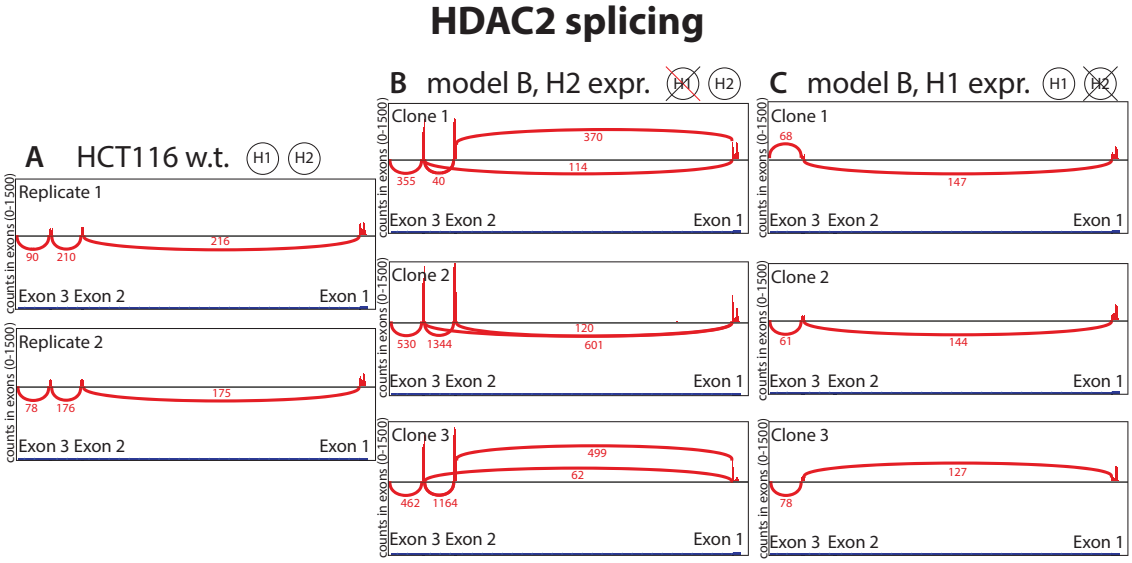

Figure 6.2 Positive controls of the transcriptomes on the basis of splicing between the exons 1-2-3 of HDAC2. RNASeq reads between intron 1, intron 2 and intron 3 of HDAC2 are shown for two replicates of HCT116 wild type cells (part **A**), three clones of the system B cells with a conditional HDAC2 expression and both endogenous HDAC1 and HDAC2 knockouts (part **B**) as well as three clones with a conditional HDAC1 expression and both endogenous HDAC1 and HDAC2 knockouts (part **C**). Sashimi plots were generated with the tool IGV[141].

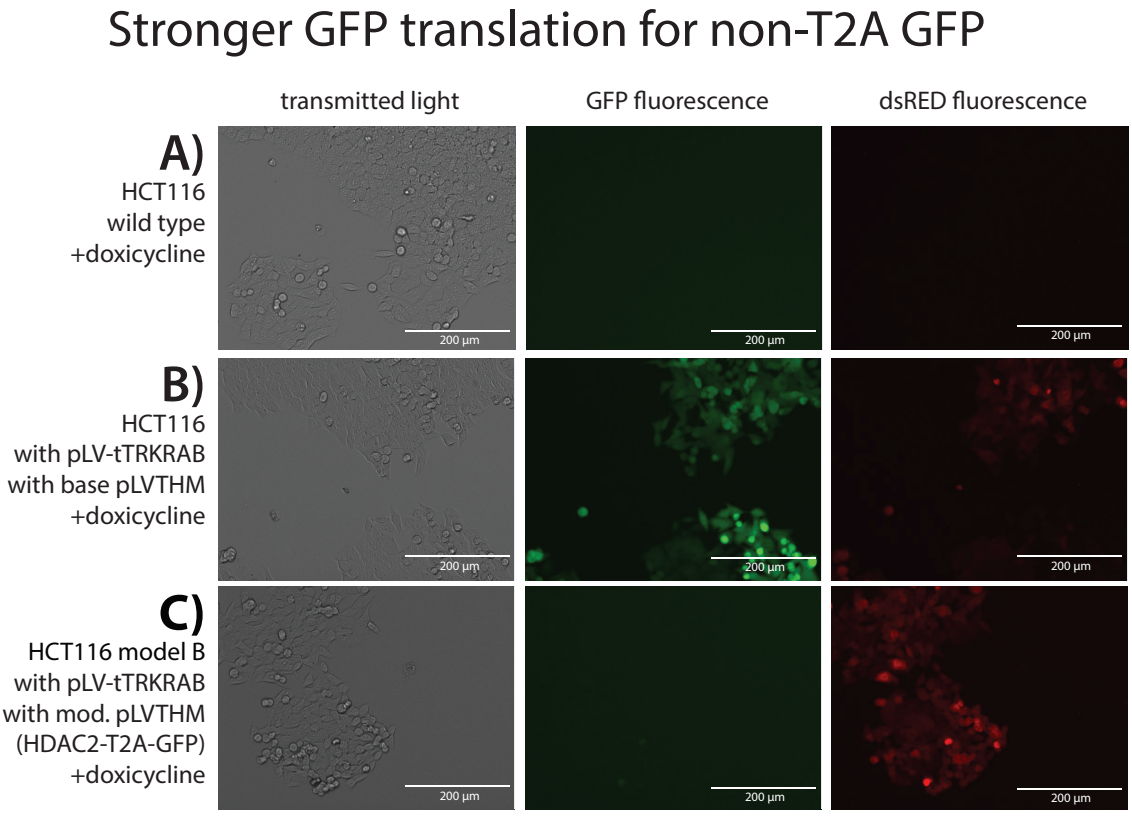

Figure 6.3 Fluorescencemicroscopy shows lower GFP fluorescence from the EF1α-HDAC-T2A-GFP transgene compared to the EF1α-GFP transgene. Fluorescence microscopy images with transmitted light (left), GFP fluorescence (middle) and dsRED fluorescence (right) are depicted. **Row A)** HCT116 wild type cells. **Row B)** HCT116 cells transduced with the vector containing the repressor (pLV-tTRKRAB) and the base version of the overexpression vector (pLVTHM). **Row C)** HCT116 model B cells with a double knockout of endogenous HDAC1 and HDAC2 and the conditional overexpression of HDAC2. For the experiment all lines were cultured with doxicycline and all images were collected with an EVOS F1 fluorescence microscope.

Table 6.1 Number of cells seeded per culture in different flasks for the cell lines HCT116, Co-115, HT29 and HEK293T.

T25	two days	three days	four days	five days
HCT116	500k	350k	200k	–
HT29	550k	400k	250k	–
Co-115	–	600k	400k	200k
HEK293T	500k	330k	200k	–

T75 + 10 cm dish	two days	three days	four days	five days
HCT116	1500k	1000k	600k	300k
HT29	1650k	1200k	750k	400k
Co-115	–	3000k	2000k	1000k
HEK293T	1500k	1000k	500k	–

T225	two days	three days	four days	five days
HCT116	4500k	3000k	2000k	1000k
HT29	5000k	3600k	2250k	1200k
Co-115	–	9000k	6000k	3000k
HEK293T	4500k	3000k	1500k	–

6 well plate	two days	three days	four days	five days
HCT116	200k	130k	75k	50k
HT29	220k	160k	100k	60k
Co-115	–	240k	160k	80k

12 well plate	two days	three days	four days	five days
HCT116	70k	50k	25k	15k
HT29	80k	60k	35k	20k
Co-115	–	85k	55k	30k

Table 6.2 General RNASeq information

sample	reads	library size	RNA RIN
HCT 116 wild type rep 1	28144494	378	9.9
HCT 116 wild type rep 2	26247886	384	9.9
model B HDAC1/2 k.o. HDAC2 o.e. clone 1	29894448	396	N/A
model B HDAC1/2 k.o. HDAC2 o.e. clone 2	31852869	404	N/A
model B HDAC1/2 k.o. HDAC2 o.e. clone 3	29152975	404	N/A
model B HDAC1/2 k.o. HDAC1 o.e. clone 1	29381671	388	9.9
model B HDAC1/2 k.o. HDAC1 o.e. clone 2	31650056	380	9.9
model B HDAC1/2 k.o. HDAC1 o.e. clone 3	29079194	418	N/A

Table 6.3 Identity of Venn diagram overlaps mRNAs

gene name	**full name**
Overlap comparison 1 / comparison 3	
TM4SF18	transmembrane 4 L six family member 18
PTGS2	prostaglandin-endoperoxide synthase 2
ITGBL1	integrin, beta-like 1 (with EGF-like repeat domains)
LOC646736	uncharacterized LOC646736
DUSP10	dual specificity phosphatase 10
ATF3	activating transcription factor 3
EGR1	early growth response 1
Overlap comparison 2 / comparison 3	
GPAM	glycerol-3-phosphate acyltransferase, mitochondrial
SPARC	secreted protein, acidic, cysteine-rich (osteonectin)
GCNT4	glucosaminyl (N-acetyl) transferase 4, core 2
APOBEC3G	apolipoprotein B mRNA editing enzyme
LIPG	lipase, endothelial
SNTB1	syntrophin, beta 1
SCNN1A	sodium channel, nonvoltage-gated 1 alpha
TAGLN	transgelin
SLCO2A1	solute carrier organic anion transporter family, member 2A1
INHBB	inhibin, beta B
SERPINF1	serpin peptidase inhibitor, clade F, member 1
Overlap of all three data sets	
ANKRD1	ankyrin repeat domain 1

Table 6.4 Acetylation sites with significant differences in their HDAC1 and HDAC2 response to inhibition or expression loss.

protein	peptide sequence	site	p-value
CDC37	ELEVAEGGK(ac)AELER	K78	0,0011
ALDOA	GILAADESTGSIAK(ac)R	K42	0,0018
SHMT2	TAK(ac)LQDFK	K464	0,0063
ADIRF	TANQASDTFSGIGK(ac)K	K70	0,0063
HSPA9	HIVKEFK(ac)R	K288	0,011
SSB	VQFQGK(ac)K	K360	0,0112
NCL	AAVTPGK(ac)K	K87	0,0134
AKAP12	EGVTPWASFK(ac)K	K614	0,0168
HIST1H1E	ERSGVSLAALK(ac)K	K63	0,0196
HSPA8	VQVEYK(ac)GETK	K108	0,0212
RPL14	KITAASK(ac)K	K171	0,0214
CREBBP	SHAHK(ac)MVK	K1741	0,0215
HN1L	SIPAGAEPGEK(ac)GSAR	K142	0,022
WBP11	SGK(ac)FMNPTDQAR	K13	0,0239
NCL	AAATPAK(ac)K	K95	0,0249
NCL	GATPGK(ac)ALVATPGK	K116	0,0276
CCAR2	AGGEPWGAK(ac)KPR	K215	0,0319
BUD31	SK(ac)LEVGR	K125	0,0368
THG1L	LPTEMEGK(ac)K	K263	0,0394
HNRNPA1	SSGPYGGGGQYFAK(ac)PR	K350	0,0405
PPIA	K(ac)ITIADCGQLE	K155	0,0427
UCHL5	TSAK(ac)EEDAFHFVSYVPVNGR	K158	0,0455
MATR3	DGSASAAAK(ac)K(ac)K	K711, K712	0,0465
KHSRP	QIAAK(ac)IGGDAATTVNNSTPDFGFGGQK	K87	0,0468
RPS23	VANVSLLALYK(ac)GK	K135	0,0478

Table 6.5 List of acetylation sites exclusive identified in this study. The acetylation sites in 3.28 which are unique to this study were checked against the Uniprot database (05.06.2019) and peptides with acetylation sites that are not present in the database are summarized in the table.

#	Sequence	Protein name	location in protein
1	EGRPPEPTPAK(ac)R	SRRM2	K2602
2	KGAAIPAK(ac)GAK	NCL	K132
3	KLQANGPVAK(ac)K	NOLC1	K76
4	EAVREGRPPEPTPAK(ac)R	SRRM2	K2602
5	AAATPAK(ac)K	NCL	K95
6	SRSSAAAK(ac)LR	CENPV	K11
7	KAAVTPGK(ac)K	NCL	K87
8	KVAVATPAK(ac)K	NCL	K79
9	YIFTANK(ac)K	MED13L	K731
10	DGSASAAAK(ac)K(ac)K	MATR3	K711, K712
11	GGALPPAK(ac)R	TCOF1	K261
12	AQTK(ac)APPKPAR	NOLC1	K197
13	LSFPSIKPDTDQTLK(ac)K	DPF2	K107
14	NSNNEVACK(ac)K	WDR76	K82
15	TPSK(ac)LSEK	PBK	K12
16	SQTPERPAK(ac)K	POM121	K453
17	ISLSAPAK(ac)K	RBBP6	K1207
18	QLVSK(ac)PLSSSVSNNKR	YTHDC1	K72
19	VVPVK(ac)AK	NCL	K228
20	AAK(ac)APPK	NOLC1	K158
21	KAAATPAK(ac)K	NCL	K95
22	TVGK(ac)K(ac)QPK	AFF4	K564, K565
23	TNTTASAK(ac)VAPVR	TCOF1	K655
24	ATTKPPPAK(ac)K	NOLC1	K356
25	AEGDAKGDK(ac)AK	HMGN2	K14

Continued on next page

Table 6.5 – *Continued from previous page*

26	DISGPSPSK(ac)K	APIP	K90
27	VGRPTASK(ac)ASK	NUCKS1	K196
28	KTNTTASAK(ac)VAPVR	TCOF1	K655
29	KAEGDAK(ac)GDK	HMGN2	K11
30	IHTGEK(ac)PYK	ZNF79	K247
31	KQVVAK(ac)APVK	NOLC1	K251
32	TVVVEAGK(ac)K	TOX4	K207
33	K(ac)AAATPAK(ac)K	NCL	K88, K95
34	NNSFTAPSTVGK(ac)R	PARN	K566
35	VQLIK(ac)NGK	RPS23	K76
36	TASFSESRADEVAPAK(ac)K	ACLY	K468
37	IISLGK(ac)K	AFAP1	K332
38	MSSLGAGVTSAK(ac)K	JARID2	K323
39	ADK(ac)ARYER	HMGB1	K68
40	RLVSEK(ac)ASIFEK	LAD1	K259
41	TAAAASEK(ac)NRGPR	C19orf53	K25
42	AK(ac)KPAAAAGAK	HIST1H1E	K159
43	MSLAQK(ac)K	RPL5	K276
44	LLEDTLFPSSK(ac)K	CHAMP1	K617
45	GGISETRIEK(ac)R	EPB41L2	K956
46	QNKVEAK(ac)LR	SSB	K204
47	LATPAGLK(ac)K	POLD3	K282
48	VVTVVTTK(ac)K	DDX46	K271
49	SGAALSK(ac)K	PARP1	K505
50	SSQPLASKQEK(ac)DGTEK	HMGA1	K18
51	SVVTVAVK(ac)GNK	ZNF638	K825
52	SVIVAAK(ac)K	LRBA	K1731

Continued on next page

Table 6.5 – *Continued from previous page*

53	QSFAK(ac)PK	TWF1	K325
54	KPAAATVTK(ac)K	HIST1H1C	K168
55	MPPAEK(ac)ASR	MDC1	K1016
56	VNASASSLK(ac)K	FSCN1	K41
57	VAGGAAPSKPASAK(ac)K	NOLC1	K510
58	QAGPAPAAATAASK(ac)K	DIDO1	K626
59	TFSSSSSSK(ac)K	SMTN	K716
60	NIGK(ac)TLVTR	RPS3A	K46
61	QIAVK(ac)VEK	CASC5	K830
62	TDPECTAPIK(ac)K	CMTR1	K14
63	SIQGIHPAK(ac)K	RBM33	K1061
64	CIAAK(ac)K	EXOSC10	K856
65	IHVDFSQSVAK(ac)VK	PPIL4	K321
66	SAEPAEALVLACK(ac)R	SLC7A6OS	K28
67	GRDAFYEVLK(ac)R	FAM83G	K51
68	QLGVAK(ac)K	PPAT	K371
69	LLLSK(ac)GHSCYRPR	RPS6	K79
70	ERSGVSLAALK(ac)K	HIST1H1E	K63
71	AAFK(ac)SGK	RAI1	K1093
72	KITAASK(ac)K	RPL14	K171
73	ITAASK(ac)K	RPL14	K171
74	QWTEK(ac)HAR	UBE2T	K149
75	GRVPELPEK(ac)GSR	ZC3H13	K573
76	AFSIGK(ac)MSTAK	U2SURP	K88
77	TTVISAVGTIVK(ac)K	SAP30BP	K304
78	ANITLSGK(ac)K	C11orf98	K67
79	RYETLVGTIGK(ac)K	MPHOSPH6	K127

Continued on next page

Table 6.5 – *Continued from previous page*

80	FFGVIPSGK(ac)K	RFC1	K14
81	TQVLGK(ac)K	PHAX	K332
82	LQSSK(ac)K	NOP2	K709
83	SSIATMTSVGK(ac)SR	CCNB3	K1081
84	HALIK(ac)K	TRAP1	K652
85	YSGLTASSK(ac)K	KIAA1143	K117
86	LFGAGGGK(ac)AGK	CHMP4B	K14
87	GPLATGGIK(ac)K	TMA7	K59
88	ENLSAK(ac)R	UBA2	K623
89	RLGDSSGPALK(ac)R	SEP09	K28
90	GYGK(ac)INK	RPL7	K161
91	MTVSGK(ac)K	HBS1L	K170
92	K(ac)FGVLSDNFK	PPAT	K372
93	EAETPQAK(ac)K	NOLC1	K601
94	IK(ac)IIAPPERK	ACTC1	K330
95	VVNGAAASQPPSK(ac)R	SF3B1	K195
96	AYK(ac)QVK	CHMP5	K121
97	KSAGAAK(ac)R	HIST1H1E	K32
98	LIITLGK(ac)K	CHD9	K603
99	APAQK(ac)APAPK	RPL14	K204
100	EEGINKSEK(ac)R	PARP1	K521
101	SAVEK(ac)K	HAT1	K20
102	LRQLGVAK(ac)K	PPAT	K371
103	VK(ac)VGVNGFGR	GAPDH	K5
104	KLEELK(ac)AK	TMA7	K44
105	LALK(ac)TLSK	TSR1	K38
106	GNLK(ac)QVR	PSPC1	K8

Continued on next page

Table 6.5 – *Continued from previous page*

107	TPPEPSAK(ac)QR	PPRC1	K1398
108	VSQLLAVTGK(ac)K	CBFB	K177
109	HATLQK(ac)STK	TRIM28	K272
110	TSTGAPAAIK(ac)K	CAPG	K137
111	VRQPPAYK(ac)K	STIL	K512
112	TLGK(ac)LWR	SOX9	K141
113	SQETPATK(ac)K	SNRPA	K122
114	KVAEK(ac)EAK	KARS	K36
115	ARVVLK(ac)YR	SRP9	K30
116	TLPSTSSSGSK(ac)R	NFIC	K280
117	KAVIVGK(ac)ESK	CDK13	K566
118	LALK(ac)TGIVAK	C19orf43	K128
119	QHSLLK(ac)R	RPS15	K58
120	KPAAAAGAK(ac)K	HIST1H1E	K168
121	GAVGEQLGK(ac)MR	TRIM72	K178
122	AAVAFK(ac)NAK	NAPG	K46
123	RINVELSTK(ac)GQK	RBM14	K149
124	TGIVAK(ac)K	C19orf43	K134
125	INVELSTK(ac)GQK	RBM14	K149
126	CIRPSVLGPLK(ac)R	FAM122B	K165
127	EFK(ac)RETGVDLTK	HSPA9	K291
128	ALLAYAFALAGNQDK(ac)R	A2M	K1162
129	VLVK(ac)QK	XRCC5	K603
130	RADAGEK(ac)PK	QARS	K673
131	KAPAQK(ac)VPAQK	RPL14	K177
132	RTDIFGVEETAIGK(ac)K	SF3A1	K486
133	IGEK(ac)VSK	TTC33	K13

Continued on next page

Table 6.5 – *Continued from previous page*

134	TPLHLAK(ac)SK	ANKRD54	K217
135	SALAPNLLTSGK(ac)K	CD3EAP	K174
136	LSDK(ac)GLK	HNRNPU	K28
137	IPAK(ac)TPPAPK	MAPT	K491
138	GK(ac)FDGAK	HMGB3	K165
139	VQIVSK(ac)K	MAP4	K997
140	QMVK(ac)FAANINK	DARS	K103
141	QYSGK(ac)FF	HNRNPK	K461
142	AGAHLQGGAK(ac)R	GAPDH	K117
143	TAMAAAK(ac)APTK	RPL24	K131
144	AAATSAK(ac)K	NCL	K62
145	KENPLQFK(ac)FR	RDX	K79
146	K(ac)FGQGSR	RPS29	K13
147	QTVGTK(ac)QPK	AFF1	K603
148	KVTAAMGK(ac)K	RPL27	K59
149	AIK(ac)LRPIAVIKG	RTCB	K496
150	AVFQANQENLPILK(ac)R	ATP1A1	K444
151	CGLPYVEVLCK(ac)NR	PPAT	K349
152	RFDEGK(ac)LK	CNN3	K156
153	TMQAVNK(ac)K	CHMP2B	K114
154	LFTSTGLK(ac)K	AKAP12	K526
155	FGFAIGSQTTK(ac)K	PCNP	K81
156	GKGDK(ac)AQIEK	HSPD1	K364
157	EGSGPIAFAHK(ac)R	DUSP12	K249
158	IRAAEK(ac)VSR	MDC1	K1025
159	LFQSDTNAMLGK(ac)K	YEATS4	K131
160	ANVK(ac)IFK	MDH1	K107

Continued on next page

Table 6.5 – *Continued from previous page*

161	IYANMFK(ac)K	FKBP5	K414
162	ATTK(ac)PPPAK	NOLC1	K351
163	KAAATSAK(ac)K	NCL	K62
164	YETLVGTIGK(ac)K	MPHOSPH6	K127
165	TTEAK(ac)MMK	ZRANB2	K43
166	KLFTSTGLK(ac)K	AKAP12	K526
167	GLGK(ac)GHK	RPL15	K176
168	RPAPEK(ac)K	DIDO1	K474
169	SVAK(ac)LEK	TPM3	K249
170	K(ac)WGFTK	RPL10	K170
171	LLAGAVK(ac)HK	FAM192A	K158
172	NQYEK(ac)HK	EIF5B	K921
173	IEVIEIMTDRGSGK(ac)K	HNRNPA1	K144
174	RK(ac)LESYFQSSK	DTX3L	K25
175	ASGYQSSQK(ac)K	HDGF	K105
176	QIEQQK(ac)K	ATP6V1E1	K68
177	VTQYK(ac)K	RPL36A	K27
178	STPVIVSATTK(ac)K	AKAP12	K1493
179	K(ac)FIQTFGK	PRKDC	K3631
180	SRDSFLK(ac)R	RPL21	K107
181	RLSYNTASNK(ac)TR	RPL34	K19
182	RTLK(ac)IPAMTIAK	HSPD1	K473
183	LLSQFLK(ac)DK(ac)LAK	CCDC65	K44, K46
184	AKDDATLSGK(ac)R	PDAP1	K172
185	NTAELQPESGK(ac)R	PPM1G	K519
186	LLIHQSLAGGIIGVK(ac)GAK	HNRNPK	K163
187	IHISK(ac)K	RPL10	K169

Continued on next page

Table 6.5 – *Continued from previous page*

188	DSPFK(ac)PK	RBBP5	K500
189	VYNVTQHAVGIVVNK(ac)QVK	RPL21	K78
190	K(ac)FYEQFSK	HSP90AA1	K436
191	TATAVAHCK(ac)R	RPS16	K26
192	LDLAGRDLTDYLMK(ac)	ACTC1	K193
193	AAHAAK(ac)TVK	PIP4K2A	K375
194	RQEQIAK(ac)R	RPS6	K230
195	K(ac)LEAAEER	STMN1	K53
196	SK(ac)GQESFKK	NPM1	K223
197	K(ac)GAAIPAK(ac)GAK	NCL	K125, K132
198	KTTTTPGRK(ac)PR	HMGA1	K82
199	KVVVSPTK(ac)K	NCL	K70
200	K(ac)EVKLPGK	HP1BP3	K533
201	LSLSK(ac)PK	BLM	K29
202	AVTTPGK(ac)K(ac)GATPGK	NCL	K109, K110
203	TTTTPGRK(ac)PR	HMGA1	K82
204	RIPIK(ac)LISK	CBLL1	K29
205	VAGGAAPSK(ac)PASAKK	NOLC1	K505
206	QQAK(ac)PVKVER	HDGFRP2	K443
207	AFVESSK(ac)LKR	YY1	K339
208	LAHPNK(ac)PK	HN1L	K110
209	KNSQK(ac)QIK	KIAA1143	K137
210	GGAESHTFK(ac)	CRIP1	K77
211	ENMK(ac)PAAK	RIF1	K1021
212	IHAAQK(ac)PYR	ZNF668	K250
213	FQAHK(ac)PAK	C19orf53	K12
214	HGLQSLGK(ac)VAIAR	PRRC2A	K49

Continued on next page

Table 6.5 – *Continued from previous page*

215	LGSSK(ac)PK	PCNP	K94
216	YYVGHK(ac)GK	MAGOHB	K16
217	GNECFQK(ac)GDYPQAMK	STIP1	K373
218	ESGPLQGK(ac)GK(ac)PR	PPRC1	K518, K520
219	ASGLAAGK(ac)GVIVAK	GART	K156
220	VHDPVTAK(ac)PK	MTHFD2	K286
221	GFGHK(ac)PGLK	ZNF746	K437
222	MVATTK(ac)PK	NOLC1	K446
223	AFDSGIIPMEFVNK(ac)	ACLY	K962
224	APGTPHSHTK(ac)PYVR	RPL18	K164
225	LHGK(ac)PIR	PTBP1	K402
226	KYIK(ac)DYMK	TPT1	K93
227	VVK(ac)QASEGPLK	GAPDH	K263
228	K(ac)YHNPK	CCT7	K231
229	QLAPNK(ac)PS	ROCK2	K1386
230	TMSAK(ac)EK	HMGB1	K55
231	THSGQK(ac)PYK	ZNF768	K343
232	GK(ac)PALSR	BRPF3	K1039
233	DK(ac)HIEEVRK	STMN1	K128
234	EVSTYIK(ac)	EEF1A1	K179
235	K(ac)HDSGAADLER	HYPK	K35
236	SDERPVHIK(ac)	TRIM33	K1127
237	EKDSPFK(ac)PK	RBBP5	K500
238	AALRPLVK(ac)PK	RPL32	K9
239	KAAVPAK(ac)R	NOLC1	K110
240	TANQASDTFSGIGK(ac)K	ADIRF	K70
241	TAGPIASAQK(ac)QPAGK	MAP4	K986

Continued on next page

Table 6.5 – *Continued from previous page*

242	IKEK(ac)YIDQEELNK	HSP90AA1	K283
243	KTAPEK(ac)SLVSDK	LAD1	K193
244	IEAVQK(ac)VNK	HDGFRP2	K560
245	AQYVLAK(ac)R	THUMPD1	K26
246	EIKLPTEMEGK(ac)K	THG1L	K263
247	RTSVLFSK(ac)K	BRPF1	K896
248	ASAISIK(ac)LGSSKPK	PCNP	K89
249	TAPEK(ac)SLVSDK	LAD1	K193
250	ASLYNAVTIEDVQK(ac)LAAFMK	PSAT1	K356
251	DTGK(ac)TPVEPEVAIHR	RPS20	K8
252	ASSK(ac)LAIMK	RFC1	K318
253	SFISPIPSK(ac)R	TCF20	K1267
254	K(ac)FLDGDELTLADCNLLPK	CLIC6	K629
255	NYVPPKGDK(ac)K	HMGB2	K85
256	NVMILTNPVAAK(ac)K	TES	K101
257	VGEVEQEAETARKDLIK(ac)	PPFIA2	K314
258	DLTKPVVTISDEPDILYK(ac)R	MRPS10	K74
259	AAPEAK(ac)K	NCL	K294
260	KGEK(ac)VPK	HMGN2	K51
261	EK(ac)AAVFR	AIMP2	K252
262	CNLLAEK(ac)QYGFCK	AHSG	K225
263	FQYCVAVGAQTFPSVSAPSK(ac)K	ADAR	K665
264	HFEATDILVSK(ac)ISR	EIF5B	K1185
265	TTAK(ac)LSTSAK	UBE2E3	K58
266	EK(ac)VMYEK	TBCA	K23
267	LFTNDCIFLK(ac)K	LYSMD2	K110
268	FNEFMTSK(ac)PK	FNBP1	K378

Continued on next page

Table 6.5 – *Continued from previous page*

269	KAEEDAALQAK(ac)K	TCOF1	K74
270	WLCPLSGK(ac)K	SRRT	K720
271	K(ac)FYEAFSK	HSP90AB1	K428
272	LVSK(ac)DGK	NCL	K424
273	LCNIFSTK(ac)FTVETASR	TOP2A	K176
274	KVEK(ac)VTISNR	HSP90AB1	K577
275	ALLAYAFALAGNQDK(ac)	A2M	K1162
276	ALVATPGK(ac)K(ac)GAAIPAK	NCL	K124, K125
277	EVKLPGK(ac)GK	HP1BP3	K540
278	TLTIVDTGIGMTK(ac)ADLINNLGTITK	HSP90AA4P	K40
279	SFFTPGK(ac)PK	PDS5B	K1124
280	SGWESYYK(ac)TEGDEEAEEEQEENLEASGDYK	XRCC6	K9
281	SASDSGCDPASK(ac)K	KDM3B	K300
282	TWIPEVHDQK(ac)ADVSAWK	DDX24	K188
283	GK(ac)PALVRR	BRD1	K877
284	YNDLYK(ac)FQQSDDLKK	OGFOD1	K97
285	AGGK(ac)PFCA	IRX4	K515
286	AFSGSGNRLDGK(ac)K	UFD1L	K238
287	VLADLAIYEPK(ac)TFK	MRPL20	K111
288	RNQSFCPTVNLDK(ac)LWTLVSEQTR	RPL27A	K77
289	LALQK(ac)NVICDK	DNAJA1	K130
290	TK(ac)GTSSFGK	RPL37	K3
291	NSNTVVFVK(ac)	TOX4	K621
292	QK(ac)PLDFSTNQK	WDHD1	K1111
293	SFPVNSDVGVLK(ac)WR	ARCN1	K363
294	QK(ac)YNVR	RPL26	K41
295	FQWDLNAWTK(ac)SAEAFGK	TRIM28	K400

Continued on next page

Table 6.5 – *Continued from previous page*

296	LDLSK(ac)NK	LRRC59	K71
297	LQMEVNDIK(ac)K	SH3KBP1	K659
298	NVIK(ac)EK	ENO1	K197
299	IHIK(ac)EK	ZNF454	K212
300	TK(ac)SLSFR	EIF3E	K409
301	EKYEK(ac)DIAAYR	HMGB2	K157
302	TKIDWNK(ac)ILSYK	CAPZA2	K273
303	GK(ac)DYYQTLGLAR	DNAJB1	K3
304	KVHVIFNYK(ac)GK	CALR	K151
305	K(ac)PPSGFK	DIDO1	K585
306	RTIAQDYGVLK(ac)ADEGISFR	PRDX1	K120
307	EEYEGPNKK(ac)PR	SFPQ	K704
308	ANAEEMTK(ac)YHSDDYIK	HDAC1	K66
309	NSTFSEIFK(ac)K(ac)	TKT	K352, K353
310	KAEDNVCVK(ac)K	MKI67	K3243
311	SSDEAVILCK(ac)TAIGALK	PSMD13	K115
312	LQEEIVNSVK(ac)	ABCB7	K745
313	CPLLK(ac)PWALTFSYGRALQASALK	ALDOA	K294
314	DSKPSSTPRSK(ac)GQESFK	NPM1	K223
315	NKGNECFQK(ac)GDYPQAMK	STIP1	K373
316	AHQCGDDDK(ac)TRPLVK	C19orf43	K170
317	QAK(ac)EMDEEDK	TMA7	K20
318	K(ac)PYCNAHYPK	LASP1	K50
319	NEK(ac)GALK	HDGF	K151
320	SIRDTPAK(ac)NAQK	NPM1	K202
321	SAAK(ac)AVKPK	HIST1H1C	K191
322	EILGTCK(ac)MLGQMTDQVADLR	VCL	K326

Continued on next page

Table 6.5 – *Continued from previous page*

323	TK(ac)PIWTRNTEDITQEEYGEFYK	HSP90AB2P	K208
324	WSSSGLPK(ac)DIDRLHNLR	DOCK1	K270
325	KGPGRPTGSK(ac)K	HMGB2	K182
326	KKPATDGAK(ac)PK	SAP130	K681
327	IHAAQK(ac)PYRCPACGK	ZNF668	K250
328	SSTTVSSFANSK(ac)PGSAKK	CUL4B	K190
329	AMDVYQK(ac)ALDLDSSCK	STIP1	K453
330	APGFGDNRK(ac)NQLK	HSPD1	K310
331	QHSITK(ac)NTAK	EDF1	K56
332	SPTPPPSSK(ac)PSSIPRK	FAM48A	K500
333	LGPNDQYK(ac)FYSVNVDYSK	NDUFA4	K63
334	IHTGQK(ac)PYK	ZNF836	K608
335	DCEECIQLEPTFIK(ac)GYTRK	STIP1	K429
336	SK(ac)NLQPK	TADA3	K124
337	SMTEAEQQQLIDDHFLFDK(ac)PVSPLLLASGMAR	CKB	K196
338	CDFTEDQTAEFK(ac)EAFQLFDRTGDGK	MYL6	K13
339	KGK(ac)YEGPK	NT5DC1	K359
340	RVIISAPSADAPMFVMGVNHEK(ac)YDNSLK	GAPDH	K139
341	KQK(ac)PLDFSTNQK	WDHD1	K1111
342	YNDLYK(ac)FQQSDDLK	OGFOD1	K97
343	IDREGK(ac)PR	RPS12	K99
344	NVASVCLQIGYPTVASVPHSIINGYK(ac)R	RPLP0	K246
345	VNVK(ac)PSVVK	ZC3H11A	K654
346	NKNDGLK(ac)PK	ADNP	K153
347	DGK(ac)PVQPVKR	ZMAT2	K39
348	KDEQEHEFYK(ac)	PSMC4	K418
349	SSILNAK(ac)NRR	MORC3	K555

Continued on next page

Table 6.5 – *Continued from previous page*

350	THPGGK(ac)PYDCK	ZNF627	K165
351	TYWVSK(ac)GSAFSTSISK	FARSA	K177
352	RFEEAAFTCEYK(ac)YDGQR	LIG1	K568
353	QQCFSK(ac)DIVENYFMR	TRIM28	K127
354	GK(ac)MSSYAFFVQTCREEHK	HMGB2	K12
355	KVVK(ac)QASEGPLK	GAPDH	K263
356	YHAAVK(ac)PFGCEECGK	ZNF316	K371
357	FSLQDPPNKK(ac)PKV	UGDH	K491
358	KMVATTK(ac)PK	NOLC1	K446
359	ELPTLK(ac)DMDFLNK	PIP4K2C	K241
360	DKEPLTAYNYK(ac)K	MINPP1	K396
361	FGMTPSK(ac)GVLFYGPPGCGK	VCP	K512
362	TIEKFEK(ac)EAAEMGK	EEF1A2	K44
363	IVGAK(ac)NSR	ZNF512	K29
364	SK(ac)PLMLIAPKPQDKK	ADNP	K266
365	FHSLK(ac)PK	EHD4	K378
366	LWSNK(ac)LTSDLTFAYER	HEXA	K488
367	SSLK(ac)PIK	NIPBL	K1029
368	HDCVGYVMK(ac)K	USP11	K775
369	CRK(ac)NHPDVASK	GTSF1	K39
370	THIAQK(ac)PYVCNNCGK	ZNF124	K288
371	GTDLWLGVDALGLNIYEK(ac)DDKLTPK	EZR	K230
372	KK(ac)PVEVK	SSRP1	K534
373	HPQLLYESK(ac)LYK	CSNK1A1	K62
374	NK(ac)PCIGK	NPAT	K1000
375	CDVDIRK(ac)DLYANTVLSGGTTMYPGIADR	ACTB	K291
376	GK(ac)PALVR	BRD1	K877

Continued on next page

Table 6.5 – *Continued from previous page*

377	VHDYK(ac)EGTPEEK	RABL3	K51
378	FKPYCNFDK(ac)YDEDHSGDDK	UBR4	K4646
379	LSAK(ac)PAPPKPEPKPK	HMGN2	K31
380	ITSGPFEPDLYK(ac)SEMEVQDAELK	PA2G4	K344
381	KAEEAGGTRLEPLK(ac)PLK	PRR12	K402
382	YGQNCHK(ac)GPPHSK	PPM1G	K166
383	SHDGAVHK(ac)PYNCSHCGK	MAZ	K335
384	AKKPAAATVTK(ac)K	HIST1H1C	K168
385	RTQVLGK(ac)K	PHAX	K332
386	K(ac)LNVTEQEK	ENO1	K81
387	YHFCEK(ac)CFNEIQGESVSLGDDPSQPQTTINK	EP300	K1203
388	KAEATGEK(ac)RPR	HMGA2	K74
389	EK(ac)GSREEK	EEF1G	K235
390	VLTANSNPSSPSAAK(ac)R	MRGBP	K200
391	TMADGNEK(ac)K	YWHAH	K77
392	AKPTGSGKEEGPAPCK(ac)QMK	MINA	K20
393	ALRDAK(ac)LDK	HSPA8	K325
394	IREYFGGFGEVESIELPMDNK(ac)TNK	HNRNPD	K218
395	EKPSYDTETDPSEGLMNVLK(ac)K	CACYBP	K196
396	LAQQMENRPSVQAALK(ac)LK	CHTOP	K70
397	QGFPMK(ac)QGVLTHGR	RPS6	K64
398	AKKPAAAAGAK(ac)K	HIST1H1E	K168
399	KASAISIK(ac)LGSSKPK	PCNP	K89
400	GVKPQAK(ac)AAK	NOLC1	K155
401	AEGDAK(ac)GDK	HMGN2	K11
402	VIRSDGAPAEGK(ac)R	THOC5	K24
403	IILGK(ac)GK	ARGLU1	K258

Continued on next page

Table 6.5 – *Continued from previous page*

404	VTGK(ac)LK	NOP2	K697
405	ESLCDSPHQNLSRPLLENK(ac)LK	U2SURP	K80
406	VQPYLDDFQK(ac)K	APOA1	K130
407	THYDAK(ac)K	NUMA1	K1624
408	LGPGGLDPVEVYESLPEELQK(ac)CFDVK	CDC37	K307
409	FVTPVPGPQGK(ac)EGK	ZNF609	K84
410	VEEIAASK(ac)CR	RPL18A	K136
411	QIEEQTIK(ac)AQK	RDX	K360
412	AAVGVK(ac)K	RPL4	K390
413	VPEGPIPPSTPK(ac)FAYGK	GLB1	K371
414	YICENQDSISSK(ac)LK	ALB	K298
415	LFPGFEIETVK(ac)NNLR	ASNS	K232
416	LSDGVAVLK(ac)VGGTSDVEVNEKK	HSPD1	K405
417	IAK(ac)LLKPQK	RBP7	K35
418	FQDNFEFIQWFK(ac)K	MAPRE3	K112
419	SLGNILQAKPTSSPAK(ac)GPPQK	TCOF1	K586
420	EK(ac)PLALYVFSHNHK	ALDH3A2	K357
421	K(ac)FAREEIIPVAAEYDK	ACADM	K54
422	AAAFEQLQK(ac)WK	TOMM70A	K168
423	EFNEEGALSVLQQFK(ac)ESDLSHVQNK	HNRNPR	K84
424	YFSSK(ac)WSFSK	WDR45B	K283
425	LSEGVTISYK(ac)SYCK	ITGB1	K398
426	VLGK(ac)DGK	THOC2	K1297
427	LIQQQLVLLLHAHK(ac)CQR	EP300	K350
428	VKLPSGSK(ac)K	RPL8	K155
429	LVSLIGSK(ac)TQIPTQR	PSMA1	K115
430	AGVNTVTTLVENK(ac)K	RPL7A	K150

Continued on next page

Table 6.5 – *Continued from previous page*

431	NILDSKPTANK(ac)K	CORO1C	K418
432	NIK(ac)ALR	HNRNPK	K66
433	EALESVEVLIK(ac)NPK	CKAP5	K308
434	THEDIEAQIREIQGK(ac)K	SF3B1	K21
435	THTGEK(ac)PFK(ac)CYK(ac)	ZNF560	K514, K517, K520
436	LTENVYK(ac)TIMEQFNPSLR	BAIAP2	K18
437	TEGKPAEVK(ac)K	MAP4	K847
438	VGLQVVAVK(ac)APGFGDNRK	HSPD1	K301
439	KPAEK(ac)PLPKPR	HDGFRP2	K282
440	AQIEK(ac)R	HSPD1	K369
441	KLEDNPK(ac)SLK	EEF1A2	K392
442	KTQDQISNIK(ac)YHEEFEK	LASP1	K121
443	GRFQDNLDFIQWFK(ac)K	MAPRE2	K155
444	EK(ac)EPIVGSTDYGKDEDSAEALLK	SPTAN1	K909
445	VLGEK(ac)GK	PKM	K261
446	NSYLEVLLK(ac)LADK	PDIA6	K322
447	KAVLFCLSEDK(ac)K	CFL1	K44
448	TK(ac)VK(ac)AK	SCAF1	K901, K903
449	AAQK(ac)TLLVSTSAVDNNEAQKK	RBM26	K709
450	EAWPGK(ac)KPTPSLLI	PPP1R8	K343
451	FDRGYISPYFINTSK(ac)GQK	HSPD1	K233
452	VFAEK(ac)WNENVQYLSEDRSVQEVLQK	ORC4	K248
453	SKIETEIK(ac)NK	CACYBP	K41
454	VVQHTK(ac)GCK	EP300	K1769
455	KWGFTK(ac)FNADEFEDMVAEK	RPL10	K175
456	FPLTTESAMK(ac)K	RPL23A	K88
457	EK(ac)PLWFDVYDAFPPLREPVFQRPR	MRPS23	K28

Continued on next page

Table 6.5 – *Continued from previous page*

458	KGPELPLVPVK(ac)R	SNRNP40	K18
459	SHTAEK(ac)PYK	ZNF610	K342
460	EVHK(ac)MVVESAYEVIK	LDHB	K233
461	DMYSFLEDMGLK(ac)	A2M	K676
462	DILEK(ac)KVEK	HSP90AA1	K581
463	LGVATVAK(ac)GVCGACK	PXN	K355
464	SK(ac)FDNLYGCRESLIDGIK	AHCY	K188
465	EVFEDAAEIRLVSK(ac)DGK	NCL	K424
466	MK(ac)FNPFVTSDR	RPL26	K2
467	TLNPVFNEQFTFK(ac)VPYSELGGK	SYT1	K214
468	NEDIPNVAVYPHNGMIDLK(ac)YFPYYGK	ATP1B3	K213
469	DLEEDHACIPIK(ac)K	EEF2	K571
470	TKFENLCK(ac)IMK	HSP90AA1	K573
471	KIGYNPDTVAFVPISGWNGDNMLEPSANMPWFK(ac)	EEF1A1	K212
472	LVGLK(ac)FMQASEDLLK	NME1	K39
473	DKQPYEQK(ac)AAK	HMGB2	K147
474	VMK(ac)FSVSPVVR	EEF2	K498
475	TQARPVGVK(ac)IPTCK	AHSA1	K203
476	AAPAPGK(ac)VGDVTPQVK	TCOF1	K244
477	AKFENLCK(ac)LMK	HSP90AB1	K565
478	CLFNHK(ac)FEESMSEK	GLG1	K342
479	ANGTSALTAQNGK(ac)AAK	NOLC1	K558
480	IGK(ac)TLPSEK	ZNF638	K1860
481	GITEECLK(ac)QPSLEQK	ACIN1	K548
482	YGSDIVPFSK(ac)VDEEQMK	XRCC5	K325
483	SETSK(ac)PGPSGLQAK	TRIP12	K289
484	EFPGFLENQK(ac)DPLAVDK	S100A10	K47

Continued on next page

Table 6.5 – *Continued from previous page*

485	SSQLLSQDTSLTGK(ac)PSKK	NPAT	K543
486	TTGQSK(ac)GFAFISFHR	EIF3G	K280
487	DYFSK(ac)FGEVVDCTLKLDPITGR	HNRNPD	K119
488	QMWSGK(ac)FSYVTPR	USP15	K353
489	LK(ac)DYAFIHFDERDGAVK	SYNCRIP	K371
490	KSQEGK(ac)PK	CAST	K56
491	YLYTLVITDK(ac)EK	RPL38	K50
492	QLFHPEQLITGK(ac)EDAANNYAR	TUBA1B	K96
493	K(ac)PLGPPPPSYTCFR	RBBP6	K150
494	HGK(ac)YMACCLLYRGDVVPK	TUBA1B	K311
495	RANSTDYGLTAAVFTK(ac)NLDK	ALDH1A3	K446
496	LADLEALK(ac)VADSK	RNASEH2A	K64
497	ARHPQLLYESK(ac)LYK	CSNK1A1	K62
498	LFFLQVK(ac)	MSN	K107
499	IDIIK(ac)HPNETDGK	DTWD1	K97
500	MEYEWK(ac)PDEQGLQQILQLLK	TNPO1	K14
501	K(ac)VTHAVVTVPAYFNDAQR	HSPA5	K164
502	KNPSNPK(ac)DK	QRICH1	K662
503	AFYPEEISSMVLTK(ac)MK	HSPA1B	K126
504	DLLVQYATGK(ac)K	SDAD1	K254
505	KSPENTEGK(ac)DGSK	HMGN3	K13
506	DTKVPNACLFTINK(ac)EDHTLGNIIK	POLR2J	K37
507	ELDPTNMTYITNQAAVYFEK(ac)GDYNK	STIP1	K272
508	QIAAIHK(ac)DLEDTEANK	SMC3	K418
509	SK(ac)KVEEAEPEEFVVEK	CBX3	K20
510	K(ac)LFAPQQILQCSPAN	TK1	K220
511	LAQMFSDMVLK(ac)DGFQPSR	TFRC	K439

Continued on next page

Table 6.5 – *Continued from previous page*

512	YKWCEYGLTFTEK(ac)	VDAC2	K85
513	TTGFGMIYDSLDYAK(ac)K	RPS24	K83
514	YVDTPFGKPSDALILGK(ac)IK	MTAP	K49
515	DMGYGNWISK(ac)PQEEK	ADAR	K1214
516	VK(ac)DEPQRR	HMGN2	K18
517	DSVVAGFQWATK(ac)EGALCEENMR	EEF2	K688
518	QDYKEGEMTLK(ac)SALALAIK	PSMA4	K187
519	YSEKEDK(ac)YEEEIK	TPM4	K184
520	YCWENFVYNDDEPFK(ac)PWK	APOBEC3F	K352
521	TCESDTLEALLLTASERPK(ac)PLLFK	UGGT1	K176
522	CGEFEK(ac)NNPDLYLK	TATDN1	K86
523	NSQK(ac)QIK	KIAA1143	K137
524	LIDGIVLTK(ac)FDTIDDK	SRPR	K589
525	ASEVEEILDGNDEK(ac)YK	SMARCB1	K106
526	IEWLESHQDADIEDFK(ac)AK	HSPA5	K617
527	SHSGK(ac)K(ac)PYQCK	ZNF561	K362, K363
528	TASLFEQK(ac)SMK	MYOF	K1944
529	RAPAPK(ac)PYVCLECGK	ZNF787	K278